

Fluctuations in Heterogeneous Catalysis: CO Oxidation as a Case Study

Von der Naturwissenschaftlichen Fakultät der Gottfried Wilhelm Leibniz
Universität Hannover zur Erlangung des Grades
Doktor der Naturwissenschaften
(Dr. rer. nat.)
genehmigte Dissertation

von
Licenciado en Física
Miguel Arnaldo Pineda Rodriguez
geboren am 05.10.1979 in Valera, Venezuela

January 2008

Referent: Prof. Dr. R. Imbihl
Korreferent: Prof. Dr. L. Schimansky-Geier
Tag der Promotion: 16. January 2008

*"We are at the very beginning of time for the human race.
It is not unreasonable that we grapple with problems.
But there are tens of thousands of years in the future.
Our responsibility is to do what we can, learn what we can,
improve the solutions, and pass them on."*

Richard Feynman (1918-1988)

Kurzzusammenfassung

Das Thema der Dissertation ist die theoretische Analyse von Fluktuationen in heterogen katalysierten Reaktionen; insbesondere die Rolle von Fluktuationen in der katalytischen CO-Oxidation auf nanoskaligen Oberflächen sollten untersucht werden. Analytische "mean-field-birth-death"-Master-Gleichungen und die entsprechenden, auf dem Gillespie-Algorithmus beruhenden, kinetischen Monte-Carlo-Simulationen der kinetischen Bistabilität in der katalytischen CO-Oxidation wurden studiert. Wie auch in zwei kürzlich publizierten Experimenten -die CO-Oxidation an einer Platin-Feldemitterspitze und derselben Reaktion an Pd-Nanoteilchen - gezeigt wurde, können intrinsische Fluktuationen Übergänge zwischen stabilen Zuständen im bistabilen Bereich induzieren. Hier wurden zunächst intrinsische Fluktuationen in Abhängigkeit von der Systemgrösse über eine Master-Gleichung untersucht, die vom Langmuir-Hinshelwood-Mechanismus der CO-Oxidation abgeleitet worden ist und als Variablen den CO- und O-Bedeckung umfasst. Nach adiabatischer Elimination der Sauerstoffbedeckung ist das Ein-Variablen-System einer analytischen Lösung zugänglich. Es wurde gezeigt, dass mit abnehmender Systemgrösse und Annäherung an den kritischen Punkt nicht mehr zwischen zwei makroskopisch stabilen Zweigen unterschieden werden kann. Unter diesen Bedingungen nähern sich die Zeitskalen der Übergänge zwischen den makroskopisch stabilen Zuständen und der Fluktuationen einander an; bei grossen Systemen und weit entfernt vom kritischen Punkt sind die Zeitskalen hingegen wohl separiert. Die entsprechenden stationären Lösungen der Wahrscheinlichkeitsverteilung und die mittlere "first passage time", die mittels des reduzierten Modells berechnet wurden, gleichen den numerischen Lösungen, die für das Zwei-Variablen-Modell erhalten wurden. In der katalytischen CO-Oxidation an Pt(110) wurden bei relativ hohem Druck (10^{-2} mbar) stochastische Musterbildungen gefunden, deren Nukleation Dichtefluktuationen der Adsorbate zugeschrieben wurde. Um die Fluktuationen in der CO-Oxidation bei höheren Drücken zu modellieren, wurde eine Reaktions-Diffusions-Master-Gleichung formuliert, die die Zunahme der Fluktuationen bei kleiner werdender Diffusionslänge beschreiben sollte. Analytische Lösungen konnten in einer reduzierten Ein-Variablen-Master-Gleichung erhalten werden, die sich ergibt, wenn die "mean-field"-Näherung angewendet und Sauerstoff adiabatisch eliminiert wird. Es wurde gezeigt, dass als Folge einer symmetrie-brechenden Bifurkation ein Phasenübergang 1. Ordnung auftritt. Die entsprechenden stationären Lösungen der nicht-linearen Master-Gleichung wurden auch in raumzeitlichen Monte-Carlo-Simulationen mit dem Gillespie-Algorithmus erhalten. Schliesslich wurde ein stochastisches Hybridmodell formuliert, das repulsive CO-

O- und O-O-Wechselwirkungen der Adsorbate mit einschliet. Die Sauerstoffbedeckung als schnelle Variable wurde adiabatisch eliminiert und das Phasendiagramm im Parameter-
raum konstruiert. Kritische Fluktuationen um die stabilen Zustände herum wurden auch
als Funktion der Systemgrösse untersucht.

Schlüsselwörter: Fluktuationen, Master-Gleichungen, Gillespie-Algorithmus.

Abstract

The topic of this Thesis is the theoretical analysis of fluctuations in heterogeneous catalysis. In particular, we study the role of fluctuations on the nonlinear dynamics in CO oxidation on nanoscale surfaces. Analytical mean-field birth-death-type master equation studies and corresponding Gillespie-type kinetic Monte Carlo simulations of the kinetic bistability of CO oxidation were carried out in this work. As has been observed, *e.g.* in recent experiments of CO oxidation on a Pt field emitter tip and on Pd nanoparticle surfaces, internal fluctuations can induce transitions between the two stable states of the bistable region. Here, at first the internal fluctuations due to finite size effects are studied by a master equation with a Langmuir-Hinshelwood mechanism for CO and oxygen. Analytical solutions can be found in a reduced one-component model after adiabatic elimination of the oxygen coverage. It is shown that near the critical point, with decreasing surface area, one can not distinguish between two macroscopically stable stationary states. Under these conditions, the transition times between the macroscopic states also are no longer separated from the short time scale of the coverage fluctuations as is the case for large surface areas and far away from the critical point. The corresponding stationary solutions of the probability distribution and the mean first passage times calculated in the reduced model are supported by numerics of the full two component model. It has also been observed, *e.g.* in experiments of catalytic CO oxidation on Pt(110) at relatively high pressure (10^{-2} mbar), that stochastic patterns can be initiated by stochastic density fluctuations. In the next step, a reaction-diffusion master equation has been introduced in order to model the bistable CO oxidation on single crystal metal surfaces at high pressure where the diffusion length becomes small and local fluctuations are important. Analytical solutions can be found in a reduced one-component nonlinear master equation after applying the mean-field approximation together with the adiabatic elimination of oxygen. It is shown a symmetry-breaking bifurcation associated with a first-order phase transition. The corresponding stationary solutions of the nonlinear master equation are supported by spatial Gillespie-type Monte Carlo simulations. Finally, a stochastic hybrid mean-field model for CO oxidation with $CO - O$ and $O - O$ adsorbed repulsive interactions is introduced. The fast oxygen coverage is adiabatically eliminated and the phase diagram in the parameter space is constructed and analysed. We also study critical fluctuations and fluctuations as a function of system size as well as fluctuations around the stable states of the bistable region.

Keywords: Fluctuations, Master equation, Gillespie algorithm.

Contents

| | | |
|----------|---|-----------|
| 1 | Introduction | 1 |
| 1.1 | The phenomenon Catalysis | 3 |
| 1.2 | Heterogeneous catalysis | 6 |
| 1.3 | Fluctuations in heterogeneous catalysis | 10 |
| 1.4 | Overview | 11 |
| I | MOTIVATION AND FUNDAMENTALS | 15 |
| 2 | Experimental motivation | 17 |
| 2.1 | Introduction | 17 |
| 2.2 | Experimental techniques implemented to study fluctuations in CO oxidation | 18 |
| 2.2.1 | Field-electron microscopy (FEM) | 18 |
| 2.2.2 | Field-ion microscopy (FIM) | 19 |
| 2.2.3 | Molecular beam (MB) | 20 |
| 2.2.4 | Photoelectron emission microscopy (PEEM) | 22 |
| 2.2.5 | Ellipsometry | 23 |
| 2.3 | Fluctuation-induced transitions in CO oxidation | 24 |
| 2.3.1 | Bistability in CO oxidation | 24 |
| 2.3.2 | Catalytic CO oxidation on a Pt field emitter tip | 25 |
| 2.3.3 | Catalytic CO oxidation on Pd nanoparticles | 27 |
| 2.3.4 | Catalytic CO oxidation on Ir(111) surfaces | 29 |
| 2.4 | Fluctuation-induced pattern formation in CO oxidation | 29 |
| 2.4.1 | Catalytic CO oxidation on Pt(110) at intermediate pressures | 31 |
| 2.5 | Summary and conclusions | 32 |
| 3 | Theoretical and simulation framework | 33 |
| 3.1 | Introduction | 33 |

| | | |
|-----------|---|-----------|
| 3.2 | Markov process | 35 |
| 3.2.1 | Classical stochastic description of chemical reactions | 36 |
| 3.2.2 | Markov birth-death description | 37 |
| 3.2.3 | Global birth-death description of fluctuations | 38 |
| 3.2.4 | Local birth-death description of fluctuations | 39 |
| 3.3 | Internal and external fluctuations | 40 |
| 3.3.1 | Internal and external fluctuations modelled via master equation | 41 |
| 3.3.2 | Internal and external fluctuations modelled via Langevin equation | 41 |
| 3.3.3 | Colored fluctuations | 42 |
| 3.4 | Stochastic simulation | 42 |
| 3.4.1 | The Metropolis algorithm | 43 |
| 3.4.2 | Kinetic Monte Carlo (KMC) simulation of lattice models | 43 |
| 3.4.3 | Gillespie-like KMC simulation | 45 |
| 3.4.4 | Hybrid algorithms | 46 |
| 3.4.5 | Comparison of simulation techniques | 46 |
| 3.5 | Adiabatic reduction of fast variables from deterministic systems | 50 |
| 3.6 | Bistability in nonequilibrium systems | 50 |
| 3.7 | CO oxidation: Basic features | 52 |
| 3.7.1 | Reaction scheme | 52 |
| 3.7.2 | Bistability | 53 |
| 3.7.3 | Oscillations | 54 |
| 3.8 | Summary and conclusions | 56 |
| II | ROLE OF FLUCTUATIONS IN CO OXIDATION | 59 |
| 4 | Reduced stochastic kinetic model | 61 |
| 4.1 | Introduction | 61 |
| 4.2 | Hybrid model for CO oxidation with $O - O$ adsorbed repulsion | 62 |
| 4.2.1 | CO adsorption and desorption | 62 |
| 4.2.2 | CO surface diffusion | 63 |
| 4.2.3 | Dissociative adsorption of O_2 | 63 |
| 4.2.4 | CO_2 production | 67 |
| 4.3 | Deterministic limit: Bistability | 67 |
| 4.4 | Stochastic limit: Master equation for CO oxidation | 68 |
| 4.5 | Adiabatic reduction of oxygen from the master equation | 70 |

| | | |
|----------|---|-----------|
| 4.5.1 | Reduced master equation for the slow CO variable | 71 |
| 4.5.2 | Reduced master equation for fast oxygen variable | 72 |
| 4.5.3 | The combined system | 73 |
| 4.5.4 | Deterministic approximation for the fast oxygen variable | 73 |
| 4.6 | Summary and conclusions | 75 |
| 5 | Fluctuation-induced transitions | 77 |
| 5.1 | Introduction | 77 |
| 5.2 | Deterministic versus stochastic approach | 78 |
| 5.2.1 | Deterministic predictions: Extended single crystal surfaces | 78 |
| 5.2.2 | Stochastic predictions: Nanoscale surfaces | 79 |
| 5.3 | Reduced master equation for CO | 81 |
| 5.3.1 | Probability distributions | 83 |
| 5.3.2 | Critical fluctuations | 83 |
| 5.3.3 | The dependence of fluctuations on the system size | 86 |
| 5.4 | Transition between stable states | 86 |
| 5.5 | Summary and conclusions | 92 |
| 6 | Fluctuations and first-order phase transitions | 95 |
| 6.1 | Introduction | 95 |
| 6.2 | Stochastic reaction-diffusion model | 96 |
| 6.3 | Reaction-diffusion master equation | 98 |
| 6.3.1 | Reaction jump Markov process | 98 |
| 6.3.2 | Diffusion random walk | 99 |
| 6.4 | Mean-field approximation (MFA) | 101 |
| 6.5 | Adiabatic elimination of oxygen | 102 |
| 6.6 | Evidence for a first-order phase transition | 104 |
| 6.6.1 | Probability distribution function and effective potential | 104 |
| 6.6.2 | Order parameter | 106 |
| 6.7 | Numerical verification of MFA predictions | 111 |
| 6.7.1 | Random local and nonlocal (RLnL) interaction versus MFA | 112 |
| 6.7.2 | Local (Diffusive) interaction versus MFA | 112 |
| 6.7.3 | Nucleation and growth of islands | 119 |
| 6.8 | Summary and conclusions | 119 |

| | |
|---|------------|
| III CO OXIDATION WITH ADSPECIES REPULSIONS : | |
| A STOCHASTIC APPROACH | 123 |
| 7 A reduced stochastic hybrid model with adspecies repulsion | 125 |
| 7.1 Introduction | 125 |
| 7.2 Deterministic approach | 126 |
| 7.2.1 Hybrid and pair approximations | 127 |
| 7.3 Stochastic approach and adiabatic reduction | 128 |
| 7.3.1 Adiabatic reduction | 129 |
| 7.3.2 Bistability | 132 |
| 7.3.3 Critical Fluctuations and the dependence of fluctuations on the system size | 135 |
| 7.3.4 Fluctuations about a stable state | 139 |
| 7.4 Summary and conclusions | 141 |
| IV CONCLUSIONS AND PERSPECTIVES | 143 |
| 8 Conclusions | 145 |
| 8.1 Summary and outlook | 145 |
| 8.2 List of specific results | 147 |
| 8.3 Open issues | 150 |
| Appendices | 153 |
| A Notation and Symbols | 153 |
| B Cluster approximation for lattice models | 157 |
| B.1 The (n, m) approximation | 158 |
| C Adiabatic reduction of fast variables | 161 |
| D Mean-field approximation | 163 |
| E Spatial stochastic algorithm | 167 |
| E.1 Random local and nonlocal interaction | 167 |
| E.2 Local (diffusive) interaction | 169 |

| | |
|--|------------|
| F Rate equations from the (2,1) approximation | 171 |
| F.1 Rate equation for θ_{CO} | 171 |
| F.2 Rate equation for θ_O | 172 |
| Bibliography | 175 |
| Publications of this Thesis | 185 |
| Curriculum vitae | 187 |
| Acknowledgements | 189 |

Chapter 1

Introduction

"Nonequilibrium systems come in many varieties, and a number of not-yet-reconciled mathematical approaches can be applied to them."

David Ruelle (1935)

The natural world is built by atoms and obeys physical laws [1]. Sometimes these atoms can combine, forming new molecules. These processes are nowadays well described by the laws of quantum mechanics. However, in any chemical situation a large number of atoms or molecules are jiggling around in a very random and complicated way. Therefore, statistical methods applied to situations where there are quantum mechanical laws have been the principal tools to understand complex chemical processes. This field is called statistical mechanics and attempts to explain the macroscopic properties of matter in terms of the interactions of its microscopic constituents. Nowadays, we can distinguish between equilibrium and nonequilibrium statistical mechanics. Equilibrium statistical mechanics is concerned with certain states of matter that appear macroscopically at rest, in equilibrium and that are microscopically a superposition of states. The time is eliminated and the probability of observe a given microscopic state is given by the Boltzmann distribution. Equilibrium statistical mechanics was developed at the end of the 19th century by, among others, James Clerk Maxwell (1831-1879), Ludwig Boltzmann (1844-1906), and Josiah Willard Gibbs (1839-1903). The successes of this theory during the 20th century were tremendous. In nonequilibrium statistical mechanics¹ the dynamics cannot be neglected and the probability of observing a given microscopic state is not given by the already mentioned Boltzmann distribution. Therefore, the understanding of deterministic and

¹Also known as dissipative or irreversible statistical mechanics.

stochastic dynamics of linear and nonlinear systems is a primordial step in order to explain nonequilibrium processes in nature. When a system is outside of equilibrium, it dissipates energy as heat, associated with an irreversible increase of entropy. One can observe in such systems oscillations, spatiotemporal patterns, and a sensitive dependence on the initial conditions (chaotic dynamics). Although, nonequilibrium statistical mechanics is an area of rapid progress, an general understanding of situations far from equilibrium is limited [2].

In nonequilibrium situations, the interplay between random fluctuations and nonlinearities have nontrivial effects. Sometimes, many manifestations of nature are very complex and nonlinear, with many degrees of freedom and many possible locally stable states. Fluctuations allow the system to explore any state. This makes the natural world so diverse. There are a number of natural systems, which fall into this class of nonequilibrium systems [3, 4]. Examples are social and economical systems, many biological processes like the interior of a cell, and of most interest here, models for chemical reactions, particularly for catalysis and heterogeneous catalysis.

One can distinguish between internal and external fluctuations. For internal fluctuations (statistical fluctuations) one can think of two situations. Since the relative amplitude of fluctuations away from critical points in general scale like $(N)^{-1/2}$ with N being the number of interacting elements of the system, the first situation is clearly where the number of molecules, atoms or the size of the system involved, is small. On the other hand, the second situation is observed near critical points of instability. Here, the square root law describing the fluctuations is no longer applicable, and as in equilibrium systems the fluctuations tend to grow to produce observable effects. In contrast external fluctuations (environmental fluctuations) are parametric, or in general, environmental variability. That is parameters like temperature or pressure are not exactly constant in time but exhibit some random variations [3, 4].

Fluctuations and fluctuation-induced phenomena have been studied theoretically in many nonequilibrium systems. The constructive role of noise in these systems is well established. Phenomena like noise-induced patterns, stochastic resonances, and stochastic ratchets or Brownian motors are a few of the many examples which have been analysed [5, 6, 7, 8, 9]. In heterogeneous catalysis stochastic resonances have been reported in models of catalytic CO oxidation and catalytic NO reduction on Pt surfaces [10, 11]. The role of a ratchet potential in connection with an ac electrical field has been studied in connection with electromigration on stepped surfaces [12]. With field electron microscopy the behaviour of coverage fluctuations in CO oxidation on a Pt field emitter tip was

investigated, and it was shown that fluctuations induce transitions between the two stable kinetic stationary states that coexist in the bistable range [13, 14]. By varying the diameter of Pd particles it was demonstrated by molecular beam experiments that bistability in catalytic CO oxidation vanishes below a critical particle size [15]. The influence of external noise has been studied experimentally and theoretically with catalytic CO oxidation on an Ir(111) surface [16, 17].

This PhD Thesis uses methods of statistical mechanics, particularly the theory of stochastic processes², to study the role of fluctuations on the nonlinear dynamics of heterogeneous catalysis. Let us state from the beginning that the term fluctuations, one of the central concepts in this Thesis, is going to be considered as internal fluctuations and not fluctuations induced by some external parameters³. In the next section an introduction to catalysis is presented and the role of fluctuations in CO oxidation is briefly introduced.

1.1 The phenomenon Catalysis

Catalysis is a highly interdisciplinary field with tremendous challenges to scientists and engineers [18, 19]. Most industrial syntheses and basically all biological reactions require catalysts. Recognized as a phenomenon and utilized since 1816, catalysis obtained an extensive empirical basis in the early 20th century. Studies of catalytic mechanisms started when Langmuir-Hinshelwood kinetics became available in the mid 1920s. As it is stressed by Ostwald (1853-1932): *"a catalyst accelerates a chemical reaction without affecting the position of the equilibrium"*. It does so by forming bonds with the reacting molecules, and by allowing these to react to a product, which is then detached from the catalyst, and leaves it unaltered such that it is available for the next reaction. Thus, catalysis is a cyclic process that accelerates a chemical reaction. In simple terms, the catalytic cycle can be described as shown in Fig. 1.1.

To see how the catalyst accelerates the reaction, we need to look at the potential energy diagram in Fig. 1.2, which compares the non-catalytic and the catalytic reaction path. Note that the uncatalyzed reaction has to overcome a substantial energy barrier, whereas the barriers in the catalytic route are much lower.

Catalysis can also influence the selectivity of chemical reactions. This means that completely different products can be obtained from a given starting material by using different catalyst systems. The catalysts come in a multitude of forms, varying from atoms

²Chap. 3 presents an overview of the theory of stochastic processes and the theoretical tools used in this thesis.

³The role of external fluctuations on heterogeneous catalysis is briefly mentioned in Chap. 2.

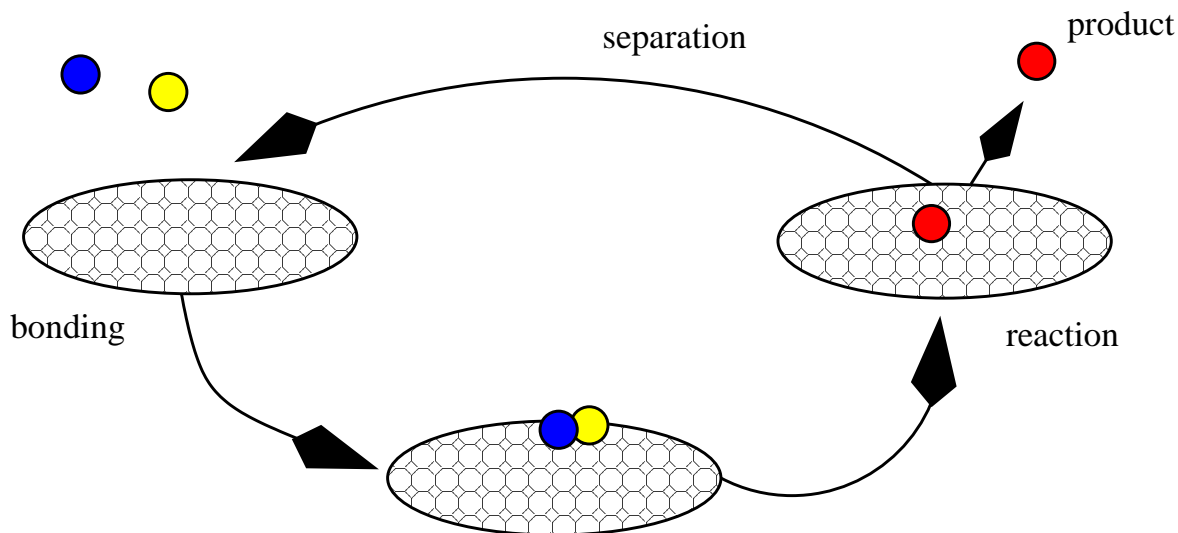


Figure 1.1: Schematic representation of a catalytic cycle. Blue and yellow circles represent molecules, the red circle is the product, and white circles are the catalyst

and molecules to large structures such as zeolite or enzymes. The numerous catalysts know today can be classified according to various criteria: structure, composition, area of application, or state of aggregation [18, 19]. From the state of aggregation, it is customary to distinguish the following three subdisciplines in catalysis: (i) homogeneous catalysis, where both the catalyst and the reactants are in the same phase; (ii) biocatalysis, where enzymes⁴ play the role; and finally (iii) heterogeneous catalysis, where solids catalyze reactions of molecules in gas or solution. By far one of the most important catalysts are the heterogeneous catalysts. *This Thesis focus on a certain aspect of heterogeneous catalysis.*

It is impossible to envision the present state of the chemical industry without catalytic reactions. Most of the products of the chemical industry are made in catalytic processes. Process involved in crude-oil and petrochemistry, require catalysts. Many environmental protections measures would be inconceivable without catalysis. However, a clear understanding of this fascinating and important phenomenon is still far away, even

⁴Enzymes are proteins that catalyze (i.e. accelerate) chemical reactions.

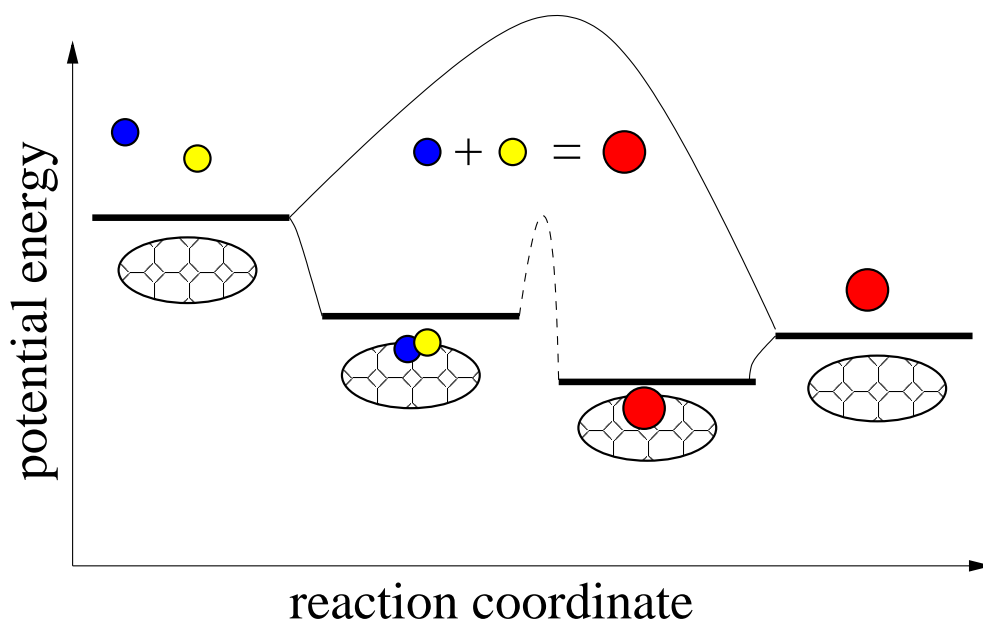


Figure 1.2: Potential energy diagram of a chemical reaction. Without a catalyst (solid line) and introducing a catalyst (dashed line)

with availability of new experimental techniques. Figure 1.3 shows a schematic classification of catalysis.

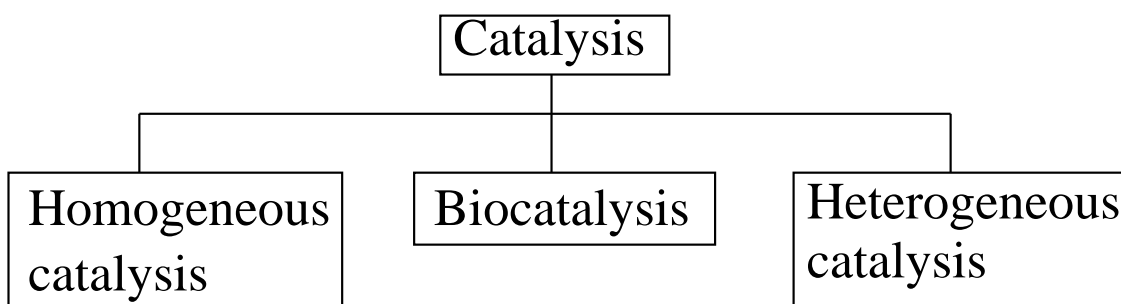


Figure 1.3: Classification of catalysis.

1.2 Heterogeneous catalysis

In heterogeneous catalysis, catalytic reactions occur at the surface. The chemical transformations occur in a flow reactor through which the reacting species pass. Atoms on the surface of the catalyst may form chemical bonds with impinging molecules, a phenomenon known as chemisorption. If existing bonds in the impinging molecule break, the process is known as dissociative chemisorption. The chemisorbed species are mobile on the surface and may bond to other particles, thus leading to new molecules, which eventually leave the surface as the desired reaction products. This subfield of catalysis is known as heterogeneous catalysis and is an important part of chemical industry but it also finds applications in environmental chemistry and energy conversion [18, 19].

Most heterogeneous catalysts consist in expensive transition metals as Pt and Pd. To use this expensive materials in an economical way, catalysts are usually nanometer-sized particles. However, this morphological change has several implications and produces the so-called size effects. Typical size effects are confinement effects, coverage fluctuations, geometric effects, electronic effects, and support effects [20]. The complexity of practical catalysts also comes from their development by purely empirical methods, e.g. by adding chemical substances and varying the composition of a catalyst. Therefore, the structural complexity together with the complexity induced by the reaction itself represents a fundamental obstacle for understanding catalysis at the molecular level.

Mechanisms of heterogeneous catalysis: Kinetic

In heterogeneous catalysis, reactions usually occur through elementary steps. However, due to the complexity of these reactions, the elementary steps are experimentally difficult to determine. Kinetics provides the framework for describing the rate at which a chemical reaction occurs. The elementary process of catalytic reactions are typically studied in surface science type experiments with single crystals as model catalyst. These studies allow to identify the elementary steps experimentally and to create microkinetic models of the reaction. However, the workhorse of real catalysis is supported catalysts where small metal particles of a few nanometer size are supported on an oxidic support material. Thus, the catalytic behavior depends also of the complexity of catalysts such as the particle size or shape. The final challenge is to transfer the knowledge acquired on simple surfaces to these more realistic systems. The difference between single-crystal studies conducted in UHV and real catalysis operating with composite materials is known as the pressure and material gap problem [21].

Heterogeneous catalysis is a natural scenery to study nonequilibrium or dissipative structures. This theme has attracted much attention since the advent of spatially resolving techniques and many fundamental questions remain still open. Experiments with simple crystal surfaces allow an experimental verification of mechanisms on the basis of which mathematical models could be formulated. For this reason, a fascinating variety of different patterns have been discovered [22, 23]. It is very common to observe in such systems rate oscillations, complex spatiotemporal patterns and chaos [24]. Experimentally, one can essentially distinguish between two type of experimental studies: experiments conducted under low pressures where the different mechanisms are mostly well established, and the corresponding elementary steps can be studied in detail [25, 26], and experiments carried out under high pressure conditions where temperature effects and strong adspecies interactions are relevant [27]. Many experimental and theoretical studies of dissipative structures in surface reactions, ranging from the simplest ones, like CO oxidation, to more complex reactions, such as the $\text{NO} + \text{NH}_3$ reaction and the oxidation of hydrocarbons have been carried out during the past years [28, 29, 30].

Catalytic CO oxidation

The catalytic oxidation of CO by O_2 on transition metal surfaces is an important process in automotive exhaust catalysis. The reaction is relatively simple and represents probably the most extensively studied reaction in the field of surface science. The catalytic cycle begins with the adsorption of CO and O_2 on the surface of a transition metal as platinum (Pt), palladium (Pd) or iridium (Ir). The stable CO bonding on transition metal surfaces is explained by the Blyholder model, original developed for metal carbonyl systems [31]. The 5σ and the 2π frontier molecular orbitals of the CO molecule are substantially modified by the presence of the metal surfaces. A filled 5σ orbital interacts with the empty $d\sigma$ metal orbitals, leading to partial transfer of electron density to the metal. At the same time filled metal $d\pi$ orbitals overlap with the 2π antibonding molecular orbital of the CO. On the other hand, O_2 molecules dissociate easily on the surface of these catalysts. This adsorption process is shown in Fig. 1.4. Once oxygen atoms are available, the reaction with CO to CO_2 can proceed almost instantaneously.

Experimentally, it is found that O adsorbed does not desorb at temperatures lower than 600 K, whereas CO adsorbed desorption starts at 400-500 K. Thus, CO molecules are bound to the surface considerably less strongly than oxygen atoms and hence may diffuse fast on the surface of close-packed metals. Finally, at temperature above 300 K, CO_2 produced interacts only weakly with the surface and desorbs immediately after its

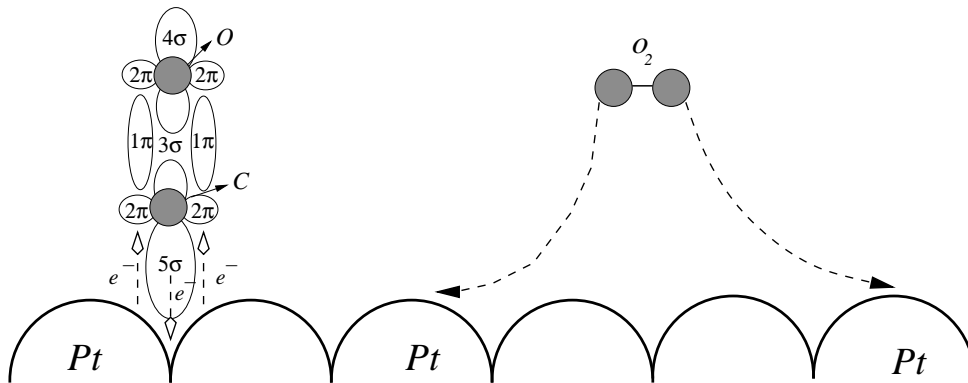


Figure 1.4: CO and oxygen adsorption on transition metals.

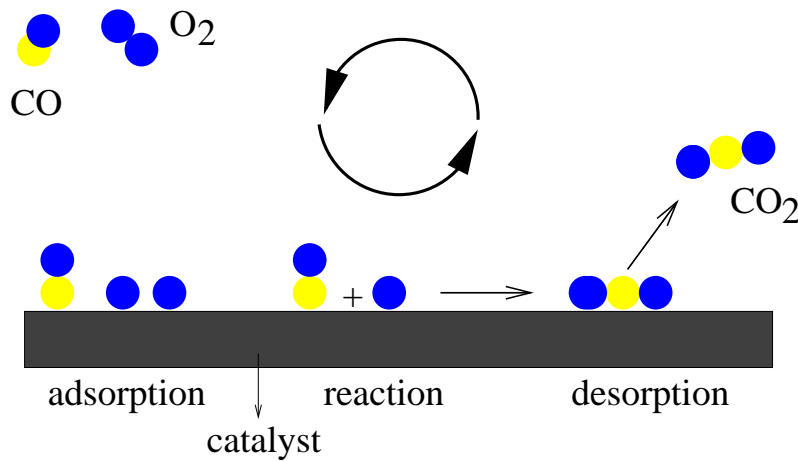


Figure 1.5: Reaction cycle of CO oxidation.

formation. Figure 1.5 shows schematically this cycle.

It has been well established that the mechanism of this reaction follows a Langmuir-Hinshelwood (LH) scheme, described by the following steps [32].

- 1) $\text{CO}_{\text{gas}} + * \rightleftharpoons \text{CO}_{\text{ads}}$ (CO – Adsorption – Desorption)
- 2) $\text{O}_{2,\text{gas}} + 2* \rightleftharpoons 2\text{O}_{\text{ads}}$ (O_2 – Adsorption)
- 3) $\text{CO}_{\text{ads}} + \text{O}_{\text{ads}} \rightleftharpoons 2* + \text{CO}_{2,\text{gas}}$ ($\text{CO}_{2,\text{gas}}$ – Production)

The first observation of rate oscillations in CO oxidation was made in the group of Wicke in the early seventies, who used a supported Pt catalyst [33, 34]. These works were followed by other reports of kinetic oscillations observed mostly in the atmospheric pressure range with transition metals, either in the form of wires, foils, ribbons, or in the form of small metals particles embedded in a zeolite matrix [35]. Since then, CO oxidation on transition metals has been the most extensively studied systems in the field of nonlinear dynamics in surface reactions [24].

To explain the origin of these kinetic oscillations, experiments with Pt and Pd single crystal surfaces were started [25]. Of the three low-index planes shown in Fig. 1.6 only the close-packed Pt(111) surface is stable in its bulklike 1×1 termination, while the more open Pt(100) and Pt(110) surfaces reconstruct in their adsorbed-free state into a quasi-hexagonal and a 1×2 geometry, respectively. However, it is found that clean Pd surfaces do not reconstruct. Almost all single crystal experimental studies were carried out under low pressure conditions ($< 10^{-3}$ mbar), where the reaction proceeds in an isothermal way. On single crystal surfaces, oscillatory kinetics was first observed in 1982 in CO oxidation on Pt(100) by G. Ertl (Nobel Laureate in Chemistry 2007) [36]. Moreover, also bistability was observed in this systems under conditions under which no oscillations occur⁵.

The bistability can be interpreted as a consequence of an asymmetric inhibition of the reaction by the reactants. Under conditions of a high O₂ flux, the surface of the crystal is largely covered by oxygen. Because oxygen influences the sticking probability of CO only moderately, the reaction rate is high and nearly proportional to the flux of CO. Once the CO flux exceeds a critical value, however, a kinetic phase transition occurs to a steady state with a predominately CO-covered surface. In contrast to adsorbed oxygen, adsorbed CO efficiently inhibits O₂ adsorption, therefore leading to a reduced reaction rate. This asymmetry leads to multistability and hysteresis, which have been observed both in high-, as well as in low-, pressure experiments with Pt and Pd surfaces [37]. While the LH scheme describes successfully this multistability, an additional step is required in order to explain the rate oscillations. This step is provided by an adsorbate-driven structural phase transition in the case of Pt surfaces and in the subsurface oxygen formation in the case of Pd catalysts [38, 39].

The development of spatially resolving techniques such as photoemission electron microscopy (PEEM) opened the possibility to go from the purely temporal phenomena to spatiotemporal pattern formation (see Sec. 2.2). Many patterns have been observed in-

⁵While Pt(111) exhibits only bistability, many different oscillations and patterns can be observed with Pt(100) and Pt(110) surfaces.

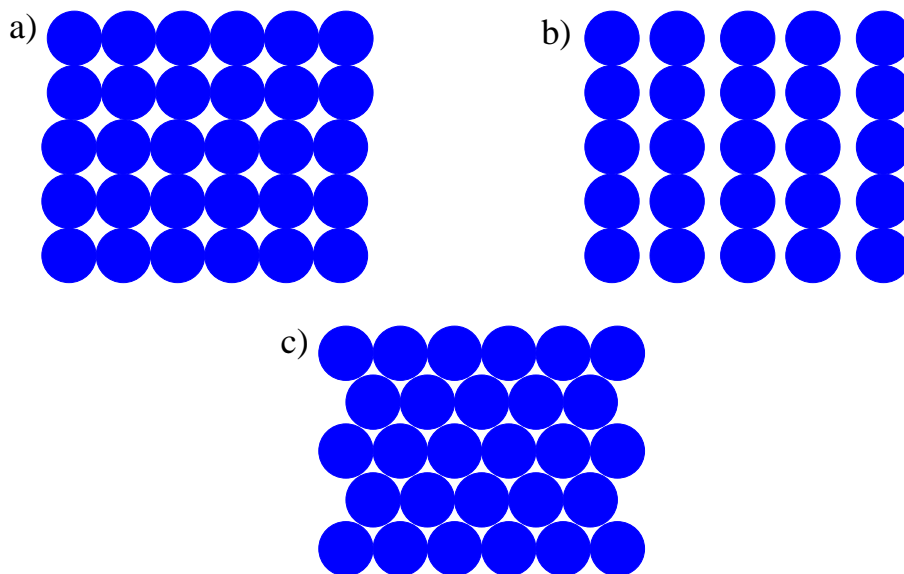


Figure 1.6: Three low index planes of Pt. a) fcc(100)-(1 × 1). b) fcc(110)-(1 × 1). c) fcc(111)-(1 × 1)

cluding rotating spiral waves, target patterns, chemical turbulence, and solitary waves [40, 41, 42, 43]. Two mechanisms provide the spatial coupling necessary to pattern formation along the catalytic surface; (i) the local coupling induced by surface diffusion of CO molecules, and (ii) the global coupling through the gas phase [44].

1.3 Fluctuations in heterogeneous catalysis

One unsolved problem in heterogeneous catalysis are the role of the stochastic fluctuations that arise as a direct consequence of the statistical nature of the elementary reaction and diffusion processes [45, 46]. Although, the study of fluctuations in chemical reactions started several years ago [3, 4], the theoretical and experimental challenge to understand the influence of internal (statistical) and external (environmental) fluctuations on the kinetic of heterogeneously catalyzed reactions is intriguing. One of the reason for this contradiction is that experimentally, it proves to be extremely difficult to identify fluctuation-induced effects in heterogeneous catalysis. Only a few experimental reports are available today. Most of these experiments have been carried out in the catalytic CO

oxidation on transition metals.

At low pressure conditions ($\leq 10^{-3}$ mbar) and high temperature (≥ 300 K) internal fluctuations have been detected only in small systems, as demonstrated in experiments with CO oxidation on a Pt field emitter tip and CO oxidation on Pd supported nanoparticles [13, 15]. Under these conditions the role of external fluctuations has been also experimentally studied with catalytic CO oxidation on Ir(111) single crystal surfaces [16]. The situation changes at high pressure close to industrial conditions. In these cases internal fluctuations can be detected even in large single crystal surfaces, as was claimed recently for CO oxidation on Pt(110) surfaces [47]. In particular, internal fluctuations in these two regimes has been analyzed by kinetic Monte Carlo (KMC) simulations [48, 49, 50]. Nevertheless, KMC simulations are essentially numerical experiments, and they do not constitute an analytic theory.

This PhD Thesis presents an analytical mean-field birth-death-type master equation study and corresponding Gillespie-type kinetic Monte Carlo simulations in order to understand the role of internal fluctuations in the kinetic bistability of CO oxidation.

Whereas most experimental studies of fluctuations in heterogeneous catalysis have been carried out with catalytic CO oxidation, the influence of fluctuation-induced effects is expected to play a role in many reactions showing similar behavior. Therefore, with the development of nanostructured systems fluctuations will become an issue for all scientists involved in the construction and analysis of such systems.

1.4 Overview

The present Thesis is a result of the studies performed at the Institute for Physical Chemistry and Electrochemistry of the Gottfried-Wilhelm-Leibniz-Universität Hannover in Hannover (Germany) between October 2004 and October 2007 under the supervision of Prof. Dr. Ronald Imbihl and Prof. Dr. Lutz Schimansky-Geier. It has been supported through a DAAD (Germany)/FUNDAYACUCHO (Venezuela) cooperation. Part of the scientific results contained in this Thesis are published or will be published in Refs. [51, 52, 53, 54], which are cited in the corresponding section of the Thesis. The experimental motivation and theoretical framework to this Thesis are provided in Part I, while in Part II and III mainly original results are presented. The description of the contents of the chapters follows.

Part I

Chapter 2

An experimental motivation to study theoretically the role of fluctuations in CO oxidation on transition metals is given. Several experimental techniques used recently to study fluctuations in CO oxidation are briefly reviewed. Finally, a few experimental evidences for fluctuation-induced effects in CO oxidation are described.

Chapter 3

The theoretical framework of the Thesis is introduced. The Markov mean-field birth-death master equation description of chemical reactions is discussed. We introduce a global and local description of fluctuations depending of the degree of the spatial inhomogeneities in the chemical systems. Fluctuations of external and internal origin are discussed. Stochastic simulation techniques are described. In particular, a description of lattices gas hybrid kinetic Monte Carlo simulations and Gillespie-type kinetic Monte Carlo simulations is given. A simple model is introduced in order to compare both simulation techniques. Finally, the adiabatic elimination of fast variables in deterministic systems as well as the bistable phenomena in nonequilibrium systems are briefly discussed.

Part II

Chapter 4

A hybrid model for CO oxidation with oxygen-oxygen repulsion introduced. Using the so-called cluster approximation, the transition probabilities for each step of the catalytical reaction are derived. The transition probabilities allow us to develop a deterministic and a stochastic description of the reaction. The oxygen, which is considered the fast variable of the system, is adiabatically eliminated from the stochastic description. The system reduction allows us to introduced a simplified version of our model.

Chapter 5

In this chapter, it is shown theoretically and by Gillespie-type kinetic Monte Carlo simulations that internal fluctuations induce transition in CO oxidation. Probability distributions, critical fluctuations, the dependence of fluctuations with the system size, and transition times are discussed.

Chapter 6

It is shown that the interplay between internal fluctuations and diffusion can induce a first-order phase transition in CO oxidation under diffusion limited conditions. A reaction-diffusion master equation is introduced to study CO oxidation under diffusion limited conditions. After applying the the mean-field approximation and after adiabatic elimination, a order parameter is introduced to characterize the phase transition. Theoretical predictions are verified by spatial Gillespie-type kinetic Monte Carlo simulations.

Part III**Chapter 7**

In this chapter, we introduce a stochastic hybrid mean-field model for CO oxidation on nanoscale surfaces with $CO - O$ and $O - O$ adsorbed repulsions. We derive it using the so-called cluster approximation. The fast oxygen coverage is eliminated adiabatically and the phase diagram in the parameter space is constructed and analysed. Finally, critical and particle number fluctuations as well as fluctuations around the stable states of the bistable behavior are analyzed.

Chapter 8

A summary of the major contributions of this dissertation and suggestion for future work is provided.

Part I

**MOTIVATION AND
FUNDAMENTALS**

Chapter 2

Experimental motivation

"It's an experience like no other experience I can describe, the best thing that can happen to a scientist, realizing that something that's happened in his or her mind exactly corresponds to something that happens in nature.... A great shock, and a great, great joy."

Leo Kadanoff (1937)

2.1 Introduction

Heterogeneous catalysis has been known as a "black magic" for a long time and the research in this field was characterized by empiricism. Now, however, thanks to the rapid development of methods in surface physics and the combination of first-principles calculations with phenomenological simulations, the elementary steps can be identified at the atomic level. One of the intriguing phenomena in heterogeneous catalysis are the so-called nanoscale effects, which exclusively arise as a consequence of the limited dimension where the reactions occur. One example are the communication effects that arise from the coupling of the kinetics between different nanofacets or nanoregions, occurring via surface diffusion. Another important nanoscale effect is the influence of coverage (internal) fluctuations¹ on the kinetics. As mentioned in the introduction, the interaction between these nanoscale fluctuations with the nonlinearities induced by the reaction itself can induce new and unexpected phenomena. In this chapter, several experimental techniques used recently to study nanoscale fluctuations as well as a series of experimental evidence

¹Fluctuations in the particle densities are known as coverage fluctuations

for fluctuation-induced contributions to the reaction rate of catalytic reactions, are briefly described.

2.2 Experimental techniques implemented to study fluctuations in CO oxidation

Fluctuations have received extensive theoretical and experimental treatment in different physical contexts for a long time, but only recently a substantial influence on the catalytic activity of chemical reactions was theoretically predicted and experimentally studied. From the experimental point of view, only a few reports for fluctuation-induced effects in heterogeneous catalysis are available in the literature. The reason is simple: Experimentally, it proves to be extremely difficult to identify fluctuation-induced effects in the global reaction kinetics of macroscopic systems. In the remainder of this chapter we will describe very briefly the experimental evidence for fluctuation-induced effects in CO oxidation, but first a series of experimental techniques used in these studies will be reviewed.

2.2.1 Field-electron microscopy (FEM)

The field emission of electrons from a cold metallic cathode in the presence of a large surface electrical field was first reported by Wood [55]. Later Schottky tried to explain the phenomena by a complete reduction of the height of the potential barrier at the surface down to the Fermi level. Finally, this emission was completely described by Fowler and Nordheim in 1928 using the new quantum mechanics [56]. Basically, quantum mechanics predicts the tunnelling of electrons due to the bending of the potential barrier because of the external electric field applied.

The phenomenon of field emission was then used to develop a microscope on the basis of the difference in work function (WF) of the various crystal planes on the surface. The field electron microscopy (FEM) itself was invented by Müller in (1936) [57]. This instrument approached, for the first time, the ideal of being able to view a surface on a scale that approached the realm of atomic dimensions and simultaneously allowed one to follow rapid changes at the surface. It gave for the first time a direct indication of the cleanness of a surface. The emitter is made in the form of a sharp "tip" producing an intense electric field around it. The electric field at the apex of the tip is inversely proportional to the radius of the tip. Electrons leave the tip with very low kinetic energy and will therefore follow paths parallel to the lines of the electrical force. Since these enter the metal tip perpendicularly, electron paths like those in Fig. 2.1 result. The image on

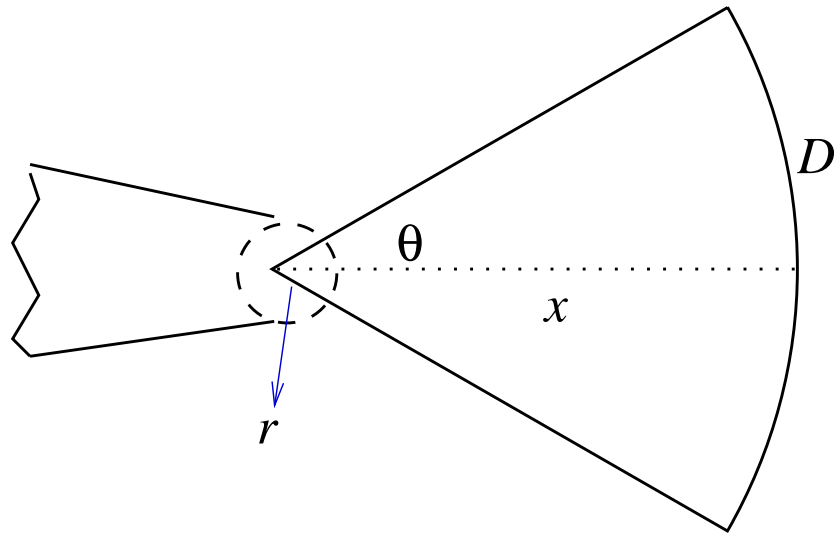


Figure 2.1: Schematic diagram showing the field electron microscopy. r , radius of curvature of the tip; x , tip to screen distance. A region of linear dimension θ will be magnified to appear as D on the screen.

the fluorescent screen is thus an electron emission map of the tip, magnified by an amount $D/\theta = x/r$. Linear magnifications of the order of 10^5 - 10^6 are possible. The resolution is limited to $\approx 20 \text{ \AA}$ by the tangential velocity of the electrons in the free-electron gas. With this apparatus it is not possible to detect individual adsorbed atoms, but only larger aggregates. The resolution is, however, sufficient to specify emission changes occurring on regions of known crystal orientation. The brightness in FEM varies with the local work function. Figure 2.2 shows a FEM image of the CO oxidation on a Pt tip [13]. The CO-covered and bare surface (low WF) are therefore imaged as bright areas whereas the oxygen-covered surface (high WF) appears dark [58]. In particular, FEM has been used to study oscillations in surface reactions [59, 60]

2.2.2 Field-ion microscopy (FIM)

Field ionisation of a H atom in a high electric field was predicted by Oppenheimer in 1928 [61]. This prediction remained untested for many years until the field ion microscopy (FIM) was invented by Müller (1951) [62]. In this device, a sharp tip of the sample material is held at a large positive potential so that field strengths at the surface approach 10^9 V/cm .

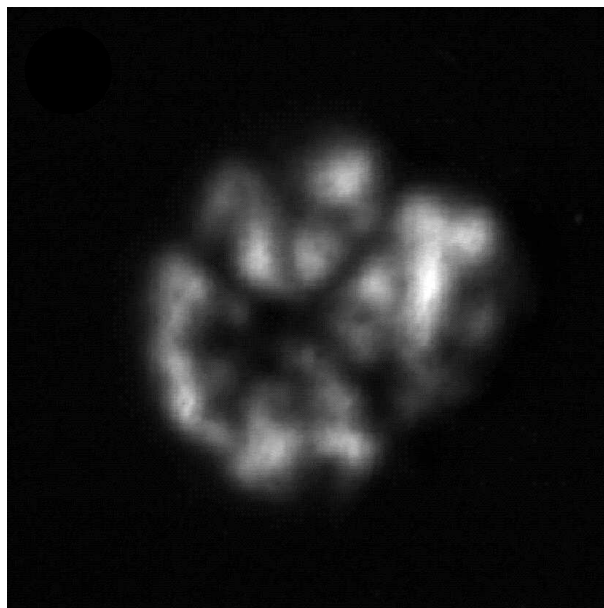


Figure 2.2: FEM image of CO oxidation on a Pt tip (from [13]).

One then admit a gas of neutral atoms, typically He or a He/H mixture, into the specimen chamber. These atoms are attracted to the solid and lose kinetic energy through multiple collisions with the surface. Eventually, they remain in the neighbourhood of the surface long enough for the electric field to ionize an electron. This process is shown in Fig. 2.3. An image of the faceted tip surface forms when the resulting positive ions rapidly accelerate away from the metal towards a fluorescent screen as is shown in Fig. 2.4.

Unfortunately, the FIM is limited to study of transition metals and their alloys since the tip itself must be stable at the fields needed to ionize the imaging gas. At sufficiently high fields, the metal atoms themselves are stripped from the surface [65].

2.2.3 Molecular beam (MB)

The MB is a spatially well defined, directed and collision-free flux of molecules. It encounters single scattering events at the sample surfaces. This implies that the flux of molecules passing through an area during a given time, can be calculated. Internal and kinetic energy of the molecules in the flux are also well defined.

The beam is prepared in a first differentially pumped chamber (source). It is generated

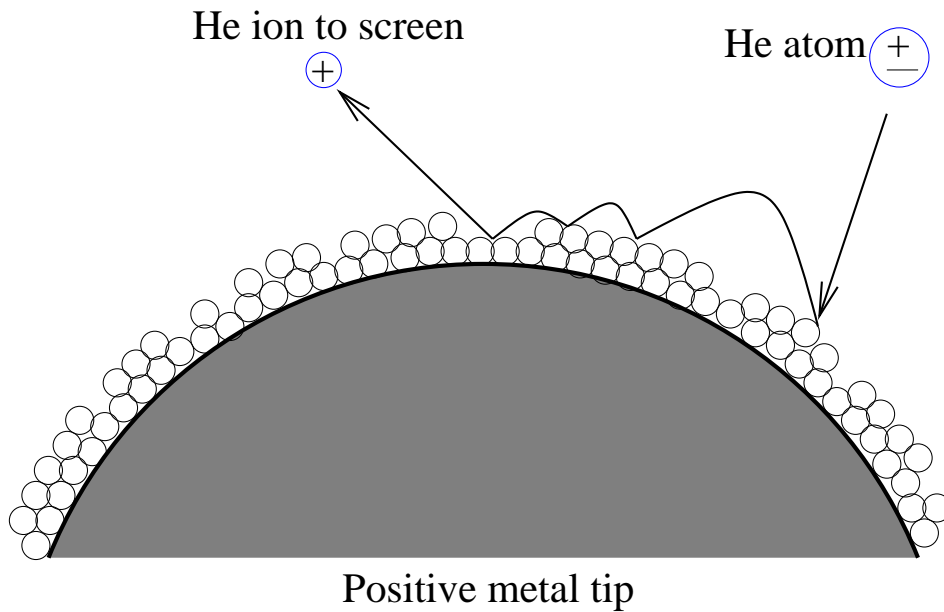


Figure 2.3: Schematic view of image formation in FIM (from [63]).

by a gas expansion from a high-pressure reservoir (nozzle) into vacuum. The centreline of the expansion is selected by a skimmer, whereas the remaining gas is efficiently pumped by several differential pumping stages. After generation, the beam can be temporally modulated by mechanical devices such as shutters or choppers. The pressure difference between the reservoir and vacuum determines the beam energy and flux. The principle of MB generation is schemed in Fig. 2.5. The methods available for the production of MBs divide into two classes, effusive sources and supersonic expansions [58].

Historically, effusive sources were the first to be developed, starting with the apparatus of Dunninger (1911) and followed by the comprehensive molecular beam programme of Stern, which started in 1919 and included the famous Stern-Gerlach experiment [66]. Effusive beams are generated by a lower pressure difference between the reservoir and ambient background. This results in broader velocity distributions. Supersonic beams are generated from a high-pressure reservoir, typically in the bar range. The large pressure difference between the reservoir and ambient pressure results in an effective equilibration of the kinetic energies in the beam. Practically, the area exposed at the sample surface remains smaller than the sample itself, so that the flux is well defined there [67].

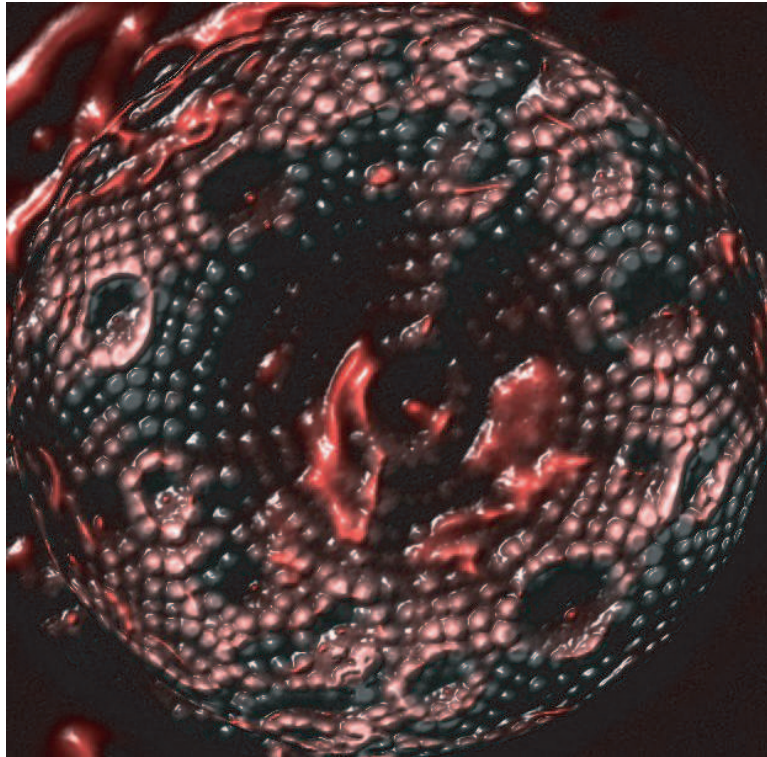


Figure 2.4: FIM of a very sharp tungsten needleless. The small round features are individual atoms. The lighter coloured elongated features are traces captured as atoms moved during the imaging process (from [64]).

2.2.4 Photoelectron emission microscopy (PEEM)

Photoelectrons are created by exposing the sample to UV light generated, for example by a D_2 discharge lamp (emission around 5-7 eV). Electron lenses to directly image the photo emitted electrons from the surface region of the specimen onto a screen, converting the electron image into visible light is the basis of the photoelectron microscopy. This microscopy dates from the early 1930s, when electron lenses and so-called emission microscopes were developed. The spatio-temporal dynamics information of the surface adlayer variation in the catalytic surface reactions is usually detected by PEEM as different grey scales of the work function patterns [68].

PEEM with a high enough lateral ($\approx 0.1 \mu m$) and temporal (≈ 20 ms) resolution is a unique tool for the investigation of real time spatio-temporal dynamics on heterogeneous

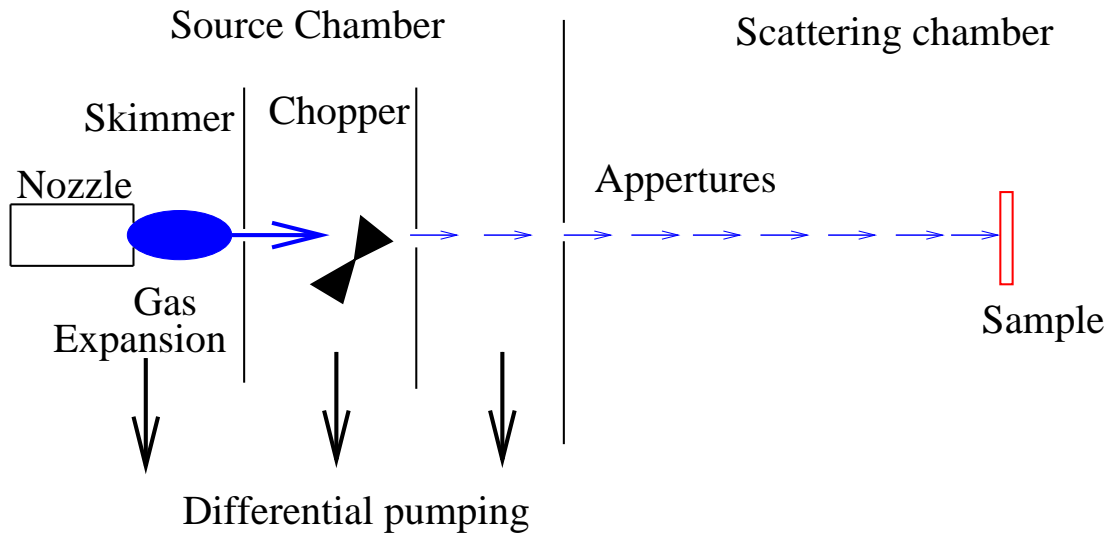


Figure 2.5: Molecular beam generation.

catalysis [68, 69].

2.2.5 Ellipsometry

Ellipsometry refers to a class of optical experiments which measure changes in the state of light polarization upon reflection from a sample. It is a powerful technique for the characterization of thin films on surfaces, which allows the determination of optical constants and thicknesses of a layer system. It provides the information not only from the surface but also the subsurface region. Furthermore, it is a light-in-light-out technique and therefore has no pressure limitations. A basic setup of an ellipsometry experiment is shown in Fig. 2.6 [27]. The light source, commonly a laser, is linearly polarized by a polarizer and reflected from the sample. In general, the reflected light is elliptically polarized, only to be converted back into linearly polarized light by a compensator, which is aligned by its fast and slow axes with the appropriate axes of the ellipse. The following analyzer, identical with the polarizer just after the light source, can now be turned to extinguish the light as it is measured by a detector. The principal ellipsometric values, the phase change and the ratio of incident to reflected amplitudes, can be derived from the settings of the compensator and the analyzer [27]. Since ellipsometry is measuring the ratio of two values, it is very robust, accurate, and reproducible. Ellipsometry has been used to image

surface reactions with the so-called Ellipsometry for surface imaging (EMSI) [70].

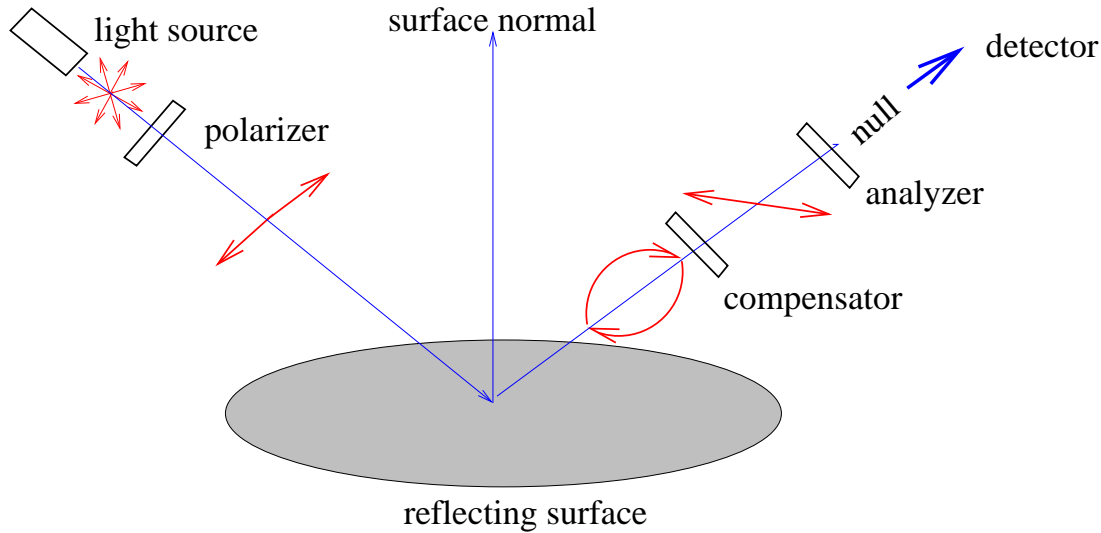


Figure 2.6: Ellipsometry setup.

2.3 Fluctuation-induced transitions in CO oxidation

2.3.1 Bistability in CO oxidation

CO oxidation on structurally stable Pt surfaces exhibits two branches of the kinetics as shown schematically in Fig. 2.7. On the active branch the surface is predominantly oxygen covered so that CO can still adsorb and react and the reaction rate therefore increases linearly with p_{CO} . On the inactive branch the surface is large CO covered and this high CO coverage inhibits the adsorption of O_2 which requires two adjacent vacant sites. On the inactive branch the rate drops with increasing p_{CO} . The hysteresis is due to the asymmetrical inhibition of the reactants O_2 and CO. Experimentally, pure bistability is observed on Pt surfaces which do not reconstruct, i.e. Pt(111) [24, 71]. The bistability terminates in a so-called cusp point when the temperature is introduced as a second control parameter. With increases the temperature the CO coverage becomes too small to allow the inhibition of O_2 adsorption. Bistability is known to give rise to front propagation and nucleation of more stable state. Thus, starting from one state, a parameter variation or local fluctuations may lead to nucleation of the other and front propagation until the whole surface has switched to this state [24].

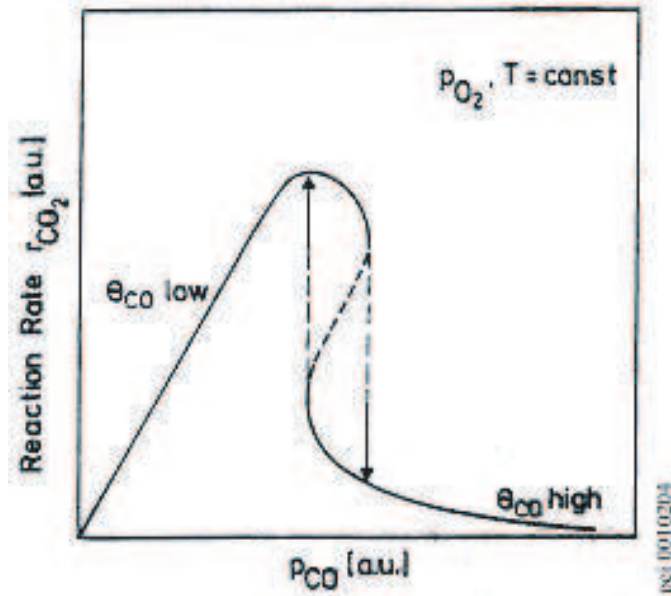


Figure 2.7: A schematic diagram showing the stationary states of the reaction rate in the bistable CO oxidation reaction. p_{O_2} and p_{CO} are the partial pressures of oxygen and CO, respectively, and T is the surface temperature.

The experiments described in this section are focused onto the role of internal (nanoscale) and external fluctuations in the kinetic bistability of CO oxidation on Pt, Pd and Ir surfaces. These experiments have shown that fluctuations of internal or external origin can induce transitions between these two states.

2.3.2 Catalytic CO oxidation on a Pt field emitter tip

Y. Suchorski *et. al* showed, in a serie of experiments with CO oxidation on a Pt field emitter tip (FET), that a reversible switching of the surface coverage from carbon monoxide rich to oxygen rich occurs in the region of bistability [13, 14, 72, 73]. They employ FIM with its high resolution of 3-4 Å to identify the surface crystallography of the area probed by FEM under reaction conditions with much lower resolution of 20 Å. The influence of the electric field was shown to be negligible in the FEM experiments. The surface of a field emitter tip which was imaged *in situ* with FEM consist of small facets of similar extension as metal particles of a supported catalyst. Therefore, the FET was considered as a model system

for a supported catalyst. Here, I will summarize some of the most important results of these experiments.

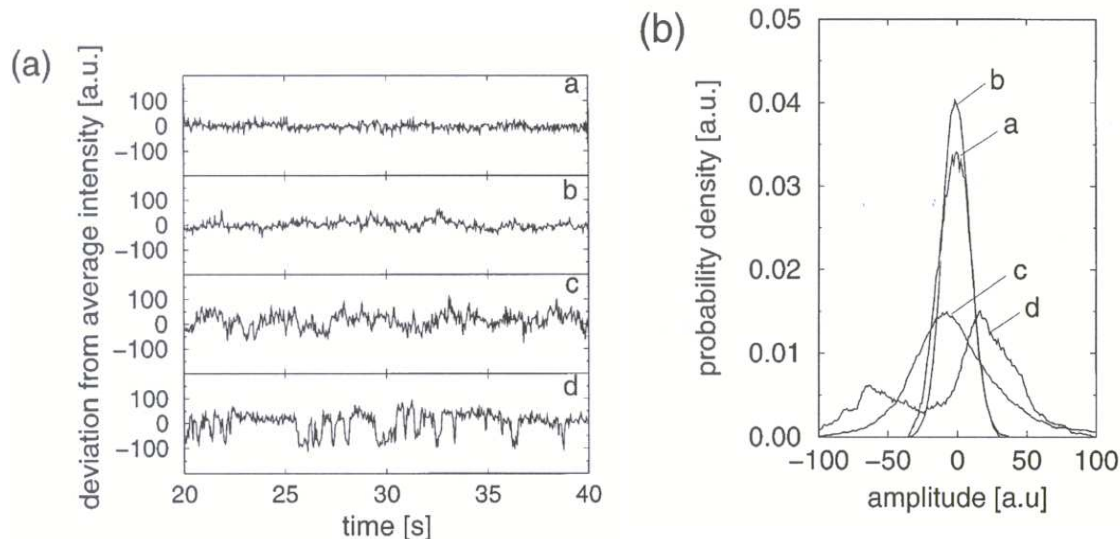


Figure 2.8: Fluctuations in catalytic CO oxidation on Pt(110) under different reaction conditions (from [13]). (a) Time series of the local ($20 \times 20 \text{ \AA}^2$) FEM brightness in the area of study. (b) Probability distributions corresponding to the time series shown in (a).

First, the bifurcation diagram for CO oxidation on a [100]-oriented Pt tip, exhibiting oscillation, bistability, and monostable regions where the tip becomes CO covered and oxygen covered, respectively was constructed [13, 14]. They found that although the various orientations on the tip differ quite strongly in their reactivity, fast CO diffusion ties the different facets together so that the tip behaves as one dynamical system. The fluctuation experiments are focused entirely on reaction conditions under which the system is bistable. Particle density fluctuations are detected as FEM brightness fluctuations. Over a facet region the fluctuations always occurred spatially uniformly, i.e., no reaction fronts could be detected within the time resolution of the experiments ($= 20 \text{ ms}$). Local fluctuations in an area of $20 \times 20 \text{ \AA}^2$ were recorded. The time series shown in Fig. 2.8 were taken from such small area in the vicinity of Pt(110) [13]. The different time series displayed in Figure 2.8a correspond to a CO-covered (inactive) and as oxygen-covered (active) surface in the monostable range (a,b) and to states in the bistable range (c,d). From the time series, probability distribution functions of the intensity fluctuations were constructed as shown in Figure 2.8b. In the monostable range relatively narrow distributions were found, but in the bistable range the distributions become rather broad. On the active branch,

the peak just broadens and become slightly asymmetric (c), but on the inactive branch (d) the distribution actually becomes bimodal. *The bimodal distribution is evidence for fluctuation-induced transitions between the two stable states.*

Secondly, they study the variation of the amplitude of fluctuations approaching the critical point (critical fluctuations) where the bistability terminates. They found that near this point the amplitude of fluctuations increases drastically like in an equilibrium phase transitions. Finally they study spatial correlations and coupling effects between different facets on the tip. They conclude that fluctuations are well correlated within one single facet but typically no correlations exist between fluctuations on different facets except for conditions very close to the critical point [72, 73]. These results also demonstrate that FEM, which has almost completely been replaced by the scanning tunnelling microscope (STM), is in fact a technique with which fluctuations in catalytic reactions can be investigated.

2.3.3 Catalytic CO oxidation on Pd nanoparticles

Inspired in the experimental results for CO oxidation on a Pt tip described above, V. Johánek *et. al* showed using molecular beam experiments that coverage fluctuations in CO oxidation on catalyst Pd nanoparticles can drastically alter their macroscopic catalytic behavior [15]. In particular, it is demonstrated that macroscopically observable bistabilities vanish completely with decreasing particle size². The effect was attributed to *fluctuations-induced transitions between two kinetic reaction regimes, with transition rates controlled by particle size.*

In this experiments the properties of the reactants were controlled by two molecular beams and the quantity of products was measured by mass spectroscopy. A combination of two different preparation methods, physical vapor deposition (PVD) and electron beam lithography (EBL) were used. PDV typically allows preparation of particles down to 1-10 nm diameter, whereas EBL allows preparation of particles above 10 nm. Small particles in the range of a few nanometres in diameter were prepared by metal evaporation and growth of Pd on a well-defined alumina film on a NiAl(110) single crystal surface. In order to obtain larger particles sizes model catalysts were prepared by means of EBL [15]. Figure 2.9 shows the size-dependent behavior of the kinetic bistability for CO oxidation on Pd nanoparticles. They investigated the transient behavior in the region where a transition from the O-rich to the CO -rich regime occurs and where hysteresis is expected.

For large particles of the model catalyst I, the transient behavior is quite similar to the

²Normally, internal fluctuations are inverse proportional to the system size

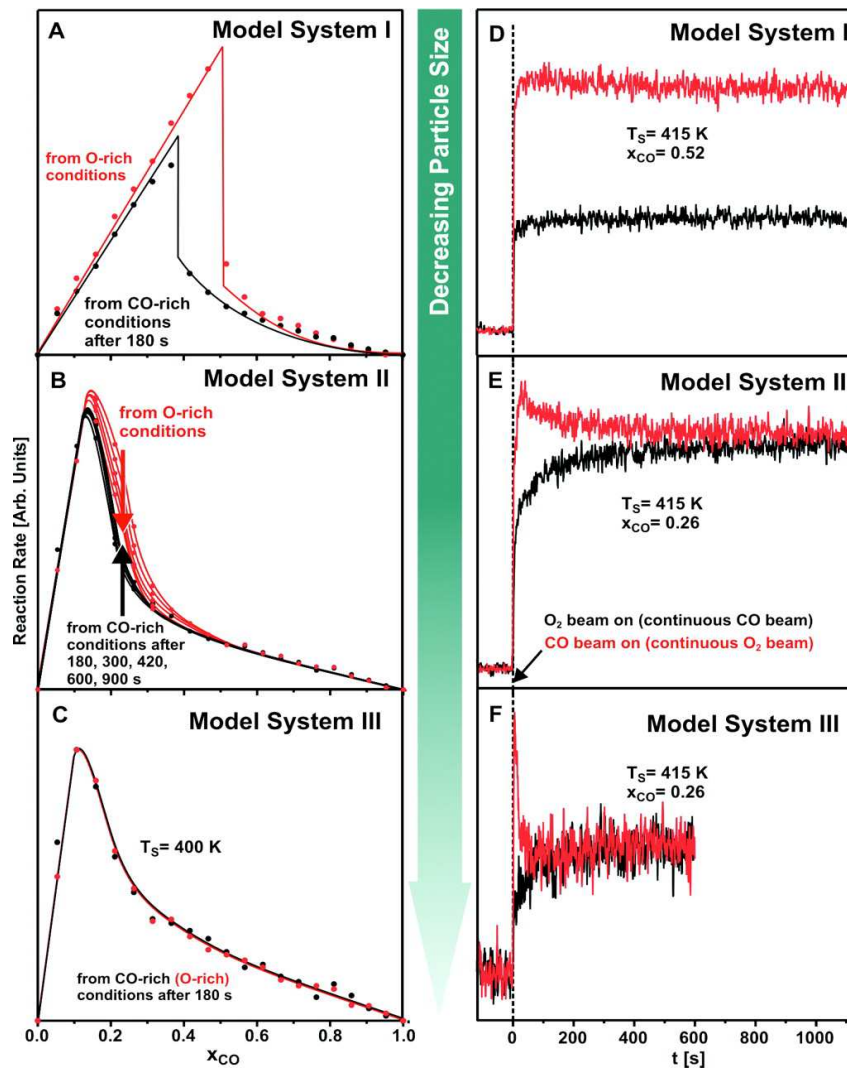


Figure 2.9: CO_2 production rates at steady state as a function of the fraction of CO in the total flux x_{CO} (left) and during the transient as a function of time. Red: CO-precovered, black: O-precovered. The bistability vanishes with smaller particle size (from [15]).

deterministic predictions. Preparing the surface either in an O or CO precovered state, two different reactive states are obtained which are perfectly stable within the experimental accuracy. When they proceed to smaller particles of the model system II, they observed that, although different reaction rates are initially established by either starting from O- or CO-rich conditions, these differences vanish slowly but completely on a typical time scale.

Also, for smallest particles of model system III, a common steady-state rate, is reached. They showed also that the width of the bistable region rapidly decreased with increasing defect density³.

2.3.4 Catalytic CO oxidation on Ir(111) surfaces

Recently, also the role of external fluctuations in CO oxidation on large Ir(111) surfaces was studied using Photoelectron Emission Microscopy (PEEM) [16]. S. Wehner *et. al* used PEEM for this investigation, since CO and O covered areas on the Ir(111) surface turn out to exhibit sufficient work function contrast and also because the rates of CO adsorption and desorption, O adsorption, CO+O reaction, and CO and O diffusion are known rather precisely. As in the previous cases, in the bistable range, at an one appropriate flux of CO, two CO_2 rates, high or low, can be measured. Oxygen covered fractions of the surface appear black, CO covered fractions appear gray, and uncovered regions appear light gray. *They observe that with the application of noise to the CO flux, transitions from upper (lower) to the lower (upper) branch of the hysteresis or bistability can be induced.* Depending on the noise strength the time required to complete the transition spans the range from a few seconds (large noise) to several hours (small noise). Figure 2.10 displays PEEM pictures recorded during experiments as function of the noise intensity denoted by ΔY [16]. As seen in Fig. 2.9(a), starting with a CO covered surface (low CO_2 rate branch) and small noise, oxygen islands appear and grow slowly, and finally the surface is oxygen covered (high CO_2 rate branch) and remains so for a long time. In Fig. 2.9(b), the noise level was increased, consequently the transition from a CO covered surface to an O covered one is significantly faster. In contrast to the previous case, several islands are formed and growth. Finally in Fig. 2.9(c), the noise is strong enough to produce more islands and reduce the transition times.

2.4 Fluctuation-induced pattern formation in CO oxidation

The previous experiments were carried out at low pressures i.e, below 10^{-4} mbar. Under these conditions, each adsorbed CO molecule changes its site up to 10^6 times before the next particle impinges, thus the surface is well mixed on a length scale of about $1 \mu m$ and internal fluctuations have only important influence in small regions of a surface. However, for large surfaces ($\approx 1 cm^2$) under low pressure conditions, internal fluctuations due to the

³Structural defects like steps or impurities can be considered as small regions on the surface with different kinetics parameters.

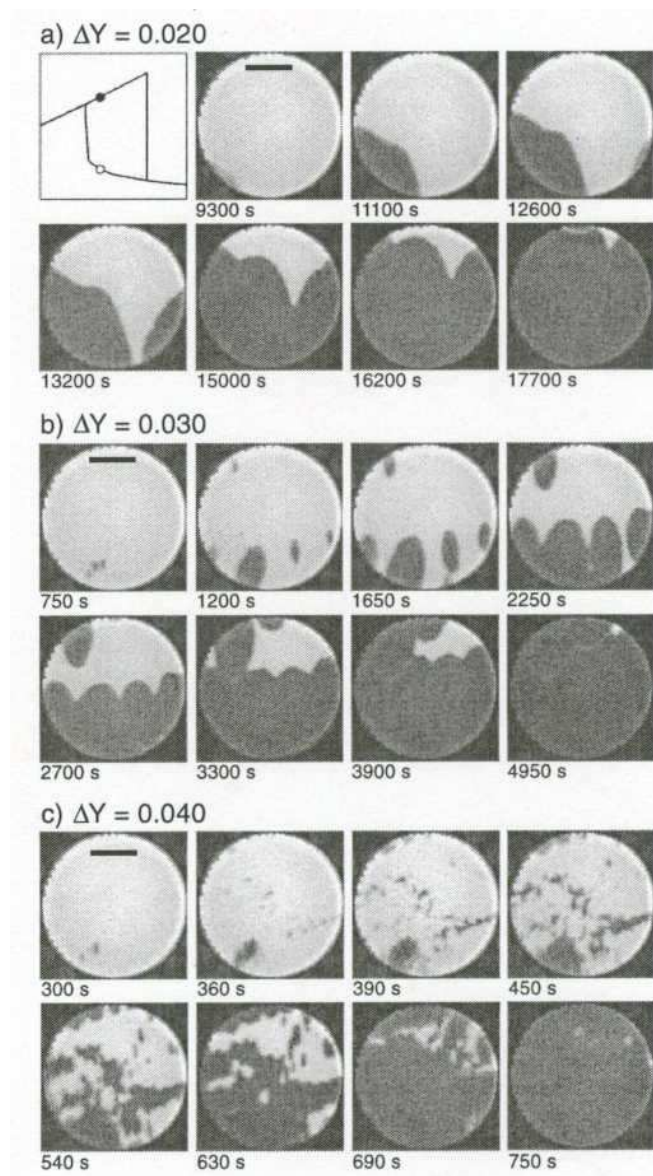


Figure 2.10: PEEM images showing randomly nucleating oxygen islands recorded during the ongoing reaction in the bistable range at a given external noise intensity ΔY . The horizontal black bar corresponds to $100 \mu\text{m}$ (from [16]).

discrete nature of the reaction processes are averaged out and not detected in experiments. The experiment described in this section corresponds to a situation when CO oxidation is carried out under high pressure conditions ($\approx 10^{-2}$ mbar). The diffusion length may, at

these higher pressures, decrease due to (i) the low diffusivity which results from a densely populated surface and (ii) due to a short residence time caused by repulsive particle interactions and a high impingement rate. Finally, it reaches a scale on which fluctuations become important inside small patches of the surface, which are, however large enough to lead to macroscopically detectable consequences, i.e, nucleation of fronts.

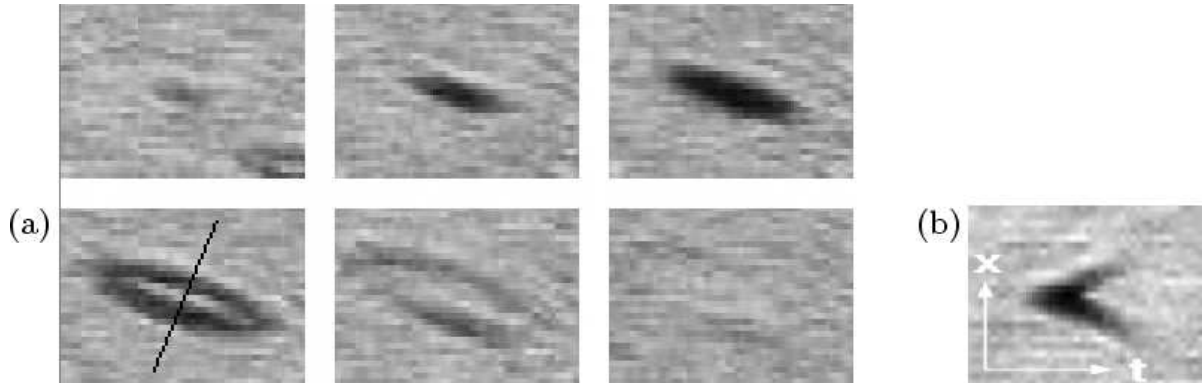


Figure 2.11: (a) Pt(110) surface exhibiting raindrop patterns with EMSI (Ellipsomicroscopy for surface imaging) at $p_{CO} = 7 \times 10^{-3}$ mbar and $p_{O_2} = 2.2 \times 10^{-2}$ mbar. (b) Space-time diagram of the raindrop ($1.6 \text{ s} \times 100 \mu\text{m}$) (from [47]).

2.4.1 Catalytic CO oxidation on Pt(110) at intermediate pressures

Recently, it was reported that at intermediate pressures ($\approx 10^{-2}$ mbar) internal fluctuations can induce spontaneously pattern formation in CO oxidation on Pt(110) at intermediate pressures [47]. The patterns were recorded at these high pressure with Ellipsomicroscopy for surface imaging (EMSI) [47, 70]. The experimental observation with Pt(110) at intermediate pressures (called "raindrop patterns") is reproduced in Fig. 2.11. The CO partial pressure was stepwise increased to a value just before the whole surface would switch to the CO-covered state. CO nuclei could be seen to originate at various random places forming a ring-shaped pattern that was subsequently destroyed. Thermokinetic effects are consequence of the temperature increases caused by the reaction heat at 10^{-2} mbar: In combination with the asymmetric inhibition of adsorption and the strong temperature dependence of CO desorption. An O-covered surface exhibits a high reaction rate and therefore become hot, while a CO covered areas keeps the catalyst cool. This effect constitutes the first example of mesoscopic pattern formation in a surface reaction

that is initiated by internal fluctuations and cannot be fully captured in a deterministic description [47].

2.5 Summary and conclusions

In the present chapter, after introduce some techniques recently used to study fluctuations in CO oxidation, a short description of the few experimental evidence for fluctuation-induced transitions in CO oxidation on Pt, Pd, and Ir surface as reported by Y. Suchorski *et. al* [13, 14, 72, 73], V. Johánek *et. al* [15], and S. Wehner *et. al* [16], has been presented. With field electron microscopy the behavior of internal fluctuations in the CO oxidation on a Pt field emitter tip was investigated by Y. Suchorski *et. al* and it was shown that these fluctuations induce transitions between the two kinetically stable stationary states that coexist in the bistable range shown in Fig. 2.7 [13, 14, 72, 73]. V. Johánek *et. al* demonstrated by molecular beam experiments that varying the diameter of Pd particles the bistability in CO oxidation vanishes below a critical particle size [15]. On the other hand, S. Wehner *et. al* showed recently, using photoelectron emission microscopy, that external fluctuations of sufficient strength imposed on the CO flux can induce transitions between a fully CO covered state into a fully O covered state (or vice versa). Finally, one experimental evidence for fluctuation-induced pattern formation in CO oxidation on a Pt(110) surfaces was reported [27, 47, 70].

The experimental study of fluctuations in heterogeneous catalysis is still in its infancy. Only few experimental studies in this field are available. New techniques with more spatio-temporal resolution are needed in order to detect fluctuations, which usually are presented in extreme condition as for example in small nanoparticles and high pressures. It can be expected that these studies will also demonstrate the role of fluctuations in oscillatory kinetics, spiral waves, and many other dissipative structures observed in CO oxidation on transition metals.

Chapter 3

Theoretical and simulation framework

"The sciences do not try to explain, they hardly even try to interpret, they mainly make models. By a model is meant a mathematical construct which, with the addition of certain verbal interpretations, describe observed phenomena. The justification of such a mathematical construct is solely and precisely that it is expected to work."

John von Neumann (1903-1953)

3.1 Introduction

The present chapter is dedicated to summarise the theoretical framework of this Thesis. It is constructed using the so-called theory of stochastic process applied to chemical reactions. We start with the well known result from statistical mechanics which reads that if the average number of molecules in a chemical reaction is of the order of N , the fluctuations about this average will be of the order of $N^{-1/2}$. Usually, in many chemical reactions N is typically in the range $10^{20} - 10^{25}$ and the square root of the extent of fluctuations is therefore essentially negligible. Thus, under these conditions, chemical reactions can be described by deterministic process. By a process, we mean any function \mathbf{X} of time t that can be regarded as specifying the instantaneous density of molecules (the coverage) of some chemical reaction. We say that a process is deterministic if a knowledge of its values up to and including time t allows us to unambiguously predict its value at any infinitesimally later time $t + dt$. An important subclass of deterministic process is comprised of those

that are memoryless. Here, the value $\mathbf{X}(t)$ alone uniquely determines $\mathbf{X}(t + dt)$, so the process can advance in time without having to recall its past values. An example of these without memory deterministic processes is one for which the value $\mathbf{X}(t + dt)$ is obtained from the value $\mathbf{X}(t)$ through a equation of the form

$$\mathbf{X}(t + dt) = \mathbf{X}(t) + \mathbf{f}(\mathbf{X}(t), t)dt, \quad (3.1)$$

where \mathbf{f} is some ordinary function. After some algebra we see that this process is simply the solution of the ordinary differential equation

$$\frac{d\mathbf{X}}{dt} = \mathbf{f}(\mathbf{X}, t), \quad (3.2)$$

subject to some prescribed initial condition $\mathbf{X}(t_0) = \mathbf{x}_0$. There are situations, however, such as in diffusion controlled reacting systems, reactions in biological cells or the diffusion-reaction in nanoscale solid catalysts, where the conventional deterministic description would be inadequate. Other situation where the deterministic description breaks down is near the points of instability. The square root law describing the fluctuations is no longer applicable, and the fluctuations tend to grow to producing strong effects.

This type of situations frequently encountered in chemical reaction systems justifies the application of mathematical tools developed from stochastic process theory. We say that a process is stochastic if a knowledge of its values up to and including time t allows us to *probabilistically* predict its value at any infinitesimally later time $t + dt$. More precisely, the values $\mathbf{X}(t')$ for $t' \leq t$ determinate the probability that $\mathbf{X}(t + dt)$ will be equal any particular value for any given positive infinitesimal dt ¹. If that probability happens always to be zero for all values but one, then we are dealing once again with a deterministic process. Finally, we see that a knowledge of all the values of a stochastic process prior to and including time t will only allow us to make *probabilistic predictions* about the value of the process at time $t + dt$. As in the case of a deterministic process, an important subclass of stochastic processes is comprised of those that are memoryless. This memoryless stochastic process is called a Markov process and will be described in next section [74].

¹Clearly $\mathbf{X}(t')$ represents a random or stochastic variable which is defined by a probability distribution.

3.2 Markov process

For memoryless stochastic processes, the probabilities assigned to the possible values of $\mathbf{X}(t + dt)$ on the basis of the value $\mathbf{X}(t)$ alone cannot be sharpened by taking cognizance of any values $\mathbf{X}(t')$ for $t' \leq t$; so the process just forget those past values. Thus, a Markov process $\mathbf{X}(t)$ is the state function of some system whose state value at time $t + dt$ can be probabilistically predicted from its state value at time t , but in a way that cannot be improved upon by taking account of the state values prior to time t . The name given to memoryless stochastic processes is that of the Russian mathematician A. A. Markov (1856-1922). The Markov process can be further subclassified depending on the nature of

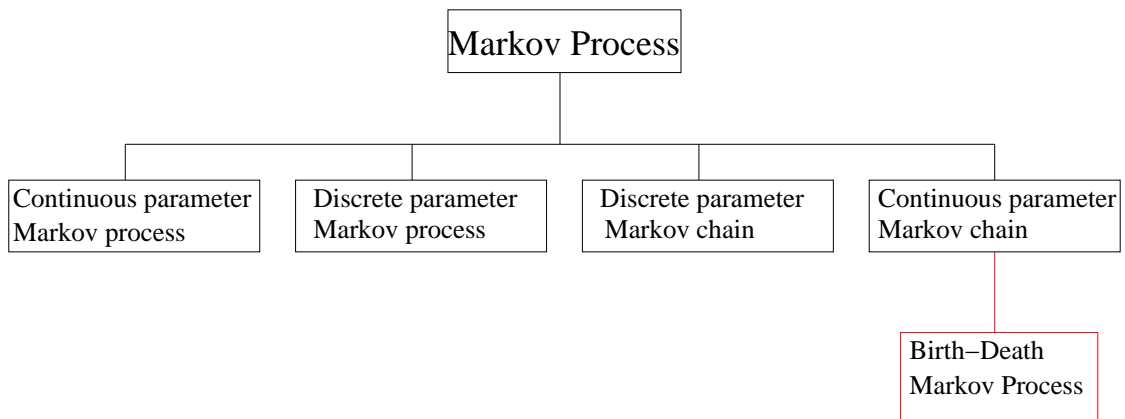


Figure 3.1: Classification of Markov processes. In this Thesis we will concerned with birth-death Markov processes.

the state-space $\mathbf{X}(t)$ and the parameter time t (see Fig. 3.1) [3, 4, 75]. Thus discrete state-discrete time processes that satisfy the Markovian assumption are said to form a discrete parameter Markov chain, while the discrete state-continuous time processes are said to form a continuous parameter Markov chain. Similarly, continuous state-discrete time and continuous state-continuous time process are correspondingly referred to as discrete parameter Markov process and continuous parameter Markov processes. In this Thesis we will concentrate basically on continuous parameter Markov chains or discrete-state-continuous parameter Markov processes. In particularly, we shall be concerned with some of the processes that belong to the category of this continuous parameter Markov chain, the so-called birth-death Markov process.

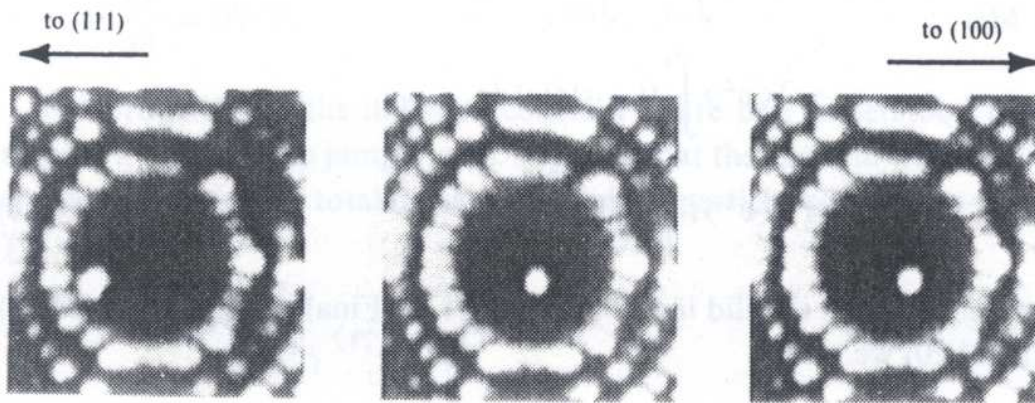


Figure 3.2: Field ion microscopy images of diffusion of rhenium atoms on W(211). Successive images are separated by 60 second intervals (from [65])

3.2.1 Classical stochastic description of chemical reactions

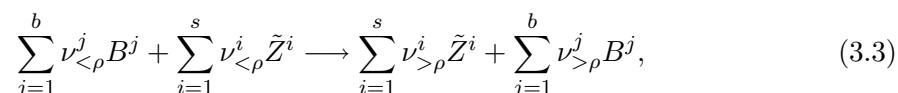
Under some conditions, chemical systems can be described as classical stochastic many-particle systems. In order to understand this notion, let us, consider the experimental study of diffusion of atoms on metals surfaces using field ion microscopy as shown in Fig. 3.2. On a fundamental level a freshly deposited diffusing atom is described by a quantum-mechanical wave function that evolves under the influence of various interactions with the substrate and the environment. However, monitoring the particle by field ion microscopy, it seems to behave as a classical object that hops occasionally from one lattice site to another. In fact, the deposited atom is exposed to a complex variety of interactions and entanglement with the environment which lead to a continuous decoherence of the quantum state [76, 77]. This process keeps the wave package pinned to a certain lattice site as time proceeds. The opposing quantum effect of recoherence, however, leads to occasional tunnelling through the surrounding energy barriers. Immediately after tunnelling, decoherence again localizes the wave function at the site, destroying all information encoded in quantum-mechanical phases. This means that several subsequent tunnelling events are effectively uncorrelated, provided that they are separated by time intervals that are much larger than the typical decoherence time. It is this separation of time scales that allows one to consider the particles as a classical object. Using this

classical picture it is no longer necessary to consider the full wave function of the particle, rather it is sufficient to characterize its state by the index of the lattice site to which it is pinned at time t and the effective transition rates by which it hops to its nearest neighbors. This interpretation can be extended to the chemical reactions used in this Thesis, because in this case, we keep count of the total numbers of reactant and product molecules and use the macroscopic rate law to model the transition rates between the possible states in a classical molecule number space.

3.2.2 Markov birth-death description

In some system of N species the occurrence of an event such as a reaction may lead to both an increase and a decrease in total population N , this process is known as a birth and death processes. Some simple birth-death processes are: the Poisson process, the radioactive decay process, the random telegraph process, and the payroll process [74]. A theory of chemical fluctuations based on the notion of a birth and death process was first proposed by Delbrück (1906-1981) [78]. This simple theory in essence keeps count of the total numbers of reactant and product molecules and uses the macroscopic rate law to model the transition rates between the possible states in a classical molecule number space.

More quantitatively, let consider a set of reactions $\rho = 1, 2, \dots, r$ of the form



involving the intermediate species $\tilde{\mathbf{Z}} = \{\tilde{Z}^i\}_{i=1}^s$ and the species $\{B^j\}_{j=1}^b$ supplied at constant concentration by reservoirs. An elementary event of the reaction ρ changes the integer number \tilde{Z}^i of molecules by an amount equal to the stoichiometric coefficients $\nu_{\rho}^i = \nu_{>\rho}^i - \nu_{<\rho}^i$, with $i = 1, 2, \dots, s$, with transition rate $W_{\rho}(\tilde{\mathbf{Z}})$. This description assumes that the molecules can diffuse infinitely fast and consequently the system is considered as well mixed. In cases where the diffusion of molecules is local, new reaction steps considering the exact position of the molecules have to be introduced.

This well mixed system can be represented as a Markov birth-death process in the number of molecules, where the probability $P(\tilde{\mathbf{Z}}; t)$ of having a determinate number of molecules in a volume A at time t is governed by the so-called stochastic master equation [3, 4, 79].

3.2.3 Global birth-death description of fluctuations

A global description of fluctuations try the system as a whole and discards aspect of fluctuations associated with such properties as the size, range over which these fluctuations extend, and correlation length over which two parts of the system can feel each other [3, 4, 79]. In this case the system is treated as if it remained homogeneous, and thus, described by a master equation of the form

$$\frac{d}{dt}P(\tilde{\mathbf{Z}}; t) = \sum_{\rho=1}^r [W_{\rho}(\tilde{\mathbf{Z}} - \mathbf{v}_{\rho}/\tilde{\mathbf{Z}})P(\tilde{\mathbf{Z}} - \mathbf{v}_{\rho}; t) - W_{\rho}(\tilde{\mathbf{Z}}/\tilde{\mathbf{Z}} - \mathbf{v}_{\rho})P(\tilde{\mathbf{Z}}; t)], \quad (3.4)$$

where $\tilde{\mathbf{Z}} = \{\tilde{Z}^i\}_{i=1}^s$ is the population vector and $\mathbf{v}_{\rho} = \{\nu_{\rho}^i\}_{i=1}^s$ the stoichiometric vector. This is a linear differential-difference equation for $P(\tilde{\mathbf{Z}}; t)$ with nonlinear coefficients. In this form the meaning of this equation becomes clear: "the master equation is a gain-loss equation for the probability of the separate states"². Several methods can be apply to solve these equations, but in general, only for a handful of cases is a complete analytical solution of these equations possible. For most other situations it is necessary to develop approximation schemes. Different approximations of the master equation have been introduced. We will mention briefly only a few of these approximations, but a complete description of them is not necessary to understand the main results of this Thesis [3, 4, 79].

Fokker-Planck approximation

In this approximation the so-called Fokker-Planck equation is introduced as special case of master equation. This equation is a differential equation more easier to solve than the master equation. But, it is an approximate description for any Markov process whose individual jumps are small. This approximation is useful for linear processes, but its use in nonlinear situations can sometimes lead to erroneous results [80].

Systematic expansion of the master equation

This approximation consists in the systematic expansion of the master equation in some suitably chosen parameter. Here, it is necessary to select a parameter that appears in the master equation(i.e. in the transition probability), for large values of which the fluctuations are small. In many instances, this parameter could simply be the size of the system. This method is usually applied to nonlinear situations [3, 4, 79].

²The name "master equation" first appeared in A. Nordsieck, W. E. Lamb, and G. E. Uhlenbeck, *Physica* **7**, 344 (1940). Sometimes the more specific name "Pauli master equation" is used.

Hamilton-Jacobi formulation

This approximation was proposed by Kitahara and the idea is to convert the master equation in a Hamilton-Jacobi equation [3, 4, 79].

The Langevin approach

This approximation is used to find the effects of fluctuations in macroscopically known systems. The fluctuations are introduced by adding random terms to the deterministic equations of motion. This approach is mathematically equivalent to the Fokker-Planck equation, and thus, it relates to the master equation description [3, 4, 79].

3.2.4 Local birth-death description of fluctuations

The global birth-death formalism shown above is subject to a number of objections [3, 4, 79]: (1) the inadequacy of the approach to take account spatial variations, and (2) the lack of a rigorous microscopic justification of the Markov master equation in the number of particle space. The latter, while of considerable importance, will not be considered in this Thesis.

The global homogeneous theory rest on the assumption that the processes which tend to distribute the particles uniformly (diffusion) in a given volume of system are far too rapid in relation to the processes that alter the particle number (chemical reactions). Clearly, this situation may not always hold true and spatial inhomogeneities can develop. It is desirable therefore to provide a simple means of taking account of these inhomogeneities. Such a formalism can be easily developed if one discretise that space in terms of number of cells. Each cell is presented as a $L \times L$ site square lattice. A important conditions of this approximation is that the probability that a molecule diffuses out of a given cell must exceed the probability that the molecule undergoes a reactive event within the cell. Thus, within each cell it is assumed that the reaction is homogeneous so that the usual concept of global description holds. It is assumed that the cells are interconnected by transport to and from the cell to surrounding. Finally, the two mechanisms of reaction and transport responsible for the generation and loss of species from a cell can thus be written in terms of the birth-death formalism.

To illustrate the point we shall consider the set of reactions shown in Eq. 3.3 to represent the dynamics inside each cell. In particularly and for simplicity we will consider the simple case of a single specie $\tilde{\mathbf{Z}} = \left\{ \tilde{Z}_j^1 \right\}_{j=1}^M$, where \tilde{Z}_j represents the number of molecules of this specie in the cell j . The state of the system, subdivided into M cells, can then be described

in terms of the evolution of the probability function $P(\tilde{\mathbf{Z}}; t)$. Thus, a reaction-diffusion master equation can be constructed with the form

$$\frac{dP(\tilde{\mathbf{Z}}; t)}{dt} = \frac{dP^{reac}}{dt} + \frac{dP^{diff}}{dt}, \quad (3.5)$$

where the reaction part obviously will have a form similar to the master equation of the global description

$$\frac{dP(\tilde{\mathbf{Z}}; t)^{reac}}{dt} = \sum_{j=1}^M \sum_{\rho=1}^r [W_{\rho}^j(\tilde{Z}_j^1 - \nu_{\rho,j}^1 / \tilde{Z}_j^1) P(\tilde{Z}_j^1 - \nu_{\rho,j}^1; t) - W_{\rho}^j(\tilde{Z}_j^1 / \tilde{Z}_j^1 - \nu_{\rho,j}^1) P(\tilde{Z}_j^1; t)], \quad (3.6)$$

but the new diffusion part must be written as

$$\frac{dP(\tilde{\mathbf{Z}}; t)^{diff}}{dt} = d \sum_{j=1}^M \sum_{\mu=1}^2 [M_{\mu}^j(\tilde{Z}_j^1 - 1 / \tilde{Z}_j^1) P(\tilde{Z}_j^1 - 1, \tilde{Z}_{j+l}^1 + 1; t) - M_{\mu}^j(\tilde{Z}_j^1) P(\tilde{Z}_j^1; t)]. \quad (3.7)$$

l denotes the nearest neighbors of the cell j . Note that new transition probabilities M_{μ}^i are introduced. They correspond to the gain and loss of number of species in a cell as consequence of diffusion between cells. Finally, d refers to the microscopic diffusive constant that is related to the chemical diffusive coefficient D in the continuum limit by [4, 79]:

$$D = L^2 d. \quad (3.8)$$

In the general case shown Eq. 3.3 where the number of species is s , a general master equation for $\tilde{\mathbf{Z}} = \{\tilde{Z}_j^i\}_{i=1, j=1}^{s, M}$ must be analyzed. Finally, this equation can be solved by the methods mentioned above [3, 4, 79].

3.3 Internal and external fluctuations

The treatment presented thus far only considered the presence of internal fluctuations. The internal fluctuations are self-originated in the system and reflect the underlying statistical nature of the processes. These fluctuations are described by a Markovian master equation and in the thermodynamic limit vanish altogether.

In contrast to these internal fluctuations, the external ones are not self-originated and owe their existence to the coupling of the system to a fluctuating environment. These fluctuations reflect the statistical nature of the environment and they can thus become

important even in the thermodynamic limit. Since these fluctuations occur at macroscopic level, a logical way of incorporating them in the analysis would lead to a stochastic differential equation [3]. In many practical applications it is possible to decide which of these types of fluctuations are important in the analysis. There would, however, be situations, where both types of fluctuations would contribute to the total evolution of the system. The analysis of the simultaneous presence of internal and external fluctuations can be handled in the following two ways [3, 75].

3.3.1 Internal and external fluctuations modelled via master equation

As before the internal fluctuations are modelled via the master equation formulation. The external fluctuation is then incorporated through an appropriate variation in the external parameter that enters the transition probabilities in the master equation (i.e, pressure or temperature in the case of chemical reactions). The master equation can be written as

$$\frac{d}{dt}P(\tilde{\mathbf{Z}}; t) = \sum_{\rho=1}^r [W_{\rho}(\tilde{\mathbf{Z}} - \mathbf{v}_{\rho}/\tilde{\mathbf{Z}})P(\tilde{\mathbf{Z}} - \mathbf{v}_{\rho}; t) - W_{\rho}(\tilde{\mathbf{Z}}/\tilde{\mathbf{Z}} - \mathbf{v}_{\rho})P(\tilde{\mathbf{Z}}; t)]. \quad (3.9)$$

In order to introduce the external fluctuations, we can identify the existence of fluctuating parameters in the functions $W_{\rho}(\tilde{\mathbf{Z}} - \mathbf{v}_{\rho}/\tilde{\mathbf{Z}})$ or $W_{\rho}(\tilde{\mathbf{Z}}/\tilde{\mathbf{Z}} - \mathbf{v}_{\rho})$. Taken for example, the simple case where $W_{\rho}(\tilde{\mathbf{Z}} - \mathbf{v}_{\rho}/\tilde{\mathbf{Z}})$ alone fluctuates we can write

$$W_{\rho}(\tilde{\mathbf{Z}} - \mathbf{v}_{\rho}/\tilde{\mathbf{Z}}) = W_{\rho}^0(\tilde{\mathbf{Z}} - \mathbf{v}_{\rho}/\tilde{\mathbf{Z}}) + W_{\rho}^1(\tilde{\mathbf{Z}} - \mathbf{v}_{\rho}/\tilde{\mathbf{Z}})\xi(t), \quad (3.10)$$

where $W_{\rho}^0(\tilde{\mathbf{Z}} - \mathbf{v}_{\rho}/\tilde{\mathbf{Z}})$ represents the nonfluctuating part. It is often convenient to define $\xi(t)$ as a Gaussian white noise with zero mean and correlation $\langle \xi(t)\xi(t') \rangle = 2D\delta(t-t')$ [3]. The parameter D signifying the intensity of the fluctuation and remains a finite quantity in the thermodynamic limit. Thus, external fluctuations are known as multiplicative fluctuations or noise.

3.3.2 Internal and external fluctuations modelled via Langevin equation

Consider the macroscopic equation

$$\frac{d\theta}{dt} = f(\theta, p), \quad (3.11)$$

Thermal internal fluctuations are introduced by adding a fluctuation or noise term

$$\frac{d\theta}{dt} = f(\theta, p) + A^{-1}\xi_1(t), \quad (3.12)$$

where A is the size of the system and $\xi_1(t)$ is a Gaussian white noise with zero mean and correlation $\langle \xi_1(t)\xi_1(t') \rangle = 2D_1\delta(t-t')$. Finally, the equation taking into account at the same time internal and external fluctuations is then

$$\frac{d\theta}{dt} = f^0(\theta, p) + f^1(\theta, p)\xi_2(t) + A^{-1}\xi_1(t), \quad (3.13)$$

where $\xi_2(t)$ is a Gaussian white noise with zero mean and correlation $\langle \xi_2(t)\xi_2(t') \rangle = 2D_2\delta(t-t')$ [3].

3.3.3 Colored fluctuations

So far we have assumed, that the fluctuation term were Gaussian and white. This is a very reasonable assumption for internal fluctuations, which represents many irrelevant degrees of freedom evolving in very short temporal and spatial scales. Nevertheless, in realistic experiments in which fluctuations are introduced through some external device, one has to take into account the spatiotemporal structure of the fluctuations. One can then prescribe that the fluctuations are still Gaussian but with a finite time-correlation. The finite width of the correlation-time makes the process non-Markovian [5].

3.4 Stochastic simulation

Most statistical mechanics systems like some complex chemical system cannot be solved explicitly. One of the more important tools for extracting answers out of statistical mechanics of real systems are through simulations. If one is interested in the microscopic structure of the system, molecular dynamics simulations, which consider atoms moving according to the to Newton's laws, are used [65]. But, if one is not interested in detailed dynamics trajectories of the system, one can use the so-called Monte Carlo simulations.

The basis of the Monte Carlo methods is that the deterministic equations of molecular dynamics simulations are replaced by "stochastic" transition for the process in the system. The name Monte Carlo was coined by John von Neumann (1903-1953) and refers to the random sampling of numbers, in analogy to gambling in Monte Carlo, Monaco, a city well known for its casinos. This Monte Carlo methods or stochastic algorithms have been used

to explore equilibrium and nonequilibrium processes. Here, we will review some of them.

3.4.1 The Metropolis algorithm

This algorithm is the basis of applications to equilibrium systems. This method is an algorithm developed by Nicholas Metropolis (1915-1999) that originates simply from the Boltzmann distribution [81]. Consider the thermodynamic average y of a variable with values y_i in state i that has energy E_i ,

$$y = \frac{\sum_i y_i P_i}{\sum_i P_i}, \quad (3.14)$$

in which the probabilities $P_i = e^{-E_i/k_B T}$, where k_B is the Boltzmann's constant and T is the absolute temperature. If the system is initially in a state i , detailed balance³ requires that the rate of transitions W_{ij} from state i to state j satisfies

$$P_i W_{ij} = P_j W_{ji} \quad (3.15)$$

or

$$\frac{W_{ij}}{W_{ji}} = \frac{P_j}{P_i} = e^{-(E_j - E_i)/k_B T}. \quad (3.16)$$

The right-hand side of this equation is known, so to generate a set of states with the distribution P_i , the W_{ij} are chosen as

$$W_{ij} = \begin{cases} 1, & \text{if } P_j > P_i; \\ e^{-(E_j - E_i)/k_B T}, & \text{if } P_j \leq P_i. \end{cases} \quad (3.17)$$

A random number $r \in (0, 1)$ is then selected and the system is moved to state j only if $r < e^{-(E_j - E_i)/k_B T}$.

3.4.2 Kinetic Monte Carlo (KMC) simulation of lattice models

In the Kinetic Monte Carlo (KMC) simulation of lattice models the systems are described by finite lattice models with L^2 sites and periodic boundary conditions. The sites are designated as either occupied or vacant [82]. A specification of all possible transitions

³The detailed balance principle merely states that in equilibrium the sum of all transitions per unit time into any state i must be balanced by the sum of all transitions from i into other states j .

between different configurations of the lattice, together with the associated rates, completely prescribes the evolution of the model for the process of interest. Let n_j denote the occupancy of site j , n the configuration of the entire system, and $P(n;t)$ the probability for the system to be in this configuration at time t . Implicitly, these probabilities involve ensemble averaging which, in the context of KMC simulation, may correspond to averaging over a large number of simulation trials. Then, evolution is described exactly by the master equation [3]

$$\frac{d}{dt}P(n;t) = \sum_{n'} W(n',n)P(n';t) - \sum_{n'} W(n,n')P(n;t), \quad (3.18)$$

where $W(n' \rightarrow n)$ denotes the prescribed rate of transitions from configuration n' to n . These two configurations will differ only in the occupancy of a site for adsorption or desorption, but in the occupancy of a pair of sites for diffusion. On the right hand side of this equation, the first (second) term reflects gain (loss) in the population of configuration n . We note that for a Markov process, specifying a rate for each microscopic process actually means there is an exponential waiting-time distribution between events associated with this process, with the mean waiting-time between consecutive events given by the inverse of the rate.

Basic algorithm

We assume that the model in study incorporates a variety of distinct atomistic process, which we label by ρ (e.g., $\rho =$ adsorption, desorption, diffusion, reaction, etc.). Furthermore, we suppose that each process, ρ , occur with only a finite number of microscopic rates, $W_\rho(m)$, for $m = 1, 2, \dots$, depending on the local environment. We let $W_\rho(max)$ denote the maximum of the $W_\rho(m)$, for each ρ . We then set $W_{tot} = \sum_\rho W_\rho(max)$, and define $p_\rho = W_\rho(max)/W_{tot}$, so that $\sum_\rho p_\rho = 1$. Then, one first selects a site, and select a process, ρ , with probability, p_ρ , reflecting the maximum rate for that process ρ . Finally, one implements this process (if allowed) with a probability, $q_\rho = W_\rho/W_\rho(max) \leq 1$, where W_ρ is the actual rate for the process ρ at site j . This means that W_ρ is one of the $W(m)$, with m determined by the local environment of sites j . One can also connect the simulation time (the number of times a site is chosen) with the physical time. On each occasion a site is chosen, we increment the physical time by δt , where $L^2 W_{tot} \delta t = 1$. Thus, after one attempt per site, the physical time has increased by $1/W_{tot}$.

3.4.3 Gillespie-like KMC simulation

The Gillespie algorithm is the Monte Carlo simulation technique implemented in this Thesis. This algorithm was developed by D. T Gillespie in 1976. It generates a statistically correct trajectory (possible solutions) of the stochastic master equation [83, 84, 85]. Here, we assume that the system or volume is well mixed⁴ and one may represent the system simply by the number of each species of molecules⁵. Under this approximation, the probability that a certain reaction ρ will take place in the next instant of time dt is given by $W_\rho dt$, where W_ρ are the transition rates and depend of the different system parameters. We introduce the reaction probability density function $P(\tau, \rho/\tilde{\mathbf{Z}})$ defined such that $P(\tau, \rho/\tilde{\mathbf{Z}})$ = probability that given the state $\tilde{\mathbf{Z}}$ at time t , the next reaction in a volume will occur in the infinitesimal time interval $(t + \tau, t + \tau + d\tau)$ and will be an ρ reaction.

To find an expression for $P(\tau, \rho/\tilde{\mathbf{Z}})$ we note that it is equal to the probability of no reaction over time interval $(t, t + \tau)$, $P_0(\tau/\tilde{\mathbf{Z}})$ multiplied by the probability that ρ will occur over time interval $(t + \tau, t + \tau + d\tau)$, namely, $W_\rho d\tau$. Thus,

$$P(\tau, \rho/\tilde{\mathbf{Z}}) = P_0(\tau/\tilde{\mathbf{Z}})W_\rho d\tau. \quad (3.19)$$

It turns out that $P_0(\tau/\tilde{\mathbf{Z}})$ has the form [83]

$$P_0(\tau/\tilde{\mathbf{Z}}) = e^{-\sum_{\rho=1}^r W_\rho d\tau}, \quad (3.20)$$

from which we may conclude that

$$P(\tau, \rho/\tilde{\mathbf{Z}}) = \begin{cases} W_\rho e^{-W_o \tau}, & \text{if } 0 \leq \tau < \infty; \\ 0, & \text{otherwise.} \end{cases} \quad (3.21)$$

where $W_o = \sum_{\rho=1}^r W_\rho$ and r the number of reactions. By noting that $P(\tau, \rho/\tilde{\mathbf{Z}})$ is separable, we see that at any point we can pick τ and ρ from the distribution $P(\tau, \rho/\tilde{\mathbf{Z}})$ by choosing two random numbers r_1 and r_2 from the interval (0,1) and setting τ and ρ such that

$$\tau = \frac{1}{W_o} \ln \frac{1}{r_1}, \quad (3.22)$$

⁴The nonreactive collisions occur far more often than the reactive collisions and, hence, that fast dynamics of motion can be neglected.

⁵This approximation corresponds to a global description of fluctuations, where the probability of observe a determinate number of molecules is given by Eq. 3.4

$$\sum_{\mu=1}^{\mu=\rho-1} W_{\mu} < r_2 W_o \leq \sum_{\mu=1}^{\mu=\rho} W_{\mu}. \quad (3.23)$$

In summary, after setting the initial species population $\tilde{\mathbf{Z}}$ and reaction constants the algorithm is:

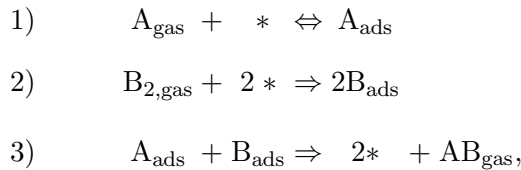
- (1) Calculate W_{ρ} ($1 \leq \rho \leq r$).
- (2) Generate r_1 and r_2 and calculate τ and ρ according to Eqs. (3.22) and (3.23).
- (3) Increase t by τ and adjust $\tilde{\mathbf{Z}}$ to take account of an occurrence of a reaction ρ .

3.4.4 Hybrid algorithms

One of the main problems of KMC simulation are the simulation of diffusion. In many physico-chemical systems the rate constant for diffusion is much longer than those for other reactions. For example, experimental studies show that diffusion of CO on a Pt(111) surface at 300 K is greater than ten orders of magnitude faster than CO-O reaction event [86]. As consequence of this separation of time scales, KMC simulations of diffusion events are impractical. During such a simulation, the events chosen are mostly diffusion events with rare reaction events. The hybrid treatment basically consider a full lattices model description of the slow events and a standard mean-field treatment⁶ is used to describe the highly mobile particles [87, 88, 89].

3.4.5 Comparison of simulation techniques

It is instructive to compare the different simulation technique using simple examples. Here, it is used the monomer-dimer ($A + B_2$) model without lateral interactions which schematically can be written as



with $*$ and (ads) denoting a vacant adsorption site and adsorbed molecules or atoms, respectively. Note that the monomer-dimer model mimics CO oxidation on single-crystal surfaces. In general, one can use other models like the dimer-dimer model and the triple-dimer model [90].

⁶The mean-field treatments consider that the fast adspecies are distributed randomly on the lattices.

Here, we show simulations results of this system by (i) hybrid kinetic Monte Carlo simulations with a mean-field treatment of A and a lattice-gas treatment of B [91]; and (ii) Gillespie-type Monte Carlo simulation of the numbers of reactant adspecies in a well-mixed model [51].

Hybrid kinetic Monte Carlo simulations

Here, we assume that, due to rapid diffusion, A_{ads} is distributed randomly on the non- B_{ads} sites at all times. Thus, one tracks the number, N_B , and location of all B_{ads} on the square lattices of adsorption sites, but only tracks the number, N_A , of A_{ads} . At each Monte Carlo step, one randomly selects between adsorption, desorption, reaction, etc., with weights determined by the relative rates for these processes. When deciding whether to adsorb or desorb A , or to react a B_{ads} with an A_{ads} , it is necessary to decide whether a chosen non- B_{ads} site is occupied by one randomly distributed A_{ads} . We say that such a site is occupied by A_{ads} with probability $p = N_A/N_Z$, where $N_Z = N - N_B$ denotes the total number of non- B_{ads} . Thus if it is decided to attempt A_{gas} -adsorption (A_{ads} -desorption) at a selected non- B_{ads} site, such adsorption (desorption) is implemented with probability $1 - p$ (p), measuring the probability that the site is empty (occupied by A_{ads}), then N_A is incremented by $+1$ (-1). Reaction and B -adsorption are treated similarly. Here the impingement rates are normalized so that $y_A + y_B = 1$, which sets the time scale, and also sets $y = y_A$. We consider that reaction rate $k = 1$. Finally, the desorption rate is denoted by d . Figure 3.3 shows the time variation of the coverage θ_A and θ_B , of A_{ads} and B_{ads} , respectively. We use $d = 0$ and $y = 0.45$. Note that the system evolves to a stable state of low A_{ads} coverage and high B_{ads} coverage.

Gillespie-like kinetic Monte Carlo simulation

To implement the Gillespie algorithm, basically what we need are the transition probabilities for each reaction step. These transition probabilities can be obtained from the hierarchical rate equations for the model. These equations describe the evolution of coverage as a function of time. We consider, as an example, a simplified version of these equations

$$\frac{d\theta_A}{dt} = y(1 - \theta_A - \theta_B) - d\theta_A - 4k\theta_A\theta_B, \quad (3.24)$$

$$\frac{d\theta_B}{dt} = 2(1 - y)(1 - \theta_A - \theta_B)^2 - 4k\theta_A\theta_B. \quad (3.25)$$

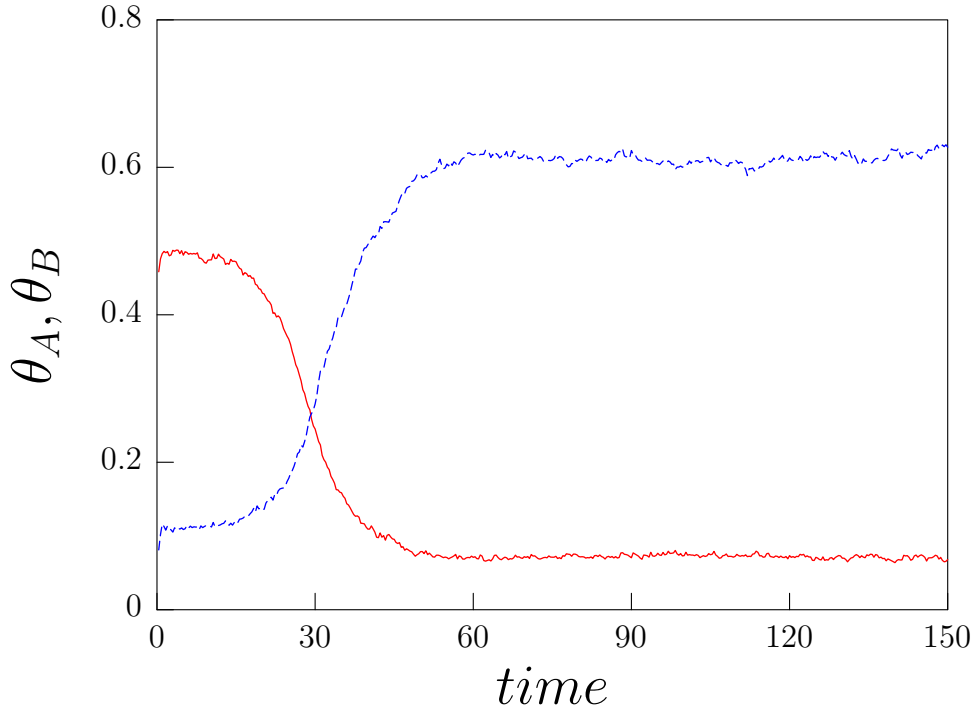


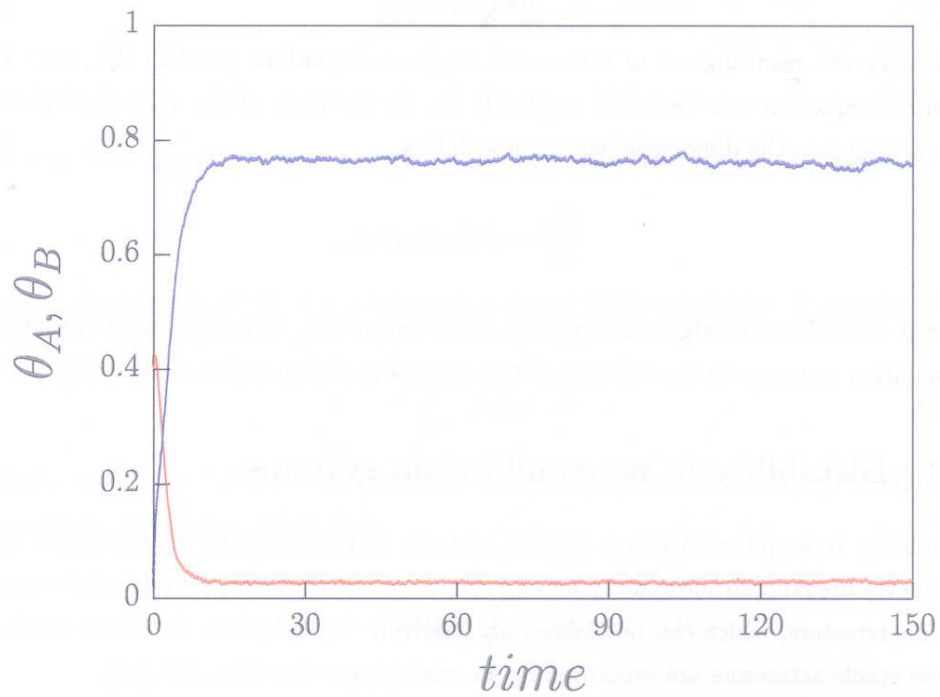
Figure 3.3: Hybrid kinetic Monte Carlo simulations of a lattice model. Time series of θ_A (red line) and θ_B (blue line) for $y = 0.45$ and $L^2 = 10000$

where, $\theta_A = N_A/N$ and $\theta_B = N_B/N$. $N = L^2$ is the size of the system. With d and k denoting desorption and reaction constant rates, respectively. Finally, y is the impingement constant rate of A_{gas} .

From the rate equations transition probabilities can be derivate (Table 3.1). Now, we can implement the algorithm. Note that we have four reaction steps ($\rho = 1, \dots, 4$) and $W_o = W_1 + W_2 + W_3 + W_4$. Figure 3.4 shows the time variation of the coverage θ_A and θ_B , of A_{ads} and B_{ads} , respectively. We use $k = 1$, $d = 0$, $y = 0.45$ and $N = 10000$. Note that the system evolves to a stable state of low A_{ads} coverage and high B_{ads} coverage. The time series shown in this figure are in qualitatively agreement with the results from hybrid kinetic Monte Carlo simulations. The hybrid kinetic Monte Carlo simulations considered here takes into account spatial correlations for B_{ads} and it is expected to be more realistic that the predictions from the Gillespie algorithm, which takes into account the transition probabilities from the over-simplified rate equations 3.24 and 3.25.

| Reaction step | Transition probability |
|---|---|
| $A_{\text{gas}} - \text{Adsorption}$ | $W_1 = y(N - N_A - N_B)$ |
| $A_{\text{ads}} - \text{Desorption}$ | $W_2 = dN_A$ |
| $B_{2,\text{gas}} - \text{Adsorption}$ | $W_3 = \frac{2(1-y)(N - N_A - N_B)^2}{N}$ |
| $A_{\text{ads}} - B_{\text{ads}} - \text{Reaction}$ | $W_4 = \frac{4kN_A N_B}{N}$ |

Table 3.1: Transition probabilities for the reaction process.

Figure 3.4: (Color online) Gillespie-type kinetic Monte Carlo simulations. Time series of θ_A (red line) and θ_B (blue line) for $y = 0.45$ and $N = 10000$

3.5 Adiabatic reduction of fast variables from deterministic systems

The adiabatic reduction approximation is a technique used to remove highly reactive species from deterministic models of chemical reactions. Frequently, ordinary differential equations (ODE's) are used to model these chemical reactions in the deterministic limit, where θ_A and θ_B are the coverage of the slow and fast variables, respectively. Let us consider the following ODE's

$$\frac{d\theta_A}{dt} = f(\theta_A, \theta_B), \quad \epsilon \frac{d\theta_B}{dt} = g(\theta_A, \theta_B) \quad (3.26)$$

The idea of adiabatic reduction on Eq. 3.26 is to set the production rates of the fast variable to zero,

$$g(\theta_A, \theta_B) = 0, \quad (3.27)$$

and solve the resulting set of differential algebraic equations (DAES) [92, 93]. If the algebraic equation can be solved explicitly for θ_B in terms of θ_A , then $\theta_B(\theta_A)$ can be substituted into the differential equation as follow

$$\frac{d\theta_A}{dt} = f(\theta_A, \theta_B(\theta_A)), \quad (3.28)$$

then it eliminates the algebraic equation from the model. The solution of the adiabatic elimination converge to the solution of the original model as ϵ goes to zero [94].

3.6 Bistability in nonequilibrium systems

Bistability is found with many natural systems and is generally characterized by the symmetry breaking in the state space of a system due to the simultaneous existence of two stable attractors, which can be reached alternatively dependent on the initial conditions. These stable attractors are separated by an unstable one (see Fig. 3.5) [95].

If the system is characterized by a single state variable θ which depends only on time, but not on space, its temporal evolution is given by

$$\frac{d\theta}{dt} = f(\theta, p), \quad (3.29)$$

where p represents the control parameters. The function $f(\theta, p)$ allows direct identification

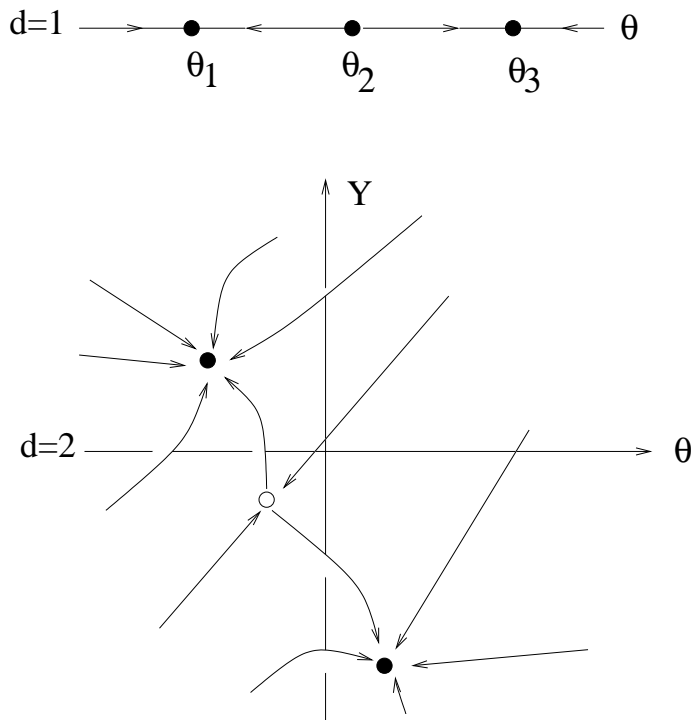


Figure 3.5: Bistability in state space with one and two degrees of freedom.

of the range of bistability within the parameter space p . Now, a potential V may be defined as

$$V = - \int_{\theta}^{\theta_0} f(\tilde{\theta}, p) d\tilde{\theta}. \quad (3.30)$$

If the function $f(\theta, p)$ is bistable, the potential will exhibit a double-well shape. The stable θ_1 and θ_3 are at the same level of V if

$$S = V(\theta_3) - V(\theta_1) = \int_{\theta_3}^{\theta_1} f(\tilde{\theta}, p) d\tilde{\theta} = 0, \quad (3.31)$$

where S is denoted as a supersaturation.

In a spatially extended system the state variable will also depend on the spatial coordinate x , and local bistability of $f(\theta, p)$ will give rise to nucleation and propagation of fronts. The system is described by a reaction-diffusion equation of the type

$$\frac{\partial \theta(x, t)}{\partial t} = f(\theta, p) + D \nabla^2 \theta, \quad (3.32)$$

where D is the diffusion coefficient. In general, if the solution $\theta(x, t)$ of the one-dimensional reaction-diffusion equation is known, then its front propagation velocity c_f is given by

$$c_f = \frac{\int_{\theta_3}^{\theta_1} f(\theta) d\theta}{\int_0^\infty (\partial\theta/\partial x)^2 dx} = S/X. \quad (3.33)$$

This means that the front velocity is dependent on the potential difference S and a term X , which is analogous to a surface tension of the profile. This relation holds for propagation of a wave front in a two-dimensional isotropic medium, in which the velocity of a wave front with curvature χ is given by

$$c(\chi) = c_f - D\chi = D \left(\frac{1}{R_c} - \frac{1}{R} \right), \quad (3.34)$$

where R is the curvature radius. This equation reflects the fact that a nucleus will only grow if its radius exceeds the critical value R_c , otherwise it will shrink. The critical radius R_c for nucleation is easily derived as

$$R_c = D/c_f. \quad (3.35)$$

3.7 CO oxidation: Basic features

In previous sections, basic concepts of the Markov process description of chemical reactions, stochastic simulation techniques, and bistability in nonequilibrium systems were summarized. We now turn to the specific system, the catalytic oxidation of CO on transition metals, that will serve as a model system for the theoretical studies throughout this work. This reaction is one of the most studied heterogeneous catalytic surface reactions [18]. It shows a particularly rich dynamics including oscillations, bistability and a great variety of spatiotemporal phenomena [24, 71].

3.7.1 Reaction scheme

It is well known that the catalytic oxidation of CO on transition metals like Pt or Ir proceeds via a Langmuir-Hinshelwood mechanism [32]. The reaction can be summarized

in the following scheme,



where $*$ stands for a free adsorption site and the index "ads" denotes adsorbed molecules or atoms. Before the reaction can take place, both CO and oxygen have to adsorb from the gas phase on the catalytic surface. At typical temperatures, desorption of CO has to be taken into account, whereas oxygen desorption can be neglected. An adsorbed CO molecule can react with an adsorbed oxygen atom from a neighboring lattice site to form carbon dioxide which is immediately released into the gas phase, leaving two vacant sites for adsorption of new particles. A weakly bound precursor state during CO adsorption allow hopping of the CO molecule between different location so that binding to an adequate adsorption site becomes more likely. For the typical temperature considered here, no similar mobility for oxygen is observed.

3.7.2 Bistability

In catalytic CO oxidation the bistable behavior is induced by a asymmetric inhibition. The oxygen adsorbate layer exhibits an open structure with empty sites in between, always allowing the adsorption of additional CO. On the other hand, CO forms a compact adsorbate, completely covering and thus poisoning the catalyst surface against additional adsorption of oxygen so that no reaction can take place. This behavior induces bistable dynamics in a wide range of parameters, where a mainly oxygen covered reactive state coexists with a CO covered non-reactive state [24].

Bistability in CO oxidation on Pt(111)

Multistability and hysteresis effects in catalytic CO oxidation have been observed with a structural stable Pt(111) surface [24]. In order to study theoretically catalytical CO oxidation on Pt(111) surfaces, one can denote the surface concentrations (coverage) by θ_{CO} and θ_O , and assume the rate of CO_2 formation is given by $r = k_3\theta_O\theta_{CO}$ then the

state variables θ_O and θ_{CO} are determined by the following set of two coupled ODE's

$$\frac{d\theta_{CO}}{dt} = k_1 p_{CO} \left[1 - \left(\frac{\theta_{CO}}{\theta_{CO}^s} \right)^q \right] - k_2 \theta_{CO} - k_3 \theta_{CO} \theta_O, \quad (3.36)$$

$$\frac{d\theta_O}{dt} = k_4 p_{O_2} \left[1 - \frac{\theta_{CO}}{\theta_{CO}^s} - \frac{\theta_O}{\theta_O^s} \right]^2 - k_3 \theta_{CO} \theta_O. \quad (3.37)$$

The rate k_1 and k_4 are proportional to the sticking coefficient for CO and O_2 , respectively. θ_{CO}^s and θ_O^s are the saturation coverages of adsorbed CO and O, respectively. $q > 1$ models the precursor-type kinetics of CO adsorption. The parameters k_2 and k_3 are temperature dependent (because the activation energy). We consider values of all parameters realistic for Pt(111), as extracted from experimental results. These values are listed in Table 3.2 [96]. The partial pressures p_{CO} and p_{O_2} play the role of control parameters. Figure 3.6 shows the calculated variation of the reaction rate r with p_{CO} at various temperatures for fixed p_{O_2} . The cusp is in this case at $T = 549$ K. Below this temperature, the reaction rate jumps suddenly from a high to a very low value upon increasing p_{CO} . As p_{CO} is decreased again at fixed T , the jump occurs at a lower value of p_{CO} . This hysteresis marks the range of bistability.

3.7.3 Oscillations

Catalytic CO oxidation comprises also an internal negative feedback loop, which is an essential prerequisite for oscillatory dynamics. This loop is established by the structural transition of the Pt(110) and Pt(100) surfaces. For example, in a Pt(110) surface the structural transition occurs between the structural transition between the (1×2) missing row phase and the (1×1) bulk terminated structure. The sticking coefficient of oxygen is higher on the (1×1) structure as compared to the (1×2) surface. For an appropriated choice of parameters, adsorption of CO will dominate on the (1×2) surface, eventually inducing a lifting of the reconstruction to the (1×1) structure. On the (1×1) surface, however, the sticking probability of oxygen is increased leading now to a preferred adsorption of oxygen and, consequently, to an enhanced consumption of adsorbed CO due to reaction. If the CO coverage has dropped below 0.5 ML, the surface starts to reconstruct until the (1×2) missing row structure is reestablished at CO coverages below 0.2 ML. Now, the sticking probability for oxygen is reduced again and the process can start all over (see Fig. 3.7) [24].

Kinetic oscillations in catalytic CO oxidation have been investigated on Pd(110) and Pd(111) [24]. Since clean Pd surfaces do not reconstruct, the operation of a reconstruction

| | |
|---|-----------------------------------|
| <i>CO</i> : $k_1 = k_{CO}s_{CO}$ | |
| $k_{CO} = 1.919 \times 10^5 \text{ MLs}^{-1}\text{mbar}^{-1}$, | $s_{CO} = 0.84$ |
| $\theta_{CO}^s = 0.5 \text{ ML}$, | $q = 2$ |
| <i>O₂</i> : $k_4 = k_O s_O$ | |
| $k_O = 3.589 \times 10^5 \text{ MLs}^{-1}\text{mbar}^{-1}$, | $s_O = 0.06$ |
| $\theta_{CO}^s = 0.25 \text{ ML}$ | |
| <i>Rates</i> : $k_i = k_i^o \exp * (-E_i/RT)$ | |
| k_2 : <i>CO</i> desorption | |
| $k_2^o = 1.25 \times 10^{15} \text{ s}^{-1}$, | $E_2 = 34.9 \text{ kcalmol}^{-1}$ |
| k_3 :reaction | |
| $k_3^o = 1.645 \times 10^{14} \text{ s}^{-1}\text{ML}^{-1}$, | $E_2 = 24.1 \text{ kcalmol}^{-1}$ |
| D_{CO} : <i>CO</i> diffusion | |
| $D_{CO}^o = 10^{-8} \text{ m}^2\text{s}^{-1}$, | $E_d = 7 \text{ kcalmol}^{-1}$ |

Table 3.2: Parameters of the model for Pt(111) (from [96]).

mechanism similar to Pt surfaces at first seemed to be excluded. In contrast to oxygen adsorption on Pt surface, oxygen adsorption on Pd surfaces is not structure sensitive and therefore a reconstruction mechanism cannot work in the same way as on Pt surfaces. For example, the oscillation mechanism for Pd(110) is in fact based on the ability of Pd catalysts to incorporate oxygen, such that a subsurface oxygen species is formed. The role of subsurface oxygen in the oscillation mechanism, is the reversal of the usual clockwise hysteresis in the CO_2 production rate upon variation of p_{CO} , into a counterclockwise hysteresis under conditions where rate oscillations occur [97].

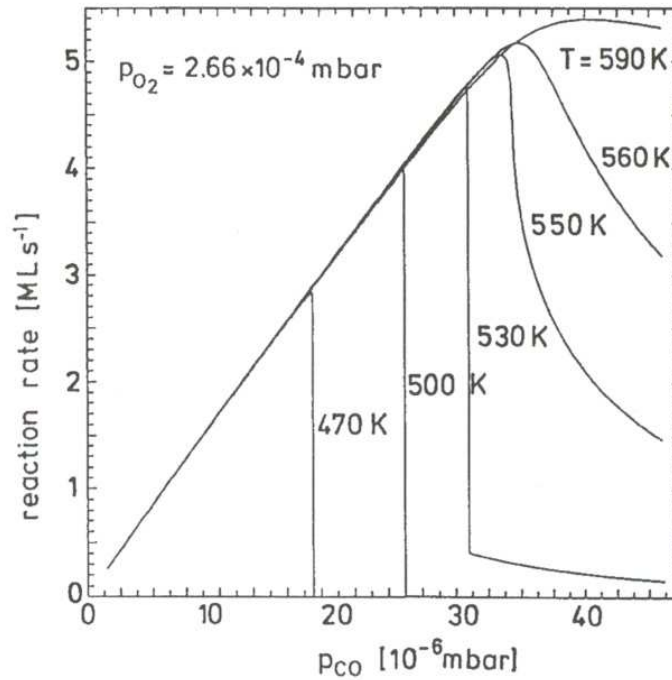


Figure 3.6: CO_2 production rate r increasing CO pressures and at different temperatures ($p_{\text{O}_2} = 2.66 \times 10^{-4} \text{ mbar}$) (from [96]).

3.8 Summary and conclusions

This chapter introduced the theoretical framework used in this Thesis. Here, it is shown that if the size of the system in consideration is small or the control parameters are near points of instabilities, the deterministic description of chemical reactions breaks down. This invalidity of the deterministic predictions is produced by the strong random variable fluctuations present in these regimes. Thus, in order to include these fluctuations in chemical reactions, several tools from the theory of stochastic process, in particular a special class of these processes that are known as Markov Process, have to be implemented. A convenient mathematical description of these Markov processes is the so-called master equation. Nevertheless, we must appreciate that the Markov assumption is more of a mathematical convenience and real systems may be described only approximately as Markov processes. This necessitates the choice of a proper variable to denote the state space. For example, we can think of a simple decomposition type of reaction where the

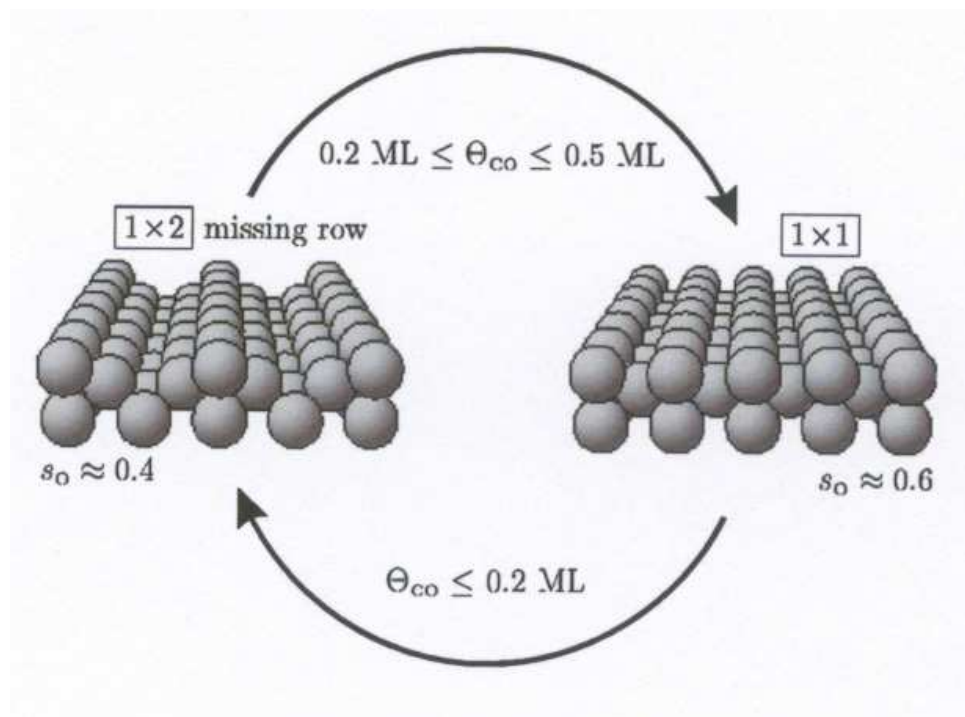


Figure 3.7: Schematic illustration of the adsorbate induced structural transition of the Pt(110) surface.

reactant breaks up due to collisions. Thus, if we were to monitor the concentration of the reactant, the change of concentration between times t and $t + dt$ has certain probability distribution that would depend only on the concentration at time t . The mode by which this concentration was reached, or the previous concentration history, is immaterial. Thus a process described with concentration as a random variable can be treated as a Markov process. Let us now suppose that such a reaction occurs in presence of a catalyst that loses its activity in proportion to the concentration of reactant it processes. Clearly, the change in concentration now depends not only on the concentration at that instant, but also on the activity of the catalyst, which requires a knowledge of the concentration history. Concentration cannot any more then be used as a random variable to describe the system as a Markov process. It is possible, however, to treat the system as a two-component (concentration-activity) Markov process.

Several stochastic simulation techniques were introduced. The nonequilibrium nature of the catalytic CO oxidation permits to use both kinetic Monte Carlo simulation of nonequi-

librium lattice models and Gillespie-like Monte Carlo simulation. If one is interested in an atomistic or more realistic description of the system, kinetic Monte Carlo simulations of lattice models is more useful. But, if the idea is to obtain a more qualitatively description, Gillespie-like kinetic Monte Carlo simulation may be used. The construction of a model for a KMC simulation can often benefit from a related classical or quantum molecular dynamics simulation to identify the important physical process and estimate the prefactors and kinetic barriers. The transition rates are particular to the process of interest and must be determined either by direct calculations, from a first-principles calculation or by molecular dynamics simulations, or inferred from experiment. These kinetics simulations together with multiscale modelling using hybrid algorithms play a key role in heterogeneous catalysis. The adiabatic elimination technique is introduced as a good approximation to eliminate fast variables from systems with time scales that span many orders of magnitude. We also discussed the bistability phenomena in nonequilibrium system. Finally, basic concepts of catalytic CO oxidation on transition metals are summarized.

In this Thesis, we shall use the Gillespie algorithm as simulation technique. To obtain realistic results for CO oxidation, the so-called cluster approximation (see Appendix B) is implemented in order to derive realistic transition probabilities.

Part II

**ROLE OF FLUCTUATIONS IN
CO OXIDATION**

Chapter 4

Reduced stochastic kinetic model

"A great many quantities have been proposed as measures of something like complexity. In fact, a variety of different measures would be required to capture all our intuitive ideas about what is meant by complexity and its opposite, simplicity."

Murray Gell-Mann (1929)

4.1 Introduction

This chapter introduces a stochastic kinetic model for CO oxidation. Here, we focus on the catalytic CO oxidation on crystal surfaces without reconstruction¹. The nonequilibrium nature of this surface reaction system supports the occurrence of many interesting dissipative structures. One of the more studied features is pattern formations with a characteristic length scale of microns which can be observed using in-situ surface-sensitive microscopy techniques. In particular, we are interested in a model for CO oxidation able to produce bistability (*a stable reactive steady state with high CO₂ production rate coexists with a stable inactive state with a low CO₂ production rate*) [24].

As mentioned in the introduction, CO oxidation is one of the most simple pattern-formation chemical reactions in surface science, and the key underlying atomistic processes are described by the so-called Langmuir-Hinshelwood (LH) mechanism.

For CO oxidation under typical conditions, CO_{ads} is highly mobile, and its diffusion rate controls the length scale of spatial patterns observed during the reaction. In contrast,

¹For example CO oxidation on Pt(111) [98, 99] or Pd(100) [100] surfaces.

O_{ads} is relatively immobile. Thus, CO_{ads} is in a locally equilibrated state. This results in nonequilibrium conditions. We note that O_{ads} mobility can be significant in CO oxidation at higher temperatures although its is always far less than CO_{ads} mobility [24, 25]. Thus, we will not include O_{ads} mobility (rate of oxygen diffusion $h_O = 0$) in our model. There are a number of different levels of modelling, depending in part on the extent to which adspecies interactions are incorporated² [101]. Here, we use a "minimally interacting model incorporating only $O_{ads} - O_{ads}$ repulsive interactions" [102]. In this case, O_{ads} can exhibit ordered phases. Now CO_{ads} is randomly distributed on all available sites. Further simplification is achieved if there exists a fast mobility of O_{ads} and if the interactions are totally eliminated. In this case, randomly distributed adspecies can be analysed by classic mean-field rate equations, and the equations become exact. In our minimal interacting model, a more sophisticated approximation has to be used in order to describe $O_{ads} - O_{ads}$ interaction.

Our intention is to perform a mean-field birth-death description of CO oxidation using the above mentioned reaction steps. *In the mean-field approximation one only tracks the total numbers (or equivalently coverage) of different species and their increment and decrement using macroscopic rate laws to model the respective transition rates.* It means that the total number of adspecies (or total coverage) is the random variable used in our model. Consequently, a Markov birth-death description is applied [51].

4.2 Hybrid model for CO oxidation with $O - O$ adsorbed repulsion

To take into account correctly fast CO_{ads} diffusion and oxygen ordering at the level of the mean-field description, a hybrid description has been used together with the so-called cluster approximation. The application of cluster approximation to CO oxidation has a long history [103, 104, 105, 106, 107, 108, 109]. This section starts deriving the transition probabilities of our model step by step.

4.2.1 CO adsorption and desorption

In real CO oxidation experiments, CO_{gas} adsorbs associatively on different sites of the surface with different binding energies. In a mean-field birth-death description, the adsorption site properties are irrelevant because in this case we are only interested in the

²In Chap. 7 we analyze a model with $CO - O$ and $O - O$ adspecies interactions

total number of adsorbed species and not in detailed atomic configurations³. Thus, CO_{gas} adsorbs on the surfaces at rate proportional to p_{CO} . Considering that oxygen atoms are also adsorbed on the surface, the transition probability for CO_{gas} adsorption can be written as

$$W_1(N_{CO}/N_{CO} + 1) = p_{CO}(A - N_{CO} - N_O), \quad (4.1)$$

where N_{CO} and N_O are the total number of adsorbed CO and oxygen molecules, respectively. We require, $0 < N_{CO,i} + N_{O,i} \leq A$, where A represents the area of the surface. On the other hand, CO_{ads} molecules can desorb from the surface into the gas phase at rate d . The parameter d correspond to the temperature in experiments, because CO_{ads} desorption is the strongest activated step in the LH sequence. Finally, the transition probability for the desorption step is

$$W_2(N_{CO}/N_{CO} - 1) = dN_{CO}. \quad (4.2)$$

4.2.2 CO surface diffusion

As mentioned above, for CO oxidation under typical conditions, the surface hop rate or diffusion of CO_{ads} is many orders of magnitude higher than the rates for other processes like adsorption, desorption, reaction, and diffusion of O_{ads} . In this case, due to the rapid diffusion, CO_{ads} is distributed randomly on the non- O_{ads} sites at all times (rate of CO diffusion $h_{CO} \rightarrow \infty$). Basically, we assume a uniform distribution of CO_{ads} on all non- O_{ads} sites. Then we say that the local number of CO_{ads} molecules on non- O_{ads} sites is

$$N_{CO}^{loc} = \frac{N_{CO}}{N_Z}, \quad (4.3)$$

where $N_Z = A - N_O$ denotes the total number of non- O_{ads} sites or the total surface area not occupied by O_{ads} [91].

4.2.3 Dissociative adsorption of O_2

In real experimental situations, oxygen has preferred absorption sites which inside our mean-field description are irrelevant. $O_{2,gas}$ adsorbs dissociatively at diagonal nearest-neighbor (NN) empty sites at rate p_{O_2} , provided that all six additional NN sites to these are unoccupied by O_{ads} . O_{ads} does not desorb at $T \leq 600$ K and as mentioned above is practically immobile at low T ($T \leq 500$ K) [102]. This prescription of oxygen adsorption was introduced by Evans *et al.* [102], and is termed the "eight-site rule" since an ensemble of eight sites not occupied by O_{ads} are required for adsorption (see Fig. 4.1). This rule

³We do not take into account the differences between bridge, fourfold or on-top sites [65].

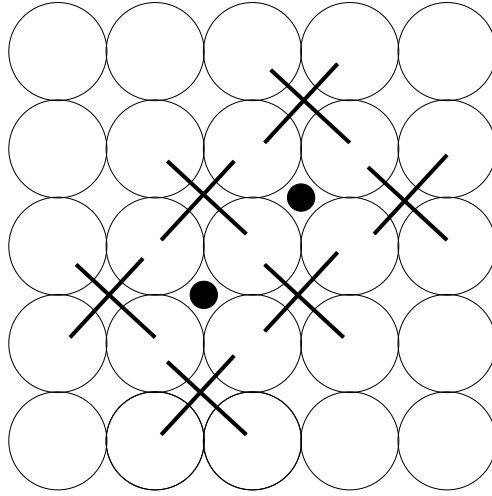


Figure 4.1: Schematic of $O_{2,gas}$ adsorption on a lattice. The two black circles represent O atoms. Crosses denote the six additional sites not occupied by O .

was originally applied to describe dissociative adsorption of oxygen on Ni(111) [110] and Pd(100) [111, 112]. Together with the immobility of O_{ads} , this adsorption rule ensures that no adjacent pairs of $O_{ads} - O_{ads}$ are created during the reaction. As a consequence, the oxygen adlayer tends to display (2×2) superlattice ordering. Such ordering in oxygen adlayer has been observed experimentally for metal(100) surfaces with the exception of Pt(100) where O_{ads} displays more complicated superlattice ordering [113]. Note that the eight-site rule prevents any unphysical poisoning by O adsorbed as contained in the classic Ziff-Gulari-Barshad model for a monomer-dimer reaction [114].

Figure 4.1 shows a schematic lattice model description of $O_{2,gas}$ adsorption which can be correctly described by kinetic Monte Carlo simulations of lattice models [100, 101, 102]. However, in our case we are interested in deriving mean-field transition probabilities which at the same time should be able to reflect this NN $O_{ads} - O_{ads}$ repulsion. Let us denote E empty sites, and Z , sites not occupied by O_{ads} . We let $\{J\}$ denote the fraction of sites in state $J = CO, O, E$, or Z . Thus, the fraction of eight-site configurations may be written

as

$$\left\{ \begin{array}{cccc} & & Z & \\ & & Z & E & Z \\ Z & E & Z & & \\ & Z & & & \end{array} \right\}. \quad (4.4)$$

Simplification is possible since that CO_{ads} molecules are randomly distributed on Z sites to obtain

$$\left\{ \begin{array}{cccc} & & Z & \\ & & Z & E & Z \\ Z & E & Z & & \\ & Z & & & \end{array} \right\} = (\{E\}/\{Z\})^2 \left\{ \begin{array}{cccc} & & Z & \\ & & Z & Z & Z \\ Z & Z & Z & & \\ & Z & & & \end{array} \right\}. \quad (4.5)$$

There is no simple exact expression for the configuration of Z sites. Thus, one needs a reasonable approximation. Here one can invoke the standard cluster approximation (see Appendix B) [103, 104, 105, 106, 107, 108, 109]. In a simplified version of this approximation we let $\{J'J\}$ denote the probability that the left site in a specific NN pair is in state J' , and the right one is in state J , etc. Then, from conservation of probability, one has that, *e.g.*,

$$\{ZZ\} + \{OZ\} + \{ZO\} + \{OO\} = 1, \quad (4.6)$$

where $\{OO\} = 0$ and $\{OZ\} = \{ZO\} = \{O\}$, so $\{ZZ\} = 1 - 2\{O\}$. Similar notation is adopted for probabilities of configurations of various larger sets of sites.

One finally obtains

$$\left\{ \begin{array}{cccc} & & Z & \\ & & Z & Z & Z \\ Z & Z & Z & & \\ & Z & & & \end{array} \right\} \approx \{ZZ\}^8 / \{Z\}^8 = (1 - 2\{O\})^8 / (1 - \{O\})^8. \quad (4.7)$$

Inserting Eq. 4.7 in Eq. 4.5 and using

$$\{E\} = 1 - \{O\} - \{CO\}, \quad (4.8)$$

and

$$\{Z\} = 1 - \{CO\}, \quad (4.9)$$

one obtain

$$\left\{ \begin{array}{cccc} & & Z & \\ & Z & E & Z \\ Z & E & Z & \\ & Z & & \end{array} \right\} \approx \frac{(1 - \{O\} - \{CO\})^2 (1 - 2\{O\})^8}{(1 - \{O\})^{10}}. \quad (4.10)$$

Note that $\{J\}$ is equal to the so-called coverage ($\theta_J = N_J/A$). Using coverage notation in Eq. 4.10, it is easy to show that the fraction of eight-site configurations as a function of the number of adspecies can be written as

$$\left\{ \begin{array}{cccc} & & Z & \\ & Z & E & Z \\ Z & E & Z & \\ & Z & & \end{array} \right\} \approx \frac{(A - N_O - N_{CO})^2 (A - 2N_O)^8}{(A - N_O)^{10}}. \quad (4.11)$$

In the same way, the number of eight-site configurations is

$$N \left\{ \begin{array}{cccc} & & Z & \\ & Z & E & Z \\ Z & E & Z & \\ & Z & & \end{array} \right\} \approx A \frac{(A - N_O - N_{CO})^2 (A - 2N_O)^8}{(A - N_O)^{10}}. \quad (4.12)$$

Finally, one can verify that the transition probability for the dissociative adsorption of oxygen is given by

$$W_3(N_{CO}/N_{CO} - 1) = 2p_{O_2} N \left\{ \begin{array}{cccc} & & Z & \\ & Z & E & Z \\ Z & E & Z & \\ & Z & & \end{array} \right\}, \quad (4.13)$$

or using Eq. 4.12

$$W_3(N_{CO}/N_{CO} - 1) = 2p_{O_2} A \frac{(A - N_O - N_{CO})^2 (A - 2N_O)^8}{(A - N_O)^{10}}. \quad (4.14)$$

It is important to note that for $N_O = A/2$, we obtain $W_3 = 0$. It means that the surface can not be completely covered by oxygen, and thus, the unphysical oxygen poisoning state is eliminated. However, the cluster approximation predictions are not precise at high

coverage. This failure derives in part from the feature that the cluster approximation does not account for an observed dramatic symmetry-breaking of the reaction model for high O_{ads} [102].

4.2.4 CO_2 production

Obviously, in the cluster approximation the transition probability for the reaction rate must be written as

$$W_4(N_{CO}, N_O/N_{CO} - 1, N_O - 1) = 4k\{COO\}. \quad (4.15)$$

where the factor 4 corresponds to the coordination number of the square lattice and k is the probability for CO_{ads} and O_{ads} reaction. Further simplification of this pair configuration is possible exploiting the feature that CO_{ads} molecules are randomly distributed on Z sites. In particular, one has

$$\{COO\} = (\{ZO\}\{CO\})/\{Z\} = \{CO\}\{O\}/(1 - \{O\}). \quad (4.16)$$

Thus, the corresponding transition probability as a function of the number of adspecies is

$$W_4(N_{CO}, N_O/N_{CO} - 1, N_O - 1) = 4kN_{CO}N_O/(A - N_O) = 4kN_ON_{CO}^{local}. \quad (4.17)$$

4.3 Deterministic limit: Bistability

Note that if the surface area $A \rightarrow \infty$, then the number of adsorbed molecules N_J also increases, and thus, $\theta_J = \lim_{A \rightarrow \infty} N_J/A = const$. In this limit the stochastic processes approximate the solution of the initial value problem given by ODE's. In this section, we start with the mean field dynamics

$$\frac{d\langle\theta_{CO}\rangle}{dt} = \frac{\langle W_1 - W_2 - W_4 \rangle}{A}, \quad (4.18)$$

$$\frac{d\langle\theta_O\rangle}{dt} = \frac{\langle W_3 - W_4 \rangle}{A}. \quad (4.19)$$

In the limit $A \rightarrow \infty$ and using the well known fact that fluctuations of the concentrations vanish like $(A)^{-1/2}$, it is easy to show that the ODE's can be written as

$$\frac{d\theta_{CO}}{dt} = p_{CO}(1 - \theta_{CO} - \theta_O) - d\theta_{CO} - \frac{4k\theta_{CO}\theta_O}{(1 - \theta_O)}, \quad (4.20)$$

$$\frac{d\theta_O}{dt} = 2p_{O_2} \frac{(1 - \theta_{CO} - \theta_O)^2(1 - 2\theta_O)^8}{(1 - \theta_O)^{10}} - \frac{4k\theta_{CO}\theta_O}{(1 - \theta_O)}, \quad (4.21)$$

where we used the fact that for small fluctuations $\langle \theta_O \theta_{CO} \rangle \approx \langle \theta_O \rangle \langle \theta_{CO} \rangle$. Unfortunately, Eqs. 4.20 and 4.21 cannot be solved analytically. Therefore, the states of the deterministic system are found numerically. For sufficiently low desorption d , the reaction exhibits bistability in a p_{CO} pressure range. In the bistable region the stable stationary states are connected by an unstable saddle state. For appropriate initial conditions, the system resides on one of two stationary states for an indefinite period of time. This bistability region vanishes as $d \rightarrow d_c$, where $d = d_c$ correspond to a cusp bifurcation. At this point the two stable stationary states and the unstable one are equals. Figure 4.2(a) shows the phase diagram of the stationary states $\theta_{CO_{st}}$ and $\theta_{O_{st}}$ in the (p_{CO}, d) plane. The cusp is located at $d_c \approx 0.048$ and $p_{CO} \approx 0.40$, which corresponds to James *et al.* [102, 115, 116]. For high p_{CO} we obtain an inactive state and for low p_{CO} a reactive state with high and low CO_{ads} coverage respectively. We choose $p_{CO} + p_{O_2} = 1$, which sets the time scale in the model, and also set $p_{O_2} = 1 - p_{CO}$. We also choose $k = 1$, but other values produce qualitatively similar results.

Solutions of ODE's have limited domain of attraction, such that only solutions in this domain tend to the corresponding stable solution. Figure 4.2(b) shows an schematic example of deterministic predictions for bistability. Here, $\theta_{st}(1, 2)$ represent stable states with its respective domain of attraction limited by the position of the unstable state which is denoted by θ_{unst} . Basically, the macroscopic rate laws without fluctuations effects predict, that the system resides on one of two stationary stable states for an indefinite period of time.

4.4 Stochastic limit: Master equation for CO oxidation

In order to go to the stochastic limit, we have to return to the Markovian transition probabilities derived in the previous section and to concentrate on finite values of A . Table 4.1 summarizes these transition probabilities. Let us denote the populations by a vector $\tilde{\mathbf{Z}} = \left\{ \tilde{Z}^i \right\}_{i=1}^2 = \{N_{CO}, N_O\}$, and its change for each of the four processes denoted by ρ

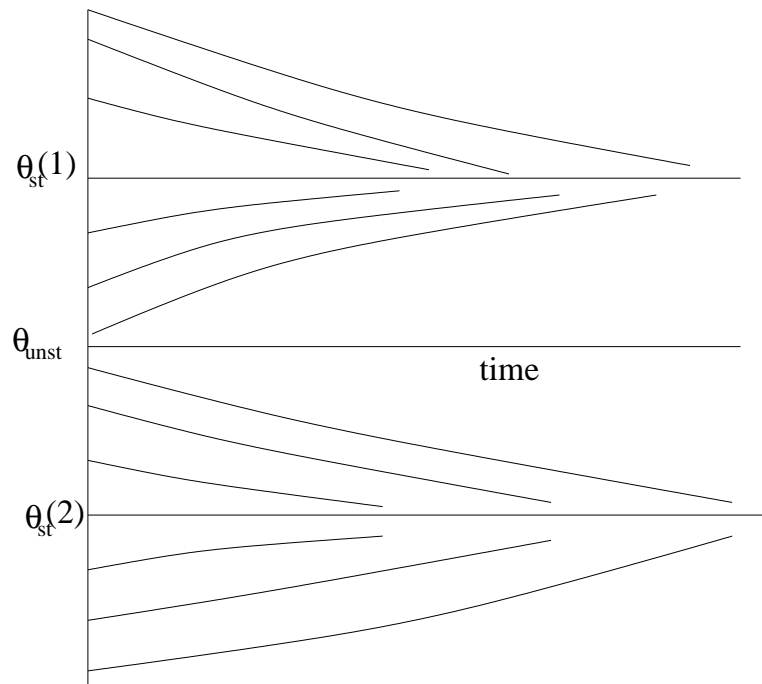
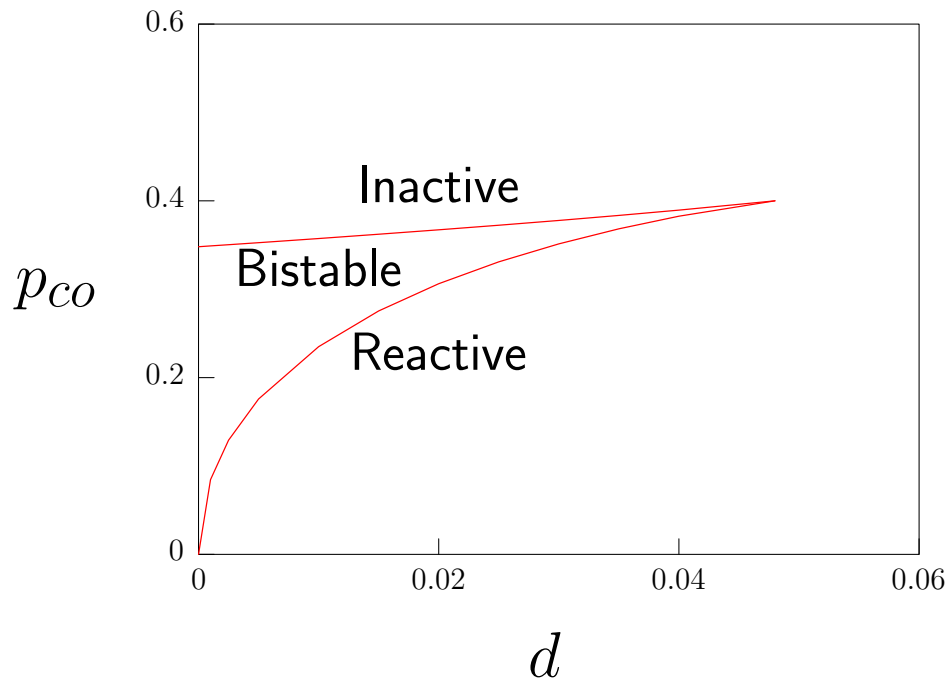


Figure 4.2: *a*) Steady- state diagram in the (p_{CO}, d) plane showing the bistable region as well as the reactive and inactive state [from the deterministic approach, Eqs. 4.20 and 4.21]. *b*) Schematic deterministic prediction for bistability. All solutions other than θ_{unst} itself tend to either $\theta_{st}(1)$ or $\theta_{st}(2)$.

| Reaction step | Transition probability |
|--|--|
| $\text{CO}_{\text{gas}} - \text{Adsorption}$ | $W_1 = p_{\text{CO}}(A - N_{\text{CO}} - N_{\text{O}})$ |
| $\text{CO}_{\text{ads}} - \text{Desorption}$ | $W_2 = dN_{\text{CO}}$ |
| $\text{O}_{2,\text{gas}} - \text{Adsorption}$ | $W_3 = 2p_{\text{O}_2} A \frac{(A - N_{\text{O}} - N_{\text{CO}})^2 (A - 2N_{\text{O}})^8}{(A - N_{\text{O}})^{10}}$ |
| $\text{CO}_{\text{ads}} - \text{O}_{\text{ads}} - \text{Reaction}$ | $W_4 = 4k N_{\text{CO}} N_{\text{O}} / (A - N_{\text{O}})$ |

Table 4.1: Transition probabilities for CO oxidation on unreconstructed noble metal surfaces.

with a vector $\mathbf{v}_\rho = \{v_\rho^i\}_{i=1}^2$. Hence, the temporal dynamics of the time-dependent probability for the occupation of N_{O} sites with oxygen and N_{CO} sites with carbon monoxide $P(N_{\text{CO}}, N_{\text{O}}; t)$ is governed by the homogeneous master equation

$$\frac{d}{dt} P(\tilde{\mathbf{Z}}; t) = \sum_{\rho=1}^4 [W_\rho(\tilde{\mathbf{Z}} - \mathbf{v}_\rho / \tilde{\mathbf{Z}}) P(\tilde{\mathbf{Z}} - \mathbf{v}_\rho; t) - W_\rho(\tilde{\mathbf{Z}} / \tilde{\mathbf{Z}} - \mathbf{v}_\rho) P(\tilde{\mathbf{Z}}; t)]. \quad (4.22)$$

Obviously, this master equation represents a global birth-death description of fluctuations. Now, it is possible to apply the Gillespie algorithm to this equation [51]. Nevertheless, to derivate analytical solutions of this nonlinear equations is in general quite difficult. Thus, we have to turn to approximations [51].

4.5 Adiabatic reduction of oxygen from the master equation

Theoretical methods for the adiabatic elimination of fast-relaxing variables from master equations have received a great deal of interest in the last years [117, 118, 119, 120, 121, 122, 123, 124]. This is motivated partially by the fact that in most cases it is difficult or impossible to solve this equation. It is also known that for large complicated chemical networks, model reduction often provides a way to efficient computational methods. *These techniques assume that fast variables are in a quasi-steady state with respect to the*

remaining slow variables. If the quasi-steady state distributions conditioned on the slow variables can be determined, then they can be used to eliminate the fast variables. Under some conditions one can approximate the corresponding fast variable using Langevin or deterministic equations [125].

The adiabatic elimination can be justified for our model by direct integration of Eqs. 4.20 and 4.21, which reveals that a slowly varying trajectory in phase space with almost constant oxygen coverage is rapidly reached from any initial condition, which nearly coincides with the nullcline $d\theta_O/dt = 0$. Hence θ_O is a fast variable. One early application of the fast variable elimination method to a deterministic model of CO oxidation was developed by Bär *et al.* [96]. In principle, one can use the previous result of time scale separation in order to justify the application of the fast variable elimination method to stochastic systems. Nevertheless, the trajectories of our model in phase space are random, and a clear time scale separation between θ_O and θ_{CO} is not evident. Figure 4.3(a) shows several stochastic trajectories from the two dimensional master equation, for relative large A , together with the nullcline $d\theta_O/dt = 0$ and $d\theta_{CO}/dt = 0$. In this limit, it is evident that the nullcline $d\theta_O/dt = 0$ (solid line) is rapidly reached from any initial conditions.

4.5.1 Reduced master equation for the slow CO variable

We consider $\tilde{\mathbf{Z}} = \{N_{CO}, N_O\}$, with the stoichiometric coefficients $\mathbf{v}_1 = \{1, 0\}$, $\mathbf{v}_2 = \{-1, 0\}$, $\mathbf{v}_3 = \{0, 2\}$, and $\mathbf{v}_4 = \{-1, -1\}$. If we take from the time scale separation that

$$P(N_{CO}, N_O; t) = G(N_{CO}; t)H(N_O : N_{CO}; t), \quad (4.23)$$

then oxygen can be adiabatically reduced from Eq. (4.22). Note that $H(N_O : N_{CO}; t)$ is the conditional probability distribution for N_{CO} being kept constant. We also require

$$\sum_{N_{CO}} G(N_{CO}) = 1, \quad (4.24)$$

$$\sum_{N_O} H(N_O : N_{CO}) = 1. \quad (4.25)$$

Inserting Eq. 4.23 into Eq. 4.22 and summing up over N_O , we obtain

$$\begin{aligned} \frac{d}{dt}G(N_{CO}; t) &= \tilde{W}_1(N_{CO} - 1)G(N_{CO} - 1; t) + \tilde{W}_2(N_{CO} + 1)G(N_{CO} - 1; t) \\ &\quad - (\tilde{W}_1(N_{CO}) + \tilde{W}_2(N_{CO}))G(N_{CO}; t) \end{aligned}$$

$$\begin{aligned}
& + \sum_{N_O} (W_3(N_O - 2)H(N_O - 2 : N_{CO}; t) \\
& - W_3(N_O)H(N_O : N_{CO}; t))G(N_{CO}; t).
\end{aligned} \tag{4.26}$$

The last term of this equation must be zero because it does not contribute to the variation of N_{CO} . Thus, one may write

$$\begin{aligned}
\frac{d}{dt}G(N_{CO}; t) & = \tilde{W}_1(N_{CO} - 1)G(N_{CO} - 1; t) + \tilde{W}_2(N_{CO} + 1)G(N_{CO} - 1; t) \\
& - (\tilde{W}_1(N_{CO}) + \tilde{W}_2(N_{CO}))G(N_{CO}; t),
\end{aligned} \tag{4.27}$$

where

$$\tilde{W}_1(N_{CO}) = \sum_{N_O} W_1(N_{CO}, N_O)H(N_O : N_{CO}), \tag{4.28}$$

and

$$\tilde{W}_2(N_{CO}) = \sum_{N_O} (W_2(N_{CO}) + W_4(N_{CO}, N_O))H(N_O : N_{CO}), \tag{4.29}$$

are the conditional expectations of $W_1(N_{CO}, N_O)$ and $W_2(N_{CO}) + W_4(N_{CO}, N_O)$, respectively. The conclusion of this analysis is that the evolution of $G(N_{CO}; t)$ depends on the conditional probability distribution $H(N_O : N_{CO})$.

4.5.2 Reduced master equation for fast oxygen variable

Note that the vector $\tilde{\mathbf{Z}} = \{N_{CO}, N_O\}$ is a Markov process that obeys the Markovian master equation 4.22 and can be simulated by the Gillespie algorithm. Note also that if we consider that N_O evolves only through $W_3(N_O : N_{CO})$ and $W_4(N_O : N_{CO})$, where N_{CO} is a constant parameter that does not evolve, then N_O alone is also a Markov variable which satisfies the following master equation [126, 127, 128]

$$\begin{aligned}
\frac{d}{dt}H(N_O : N_{CO}; t) & = W_3(N_O - 2)H(N_O - 2 : N_{CO}; t) - W_3(N_O)H(N_O : N_{CO}; t) \\
& + W_4(N_O + 1)H(N_O + 1 : N_{CO}; t) - W_4(N_O)H(N_O : N_{CO}; t),
\end{aligned} \tag{4.30}$$

with N_{CO} being kept constant.

4.5.3 The combined system

Due to the time scale separation $H(N_O : N_{CO}; t)$ will quickly relax to a stationary distribution⁴. This equilibration implies that we should approximate Eq. 4.30, as

$$\frac{d}{dt}H(N_O : N_{CO}; t) \approx 0. \quad (4.31)$$

Thus, the resulting coupled master equations of our model are

$$\begin{aligned} \frac{d}{dt}G(N_{CO}; t) = & \tilde{W}_1(N_{CO} - 1)G(N_{CO} - 1; t) + \tilde{W}_2(N_{CO} + 1)G(N_{CO} - 1; t) \\ & - (\tilde{W}_1(N_{CO}) + \tilde{W}_2(N_{CO}))G(N_{CO}; t), \end{aligned} \quad (4.32)$$

$$\begin{aligned} 0 \approx & W_3(N_O - 2)H(N_O - 2 : N_{CO}; t) - W_3(N_O)H(N_O : N_{CO}; t) \\ & + W_4(N_O + 1)H(N_O + 1 : N_{CO}; t) - W_4(N_O)H(N_O : N_{CO}; t), \end{aligned} \quad (4.33)$$

where the conditional transition probabilities are given by Eqs. 4.28 and 4.29. Note that Eq. 4.32 is an one-step master equation with a well-know solution [3]. Now the more difficult part will be computing $H(N_O : N_{CO}; t)$ which is no more an one-step master equation; indeed, this will usually have to be done approximately [126].

4.5.4 Deterministic approximation for the fast oxygen variable

Figure 4.3(b) shows a solution of Eq. 4.33 for $\theta_{CO} = N_{CO}/A = \text{const}$. It is clear that $H_{st}(N_O : N_{CO} = \text{const})$ is a sharply peaked monomodal function around N_O . Thus $N_O = A\theta_O$ is solution of

$$\frac{d\theta_O}{dt} = 2p_{O_2} \frac{(1 - \theta_{CO} - \theta_O)^2(1 - 2\theta_O)^8}{(1 - \theta_O)^{10}} - \frac{4k\theta_{CO}\theta_O}{(1 - \theta_O)} = 0, \quad (4.34)$$

for each $N_{CO} = A\theta_{CO}$ [51]. Note that we approximate the stochastic fast variable by using the deterministic equation corresponding to this variable. It is just an approximation, which holds true for sharply single peaked function $H_{st}(N_O : N_{CO} = \text{const})$. A generalisation obviously must include higher moments, too [129].

⁴A more precise way of stating this requirement is to say that the fast variable equilibrate (relax) before the expected time to the first slow reaction.

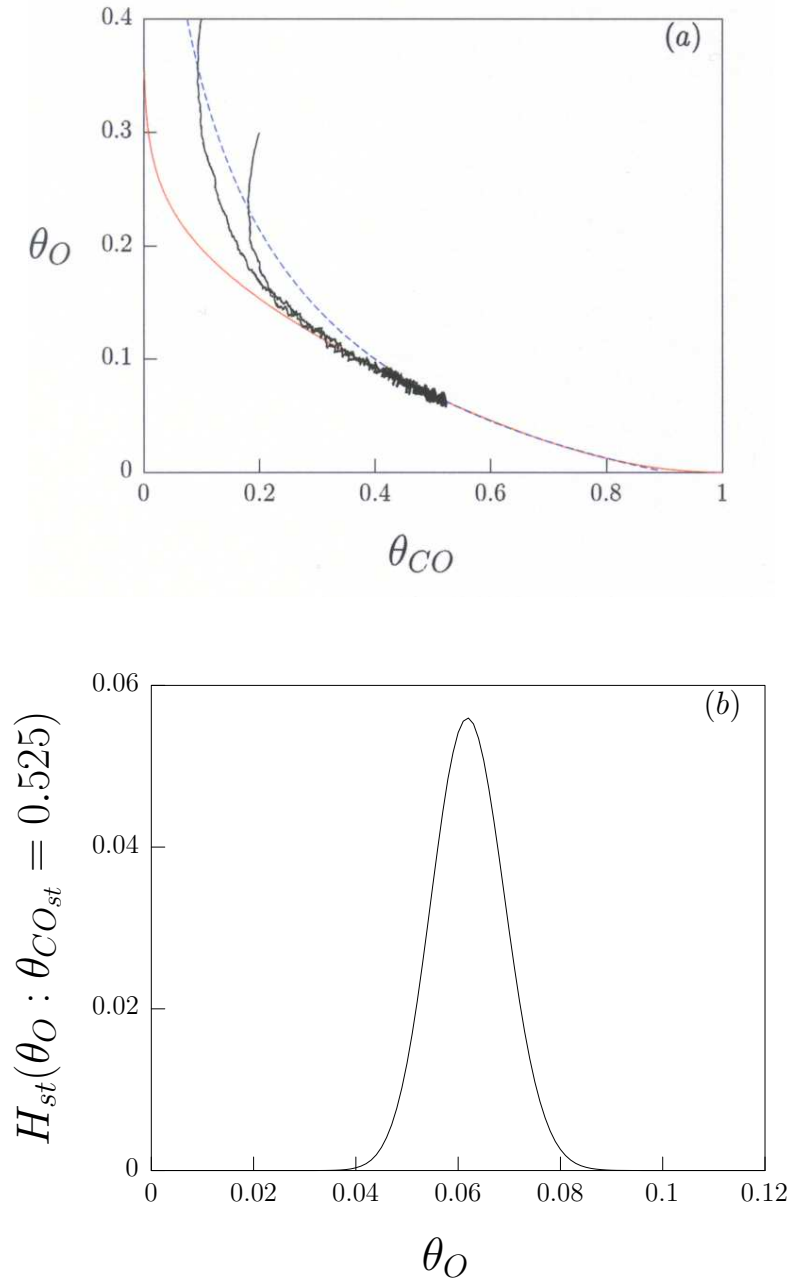


Figure 4.3: Phase space plane of the deterministic approach as well as the conditional stationary probability distribution $H_{st}(\theta_O : \theta_{CO_{st}})$ from the Gillespie algorithm. *a*) Several stochastic trajectories for different initial conditions and relative large A , together with the nullcline $d\theta_O/dt = 0$ (solid lines) and $d\theta_{CO}/dt = 0$ (dashed line). The nullcline $d\theta_O/dt = 0$ is rapidly reached from any initial condition. *b*) $H_{st}(\theta_O : \theta_{CO_{st}} = 0.525)$ in the coverage space with $A = 1000$. This conditional probability distribution is sharply peaked and unimodal around the mean value $\langle \theta_O \rangle = \theta_O = 0.065$. The CO pressure and the desorption are constant at $p_{CO} = 0.38645$, and $d = 0.04$.

4.6 Summary and conclusions

In this chapter, we have analyzed a model for CO oxidation which incorporates superlattice ordering of O_{ads} as well as a rapid mobility of CO_{ads} . It is shown that in the deterministic limit the model exhibits bistability, which is lost at a cusp bifurcation or "critical point" when the desorption rate d for CO_{ads} exceeds a critical value. Then, the internal fluctuations were taken into account by a stochastic Markov birth-death process by using the so-called master equation. This equation describes the evolution of the probability distribution for the number of molecules in a chemical system that is well mixed. One disadvantage of this master equation is that an analytical solution is not available in general. Nevertheless, this problem was solved by introducing the technique of adiabatic elimination of fast variables (In Appendix B, a general method for the elimination of fast variables from the master equation is derived).

These techniques assume that fast variables are in a quasi-steady state with respect to the remaining slow variables. If the quasi-steady state distributions conditioned on the slow variables can be determined, then they can be used to eliminate the fast variables. We showed that N_{CO} is the slow variable and N_O the fast one. Therefore, we used the adiabatic approximation to eliminate N_O , together with the hybrid model idea for fast CO diffusion to show that the dynamic of the slow N_{CO} variable may be describe by the following master equation

$$\begin{aligned} \frac{d}{dt}G(N_{CO};t) = & \tilde{W}_1(N_{CO} - 1)G(N_{CO} - 1;t) + \tilde{W}_2(N_{CO} + 1)G(N_{CO} - 1;t) \\ & - (\tilde{W}_1(N_{CO}) + \tilde{W}_2(N_{CO}))G(N_{CO};t), \end{aligned} \quad (4.35)$$

where \tilde{W}_1 and \tilde{W}_2 are the conditional expectations of $W_1(N_{CO}, N_O)$ and $W_2(N_{CO}) + W_4(N_{CO}, N_O)$. The relaxation to equilibrium of the fast oxygen variable is modelled using the following deterministic equation

$$0 = 2p_{O_2} \frac{(1 - \theta_{CO} - \theta_O)^2 (1 - 2\theta_O)^8}{(1 - \theta_O)^{10}} - \frac{4k\theta_{CO}\theta_O}{(1 - \theta_O)}, \quad (4.36)$$

where $N_{CO} = A\theta_{CO} = const.$

Obviously, the deterministic approximation for the fast oxygen variable takes into account that the fluctuations are small. For instance, this approximation considers that $\langle \theta_O \theta_O \rangle \approx \langle \theta_O \rangle^2$. This implies that the variance is equal zero, and hence the $N_O = A\theta_O$ is a variable with no fluctuations. Thus, it is a crude approximation and a generalisation

obviously must include higher moments.

It is important to emphasize that our model is still rather simplistic. To precisely describe behavior in real systems, more realistic and complicated reaction models must be utilized. These should incorporate $CO_{ads} - O_{ads}$ and $CO_{ads} - CO_{ads}$ interactions in addition to the repulsive $O_{ads} - O_{ads}$ considered here. Also, it is possible to incorporate in a more realistic model O_{ads} diffusion.

Chapter 5

Fluctuation-induced transitions

"In other words, the impossibility of an uncompensated decrease of entropy seems to be reduced to an improbability."

Josiah Willard Gibbs (1839-1903)

5.1 Introduction

Catalytical reactions have been studied extensively on extended single crystal surfaces. However, as mentioned in Chap. 2, recent interest has turned to reactions on nanoscale systems, *e.g.*, on supported nanoparticles [15] or on metal field emitter tips (FET's) with facet dimensions of ≈ 10 nm [13]. In these systems, fluctuation effects are very pronounced due to their small size. CO oxidation on extended surfaces typically exhibits robust bistability. In previous chapters it was shown that this bistability derives from the nonlinear Langmuir-Hinshelwood kinetics together with long-range spatial interaction due to fast CO surface diffusion. However, experimental studies for nanoscale systems suggest a loss of bistability due to internal fluctuation-induced transitions between stable branches [15, 13]. It was also shown that the amplitude of fluctuations diverges upon approaching the bifurcation point terminating the bistable range of the reaction [13]. If these experiments are carried out at low pressure or high temperature, CO molecules can diffuse very fast on the surface and a well-stirred system is formed which exhibits homogeneous fluctuations. Thus spatially homogeneous transitions from a stable state to the other stable state and vice versa can be observed. *In this chapter we show that this behavior is captured qualitatively by a master equation analysis based on mean-field kinetics and by corresponding Gillespie-type kinetic Monte Carlo simulations* [51].

5.2 Deterministic versus stochastic approach

Normally, the stochastic description of a phenomenon differs of macroscopic deterministic predictions. Deterministic macroscopic rate laws describe chemical reactions by concentration averages. On the other hand, it is well known that chemical reactions are affected by internal fluctuations because of the stochastic nature of elementary processes. Therefore, a stochastic analysis is fundamental. For a catalytic reaction, which should take place on small metal particles of typically a few nanometer diameter, a clear distinction between deterministic and stochastic predictions is important. Of particular interest for us is the bistable behavior in *CO* oxidation on nanoscale surfaces because a clear characterisation of bistability in those small systems is still far from complete.

5.2.1 Deterministic predictions: Extended single crystal surfaces

In *CO* oxidation on well-defined extended single crystal surfaces at low pressure ($\leq 10^{-4}$ mbar) and typical temperatures (≈ 500 K) there are about 10^6 site changes due to diffusion of an adsorbed *CO* molecule per adsorption event. Therefore the surface can be regarded as being locally well-mixed (on the order of the diffusion length which amounts to $\leq 1\mu\text{m}$). In this case internal fluctuations due to the discrete nature of the reaction process are averaged out. Simple deterministic rate equations should thus be applicable and have indeed been very successful in reproducing a large number of experimental finding, such as bistability, oscillations, spirals, pulses, fronts, turbulence, and solitary waves [24, 130].

Our interest is study the kinetic bistability of *CO* oxidation. We use the deterministic model, incorporating $O_{ads} - O_{ads}$ repulsive interactions and fast *CO* diffusion, which was introduced in Chap. 4. We will show that the reduced version of this model still is able to exhibit bistability. Let us consider the reduce model

$$\frac{d\theta_{CO}}{dt} = p_{CO}(1 - \theta_{CO} - \theta_O) - d\theta_{CO} - \frac{4k\theta_{CO}\theta_O}{(1 - \theta_O)}, \quad (5.1)$$

$$0 = 2p_{O_2} \frac{(1 - \theta_{CO} - \theta_O)^2(1 - 2\theta_O)^8}{(1 - \theta_O)^{10}} - \frac{4k\theta_{CO}\theta_O}{(1 - \theta_O)}. \quad (5.2)$$

Solving for θ_O one obtains

$$\theta_O = g(\theta_{CO}, p_{O_2}, k), \quad (5.3)$$

and finally

$$\frac{d\theta_{CO}}{dt} = p_{CO}(1 - \theta_{CO} - g(\theta_{CO})) - d\theta_{CO} - \frac{4k\theta_{CO}g(\theta_{CO})}{(1 - g(\theta_{CO}))}. \quad (5.4)$$

Figure 5.1 shows $\frac{d\theta_{CO}}{dt}$ versus θ_{CO} . Note that the bistability is still reproduced by the one-dimensional model. The macroscopic rate laws without fluctuations effects predict, that the system resides on one of two stationary stable states for an indefinite period of time. As in Chap. 4, we choose $p_{CO} + p_{O_2} = 1 = k$ and consider system behavior as a function of p_{CO} .

5.2.2 Stochastic predictions: Nanoscale surfaces

In order to compare the deterministic predictions with the stochastic approach, Gillespie-type KMC simulations of the whole master equation 4.22 are shown Fig. 5.2. Figure 5.2(a) demonstrates that, with increasing particle number, the width of the joint probability maxima, obtained from the whole system by Gillespie algorithm, becomes more narrow, simultaneously the population approach becomes more similar to the deterministic description (non-transitions between the two stable states occur). In fact, for $A \rightarrow \infty$, the maxima

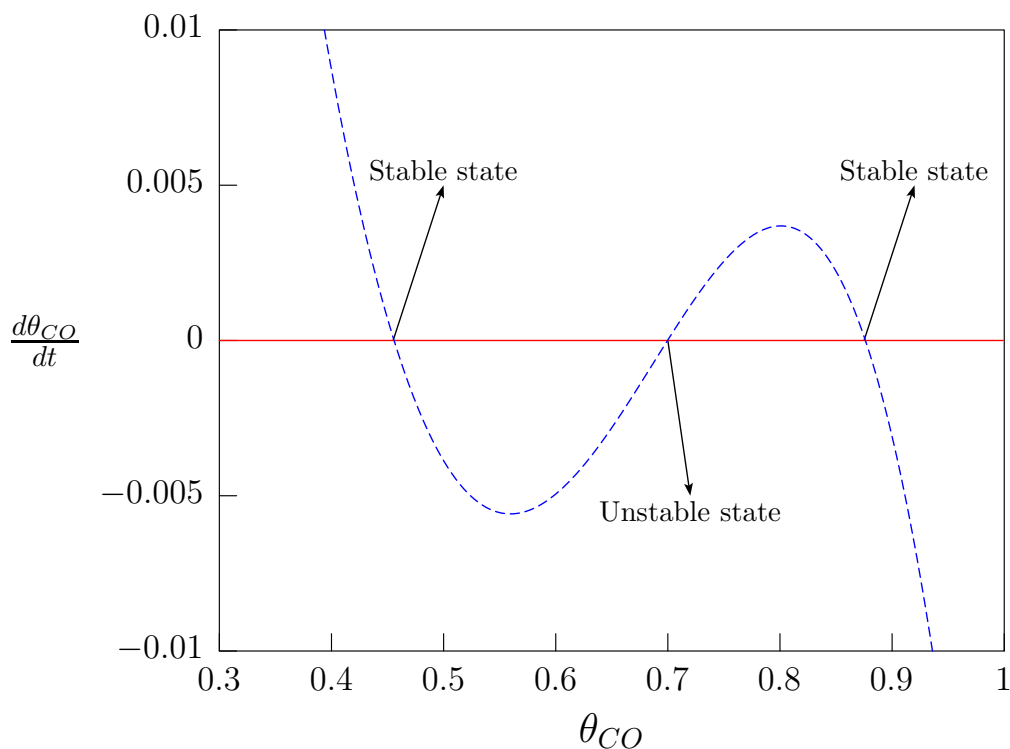


Figure 5.1: Stable and unstable solutions of Eq. 5.4 for $p_{CO} = 0.36715$ and $d = 0.030$ (dashed line). The intersection of the dashed line with $\frac{d\theta_{CO}}{dt} = 0$ (solid line) are the respective solutions.

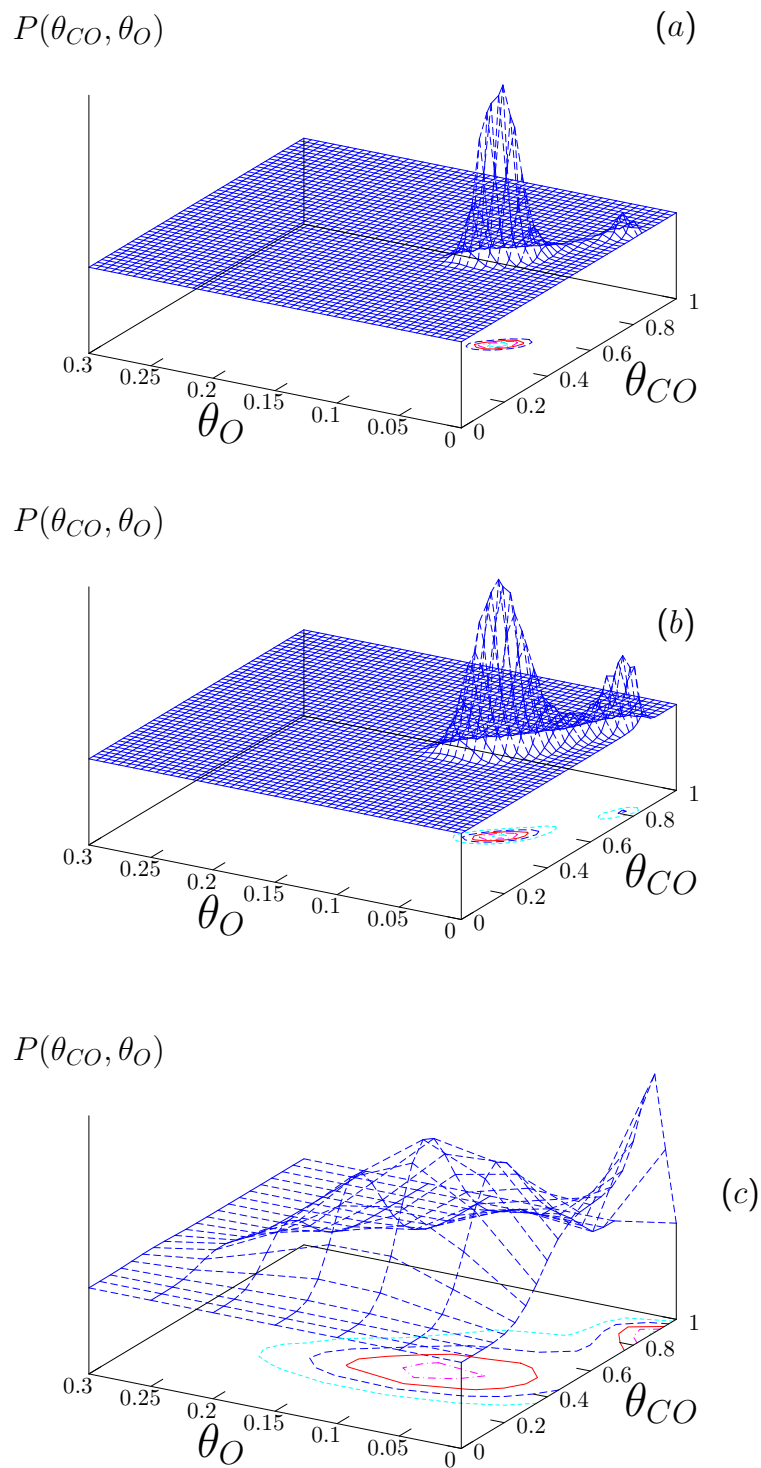


Figure 5.2: Influence of the surface area A on the dynamics of the reaction. Joint probability distribution in the coverage space for three different values of A with $p_{CO} = 0.38645$ and $d = 0.040$. The initial conditions are $\theta_{CO} = 0.525$ and $\theta_O = 0.065$. (a) $A = 1000$; (b) $A = 500$; (c) $A = 20$.

of the probability distribution coincide with the stable stationary states ($\theta_{CO} = 0.525$, $\theta_O = 0.065$) or ($\theta_{CO} = 0.825$, $\theta_O = 0.00951$), depending on the initial condition and parameter values [95].

On the other hand, we expect that for small systems the deterministic predictions become incorrect. Because the number of particles decreases, the amplitude of fluctuations of the coverage increases. Consequently, the width of the probability distributions in coverage space increases and spontaneous transitions between both reaction regimes become more frequent (Fig. 5.2(b)). Figure 5.2(c) shows that for a small number of particles, the transitions are accelerated and the macroscopic bistability tends to disappear [131, 132].

5.3 Reduced master equation for CO

Several Markovian stochastic models of the birth-death-type have been introduced to study oscillations [133, 134, 135] and bistability [48] in CO oxidation on nanoscale system, but until now analytical solutions of the master equation for these systems were unavailable. In this section we derive an analytical expression for the stationary probability distribution. It is easy to show that

$$\tilde{W}_1(N_{CO}) = p_{CO}(A - N_{CO} - \langle N_O \rangle), \quad (5.5)$$

and

$$\tilde{W}_2(N_{CO}) = dN_{CO} + \left\langle \frac{4N_O N_{CO}}{(A - N_O)} \right\rangle, \quad (5.6)$$

where $\langle N_O \rangle$ and $\langle 4N_O N_{CO}/(A - N_O) \rangle$ are the conditional expectation values of N_{CO} and $4N_O N_{CO}/(A - N_O)$ respectively.

From Sec. 4.5 we known that $H_{st}(N_O : N_{CO_{st}})$ is a sharply peaked function around $\langle N_O \rangle$. Thus, the average of the nonlinear Eq. 5.6 can be replaced by the nonlinear equation of the average

$$\tilde{W}_2(N_{CO}) = dN_{CO} + \frac{4N_{CO} \langle N_O \rangle}{(A - \langle N_O \rangle)}. \quad (5.7)$$

Using $\langle \theta_O \rangle = \theta_O = N_O/A$, which is obtained from the nullcline $d\theta_O/dt = 0$ by utilizing the well known Newton-Raphson method, it is now possible to calculate for every value of $\theta_{CO} = N_{CO}/A$ the conditional expectation values from Eqs. 5.5 and 5.7. This allows us to obtain $G_{st}(\theta_{CO})$ after solve the reduced master Eq. 4.27. Table 5.1 summaries the previous analysis. Note that the dynamic represented by these new transition probabilities is similar to the dynamic of Schlögl-type models [136, 137, 138]. These transition probabilities

| Event | Transition probability |
|---------------------------------|--|
| $N_{CO} \rightarrow N_{CO} + 1$ | $\tilde{W}_1 = p_{CO}(A - N_{CO} - \langle N_O \rangle)$ |
| $N_{CO} \rightarrow N_{CO} - 1$ | $\tilde{W}_2 = dN_{CO} + \frac{4N_{CO}\langle N_O \rangle}{(A - \langle N_O \rangle)}$ |

Table 5.1: Transition probabilities for the reduced master equation.

generate the following master equation

$$\begin{aligned} \frac{d}{dt}G(N_{CO}; t) &= \tilde{W}_1(N_{CO} - 1)G(N_{CO} - 1; t) + \tilde{W}_2(N_{CO} + 1)G(N_{CO} - 1; t) \\ &\quad - (\tilde{W}_1(N_{CO}) + \tilde{W}_2(N_{CO}))G(N_{CO}; t). \end{aligned} \quad (5.8)$$

This master equation represents a one-step birth-death Markov process for which only jumps of size +1 or -1 are allowed. In order to solve this master equation let us now suppose that the probability distribution $G(N_{CO}; t)$ approaches a stationary shape including macroscopic transitions between the stable states of the deterministic approach. The final shape of $G(N_{CO}; t)$ is in agreement with the solution $dG_{st}(N_{CO})/dt = 0$, with boundary condition $G_{st}(N_{CO} \rightarrow \infty) = 0$. In this case detailed balance holds and one finds

$$\tilde{W}_1(N_{CO} - 1)G_{st}(N_{CO} - 1; t) = \tilde{W}_2(N_{CO})G_{st}(N_{CO}; t), \quad (5.9)$$

and subsequently

$$G_{st}(N_{CO}) = \prod_{N=1}^{N_{CO}} \frac{\tilde{W}_1(N-1)}{\tilde{W}_2(N)} \left(1 + \sum_{n=1}^A \prod_{N=1}^n \frac{\tilde{W}_1(N-1)}{\tilde{W}_2(N)} \right)^{-1}. \quad (5.10)$$

This equation is the normalised stationary probability distribution for the occupation of sites with N_{CO} molecules [51, 74, 95].

5.3.1 Probability distributions

It is instructive to compare probability distributions from Eq. 5.10 and Gillespie-type KMC simulations of the whole master equation. Figure 5.3 shows the stationary probability distribution $G_{st}(\theta_{CO})$ in the bistable and monostable regions. Red solid lines correspond to Eq. 5.10 and blue dashed lines correspond to simulations of the whole system by using the Gillespie stochastic algorithm. Figures 5.3(a) and 5.3(c) show the probability distribution function in the monostable reactive and inactive regions with low and high θ_{CO} , respectively. On the other hand, Fig. 5.3(b) shows the same probability distribution in the bistable region where the two regimes coexist. The agreement between both, the analytical theory and the simulation is reasonably good.

5.3.2 Critical fluctuations

At this point, let us return to the deterministic phase diagram (p_{CO}, d) in Fig. 4.2, close to the critical point d_c . It is known from the theory of fluctuations in nonequilibrium systems that long-range correlations between macroscopic fluctuations emerge in the vicinity of and below the critical point of a nonequilibrium instability. As a consequence, the amplitude of fluctuations rises near this point [79].

In Fig. 5.4(a), the stationary probability distribution obtained from the theoretical adiabatic elimination is shown for a set of parameters where the two stable stationary states possess the same probability. For parameters well apart from the cusp bifurcation, both extrema are well separated by a minimum. This reflects the deterministic behavior. Close to the critical point, where the two stable stationary points and the unstable one merge, the fluctuations increase. Consequently, transitions between the reactive and inactive stable state take place.

This theoretical result of what happens near the critical point can be compared with simulations of the whole system by using the Gillespie algorithm. For this purpose, Fig. 5.4 also shows a sequence of time series for θ_{CO} . These data were taken, choosing p_{CO} near the midpoint of the bistable region, for various d approaching the critical point $d_c \approx 0.0048$.

Starting with initial conditions near the stable stationary state at low θ_{CO} and small d , the amplitude of fluctuations is insufficient for inducing transitions from the reactive to the inactive state and the low θ_{CO} persists in time, see Fig. 5.4(b). For $d \approx 0.04$, as shown in Fig. 5.4(c), transitions between the two states occur. The transition time between two states is rather long compared to the relaxation time τ_{rel} necessary to reach one stable state given an initial condition in the domain of attraction of this state. Closer to the critical point, transitions between the stable states become more frequent and one

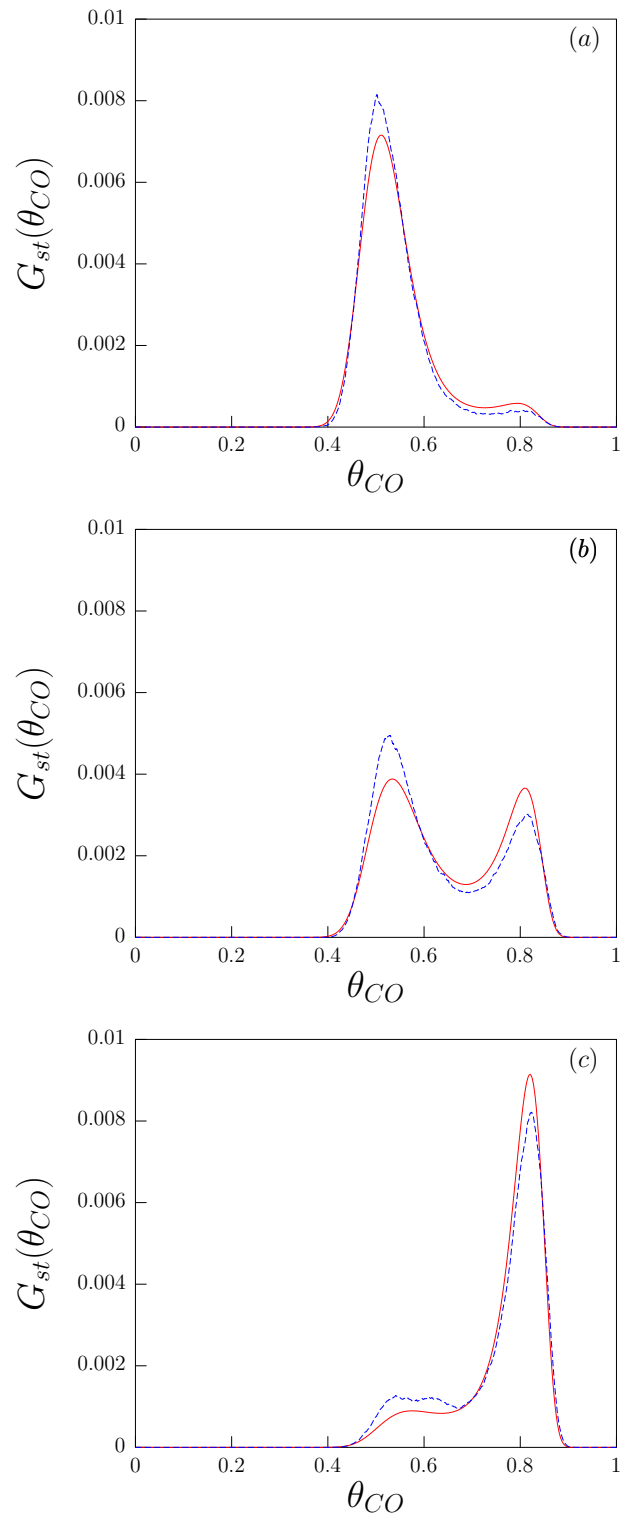


Figure 5.3: Theoretical stationary probability distribution versus probability distribution from the whole system by Gillespie-type simulations. The solid lines are theoretical results. The dashed lines are the stochastic simulations. In all Figures $d = 0.040$, and $A = 1000$. (a) $p_{CO} = 0.3840$; (b) $p_{CO} = 0.38645$; (c) $p_{CO} = 0.3890$.

is unable to distinguish between two states, see Fig. 5.4(*d*).

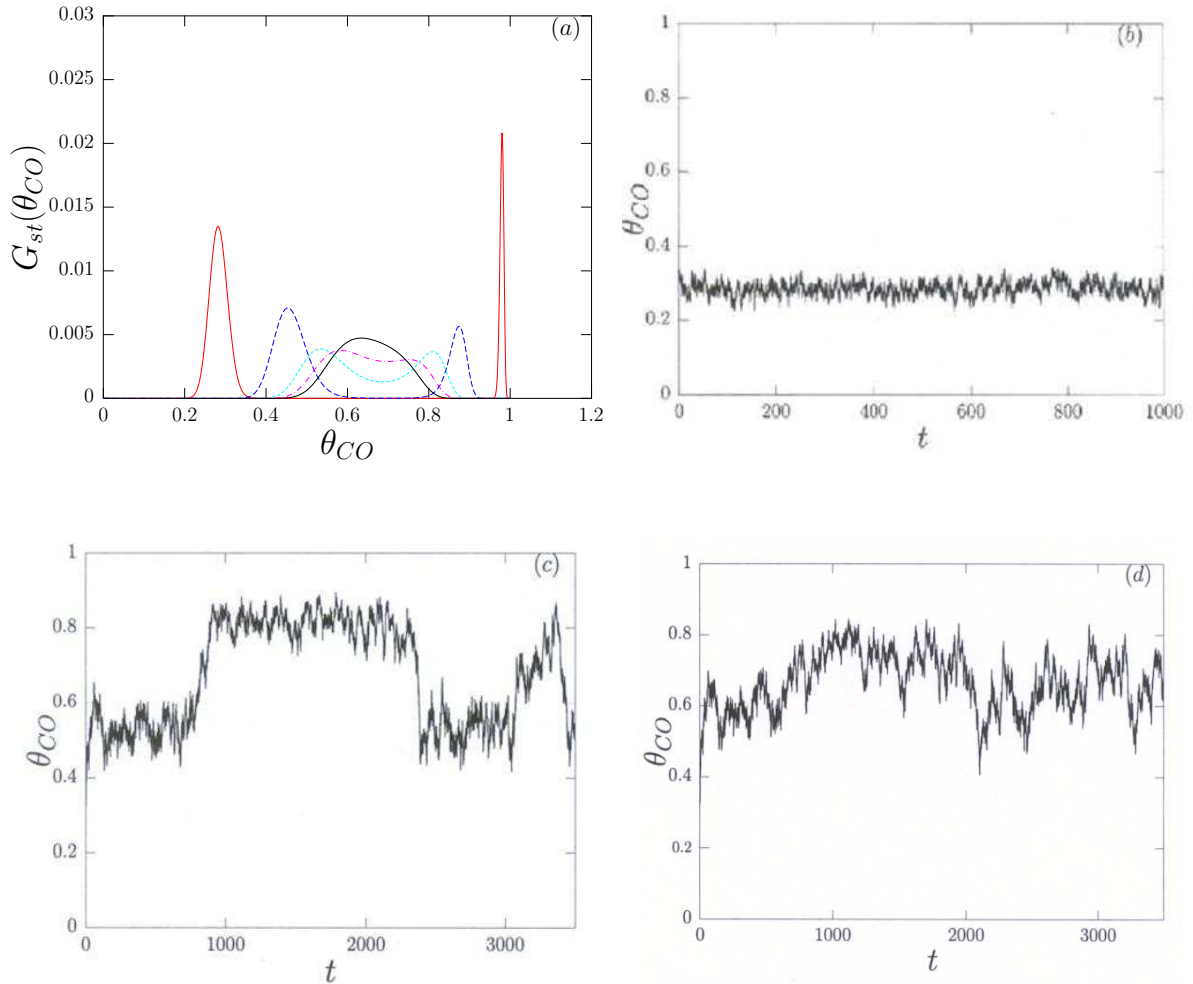


Figure 5.4: (Color online) Influence of the distance to the critical point on the fluctuations. (a) Stationary probability distribution from the theory, with (d, p_{CO}) equals to $(0.0050, 0.296)$ [red solid line]; $(0.030, 0.367)$ [dashed line]; $(0.04, 0.38645)$ [dotted line]; $(0.045, 0.0395)$ [dashed-dotted line]; $(0.048, 0.040)$ [black solid line]. (b) Time series from simulations of the whole system, corresponding to $(0.0050, 0.296)$ where no transition occurs within the simulation time. (c) The same than (b) but with $(0.04, 0.38645)$ and transitions between the two states occur at time scales larger than the relaxation time. (d) Finally, $(0.048, 0.040)$ close to the critical point, where one cannot distinguish between two stable states. The only fixed parameter is $A=1000$.

5.3.3 The dependence of fluctuations on the system size

Fluctuations in a finite volume depend on the size of this volume (internal fluctuations). Figure 5.5(a) shows the stationary probability distribution for N_{CO} molecules in the coverage space, which is calculated from the theory as a function of the system size. One is able to see the tendency of bistability to vanish depending on the number of adsorption sites A . The stationary distribution for $A = 20$ is nearly monomodal with two new small peaks induced by noise, which means noise-induced shifts of the stable stationary states, whereas bimodality with two well separated maxima starts to develop if $A \geq 200$.

Figures 5.5(b) - 5.5(d) show the corresponding time series. Decreasing the surface area and, correspondingly, the number of reactants, the transitions between the stable states are becoming more frequent and all possible coverages are populated with nonvanishing probability. For a small surface are the trajectories fluctuate around a common coverage.

5.4 Transition between stable states

From the previous sections we know that catalytic CO oxidation on a nanoscale surface undergoes transitions between the reactive and the inactive stationary states if the system is near a critical point, and if the number of adsorption sites is small. A question arises: how long does it take for a system to go from the reactive to the inactive state and vice-versa?

We will consider two intrinsic time scales. The macroscopic scale, where one observes macroscopic transitions between the two stable stationary states, and the short time scale or the relaxation time τ_{rel} , necessary to reach a stable stationary state given an initial condition inside the domain of attraction of this stable state. These scales are clearly distinct provided that the stationary distribution around the stationary state is narrow compared to the distance to the unstable state.

Declaring N_{CO}^a , N_{CO}^b , and N_{CO}^c as the particle numbers of the reactive, unstable saddle point and inactive states, respectively, the macroscopic transition times can be calculated according to [74, 95, 139, 140, 141, 142]

$$T^{ac}(N_{CO}) = \sum_{N_{CO}=N_{CO}^a}^{N_{CO}^c-1} \frac{\sum_{m=0}^{N_{CO}} G_{st}(m)}{\tilde{W}_1(N_{CO})G_{st}(N_{CO})}, \quad (5.11)$$

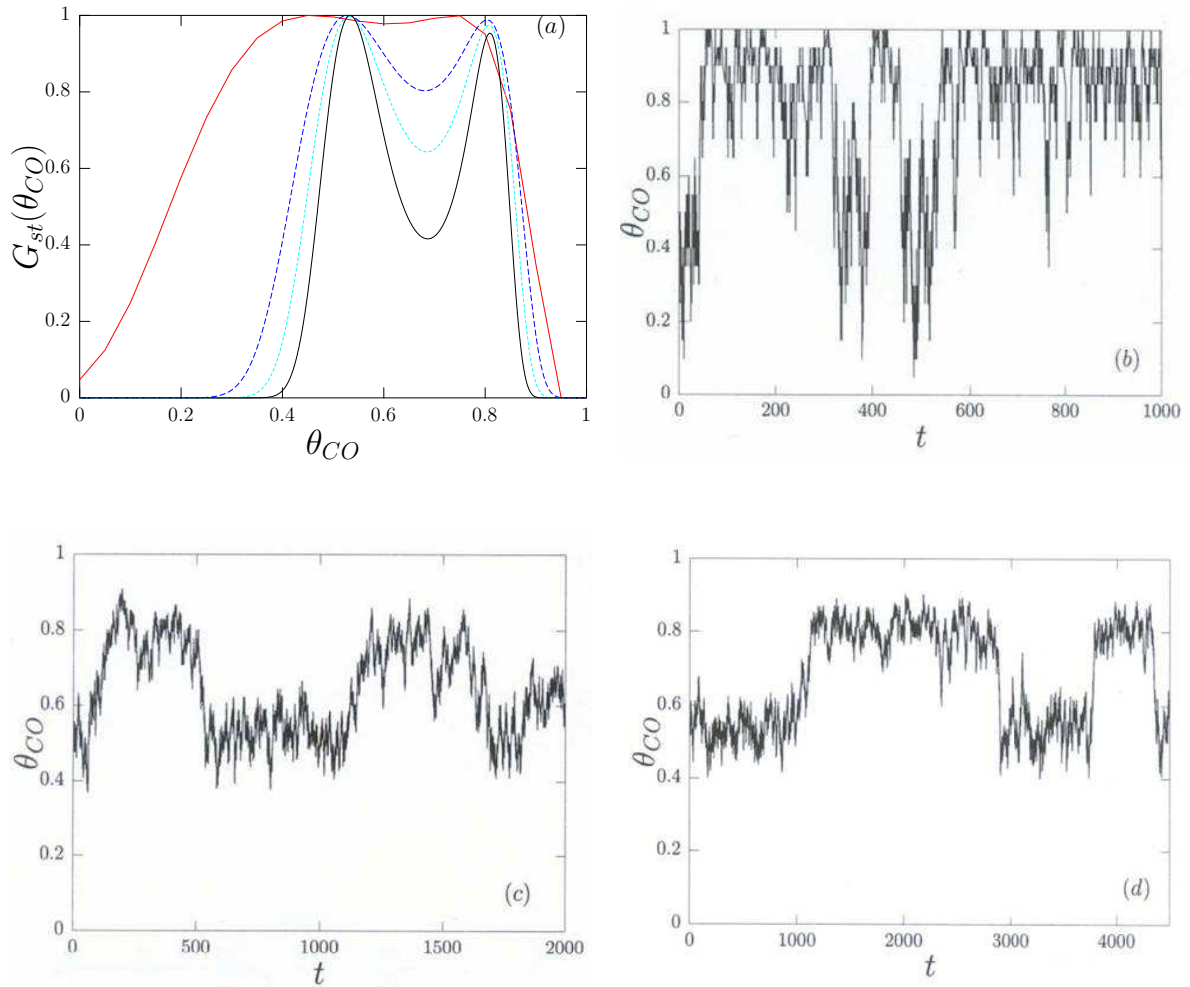


Figure 5.5: (Color online) Influence of the surface area on the fluctuations. (a) Theoretical stationary probability distribution inside the deterministically bistable region adjusted to have the same height of maxima with $A = 20$ (red solid line), 200 (dashed line), 400 (dotted line), and 800 (black solid line). For $A = 20$ one observes noise-induced shifts of the stable stationary states and a nearly monomodal distribution. The bistability is reflected by two separated maxima. This is observed if approximately $A \geq 200$. (b) The time series of the simulations of the whole system, corresponding to $A = 20$ shows large fluctuations. (c) Same as in (b) but with $A = 400$. Here, for this situation one is able to distinguish between two preferred coverage and two time scale. (d) Finally, this behaviour becomes more pronounced if $A = 800$. The CO pressure and the desorption are constant at $p_{CO} = 0.38645$ and $d = 0.04$.

the corresponding time back with

$$T^{ca}(N_{CO}) = \sum_{N_{CO}=N_{CO_c}+1}^{N_{CO}^a} \frac{\sum_{m=N_{CO}}^{\infty} G_{st}(m)}{\tilde{W}_2(N_{CO})G_{st}(N_{CO})}. \quad (5.12)$$

Figure 5.6 shows the mean transition times from Eq. (5.11) and from the simulations of the whole system. Figure 5.6(a) shows the time required to go from N_{CO}^a to N_{CO}^c as function of p_{CO} through the bistable region. Parameters give $N_{CO}^a = 525$ and $N_{CO}^c = 825$ for the stable attractors in the bistable region with $A = 1000$.

Lets first choose p_{CO} to be in the monostable reactive region of low CO coverage. For an initial state $N_{CO}^a = 525$ the mean time T_1^{ac} to do a fluctuation which ends in $N_{CO}^c = 825$ is very long. In other words, the probability of a jump is very low corresponding to Fig. 5.4(a). In the second case, where p_{CO} is in the monostable inactive region, $N_{CO}^a = 525$ is a state with low probability (see Fig. 5.4(c)), and the mean time T_2^{ac} in Fig. 5.6(a) is short because the high persistence of this inactive behavior with a large number of N_{CO}^c molecules. The calculated time in this inactive region gives a good approximation of the relaxation time necessary to reach this inactive stationary state. In the bistable region, we have transition times in between the two times above mentioned.

We introduce a potential as

$$G_{st}(\theta_{CO}) = N \exp(-A \phi(\theta_{CO})), \quad (5.13)$$

with intensive rates $m(\theta_{CO}) = \tilde{W}_2/A$ and $w(\theta_{CO}) = \tilde{W}_1/A$, and with coverage $\theta_{CO} = N_{CO}/A$ inserted yielding

$$\phi(\theta_{CO}) = \int^{\theta_{CO}} d\theta'_{CO} \ln\left(\frac{m(\theta'_{CO})}{w(\theta'_{CO})}\right), \quad (5.14)$$

we cross to an intensive description.

The time for a transition can be discussed by means of the effective potential barrier

$$\Delta\phi = \phi(\theta_{CO}^b) - \phi(\theta_{CO}^a). \quad (5.15)$$

This stochastic potential is the difference in values of $\phi(\theta_{CO})$ between the unstable saddle point θ_{CO}^b and the two local minima $\theta_{CO}^{a,b}$ corresponding to the reactive and inactive state.

The higher the potential barrier which has to be overcome for an escape between the

stable stationary states, the longer is the transition time. Note, that the mean time $T(N_{CO}^a \rightarrow N_{CO}^c)$ can be different to the reverse mean time $T(N_{CO}^c \rightarrow N_{CO}^a)$. It is also possible to calculate the mean transition times for a set of parameters p_{CO} and d along the line where the two stable states possess the same probability. Figure 5.6(b) shows the transition times for parameters in this line. In this situation the back- and forward transition times are the same. Approaching the critical point, the macroscopic

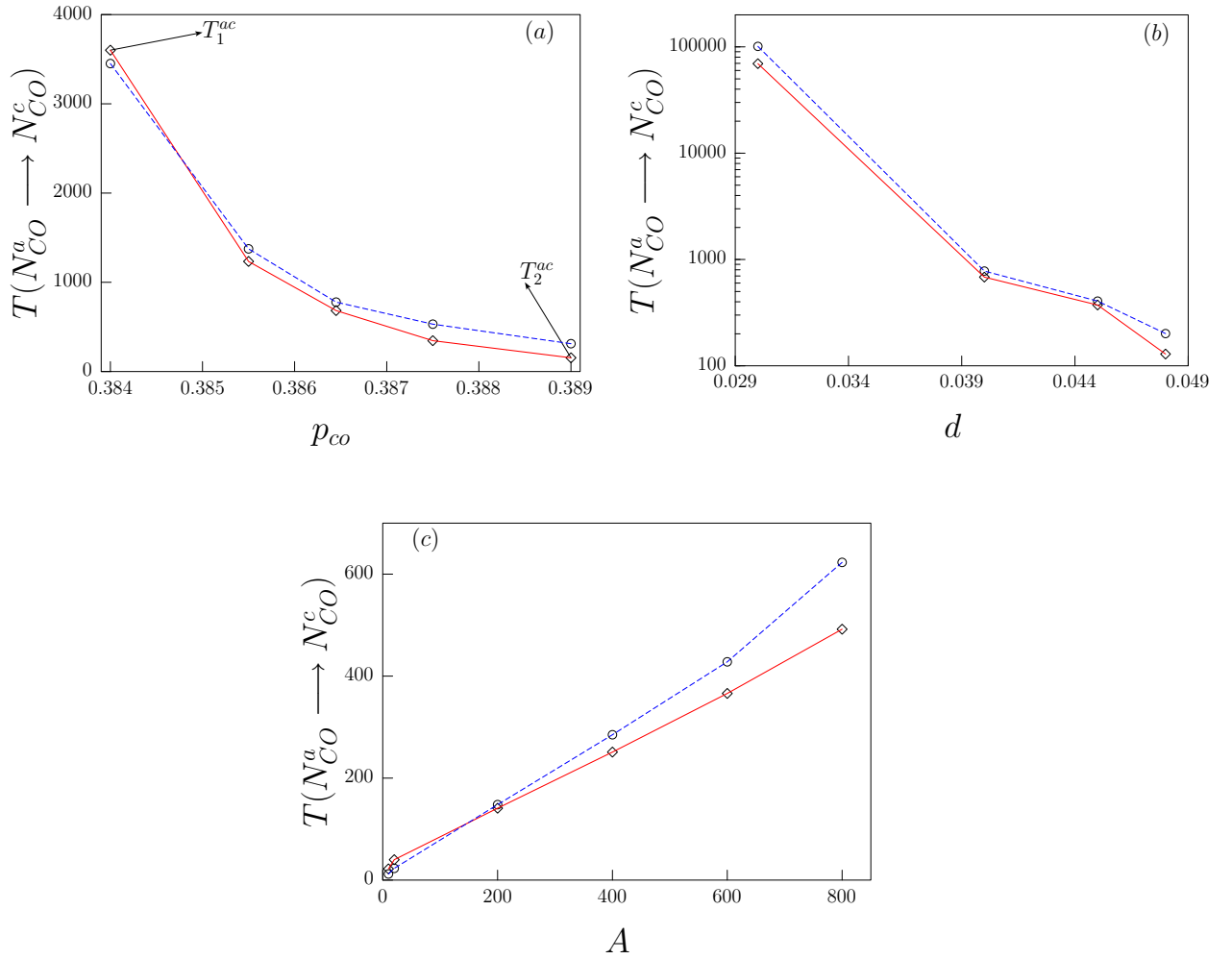


Figure 5.6: (a) Transition time $T(N_{CO}^a = 525 \rightarrow N_{CO}^c = 825)$ for varying p_{CO} through the bistable region with $d = 0.04$ and $A = 1000$. (b) Transition time in function of the desorption d and pressure p_{CO} for adsorption sites $A = 1000$. (c) Transition time in function of A for $p_{CO} = 0.38645$, and $d = 0.040$. Solid line corresponds to Eq. (5.11), and dashed line to stochastic simulations of the whole system.

transitions increase, and the transition times become smaller. Note, that this figure shows also simulations of mean transition times from the whole system.

The system size has also an impact on the transition times. For small internal noise, i.e. larger reaction surfaces, both peaks are well separated, and the transition time may be estimated by a saddle approximation with two Gaussians [3, 95].

$$T^{ac}(N_{CO}) \propto \frac{4\pi e^A \left(\phi(\theta_{CO}^b) - \phi(\theta_{CO}^a) \right)}{\left(m(\theta_{CO}^b) + w(\theta_{CO}^b) \right) A} \times \frac{1}{\left(\left| d^2\phi(\theta_{CO}^b)/d\theta_{CO}^2 \right| d^2\phi(\theta_{CO}^a)/d\theta_{CO}^2 \right)^{1/2}}. \quad (5.16)$$

Obviously, we find in the case of a large system size

$$T^{ac}(N_{CO}) \propto e^A \left(\phi(\theta_{CO}^b) - \phi(\theta_{CO}^a) \right) \xrightarrow{A \rightarrow \infty} \infty, \quad (5.17)$$

since the Arrhenius factor increases unlimited with larger surface area (number of adsorption sites). Hence, the transition time diverges yielding bistability.

In the case of a small number of adsorption sites, the amplitude of fluctuations increases, and the stationary probability distribution becomes more and more uniform. We might neglect their impact on the transition times in the sum Eq. (5.11). It results in the scaling

$$T^{ac}(N_{CO}) \propto \frac{A}{\tilde{W}_1(N_{CO})} \xrightarrow{A \rightarrow 0} \tau_{rel}. \quad (5.18)$$

This means that the time becomes short due to the rapid increase of diffusion over the drift. Consequently, the internal noise enhances the transitions and the transition time becomes comparable to the relaxation time [143]. Corresponding analytic results from the adiabatic elimination by using Eq. (5.11) is compared with simulations using the Gillespie algorithm in Fig. 5.6(c). For sufficiently small A the time scale separation between transition and relaxation times is tenuous.

Figure. 5.7 shows the transition time $T(N_{CO}^a = 525 \rightarrow N_{CO}^c = 825)$ and the relaxation time $T(N_{CO}^o = 0 \rightarrow N_{CO}^a = 525) = \tau_{rel}$ as function of the number of adsorption sites by using Eq. (5.11) [95, 143]. The transition time is approaching the relaxation time. We can estimate the relaxation time by reasoning as follows. The evolution equation for the mean of the birth-death Markov process $N_{CO}(t)$ reads

$$\frac{d\langle N_{CO}(t) \rangle}{dt} = \langle \tilde{W}_1(N_{CO}(t)) - \tilde{W}_2(N_{CO}(t)) \rangle \approx \langle \gamma(N_{CO}(t)) \rangle. \quad (5.19)$$

Expanding $\gamma(N_{CO})$ in a Taylor series about the stable state N_{CO}^{st} , and assuming that we can confine our attention to a region around N_{CO}^{st} that is small enough that

$$\frac{d\langle N_{CO} \rangle}{dt} \approx \left\langle \gamma(N_{CO}^{st}) + \gamma'(N_{CO}^{st})[N_{CO}(t) - N_{CO}^{st}] \right\rangle = \gamma'(N_{CO}^{st})[\langle N_{CO}(t) \rangle - N_{CO}^{st}]. \quad (5.20)$$

Setting $u(t) = \langle N_{CO}(t) \rangle - N_{CO}^{st}$, we see that

$$\frac{du(t)}{dt} \approx \gamma'(N_{CO}^{st})u(t). \quad (5.21)$$

The solution of this differential equation is $u(t) \approx u(0)\exp[\gamma'(N_{CO}^{st})t]$; therefore,

$$\langle N_{CO} \rangle \approx N_{CO}^{st} + [N_{CO}(0) - N_{CO}^{st}]\exp[\gamma'(N_{CO}^{st})t]. \quad (5.22)$$

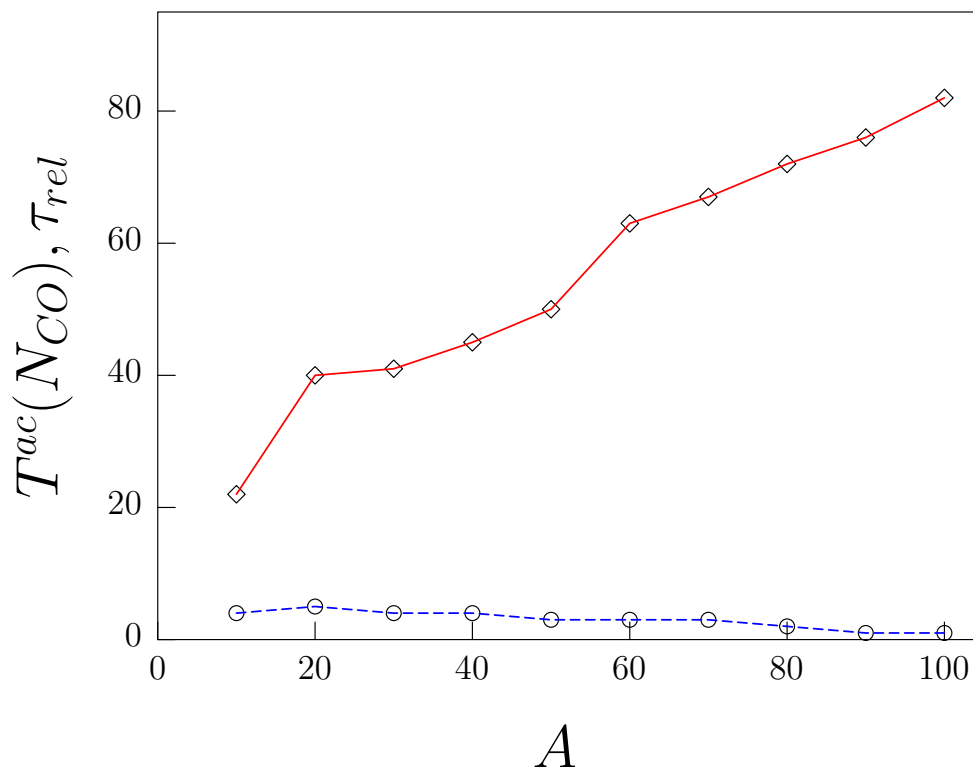


Figure 5.7: Transition time and relaxation time as a function of the size A of the catalytic area. (a) Transition time $T^{ac}(N_{CO})$ (solid line), and relaxation time τ_{rel} (dashed line) for small reacting surfaces with $p_{CO} = 0.38645$ and $d = 0.04$. Both lines were obtained using Eq. (5.11). The two time scales tend to merge for small values of A .

Recalling that $\gamma'(N_{CO}^{st}) < 0$, we conclude that $\langle N_{CO}(t) \rangle$ relaxes to $\langle N_{CO}(\infty) \rangle \approx N_{CO}^{st}$ in a time of order

$$\tau_{rel} \approx \frac{1}{-\gamma'(N_{CO}^{st})}, \quad (5.23)$$

where

$$\gamma(N_{CO}) = p_{CO}(A - N_{CO} - \langle N_O \rangle) - dN_{CO} - \frac{4N_{CO} \langle N_O \rangle}{(A - \langle N_O \rangle)}. \quad (5.24)$$

Using the following approximation (see Fig. 4.3)

$$\frac{d \langle N_O \rangle}{dN_{CO}} \approx 0, \quad (5.25)$$

one obtains

$$\gamma'(N_{CO}^{st}) \approx -p_{CO} - d - \frac{4 \langle N_O \rangle^{st}}{(A - \langle N_O \rangle^{st})}. \quad (5.26)$$

If the fluctuations are small and transitions between stable states are not allowed, this time can be taken as a reasonable estimate of the relaxation time. For example, if the stable state for $A = 1000$ is ($N_{CO}^{st} = 525$, $N_O^{st} = 65$) and the parameters of Fig. 5.7 are used, we obtain for the relaxation time $\tau_{rel} \approx 1.42$. Note that the relaxation time does not depend on A .

5.5 Summary and conclusions

Here, we have presented a theoretical framework for the stochastic bistable behavior observed in catalytic CO oxidation over a Pt field emitter tip and Pd nanoparticles. We consider low pressure conditions, therefore internal fluctuations are taken into account by a mean-field birth-death type master equation. This master equation is reduced after adiabatic elimination of one variable (namely oxygen). The reduction allows the estimation of transition times and probability distributions of adsorbed CO as a function of external parameters and system size.

We found that the fluctuations of the coverage become significant for reaction parameters approaching the critical point and for surface areas of nanoscale dimensions. As a consequence of large fluctuations, the probability distribution becomes monomodal and transitions between the stable stationary states occur on a small time scale. Finally, the macroscopic transition times are no longer separated well from the relaxation times as they do for larger surface areas and far away from the critical point. These theoretical predictions derived from the one component model have been found to be in reasonable agreement with a stochastic simulation of the whole system by the Gillespie algorithm.

At high pressure we expect also to observe fluctuation-induced transitions in CO oxidation. In order to adapt the model to such situation, we need to take into account a local description of fluctuations. This different treatment of fluctuations will be discussed in next chapter.

Chapter 6

Fluctuations and first-order phase transitions

"Science, viewed as a search for understanding the grand universe in which we find ourselves, forms a basic on which scientists can and should develop a moral vision."

Joel L. Lebowitz (1930)

6.1 Introduction

The area, in which the reactants in catalytic CO oxidation can be considered as well mixed and which therefore can be represented by a single ordinary differential equation (ODE), is given by the diffusion length of CO. On an extended single crystal surface this area is macroscopic at low pressure, but with increasing pressure the area may become smaller. The number of gas particles impinging per second on the surfaces grows proportional to the pressure and therefore the surface residence time τ of the adsorbate decreases with increasing pressure. Simultaneously the total adsorbate coverage will approach saturation limit, and since surface diffusion requires vacant sites, the diffusion rate will become very low. Since the diffusion length is given roughly by $\sqrt{\tau D_{CO}}$ the combined effect will lead to a smaller and smaller diffusion length with increasing pressure (D_{CO} is the diffusivity). Stochastic patterns ('raindrop patterns') observed in catalytic CO oxidation on Pt(110) at 10^{-2} mbar were interpreted in this way and simulations incorporating stochastic elements were able to reproduce this finding [47].

Here we propose the following approach to model the stochasticity of catalytic CO oxidation at high pressure on an extended surface. We envision the surface as being composed of an array of small compartments with identical properties inside which the adsorbates are well mixed [52, 53]. These compartments are coupled via CO diffusion. Inside each cell the diffusion is assumed to be infinitely fast and therefore each cell is represented by an ODE, which describes the bistability of the reactive system but also allows for fluctuations. The whole array of cells is represented by a reaction-diffusion master equation (RDME) which permits local fluctuations. This equation describes the evolution of the probability distribution function (PDF) for the number of adsorbed molecules. One disadvantage of this RDME is that an analytical solution is not available in general [144]. Nevertheless, this problem can be solved in part by introducing appropriate approximations. Here, we use the mean-field approach and the adiabatic elimination of fast variables.

With these two approximations, we are able to solve the RDME. These methods allow us to obtain a reduced RDME and to get theoretical expressions for the PDF of the CO coverage. In this way we can construct the phase diagram of the model as predicted by the mean-field approximation. This allows us to study the dynamic behaviour of the system depending on the cell size and on the coupling parameter between cells. We show a first-order phase transition which is characterised by an ordered symmetry-breaking state [145]. It is reflected by an abrupt change in the order parameter depending on the strength of internal fluctuations and the coupling parameter. This transition is induced by the interplay of internal fluctuations and diffusion.

6.2 Stochastic reaction-diffusion model

We use the Langmuir-Hinshelwood mechanism of previous chapters. On a macroscopically large Pt surface the reaction sequence shown above produces bistability. Two stable kinetic stationary states coexist on the parameter region of bistability. Without fluctuations the macroscopic rate laws predict that the system resides on one of two stationary stable states for an infinite period of time. Decreasing the surface size to nanoscale dimensions, fluctuations in the particle number increase and transitions between the two stable states are now possible.

However, in order to study stochastic effects under conditions of relative high pressure, a surface is divided into a square lattice of cells, which are at the same time regarded as well mixed and therefore are chosen to be smaller than the diffusion length. Each small cell is represented as a $L \times L = A$ square grid of adsorption sites and the reaction is described

using the traditional eight site model which was first introduced by James *et al.* [102]. Because we are working on a perfect single crystal surface, the cells exhibit equal catalytic activity (e.g, identical sticking coefficients). The model incorporates the following steps:

i) CO(gas) adsorbs onto single empty sites at rate p_{CO} . CO(ads) hops very rapidly to other empty sites on the cell. We consider below the case of infinitely mobile CO(ads) inside each cell [91, 102], and neglect energetic interactions between CO(ads) and other CO(ads) and O(ads) adparticles. This feature is important in order to produce the bistability observed in experiments. The distribution of CO(ads) on sites not occupied by O(ads) is random. CO(ads) desorbs from the surface at a rate d . The parameter d corresponds to the temperature in experiments, because CO desorption is the strongest activated step in the Langmuir-Hinshelwood (LH) sequence.

ii) O₂(gas) adsorbs dissociatively at diagonal nearest-neighbour (NN) empty sites at a rate proportional to p_{O_2} , provided that the additional six sites adjacent to these sites are not occupied by O(ads). This "eight-site rule" reflects the very strong NN O(ads)-O(ads) repulsion of the (2×2) superlattice ordering [111]. O(ads) is immobile in the T-range considered here due its large bonding energy, and it also cannot desorb.

iii) Each adjacent pair of CO(ads) and O(ads) can react at rate k to form CO₂, which is immediately released into the gas phase.

Here we are interested in high pressure conditions. The cells have to be well-mixed and their size at high pressure has to be chosen therefore to be of nanoscale dimensions. Consequently the deterministic description breaks down and stochastic effects become relevant. A major change concerns the treatment of CO diffusion between cells. To study this type of diffusion we adopted a similar model developed by Pavlenko *et al.* in the context of CO oxidation on nanoscale Pt facets [146]. In contrast to our case the facets there exhibited different orientations and hence a different reactivity.

iv) CO(ads) can diffuse at a finite rate from each cell to empty sites on the adjacent cells. CO(ads) would hop across a common imaginary edge of length $L = \sqrt{A}$ to adjacent empty sites at rate h (microscopic hop rate or coupling parameter). The diffusion is mimicked by the transition of CO(ads) from one cell to another at rate (in molecules per unit time) $h'N_{CO,i}$ times the probability that a site is empty in the other cells, where $h' = h/L$.

We choose $p_{CO} + p_{O_2} = k = 1$, which sets the time scale. Finally, the system is controlled by the partial pressure p_{CO} , the desorption rate d , the coupling parameter h , and the number of adsorption sites A . The model is still simplistic. It does not support oscillatory kinetics, but it describes the bistability observed in experiment [134, 135, 147, 148].

When $h = 0$, previous studies using KMC and ODE reveal bistability in this model for $d < d_C$, where d_C corresponds to a cusp bifurcation point. Two stable kinetic stationary states coexist in parameter space for a range of $p_{CO}^- < p_{CO} < p_{CO}^+$. On the active stationary state the surface is predominantly oxygen covered. On the inactive stationary state a high CO coverage inhibits O₂ adsorption and hence poisons the reaction. These stable states are connected by an unstable state producing an S-shaped plot of steady state coverage versus p_{CO} . For this model the critical parameters are $d_C = 0.048$ and $p_{CO}^C = 0.40$ [115]. Here, we use the multistable behaviour described above as prototype of bistability inside each cell.

6.3 Reaction-diffusion master equation

The master equation describes the PDF of populations in a chemical reaction [3, 4]. Normally, these master equations consider a global description of fluctuations in the sense that the system is treated as if it remained homogeneous. Of course, this description breaks down if we consider high pressure conditions. To obtain an adequate master equation formulation of the reaction diffusion system for CO oxidation, the cells of side length L are considered as well mixed and smaller than the diffusion length. We assume infinite diffusion of CO molecules inside a cell, and diffusion events between cells are considered to be much more frequent than chemical reactions. The state of the system is described by the probability distribution $P(N_{CO,i}, N_{O,i}; t)$ of finding a set of populations $\tilde{\mathbf{Z}} = \{N_{CO,i}, N_{O,i}\}$, with $i = 1, \dots, M$ denoted the number of cells. Finally the PDF is governed by the following RDME [149, 150, 151, 152, 153]:

$$\frac{dP(\tilde{\mathbf{Z}}; t)}{dt} = \frac{dP^{reac}}{dt} + \frac{dP^{diff}}{dt}. \quad (6.1)$$

The reaction and diffusion terms of this equation will be derived in next subsections.

6.3.1 Reaction jump Markov process

The transition rates $W_\rho^i(N_{CO,i}, N_{O,i})$ and population changes of the particle number of carbon monoxide ($N_{CO,i}$) and oxygen ($N_{O,i}$) inside each cell are shown in Table. (6.1):

We require, $0 < N_{CO,i} + N_{O,i} \leq A$, where a small number of adsorption sites A produces high coverage fluctuations. The term $N_{CO,i}/(A - N_{O,i})$ in $W_4^i(N_{CO,i}, N_{O,i})$ assumes that inside a cell each site adjacent to an O(ads) is occupied randomly by CO(ads).

| Reaction step | Transition probability |
|---|--|
| CO _{gas} – Adsorption | $W_1^i(N_{CO,i}/N_{CO,i} - 1) = p_{CO}(A - N_{CO,i} - N_{O,i})$ |
| CO _{ads} – Desorption | $W_2^i(N_{CO,i}/N_{CO,i} - 1) = dN_{CO,i}$ |
| O _{2, gas} – Adsorption | $W_3^i(N_{O,i}/N_{O,i} + 2) = 2p_{O_2}S_A^i(N_{CO,i}, N_{O,i}, A)$ |
| CO _{ads} – O _{ads} – Reaction | $W_4^i(N_{CO,i}, N_{O,i}/N_{CO,i} - 1, N_{O,i} - 1) = \frac{4kN_{O,i}N_{CO,i}}{(A - N_{O,i})}$ |

Table 6.1: Transition probabilities for CO oxidation on unreconstructed noble metal surfaces.

$S_A^i(N_{CO,i}, N_{O,i}, A)$ is the normalized sticking probability for oxygen, *i.e.*, the probability of finding two next NN empty sites with all six NN not occupied by oxygen (eight site rule). This term can be written as

$$S_A^i(N_{CO,i}, N_{O,i}, A) = A \frac{(A - N_{CO,i} - N_{O,i})^2 (A - 2N_{O,i})^8}{(A - N_{O,i})^{10}}. \quad (6.2)$$

Like in previous works, the reaction part of the more general RDME is expressed in the following way

$$\frac{d}{dt}P(\tilde{\mathbf{Z}}; t) = \sum_{\rho=1}^4 [W_\rho(\tilde{\mathbf{Z}} - \mathbf{v}_\rho/\tilde{\mathbf{Z}})P(\tilde{\mathbf{Z}} - \mathbf{v}_\rho; t) - W_\rho(\tilde{\mathbf{Z}}/\tilde{\mathbf{Z}} - \mathbf{v}_\rho)P(\tilde{\mathbf{Z}}; t)]. \quad (6.3)$$

where the vectors $\mathbf{v}_\rho = \left\{ v_\rho^n \right\}_{n=1}^2$ are the stoichiometric vectors. It can be shown that in the macroscopic limit of large reacting surfaces and at low pressures, this master equation reproduces the deterministic predictions [51].

6.3.2 Diffusion random walk

In order to model diffusion we assume that each absorbed CO molecule can do a random walk between adjacent cells. Like the reaction part, one can construct the transition probabilities for diffusion[150]. Table. (6.2) shows these transition probabilities.

| Reaction step | Transition probability |
|--------------------------------------|---|
| CO _{ads} (loss) – diffusion | $W_5^i(N_{CO,i}/N_{CO,i} - 1) = \frac{h'}{2s} N_{CO,i} \sum_l (1 - \theta_{CO,i+l} - \theta_{O,i+l})$ |
| CO _{ads} (gain) – diffusion | $W_6^i(N_{CO,i}/N_{CO,i} + 1) = \frac{h'}{2s} (1 - \theta_{CO,i} - \theta_{O,i}) \sum_l N_{CO,i+l}$ |

Table 6.2: Transition probabilities for CO diffusion from cell i to nearest-neighbor cells.

The sum l runs over the nearest neighbours of the cell i , and s represents the space dimension. In our case $s = 2$. $\theta_{CO,i}$ and $\theta_{O,i}$ are $N_{CO,i}/A$ and $N_{O,i}/A$, respectively. The factors in $W_5^i(N_{CO,i}/N_{CO,i} - 1)$ simply represent the transition of CO(ads) from one cell to another at a rate $h'N_{CO,i}$ times the probability that a site is empty in the first nearest neighbour cells, where $h' = h/L$. $W_6^i(N_{CO,i}/N_{CO,i} + 1)$ is interpreted in the same way. Now one can write the diffusion term of the RDME as:

$$\frac{dP^{diff}}{dt} = \sum_{i=1}^M \sum_{\rho=5}^6 [W_\rho^i(N_{CO,i}-1/N_{CO,i})P(N_{CO,i}-1, N_{CO,i+l}+1; t) - W_\rho^i(N_{CO,i})P(N_{CO,i}; t)]. \quad (6.4)$$

Notice that, as cell area is increased, we have less and less effect from diffusion. In the same way the diffusion dominates over the reaction part for small areas. This interplay between diffusion and reaction is a direct consequence of the reaction and diffusion transition probabilities which depend on L in different ways.

The coarse-grained description of our RDME is valid when CO molecules inside each cell are considered to be candidates for a reactive collision, and if the diffusion between cells occurs much more frequently than chemical reactions. This description provides a simple generalisation of deterministic reaction diffusion equations. If one is interested in stochastic effects, it is also possible to consider a reaction-diffusion Langevin equation (a deterministic reaction-diffusion equation plus a random term) which can be derived directly from the stochastic discrete model [150]. However, contrary to the Langevin approach, the RDME used here provides a mechanistic view of the dynamics at molecular level [3].

6.4 Mean-field approximation (MFA)

We begin with considering the traditional mean-field approach from the theory of equilibrium critical phenomena [149, 154, 155, 156]. In analogy with many-body theory one can expect that each cell in this approximation would interact with an averaged environment. It is well known that mean field theory gives a rough qualitative picture of the phase transition in systems of lower dimensionality, but it is not quantitatively correct. Nevertheless, we expect from the wealth of experience in equilibrium phase transitions that mean field theories will be essentially exact in four or more dimensions [157]. In this approximation, one neglects the correlation between neighbouring cells. Basically, the nearest-neighbour interaction is replaced by a global interaction through an average field. Here, $\frac{1}{2s} \sum_l (1 - \theta_{CO,i+l} - \theta_{O,i+l})$ and $\frac{1}{2s} \sum_l N_{CO,i+l}$ are replaced with $\frac{1}{M-1} \sum_{j=1, j \neq i}^M (1 - \theta_{CO,j} - \theta_{O,j})$ and $\frac{1}{M-1} \sum_{j=1, j \neq i}^M N_{CO,j}$, respectively. The cells are supposed to interact all to all throughout the global coupling.

If one considers the case that the number of cells, M , goes to infinity, one can postulate:

$$\lim_{M \rightarrow \infty} \frac{1}{M-1} \sum_{j=1, j \neq i}^M (1 - \theta_{CO,j} - \theta_{O,j}) = (1 - \theta_{CO}^m - \theta_O), \quad (6.5)$$

$$\lim_{M \rightarrow \infty} \frac{1}{M-1} \sum_{j=1, j \neq i}^M N_{CO,j} = N_{CO}^m. \quad (6.6)$$

In this limit fluctuations disappear in the averages and the cells have identical evolution with transition probabilities given in Table. (6.3).

Because oxygen does not diffuse and the sticking probability is identical in all cells, we eliminate the index i from $N_{O,i}$. We also introduce the order parameter $N_{CO}^m = A\theta_{CO}^m$, which is defined by the self-consistent equation

$$\beta(N_{CO}^m) = N_{CO}^m = \sum_{N_{CO}, N_O} N_{CO} P^{st}(N_{CO}, N_O, N_{CO}^m). \quad (6.7)$$

Note that $N_{CO}^m = A\theta_{CO}^m$ is the average value of CO molecules inside each cell. This first moment or mean value is an order parameter that determines the occurrence of a phase transition. The multiple solutions of this complicated equation reflect the possibility of bifurcations that break the ergodicity associated with the presence of a true phase transition [154]. Finally, we have a mean field coupling master equation (MFCME) without

| Reaction step | Transition probability |
|--|---|
| $\text{CO}_{\text{gas}} - \text{Adsorption}$ | $W_1(N_{\text{CO}}/N_{\text{CO}} + 1) = p_{\text{CO}}(A - N_{\text{CO}} - N_{\text{O}})$ |
| $\text{CO}_{\text{ads}} - \text{Desorption}$ | $W_2(N_{\text{CO}}/N_{\text{CO}} - 1) = dN_{\text{CO}}$ |
| $\text{O}_{2,\text{gas}} - \text{Adsorption}$ | $W_3(N_{\text{O}}/N_{\text{O}} + 2) = 2p_{\text{O}_2}S_A(N_{\text{CO}}, N_{\text{O}}, A)$ |
| $\text{CO}_{\text{ads}} - \text{O}_{\text{ads}} - \text{Reaction}$ | $W_4(N_{\text{CO}}, N_{\text{O}}/N_{\text{CO}} - 1, N_{\text{O}} - 1) = \frac{4kN_{\text{O}}N_{\text{CO}}}{(A - N_{\text{O}})}$ |
| $\text{CO}_{\text{ads}}(\text{loss}) - \text{diffusion}$ | $W_5(N_{\text{CO}}/N_{\text{CO}} - 1) = h'N_{\text{CO}}(1 - \theta_{\text{CO}}^m - \theta_{\text{O}})$ |
| $\text{CO}_{\text{ads}}(\text{gain}) - \text{diffusion}$ | $W_6(N_{\text{CO}}/N_{\text{CO}} + 1) = h'(1 - \theta_{\text{CO}} - \theta_{\text{O}})N_{\text{CO}}^m$ |

Table 6.3: Transition probabilities for CO oxidation after apply mean-field approximation.

spatial correlations,

$$\frac{dP(\tilde{\mathbf{Z}}, N_{\text{CO}}^m; t)}{dt} = \frac{dP^{\text{reac}}}{dt} + \frac{dP^{\text{MF}}}{dt}, \quad (6.8)$$

where $\tilde{\mathbf{Z}} = \{N_{\text{CO}}, N_{\text{O}}\}$.

The challenge now is to solve this MFCME in order to obtain the stationary probability distribution $P^{\text{st}}(\tilde{\mathbf{Z}}, N_{\text{CO}}^m)$, and then to solve Eq. (6.7) in order to investigate the possibility of a phase transition in our model. Like other nonequilibrium problems related to a noise-induced phase transition, $P^{\text{st}}(\tilde{\mathbf{Z}}, N_{\text{CO}}^m)$ is not available in general [129]. At this point, we are forced to introduce a new approximation, the so-called adiabatic elimination of fast variables.

6.5 Adiabatic elimination of oxygen

One can partition the system into two, the fast N_{CO} , and the slow N_{O} variables. Then we consider $\tilde{\mathbf{Z}} = \{N_{\text{CO}}, N_{\text{O}}\}$, with the stoichiometric coefficients $\mathbf{v}_1 = \{1, 0\}$, $\mathbf{v}_2 = \{-1, 0\}$, $\mathbf{v}_3 = \{0, 2\}$, $\mathbf{v}_4 = \{-1, -1\}$, $\mathbf{v}_5 = \{-1, 0\}$, and $\mathbf{v}_6 = \{1, 0\}$. From the time scale separation we have taken that $P(N_{\text{CO}}, N_{\text{O}}; t) = G(N_{\text{CO}}, N_{\text{CO}}^m; t)F(N_{\text{O}} : N_{\text{CO}}; t)$, where $F(N_{\text{O}} : N_{\text{CO}}; t)$ is the conditional probability for N_{CO} kept constant. Note also that we

changed the notation from N_O to N_O . We also require

$$\sum_{N_{CO}} G(N_{CO}, N_{CO}^m) = 1, \quad (6.9)$$

$$\sum_{\tilde{N}_O} F(N_O : N_{CO}) = 1. \quad (6.10)$$

Inserting $P(N_{CO}, N_O; t) = G(N_{CO}, N_{CO}^m; t)F(N_O : N_{CO}; t)$ into Eq. (6.8) and summing up over N_O , we obtain

$$\begin{aligned} \frac{dG(N_{CO}, N_{CO}^m; t)}{dt} = & H_1(N_{CO} - 1)G(N_{CO} - 1, N_{CO}^m; t) + H_2(N_{CO} + 1)G(N_{CO} + 1, N_{CO}^m; t) \\ & - (H_1(N_{CO}) + H_2(N_{CO}))G(N_{CO}, N_{CO}^m; t), \end{aligned} \quad (6.11)$$

where the new transition probabilities of Table. (6.4) are used.

| Event | Transition probability |
|---------------------------------|---|
| $N_{CO} \rightarrow N_{CO} + 1$ | $H_1 = p_{CO}(A - N_{CO} - N_O) + \frac{h(1-\theta_{CO}-\theta_O)N_{CO}^m}{L}$ |
| $N_{CO} \rightarrow N_{CO} - 1$ | $H_2 = dN_{CO} + \frac{4kN_ON_{CO}}{(A-N_O)} + \frac{hN_{CO}(1-\theta_{CO}^m-\theta_O^m)}{L}$ |

Table 6.4: Transition probabilities after applying mean-field approximation and adiabatic elimination of oxygen.

On the other hand, the chemical master equation of the conditional probability distribution $F(N_O : N_{CO}; t)$ with N_{CO} kept constant is given by

$$\begin{aligned} \frac{dF(N_O : N_{CO}; t)}{dt} = & W_3(N_O - 2)F(N_O - 2 : N_{CO}; t) + W_4(N_O + 1)F(N_O + 1 : N_{CO}; t) \\ & - (W_3(N_O) - W_4(N_O))F(N_O : N_{CO}; t). \end{aligned} \quad (6.12)$$

This master equation depends only on W_3 and W_4 (see Table. (6.3)). Due to the time scale separation, $F(N_O : N_{CO}; t)$ will quickly relax to a stationary distribution. Hence, moments in the conditional transition rates become stationary as well as independent of

the initial condition value N_O . Because $F^{st}(N_O : N_{CO})$ is sharply peaked and monomodal, the conditional first and higher moments are given by the stationary attractive coverage of the fast deterministic dynamic with θ_{CO} kept constant [51]. In our case, the oxygen is the fast variable, and the deterministic equation of it is given by

$$\frac{d\theta_O}{dt} = 2(1 - p_{CO}) \frac{(1 - \theta_{CO} - \theta_O)^2 (1 - 2\theta_O)^8}{(1 - \theta_O)^{10}} - \frac{4\theta_O \theta_{CO}}{(1 - \theta_O)}. \quad (6.13)$$

This last equation can be obtained from standard cluster approximation (see Chap. 3 and Appendix B).

6.6 Evidence for a first-order phase transition

Inside each cell bistable behaviour is possible, and the number of adsorption sites A is of nanoscale dimension. Thus fluctuation-induced transitions from the active to the inactive state and vice versa may occur. This property opens up the possibility to study the interplay of coverage fluctuations induced by a small number of adsorption sites, and the coupling between cells.

6.6.1 Probability distribution function and effective potential

This approximation allows us to construct a new one component nonlinear MFCME for N_{CO} alone. Considering that now $\tilde{\mathbf{Z}} = \{N_{CO}\}$, this new master equation describes the behaviour of the new probability distribution $G(N_{CO}, N_{CO}^m; t)$.

The new one-component MFCME can be written as

$$\frac{dG(\tilde{\mathbf{Z}}, N_{CO}^m; t)}{dt} = \frac{dG^{reac}}{dt} + \frac{dG^{MF}}{dt}. \quad (6.14)$$

The probability distribution $G(N_{CO}, N_{CO}^m; t)$ approaches a stationary shape, which includes macroscopic transitions between the stable states of the deterministic approach. The final shape of $G(N_{CO}, N_{CO}^m; t)$ is in agreement with the solution $dG^{st}(N_{CO}, N_{CO}^m)/dt = 0$, and vanishing probability flux. In this case detailed balance holds, and one finds

$$H_1(N_{CO} - 1)G^{st}(N_{CO} - 1, N_{CO}^m) = H_2(N_{CO})G^{st}(N_{CO}, N_{CO}^m), \quad (6.15)$$

and subsequently

$$G^{st}(N_{CO}, N_{CO}^m) = \prod_{N=1}^{N_{CO}} \frac{H_1(N-1)}{H_2(N)} \left(1 + \sum_{n=1}^A \prod_{N=1}^n \frac{H_1(N-1)}{H_2(N)} \right)^{-1}. \quad (6.16)$$

This equation is the normalised stationary PDF for the occupation of sites with N_{CO} molecules.

Firstly, we consider the case that the coupling between cells is zero and the cells are independent systems described by simple master equations which allow only global fluctuations. Inside of each cell CO molecules can diffuse infinitely fast, and this naturally produces bistability. As an example, Figure 6.1 shows a typical bimodal stationary PDF for the case when $h = 0$ with $A = 100, 400,$ and 1000 . Note that, if A decreases, the transitions between the two stable states will increase. This result is in accordance with experiments of fluctuation-induced transitions in CO oxidation on a Pt field emitter tip, and with CO oxidation on Pd nanoparticles [13, 15]. Finally, we assume that the PDF

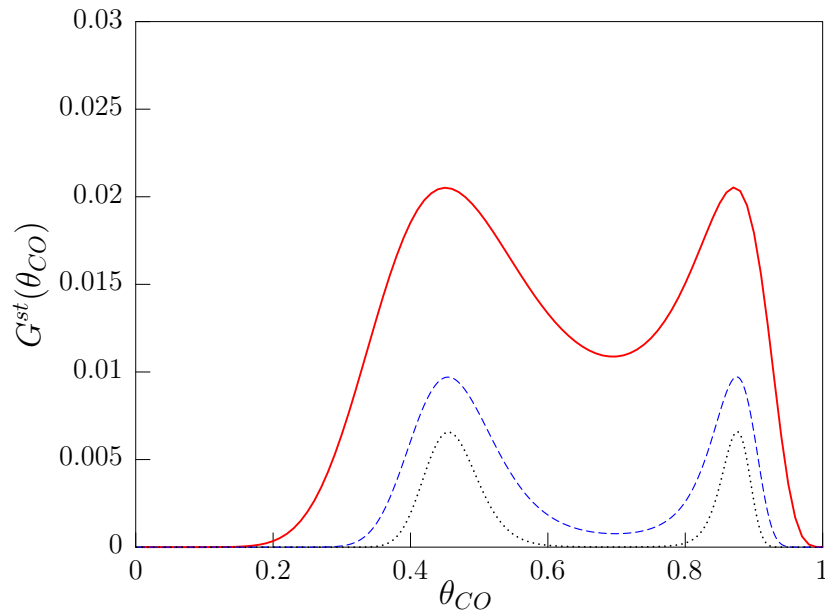


Figure 6.1: Stationary probability distribution $G^{st}(N_{CO})$ obtained from Eq. (6.16) considering only the bistable behaviour inside one single cell ($h = 0$), with $p_{CO} = 0.36715$, $d = 0.030$ and the number of adsorption sites $A = 100$ (solid line), 400 (dashed line), 1000 (dotted line).

can be written as

$$G^{st}(N_{CO}, N_{CO}^m) \propto e^{-A\phi(N_{CO}, N_{CO}^m)}, \quad (6.17)$$

and that an effective potential (EP)

$$\phi(N_{CO}, N_{CO}^m) = \frac{-\ln G^{st}(N_{CO}, N_{CO}^m)}{A}, \quad (6.18)$$

exists.

6.6.2 Order parameter

After adiabatic elimination Eq. (6.7) can be written as

$$\beta(N_{CO}^m) = N_{CO}^m = \sum_{N_{CO}, \tilde{N}_O} N_{CO} G^{st}(N_{CO}, N_{CO}^m) F^{st}(\tilde{N}_O : N_{CO}), \quad (6.19)$$

and considering

$$\sum_{N_O} F^{st}(N_O : N_{CO}) = 1, \quad (6.20)$$

the new self-consistent equation or order parameter of the system can be written as

$$\beta(N_{CO}^m) = N_{CO}^m = \sum_{N_{CO}} N_{CO} G^{st}(N_{CO}, N_{CO}^m). \quad (6.21)$$

Note that this order parameter is the mean value of the CO coverage obtained from the PDF. In our problem two cases are possible. i) The PDF is unique, and the order parameter has only one value. ii) We have several monomodal PDFs, and the order parameter has several solutions, one for each PDF.

When the coupling parameter h increases, the CO molecules can jump from cell to cell and an RDME approach is necessary. Then it is clear that the order parameter, defined by Eq. (6.21), becomes the most important variable of the model in order to study the possibility of phase transitions. A true phase transition is detected when an abrupt change in this order parameter is observed as a function of control parameters.

If the order parameter has only one solution, it is expected that the system evolves to a collective highly symmetric state. In this state of high symmetry, the cells relax to an unique mean value with only one stationary PDF. For other parameter values, multiple mean value solutions are possible and the system relaxes to a collective low symmetry state, where the cells randomly approach one or another solution depending on the initial

conditions. In this case one concludes that there are several corresponding stationary PDFs, and the mean field theory predicts a phase transition. The latter case can be understood like the breaking of the symmetry.

Figure 6.2 shows a graphical representation of Eq. (6.21). All the self-consistently determined solutions are given by the intersection of the diagonal line with the curve $\beta(N_{CO}^m)$. In Fig. 6.2(a) two typical cases are shown for two values of h and with the number of adsorption sites $A = 400$. For $h = 0.1$ only one solution is observed (solid line). In this case a homogeneous highly symmetric state dominates. As the coupling is increased, for $h = 2$ three solutions appear which represent a low symmetric state (dashed line). We remark that $\beta'(N_{CO}^m) < 1$ is sufficient for the stability of the solutions [158]. Fig. 6.2(b) shows that for $A = 100$ only one solution is observed for the whole range of h . Note, that we plot the self-consistent equation as a function of the CO coverage.

In order to clarify these latter observations, we perform an analysis of bifurcation diagrams of N_{CO}^m as function of h and the corresponding stationary PDFs. Figure 6.3(a) shows one of these bifurcation diagrams with $A = 400$. Here, one solution remains stable [the lower branch], while a new stable solution and unstable solution appear above some critical value of h . For small coupling N_{CO}^m is unique (case I) and one bimodal stationary PDF like in Fig. 6.3(b) is observed. If the coupling increases, the system behaviour departs from that of the small coupling until a bifurcation takes place to a region where two new solutions appear (cases II and III). Here, a subset of cells may have a tiny preference to the upper solution, while the rest may have a certain preference to the lower solution, with the result that the overall behaviour is not fully symmetric. In this case, the intermediate solution is unstable. These solutions, of course, correspond to three different monomodal PDFs. Figure 6.3(c) shows these PDFs. The PDF represented by the dotted line corresponds to the unstable solution, and it is not observed in simulations. Here one observes cells with high θ_{CO} coexisting with cells of low θ_{CO} . In Fig. 6.4(a), we plot the same like Fig. 6.3, but now with $A = 100$. From this figure it is clear that only the lower solution of Fig. 6.3(a) is observed and corresponds to one stable stationary PDF. Nevertheless, this PDF can change as a function of h from a bimodal shape (small h) to a monomodal shape (high h) as shown in Figs. 6.4(b) and 6.4(c).

Obviously, when one decreases the cell size and increases the parameter h , the whole system behaves in a different way. This different behaviour arises from the different scaling of the diffusion and reaction part of the RDME, as mentioned earlier. On a small surface the diffusion dominates, since fluctuations arising from diffusion come about because the molecules are jumping back and forth across the boundary of length L . Conversely, for

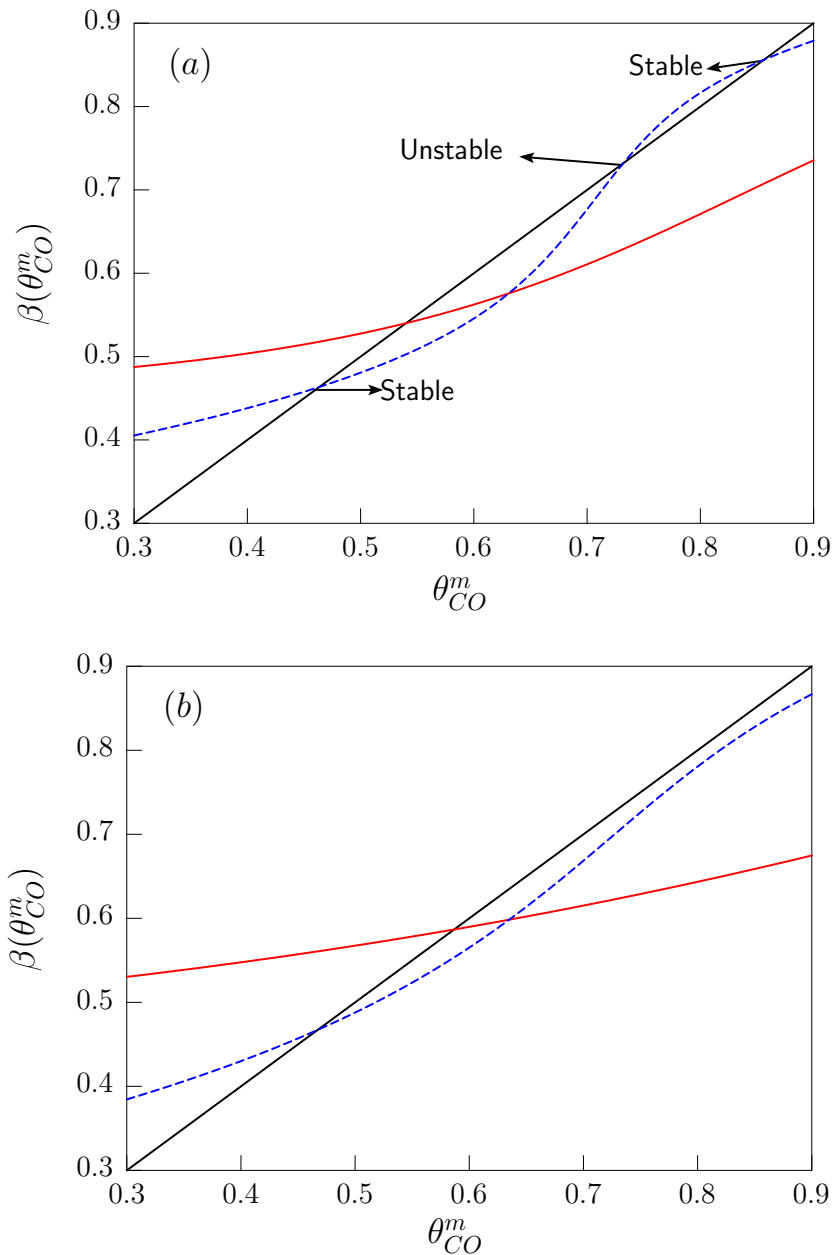


Figure 6.2: Solutions of the self-consistent equation (6.21). The solutions are given by the intersection of $\beta(N_{CO}^m)$ with the diagonal solid line. *a*) Here $A = 400$, and the solid line, which corresponds to $h = 0.1$, shows only one stable solution of this equation (highly symmetric state). On the other hand, the dashed line, which now corresponds to $h = 2$, shows three solutions (low symmetry state). *b*) In this case $A = 100$, and for the whole range of h one observes only one solution (highly symmetric state). The reaction parameters are $p_{CO} = 0.36715$ and $d = 0.030$.

larger surfaces, we find the diffusion between cells is negligible and only reaction dominates [4].

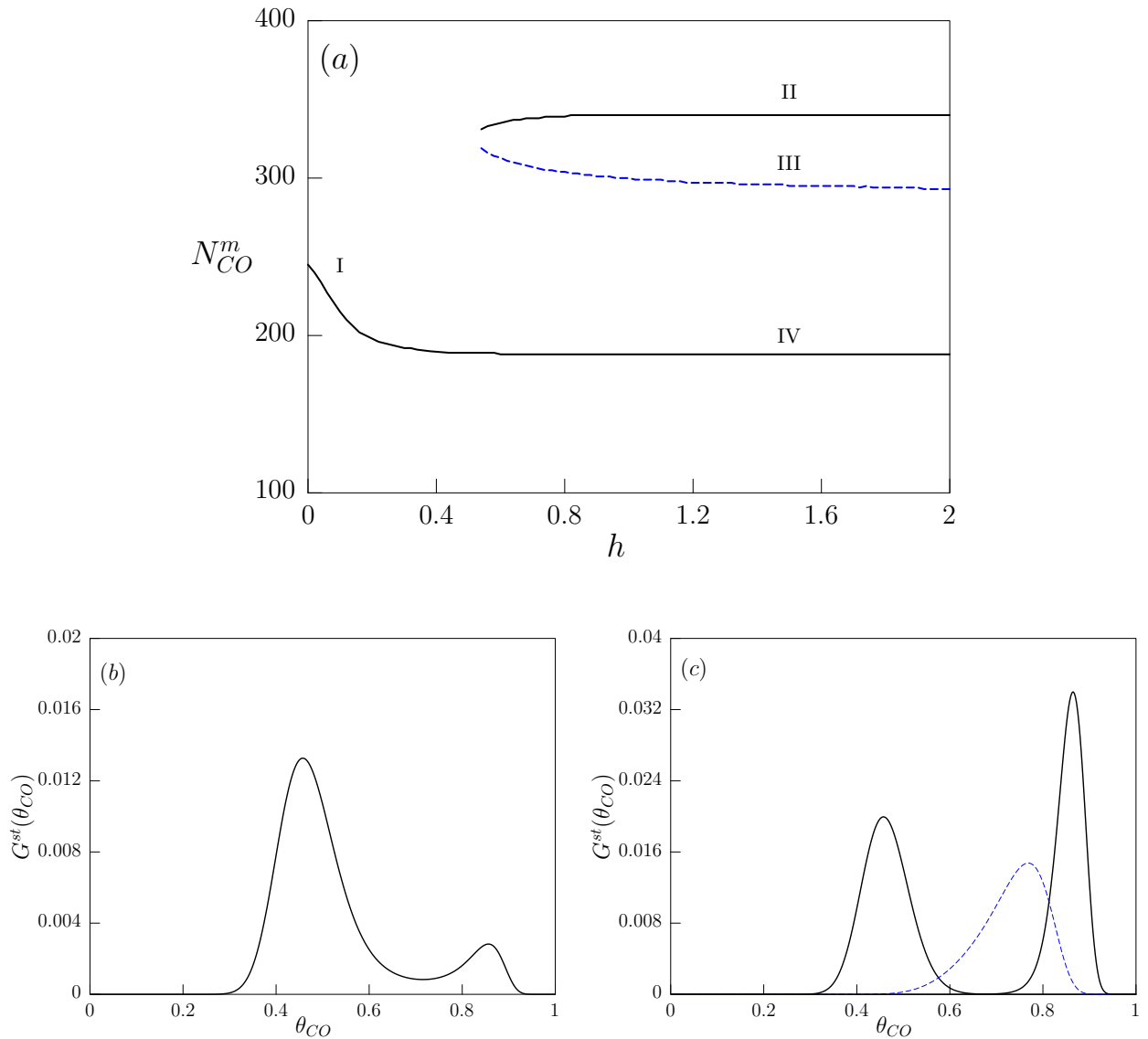


Figure 6.3: Solution of equation (6.21) as a function of the coupling parameter h and the corresponding stationary probability distribution functions. a) Here, we show the bifurcation diagram of N_{CO}^m . b) Bimodal stationary probability distribution for the case I. c) Three monomodal stationary probability distributions for the cases II, III and IV. The CO pressure and desorption rate are constant with $p_{CO} = 0.36715$ and $d = 0.030$. Each cell also has a number of sites $A = 400$.

In Fig. 6.5(a), we plotted for two values of (d, p_{CO}) the phase transition line in the parameter space (h, A) as predicted by the mean-field approximation. The curves separate regions with one unstable state and two stable ones (above each line) and a region where

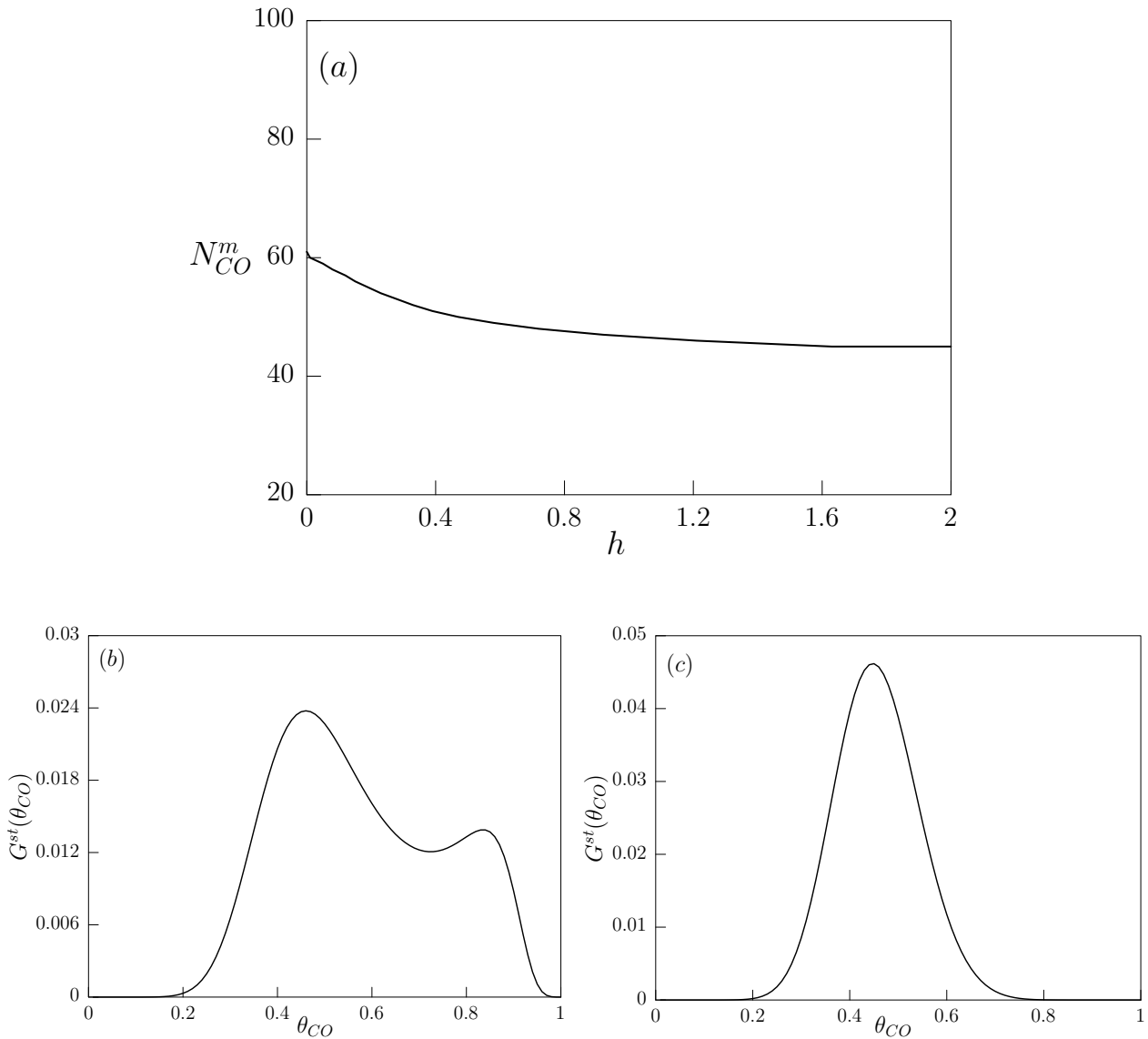


Figure 6.4: The same like Fig. 6.3, but now with $A = 100$. a) Bifurcation diagram of N_{CO}^m as a function of h . It is clear that only the lower solution of Fig. 3(a) is physical and corresponds to one stationary probability distribution function. b) and c) show that this probability distribution function can change as a function of h from a bimodal shape (small h) to a monomodal shape (high h).

only one stable solution is observed (below each line). Note that the region with two stable solutions is longer when p_{CO} and d are farther from the critical point (dashed line).

6.7 Numerical verification of MFA predictions

In order to verify the analytical results, simulations have been carried out with the Gillespie algorithm. This algorithm has received much attention in the last years [126, 127, 128, 159]. For instance, some efficient generalisations to extended systems have been introduced [160, 161]. Here, in contrast to the normal algorithm, we have taken into account the adiabatic

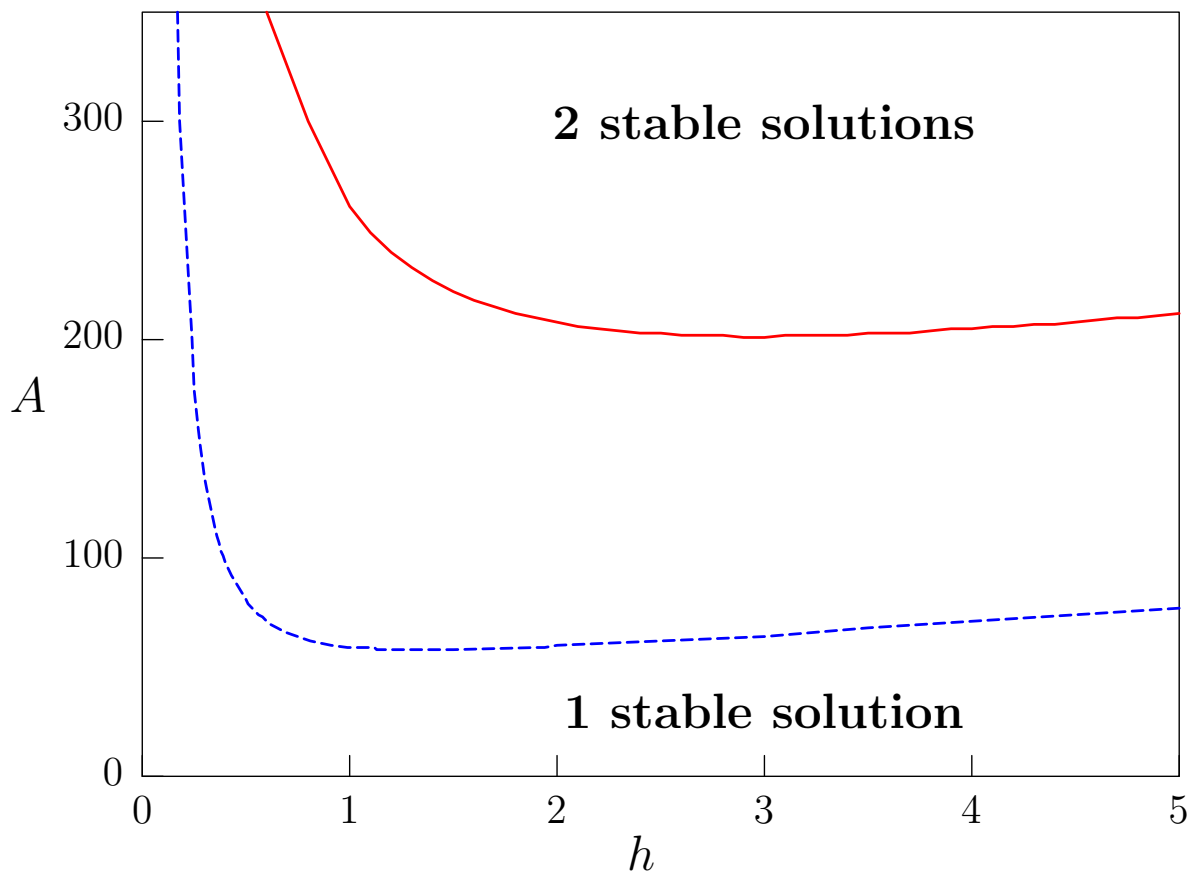


Figure 6.5: Phase diagram in the (h, A) plane as predicted by the mean-field approximation with (d, p_{CO}) equal to $(0.36715, 0.030)$ (solid line) and $(0.296, 0.0050)$ (dashed line). In the region above the curves one unstable solution of Eq. (6.21) and two stable ones appear. In the region below the curves only one stable solution of this equation is observed.

elimination of oxygen and random local and nonlocal as well as only local (diffusive) interactions between cells.

6.7.1 Random local and nonlocal (RLnL) interaction versus MFA

Here, we consider random connections between cells. It means that a given cell can change CO_{ads} molecules with any cell of the lattice at random. Thus, this kind of coupling introduces long range interactions. In this sense, simulations with our RLnL interaction system should be quite similar to the MFA predictions in the limit when the number of cells is high. Figure 6.6 shows a schematic representation of this interaction

The computer simulations have been carried out with M , the number of cells being equal to 2000. We chose appropriate initial conditions, a long simulation time and the same parameters as in the previous theoretical part. Figure 6.7(a) shows the two PDFs inside the region where two stable solutions of Eq. (6.21) exist. Note that although for finite systems there is no perfect separation into different ergodic components, the trajectories remain very long in the corresponding basin of attraction. In this case, $A = 400$, $d = 0.030$, and $p_{CO} = 0.36715$. In Fig. 6.7b the stationary PDF, but now with $A = 100$, is shown. This results are in accordance with analytical predictions. Note that the interaction form used in this case does not describe very well our reaction diffusion description of CO oxidation. For CO oxidation under the conditions considered here, CO_{ads} molecules are expected to diffuse only to nearest-neighbor cells (normal diffusion). On the other hand, the RLnL interaction is a combination of local and long range interactions. The detailed stochastic algorithm, which incorporates random local and nonlocal interactions in the Gillespie algorithm, is described in Appendix. E. It is interesting to study the relation between this kind of coupling and the so-called anomalous diffusion and Lévi flights [162]. An interesting extension could also be to use stochastic models, like the master equation used in this chapter, in order to study an array of nanoparticles with local and nonlocal coupling through the gas phase [133].

6.7.2 Local (Diffusive) interaction versus MFA

In this case, we consider that CO_{ads} molecules can only jump to nearest-neighbor cells. Obviously, this kind of transport is the correct representation of our reaction-diffusion master equation, and thus, it is expected to produce correct predictions for CO oxidation under diffusion limited conditions [53].

The idea is to compare stochastic simulations using this local interaction with MFA predictions. Here, it is expected only qualitative concordance. In our case, local interactions are confined to a 2-d lattice which represents the catalytical surface. This catalytical surface consists of different regions coupled by CO_{ads} diffusion. On the other hand, MFA considers all to all interaction between cells. This situation is more similar to a long-range or global interaction. Figure 6.8 shows a schematic representation of the local transport.

In Fig. 6.9, the comparison of the bifurcation diagram of N_{CO}^m as function of A between theory and stochastic simulation, for fixed h , is shown. For the stochastic simulation (SS) we have implemented the Gillespie algorithm taken into account the adiabatic elimination of oxygen and the diffusive or local coupling. In Fig. 6.9(a), one solution remains stable (lower branch), while a new stable solution (solid line) and unstable solution (dashed line) appear above some critical value, A_c^{MFA} . Thus, the MFA predicts a first-order phase

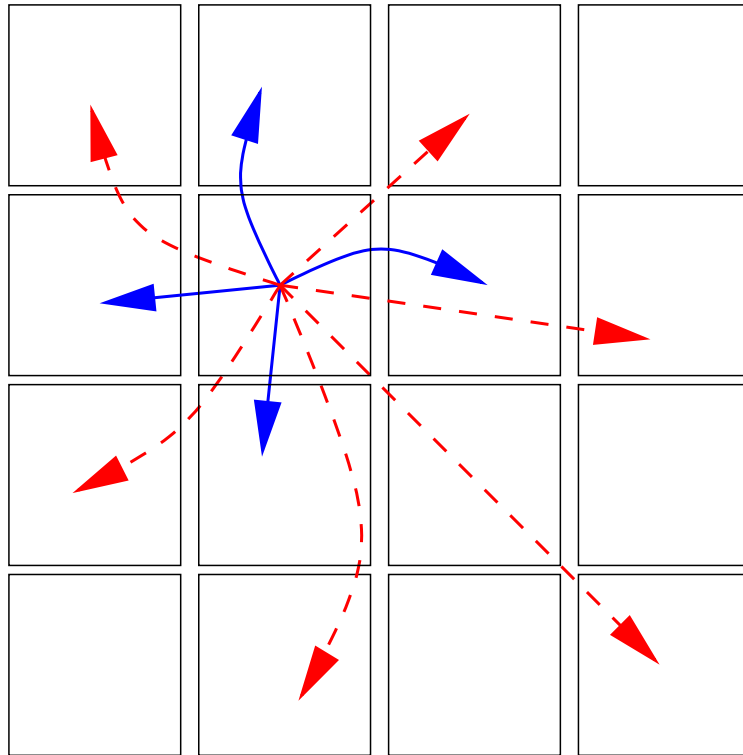


Figure 6.6: Schematic representation of the random local and nonlocal transport mechanism. Solid arrows represent local interaction. Dashed arrows represent long range interactions. CO_{ads} molecules can move from the cell in consideration to a random chosen cell on the lattices.

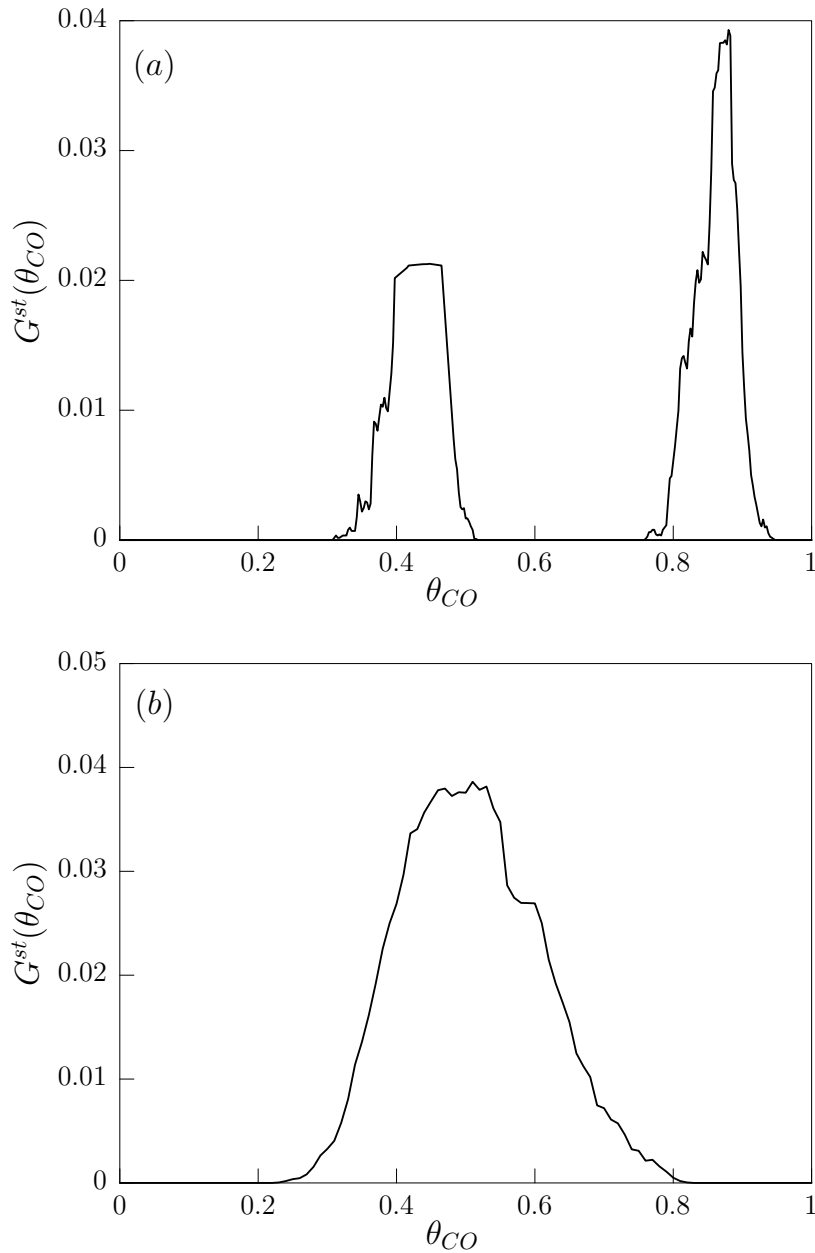


Figure 6.7: Stationary probability distribution functions of one cell, obtained from the Gillespie algorithm adopted to have random local and nonlocal interactions. *a)* Here, typical stationary probability distribution functions inside the region of low symmetry for $A = 400$ are shown. *b)* For $A = 100$, the diffusion dominates over the reaction, and a monomodal probability distribution around the mean value is obtained. This distribution is independent of the initial conditions. The computer simulations have been carried out with 2000 cells.

transition. Note that 2-d SS (circles) qualitatively confirm the existence of this first-order phase transition, but they yield a higher critical value, A_c^{SS} . Although the chemical reactions described here occur on the surface of a metal, it is interesting to note that the critical point predicted by the MFA can be reproduced by stochastic simulation using global or high dimensional coupling. Fig. 6.9(b) shows simulation (circles) and theoretical results (solid line) for relatively small h . Here, it is clear that only the lower solution of Fig. 6.9(a) is observed for small values of A . For high enough values of A , the phase transition is also expected to occur.

Figure 6.10 shows the PDF for one cell from both theory and stochastic simulations. The parameters (h, A) are chosen in the region where only one stable solution is observed. In Fig. 6.10(a), the diffusion parameter h is small, consequently the cells exhibit strong fluctuations induced basically only by reaction events. The PDF is bimodal with transitions between stable states induced by strong fluctuations. The analytical PDF is represented by the solid line and the PDF from stochastic simulations is represented by

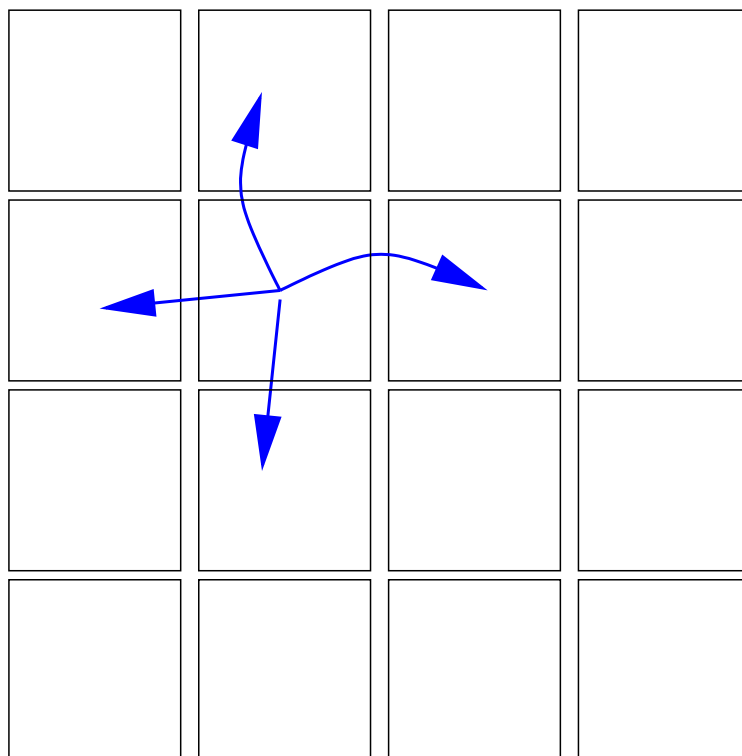


Figure 6.8: Schematic representation of the local transport mechanism. CO_{ads} molecules can move from the cell in consideration to a chosen nearest-neighbor cell on the lattice.

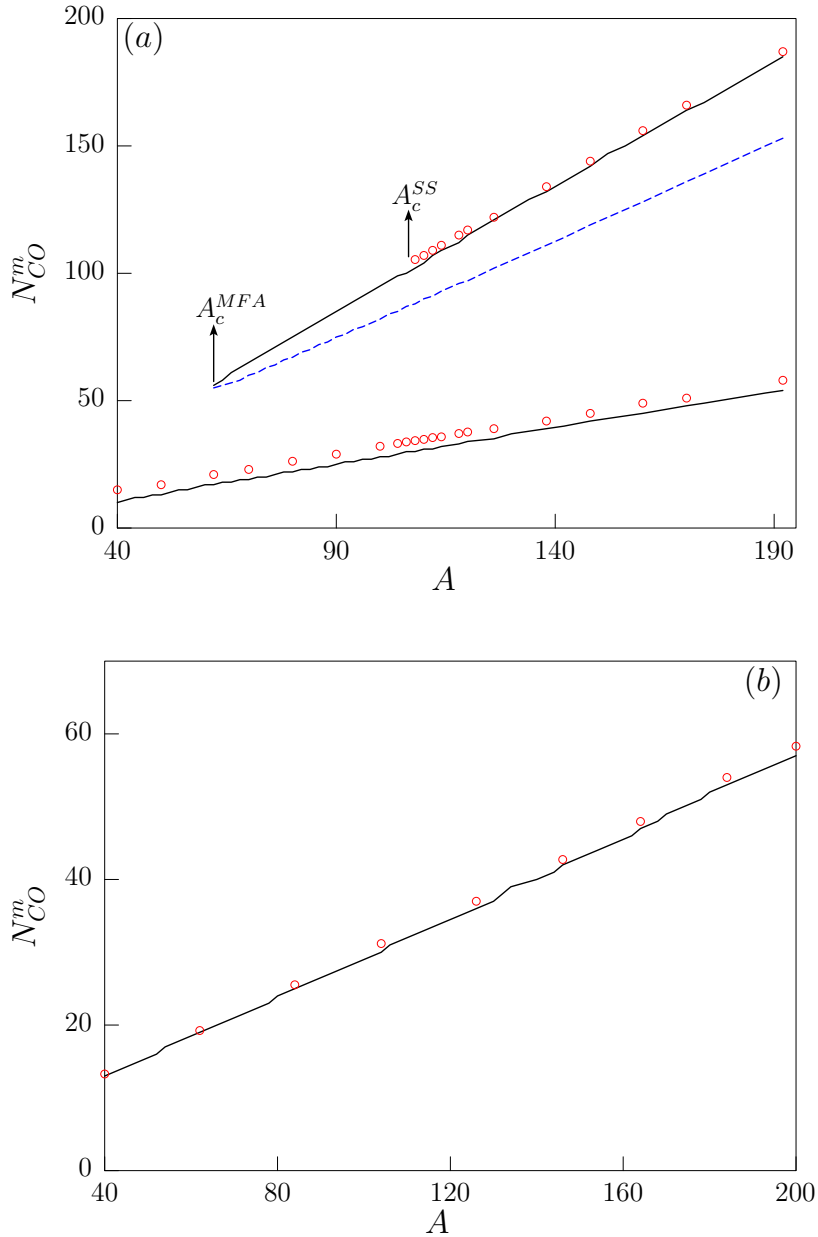


Figure 6.9: Solution of the order parameter N_{CO}^m as function of the system size A . (a) Comparison of the stable solutions of the self-consistency equation for N_{CO}^m as a function of A (solid lines) with 2-d Gillespie-like Monte Carlo simulations (circles). Here, $p_{CO} = 0.296$, $d = 0.0050$, $h = 2$ and the number of cells $M = 32 \times 32$. We use periodic boundary conditions. The unstable solution (dashed line) is not observed in simulations. A_c^{MFA} and A_c^{SS} are critical points predicted by mean-field approximation and stochastic simulations, respectively. (b) The same as (a), but now with $h = 0.1$. Here, it becomes clear that the lower solution is the only possible stable state of the system.

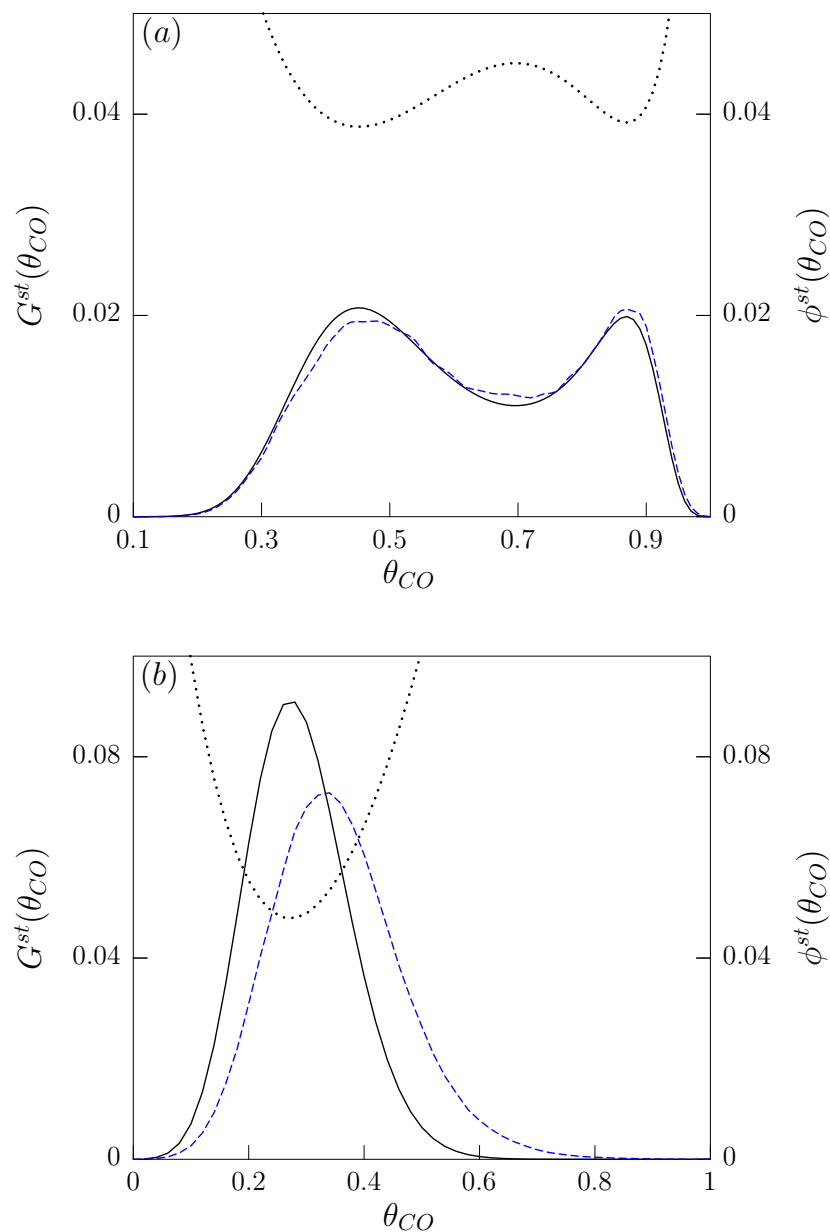


Figure 6.10: Comparison of the probability distribution functions obtained by 2-d Gillespie-like Monte Carlo simulations for 32×32 cells (dashed line) and periodic boundary conditions with the probability distribution (solid line) and the effective potential (dotted line) predicted by the mean-field approximation. (a) Here, parameters are $A = 100$, $h = 0.001$, $p_{CO} = 0.36715$, and $d = 0.030$. For these h and A , the order parameter has only one stable solution and the cells exhibit bistability as well as strong fluctuations. (b) This figure shows monomodal probability distributions from theory and simulations for $A = 50$, $h = 2.0$, $p_{CO} = 0.296$, and $d = 0.005$.

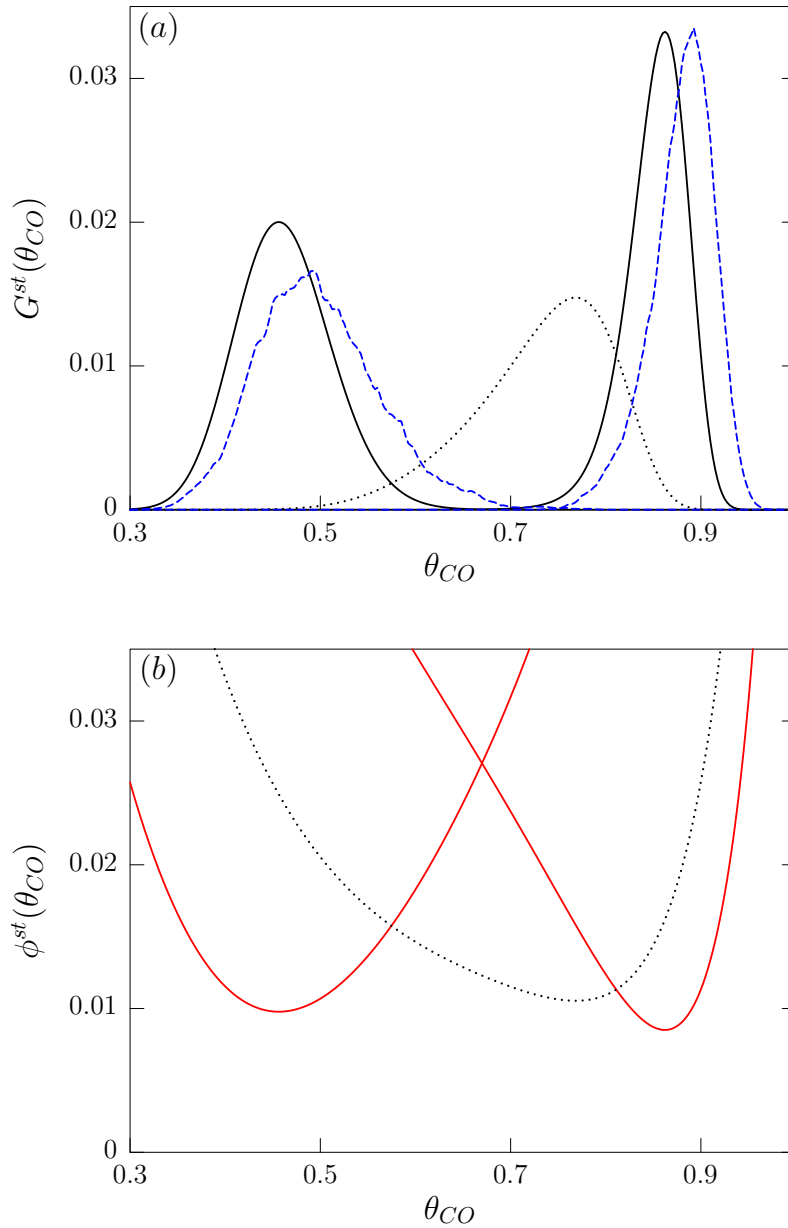


Figure 6.11: The same as Fig. 6.10, but now for parameters (h, A) inside the region of two stable solutions. (a) In this figure $h = 2.0$ and $A = 400$, and as predicted by the mean-field approximation two stable monomodal probability distributions are observed. Probability distribution functions obtained from simulations are denoted by solid lines, and probability distribution functions obtained from theory are denoted by dashed lines. The probability distribution function denoted by the dotted line is unstable. (b) This figure shows the corresponding stable effective potentials (solid lines). The effective potential denoted by the dotted line is unstable.

a dashed line. An interesting way to visualise this is through the EP (Eq. (6.18)). When the probability distribution acquires a bimodal shape the corresponding potential develops two minima (dotted line). Figure 6.10(b) shows the PDF and the EP for large h and small A . Under this conditions the PDF as well as the EP are monomodal. In this case the fluctuations are mostly consequences of the diffusive events.

Figure 6.11 now shows the PDF and EP in regions of the parameter space (h, A) where two stable solutions are observed. In these regions, three monomodal PDF's are observed corresponding to one unstable solution and two stable ones. This breaking of the system in several ergodic components is a signature of a true first-order phase transition. Figure 6.11(a) shows these PDF's from theory (solid lines) and stochastic simulations (dashed lines). The PDF represented by the dotted line is an unstable solutions of the MFME and is not observed in simulations. Figure 6.11(b) shows the corresponding effective potentials (solid line). Here again, the EP represented by the dotted line is unstable and not observed in simulations.

6.7.3 Nucleation and growth of islands

Figure 6.12 demonstrates the phenomenon of nucleation and growth usually associated with a first order-phase transition for $A = 400$, $h = 2.0$, $p_{CO} = 0.36715$ and $d = 0.030$. From Fig. 6.9(a), it is clear that the two stable states have different degrees of stability under fluctuations, which are determined by the distance of each stable state from the separatrix representing the unstable state [52]. For the parameter values used in this figure, the more stable state corresponds to the lower number of CO molecules or an active state inside a cell. Starting with a small fraction of cells with low numbers of CO molecules or reactive state and the rest of the cells with high numbers of CO molecules or an inactive state (Fig. 6.12(a)), we observe the following: First one island with a composition corresponding to active state is formed and then this island starts to grow with increasing time. This growth stops when the surface is completely covered by the active stable state. Figures 6.12(a – c) show the case when the surface is represented by a square lattice of 32×32 cells with periodic boundary conditions.

6.8 Summary and conclusions

We have analysed theoretically the interplay between internal fluctuations and diffusion in a model of the bistable CO oxidation reaction which applies to the case of a catalytic surface at high enough pressure. At higher pressure the adsorption rates grow propor-

tionally to the pressure, the diffusion length decreases, and smaller and smaller patches of the surface can be regarded as well mixed. Consequently, stochastic fluctuations become important. In this publication stochastic effects are taken into account by dividing the surface into a square lattice of nanoscale cells, each containing A adsorption sites. A reaction-diffusion master equation for the probability of finding CO and oxygen coverage at a time t , that allows local fluctuations, is introduced. We are able to solve this complicated reaction-diffusion master equation after invoking the mean-field approach together with the adiabatic elimination of oxygen. This allows an estimation of the probability distribution of adsorbed CO molecules as a function of the coupling parameter h and the number of adsorption sites A . Subsequently, the phase diagram in the parameter space (h, A) is constructed. Assuming that the bistable behaviour is possible inside each cell, we show that the phase diagram, as predicted by the mean-field approximation, is split into two regions. An analysis of the probability distribution shows evidence for the existence of a first-order phase transition associated with the bifurcation of the first moment of the CO coverage. The first moment plays the role of the order parameter which characterizes this phase transition. These analytical results have been found to be in reasonable agreement with spatially extended Gillespie-type kinetic Monte Carlo simulations, taking into account the adiabatic elimination of oxygen.

It is important to emphasize that, at high pressure, temperature effects are relevant and should also be taken into account for an improved model [163]. In this high pressure regime, due to the high coverage, energetic interactions between the adspecies will play an important role which needs to be adequately described in a realistic model. Our model can in principle be used to study fluctuations on inhomogeneous metal surfaces, where structural defects such steps or impurities are present. The structural defects can be considered as small regions on the surface with different kinetic parameters coupled by CO diffusion. An interesting extension could also be to use stochastic models, like the master equation used in this paper, in order to study an array of nanoparticles coupled globally through the gas phase. The results shown in this chapter demonstrate that noise can play an important role in catalytic systems. This opens up new perspectives for the study of noise-induced effects because conditions with a small enough mixing area will be realized in many catalytic reactions at high pressure. Our model can be used to study CO oxidation on a field-emitter tip. In this case, the different facets with different orientations are coupled by CO diffusion. Finally, our model can be extended to other catalytical systems where the mobility of adparticles is affected by high pressures as well as high coverages [86].

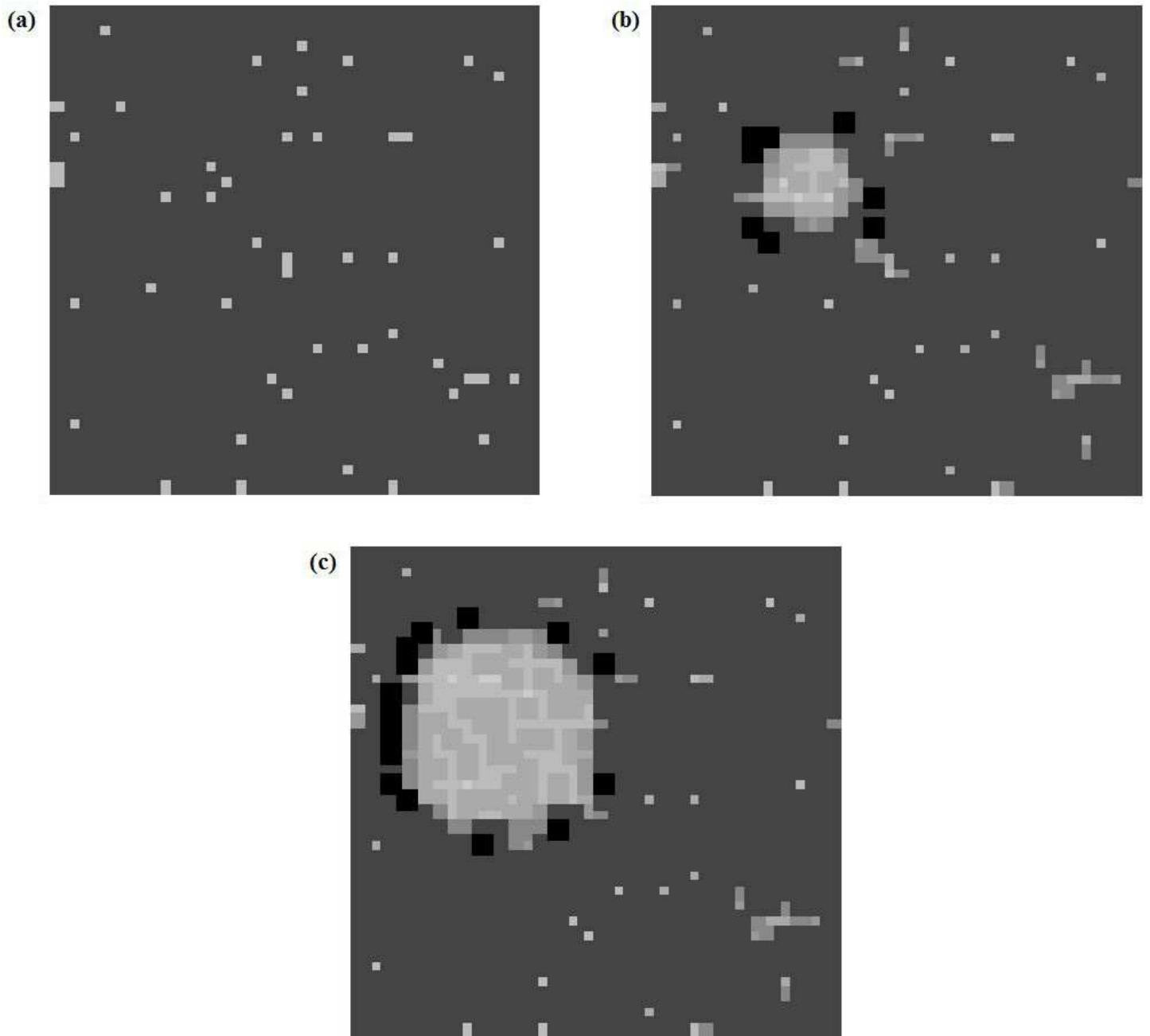


Figure 6.12: 2-d SS in grayscale of a $M = 32 \times 32$ square lattice of cells with periodic boundary conditions. Parameters are $A = 400$, $h = 2.0$, $p_{CO} = 0.36715$, and $d = 0.030$. Time increases from *a* to *c*. (*a*) Small fraction of cells with low numbers of CO molecules (reactive state) and the rest of the cells with high numbers of CO molecules (inactive state). (*b*)-(*c*) A reactive island is formed and starts to grow with increasing time.

Part III

**CO OXIDATION WITH
ADSPECIES REPULSIONS :
A STOCHASTIC APPROACH**

Chapter 7

A reduced stochastic hybrid model with adspecies repulsion

"O inventamos o Erramos."

Simón Rodríguez (1769-1854)

7.1 Introduction

The ultimate goal in the study of heterogeneous catalysis on nanoscale surfaces is to elucidate behavior at higher pressure (p) closer to industrial conditions [164]. In such regimes of higher p , the effect of adspecies interactions will play an important role [165, 166, 167, 168, 169]. Ordering of adsorbed atoms or molecules due to such interactions is a common phenomenon observed in many low-energy electron diffraction (LEED) studies [113].

In particular, atomistic lattice-gas modelling of CO oxidation on unreconstructed metal surfaces reveals the existence of phase separation of reactants into oxygen-rich and intermixed reactive states as a consequence of adspecies repulsions [49, 170]. It is shown that the system can display well-defined fluctuation-induced transitions between the two phase-separated reactive states which appear similar to those observed in studies on Pt metal field emitter tips (FET's) [13].

Apart of the implementation of realistic lattice-gas models, it is instructive and necessary to introduce toy stochastic mean-field models incorporating adspecies interactions, because kinetic Monte Carlo (KMC) simulations of lattices-gas models are only numerical experiments. In some cases theoretical analysis are needed, thus one motivation to

introduce stochastic mean-field models is to present analytical approximations. For instance, the fluctuation behavior of the bistable CO oxidation on nanoscale surfaces has been theoretically analyzed by a mean-field birth-death-type master equation, and it has been shown that near the critical point, with decreasing surface area, one cannot distinguish between two macroscopically stable stationary states [51]. These studies captured at least qualitatively the fluctuation-induced transitions experimentally observed in CO oxidation of Pt FET's and Pd nanoparticles [13, 15].

In this chapter, a stochastic hybrid mean-field model for CO oxidation on nanoscale surfaces with $CO - O$ and $O - O$ adspecies repulsive interactions is introduced. It is constructed using the so-called cluster approximation. After adiabatic elimination of the fast oxygen coverage the phase diagram in the parameter space is constructed and analysed. Finally, critical and fluctuations depending of system size as well as fluctuations around the stable states of the bistable region are analyzed.

7.2 Deterministic approach

We assume that the reaction takes place according to LH mechanism. The surface of the catalyst is a square two-dimensional lattice of active sites. The oxygen and carbon monoxide impinge randomly onto the surface and when vacant sites are available (E) they adsorb. Two adjacent vacant sites are required for oxygen molecule to adsorb dissociatively; the O_2 dissociates into O atoms, each residing on a separate surface site. As an example, first we consider the case when an atom adsorbed on the surface becomes immobile and when O-O, CO-CO and CO-O adspecies lateral repulsions between adspecies are ignored.

Hierarchical kinetic rate equations can be obtained by applying the cluster approximation (see Appendix B). It should be noted that the essence of spatial correlations implies that in general $\{OO\} \neq \{O\}^2$, etc. However, conservation of probabilities always guarantees that $\{CO\} + \{O\} + \{E\} = 1$. $\{COCO\} + \{OO\} + \{EE\} + 2\{OCO\} + 2\{COE\} + 2\{OE\} = 1$, etc [103, 106]. For finite reaction rate $k = 1$, one has

$$\frac{d\{CO\}}{dt} = p_{CO}\{E\} - 4\{COO\},$$

$$\frac{d\{O\}}{dt} = 2p_{O_2}\{EE\} - 4\{COO\},$$

$$\frac{d\{COCO\}}{dt} = 2p_{CO}\{AE\} - 2\{COCOO\} - 4 \left\{ \begin{array}{c} O \\ CO \quad CO \end{array} \right\},$$

$$\frac{d\{OO\}}{dt} = \frac{p_{O_2}}{2}\{EE\} + p_{O_2}\{OEE\} + 2p_{O_2} \left\{ \begin{array}{c} E \\ O \quad E \end{array} \right\} - 2\{OOCO\} - 4 \left\{ \begin{array}{c} CO \\ O \quad O \end{array} \right\}.$$

⋮

7.2.1 Hybrid and pair approximations

In this chapter, we are interested in behavior of the above model for CO oxidation in the regime of very large diffusion of CO_{ads} molecules. This is motivated by the observation that the hop rate for CO_{ads} is many orders of magnitude larger than the other rates in typical CO oxidation reactions. We assume that, due to very rapid diffusion, CO_{ads} is distributed randomly on the non- O_{ads} sites at all times.

Here we discuss the exact hierarchic rate equations for hybrid models with adspecies repulsions derived from the pair or (2,1) cluster approximation (see Appendix B). These hierarchic equations describe the evolution of probabilities (or coverage) for various sub-configurations of sites. Using the hybrid approximations, some simplifications arise due to feature that CO_{ads} are strictly randomly distributed. For convenience, below we express the probabilities of various configurations by the configurations themselves. Thus one has $\{CO\} = \theta_{CO}$, $\{O\} = \theta_O$, and $\{E=1-CO-O\}$, $\{COO\}$, $\{OOCO\}$, etc. represent the probabilities of an empty site, and $CO_{ads}O_{ads}$ pair, linear $O_{ads}O_{ads}CO_{ads}$ triples, etc.

In the pair or (2,1) cluster approximation, there are three single site configurations probabilities, $\{CO\}$, $\{O\}$, and $\{E\}$, and six distinct pair configurations probabilities, $\{COCO\}$, $\{OO\}$, $\{EE\}$, $\{COO\}$, $\{COE\}$, $\{OE\}$ (Note that by inversion symmetry $\{COE\} = \{ECO\}$). However, there are also conservation of probability conditions, $\{CO\} + \{O\} + \{E\} = 1$ and $\{COCO\} + \{OO\} + \{EE\} + 2\{COO\} + 2\{COE\} + 2\{OE\} = 1$. Also the single site probabilities can be determined from the pair probabilities via the relations $\{COO\} + \{COE\} + \{COCO\} = \{CO\}$, $\{COO\} + \{EO\} + \{OO\} = \{O\}$, and $\{COE\} + \{OE\} + \{EE\} = \{E\}$. Nevertheless, in the hybrid model with adspecies repulsions, further relationships exist.

We introduce a state $\{Z\} = 1 - \{O\} = \{Z^-\} + \{Z^+\}$, where $\{Z^+\}$ has nearest-neighbor oxygen atoms and $\{Z^-\}$ has no nearest-neighbor oxygen atoms. Then, one has $\{Z\} + \{O\} = 1$, $\{ZZ\} + 2\{ZO\} + \{OO\} = 1$, etc. If we consider $CO_{ads} - O_{ads}$ and

$O_{ads} - O_{ads}$ infinite repulsion, CO_{ads} is randomly distributed only on Z^- sites. Because local repulsion one also has $\{OO\} = \theta_{OO} = 0$ and $\{COO\} = \theta_{COO} = 0$.

If $\{E\} = \{E^+\} + \{E^-\}$ depending on whether the site is Z^- or Z^+ , then

$$\{E^+\} = \{Z^+\}, \quad (7.1)$$

since CO_{ads} cannot site Z^+ site, and

$$\{E^-\} = \{Z^-\} \left[1 - \frac{\{CO\}}{\{Z^-\}} \right] = \{Z^-\} - \{CO\} = \begin{Bmatrix} Z \\ Z & Z & Z \\ Z \end{Bmatrix} - \{CO\}. \quad (7.2)$$

The probability to find a CO_{ads} atom in a site is $\frac{\{CO\}}{\{Z^-\}}$, then the probability to find a site non occupied by CO_{ads} is $1 - \frac{\{CO\}}{\{Z^-\}}$.

In the cluster approximation one can write

$$\frac{d\{CO\}}{dt} = p_{CO}\{E^-\} - d\{CO\} - 4k \begin{Bmatrix} O \\ CO & O \end{Bmatrix}, \quad (7.3)$$

and

$$\frac{d\{O\}}{dt} = 2p_{O_2} \begin{Bmatrix} E \\ E & E^- & E \\ E & E^- & E \\ E \end{Bmatrix} - 4k \begin{Bmatrix} O \\ CO & O \end{Bmatrix}. \quad (7.4)$$

Then, after applying the (2,1) cluster or pair approximation and noting that $\theta_{CO} = CO$ and $\theta_O = O$, we have (see Appendix F)

$$\frac{d\theta_{CO}}{dt} = p_{CO} \left[\frac{(1 - 2\theta_O)^4}{(1 - \theta_O)^3} - \theta_{CO} \right] - d\theta_{CO} - 4k\theta_{CO}\theta_O, \quad (7.5)$$

$$\frac{d\theta_O}{dt} = 2p_{O_2} \left[\frac{(1 - 2\theta_O - \theta_{CO})^8}{(1 - \theta_O)^6(1 - \theta_O - \theta_{CO})^2} \right] \left[1 - \frac{(1 - \theta_O)^3\theta_{CO}}{(1 - 2\theta_O)^4} \right]^2 - 4k\theta_{CO}\theta_O. \quad (7.6)$$

7.3 Stochastic approach and adiabatic reduction

A square lattice of A sites with periodic boundary conditions is considered. For the stochastic description we consider the number of molecules or atoms adsorbed as variables.

Using $\theta_I = N_I/A$, we may proceed to assign rates W_ρ to the various adsorption/reaction events ($\rho = 1, \dots, r$) in the model. Finally one can construct a master equation which in general is written as

$$\frac{d}{dt}P(\tilde{\mathbf{Z}}; t) = \sum_{\rho=1}^r [W_\rho(\tilde{\mathbf{Z}} - \mathbf{v}_\rho)\tilde{\mathbf{Z}}P(\tilde{\mathbf{Z}} - \mathbf{v}_\rho; t) - W_\rho(\tilde{\mathbf{Z}}/\tilde{\mathbf{Z}} - \mathbf{v}_\rho)P(\tilde{\mathbf{Z}}; t)]. \quad (7.7)$$

Obviously, this master equation represents a global birth-death description of fluctuations for $P(\tilde{\mathbf{Z}}; t)$. Note that in this case, $\tilde{\mathbf{Z}}$ and \mathbf{v}_ρ are vectors with dimension given by the number of species. Table 7.1 shows rates or transition probabilities for the respective events. These $\rho = 1, \dots, 4$ transition probabilities can be used in the Gillespie algorithm to create trajectories which represent solutions of the general master equation 7.7.

| Event | Transition probability |
|---|--|
| $N_{CO} \rightarrow N_{CO} + 1$ | $W_1 = p_{CO} \left[\frac{(A-2N_O)^4}{(A-N_O)^3} - N_{CO} \right]$ |
| $N_{CO} \rightarrow N_{CO} - 1$ | $W_2 = dN_{CO}$ |
| $N_{CO}, N_O \rightarrow N_{CO} - 1, N_O - 1$ | $W_3 = \frac{4kN_{CO}N_O}{A}$ |
| $N_O \rightarrow N_O + 2$ | $W_4 = 2p_{O_2}A \left[\frac{(A-2N_O-N_{CO})^8}{(A-N_O)^6(A-N_O-N_{CO})^2} \right] \left[1 - \frac{(A-N_O)^3N_{CO}}{(A-2N_O)^4} \right]^2$ |

Table 7.1: Transition probabilities for CO oxidation with $CO_{ads} - O_{ads}$ and $CO_{ads} - O_{ads}$ infinite repulsion on unreconstructed noble metal surfaces.

7.3.1 Adiabatic reduction

In this subsection the adiabatic elimination of fast variables is apply to to our model [171]. We consider like in previous chapters that the oxygen is the fast variables

Master equation for the slow CO variable

We consider $\tilde{\mathbf{Z}} = \{N_{CO}, N_O\}$, with the stoichiometric coefficients $\mathbf{v}_1 = \{1, 0\}$, $\mathbf{v}_2 = \{-1, 0\}$, $\mathbf{v}_3 = \{0, 2\}$, and $\mathbf{v}_4 = \{-1, -1\}$. If we take from the time scale separation that

$$P(N_{CO}, N_O; t) = G(N_{CO}; t)H(N_O : N_{CO}; t), \quad (7.8)$$

then oxygen can be adiabatically reduced from the general master equation. Note that $H(N_O : N_{CO}; t)$ is the conditional probability distribution for N_{CO} being kept constant. We also require

$$\sum_{N_{CO}} G(N_{CO}) = 1, \quad (7.9)$$

$$\sum_{N_O} H(N_O : N_{CO}) = 1. \quad (7.10)$$

Inserting Eq. 7.8 into the general master equation and summing up over N_O , we obtain

$$\begin{aligned} \frac{d}{dt}G(N_{CO}; t) &= \tilde{W}_1(N_{CO} - 1)G(N_{CO} - 1; t) + \tilde{W}_2(N_{CO} + 1)G(N_{CO} - 1; t) \\ &\quad - (\tilde{W}_1(N_{CO}) + \tilde{W}_2(N_{CO}))G(N_{CO}; t) \\ &\quad + \sum_{N_O} (W_4(N_O - 2)H(N_O - 2 : N_{CO}; t) \\ &\quad - W_4(N_O)H(N_O : N_{CO}; t))G(N_{CO}; t). \end{aligned} \quad (7.11)$$

The last term of this equation must be zero because it does not contribute to the variation of N_{CO} . Thus, one may write

$$\begin{aligned} \frac{d}{dt}G(N_{CO}; t) &= \tilde{W}_1(N_{CO} - 1)G(N_{CO} - 1; t) + \tilde{W}_2(N_{CO} + 1)G(N_{CO} - 1; t) \\ &\quad - (\tilde{W}_1(N_{CO}) + \tilde{W}_2(N_{CO}))G(N_{CO}; t), \end{aligned} \quad (7.12)$$

where

$$\tilde{W}_1(N_{CO}) = \sum_{N_O} W_1(N_{CO}, N_O)H(N_O : N_{CO}), \quad (7.13)$$

and

$$\tilde{W}_2(N_{CO}) = \sum_{N_O} (W_2(N_{CO}) + W_3(N_{CO}, N_O))H(N_O : N_{CO}), \quad (7.14)$$

are the conditional expectations of $W_1(N_{CO}, N_O)$ and $W_2(N_{CO}) + W_3(N_{CO}, N_O)$, respectively. The conclusion of this analysis is that the evolution of $G(N_{CO}; t)$ depends on the conditional probability distribution $H(N_O : N_{CO})$.

Master equation for the fast oxygen variable

The vector $\tilde{\mathbf{Z}} = \{N_{CO}, N_O\}$ is obtained in a process that obeys the Markovian master equation 7.7 and that can be simulated by the Gillespie algorithm. Note also that if we consider that N_O evolves only through $W_3(N_O : N_{CO})$ and $W_4(N_O : N_{CO})$, where N_{CO} is a constant parameter that does not evolve, then N_O alone is also a Markov variable which satisfies the following master equation

$$\begin{aligned} \frac{d}{dt}H(N_O : N_{CO}; t) = & W_4(N_O - 2)H(N_O - 2 : N_{CO}; t) - W_4(N_O)H(N_O : N_{CO}; t) \\ & + W_3(N_O + 1)H(N_O + 1 : N_{CO}; t) - W_3(N_O)H(N_O : N_{CO}; t), \end{aligned} \quad (7.15)$$

with N_{CO} being kept constant.

The combined reduced system

$H(N_O : N_{CO}; t)$ will quickly relax to a stationary distribution. This equilibration implies that we should approximate Eq. 7.15, as

$$\frac{d}{dt}H(N_O : N_{CO}; t) \approx 0. \quad (7.16)$$

Thus, the resulting coupled master equations of our model are

$$\begin{aligned} \frac{d}{dt}G(N_{CO}; t) = & \tilde{W}_1(N_{CO} - 1)G(N_{CO} - 1; t) + \tilde{W}_2(N_{CO} + 1)G(N_{CO} - 1; t) \\ & - (\tilde{W}_1(N_{CO}) + \tilde{W}_2(N_{CO}))G(N_{CO}; t), \end{aligned} \quad (7.17)$$

$$\begin{aligned} 0 \approx & W_4(N_O - 2)H(N_O - 2 : N_{CO}; t) - W_4(N_O)H(N_O : N_{CO}; t) \\ & + W_3(N_O + 1)H(N_O + 1 : N_{CO}; t) - W_3(N_O)H(N_O : N_{CO}; t). \end{aligned} \quad (7.18)$$

Equation 7.17 is an one-step master equation with a well-know solution. The difficult part will be computing $H(N_O : N_{CO}; t)$ which is not more an one-step master equation.

Figure 7.1 shows a solution of Eq. 7.18 for $\theta_{CO} = N_{CO}/A = \text{const}$. It is clear that $H_{st}(N_O : N_{CO} = \text{const})$ is a sharply peaked monomodal function around a mean value. To simulate the fast oxygen variable we use the mean value of N_O obtained from Eq. 7.18 with keeping N_{CO} constant. In this chapter we will consider like in previous chapters that $p_{CO} + p_O = k = 1$.

7.3.2 Bistability

Table 7.2 shows the new transition probabilities derived after the adiabatic elimination of the oxygen coverage and considering the sharply peaked function $H_{st}(N_O : N_{CO} = \text{const})$. Note that in this case we use the approximation $\langle \theta_O \theta_O \rangle \approx \langle \theta_O \rangle^2$.

N_O is a mean value obtained from Eq. 7.18. In this case we will simulate directly the master equation for the fast variable using the Gillespie algorithm and then use the mean value from simulations to approximate the fast oxygen variable. Note that this procedure is different to previous chapters where the fast variable was approximated by the deterministic approximation [51, 52, 53, 54].

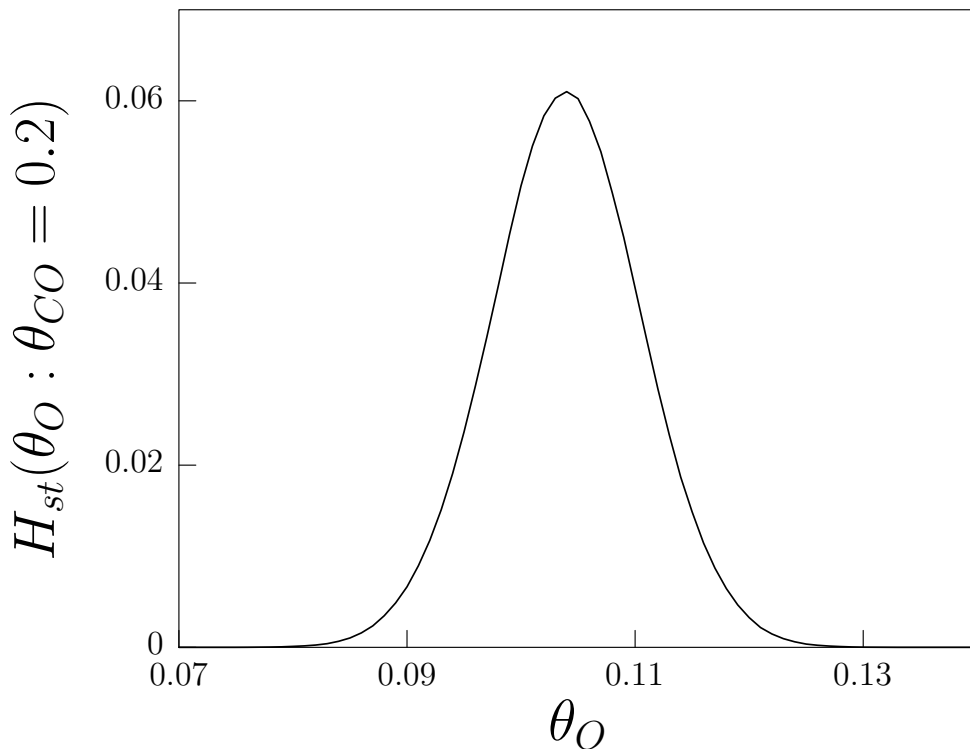


Figure 7.1: Conditional stationary probability distribution $H_{st}(\theta_O : \theta_{CO_{st}})$ from the Gillespie algorithm. In this case, $H_{st}(\theta_O : \theta_{CO_{st}} = 0.2)$ is shown in the coverage space with $A = 1000$, $p_{CO} = 0.15$ and $d = 0.030$. This conditional probability distribution is sharply peaked and unimodal around the mean value $\langle \theta_O \rangle \approx 0.105$.

| Event | Transition probability |
|---------------------------------|---|
| $N_{CO} \rightarrow N_{CO} + 1$ | $\tilde{W}_1 = p_{CO} \left[\frac{(A-2N_O)^4}{(A-N_O)^3} - N_{CO} \right]$ |
| $N_{CO} \rightarrow N_{CO} - 1$ | $\tilde{W}_2 = dN_{CO} + \frac{4kN_{CO}N_O}{A}$ |

Table 7.2: Transition probabilities for CO oxidation with $CO - O$ and $CO - O$ adspecies repulsion on unreconstructed noble metal surfaces after adiabatic elimination of N_O .

Stable states

In the rest of the chapter we will use, instead of Eq. 7.17, an alternative method to analyse the system. If a relative maximum of $G^{st}(N_{CO})$ is called a stable state of N_{CO} [74, 95], one notes that such point would have to satisfy

$$G^{st}(N_{CO}) > G^{st}(N_{CO} - 1), \quad (7.19)$$

and

$$G^{st}(N_{CO}) > G^{st}(N_{CO} + 1). \quad (7.20)$$

But from Eq. 7.17 and after invoking the detailed balance conditions

$$G^{st}(N_{CO}) = G^{st}(N_{CO} - 1) \frac{\tilde{W}_1(N_{CO} - 1)}{\tilde{W}_2(N_{CO})}, \quad (7.21)$$

and

$$G^{st}(N_{CO} + 1) = G^{st}(N_{CO}) \frac{\tilde{W}_1(N_{CO})}{\tilde{W}_2(N_{CO} + 1)}. \quad (7.22)$$

This implies that, for any relative maximum of $G^{st}(N_{CO})$

$$\frac{\tilde{W}_1(N_{CO} - 1)}{\tilde{W}_2(N_{CO})} > 1, \quad (7.23)$$

and

$$\frac{\tilde{W}_1(N_{CO})}{\tilde{W}_2(N_{CO} + 1)} < 1, \quad (7.24)$$

or equivalently

$$\tilde{W}_1(N_{CO} - 1) - \tilde{W}_2(N_{CO}) > 0, \quad (7.25)$$

and

$$\tilde{W}_1(N_{CO}) - \tilde{W}_2(N_{CO} + 1) < 0. \quad (7.26)$$

Now we define a new function $\alpha(N_{CO})$ by

$$\alpha(N_{CO}) = \tilde{W}_1(N_{CO} - 1) - \tilde{W}_2(N_{CO}). \quad (7.27)$$

We see that the preceding two inequalities can be written more simply as

$$\alpha(N_{CO}) > 0, \quad (7.28)$$

and

$$\alpha(N_{CO} + 1) < 0. \quad (7.29)$$

Finally, a N_{CO}^{st} integer is a relative maximum of $G^{st}(N_{CO})$ if:

$$\alpha(N_{CO}^{st}) = 0, \quad (7.30)$$

and

$$\alpha'(N_{CO}^{st}) < 0. \quad (7.31)$$

In our reduced model for CO oxidation with adspecies repulsions we have:

$$\alpha(N_{CO}^{st}) = p_{CO} \left[\frac{(A - 2N_O^{st})^4}{(A - N_O^{st})^3} - (N_{CO}^{st} - 1) \right] - dN_{CO}^{st} - \frac{4kN_{CO}^{st}N_O^{st}}{A} = 0, \quad (7.32)$$

and

$$\alpha'(N_{CO}^{st}) = -p_{CO} - d - \frac{4kN_O^{st}}{A} < 0, \quad (7.33)$$

where N_O^{st} is obtained from

$$\begin{aligned} 0 \approx & W_4(N_O - 2)H(N_O - 2 : N_{CO}^{st}; t) - W_4(N_O)H(N_O : N_{CO}^{st}; t) \\ & + W_3(N_O + 1)H(N_O + 1 : N_{CO}^{st}; t) - W_3(N_O)H(N_O : N_{CO}^{st}; t). \end{aligned} \quad (7.34)$$

Figure 7.2(a) shows $\alpha(N_{CO})$ as a function of N_{CO} . Note that the intersections of $\alpha(N_{CO})$ with 0 are the stable and unstable states of our reduced model with adspecies repulsions. In Fig.7.2(b), the bifurcation diagram is shown for $A = 1000$. Note that this bifurcation diagram can change as a function of A [95, 143, 146].

7.3.3 Critical Fluctuations and the dependence of fluctuations on the system size

In this section, we study the fluctuations near the critical point of a phase diagram shown in Fig. 7.2(a), and the fluctuations as a function of the system size A . It is a well known that the fluctuations increase near a critical point and that far away from a critical point the fluctuations are inversely proportional to the system size [79].

Critical fluctuations

In order to estimate the magnitude of fluctuations near the critical pint of a phase diagram, we plot in Fig. 7.3 the amplitude of fluctuations versus d for fixed p_{CO} near the critical point. We consider for simulations the original system without adiabatic elimination of oxygen coverage. The magnitude of fluctuations is

$$FF = \frac{\sum_{t=0}^T [N_{CO}(t) - \mu]^2}{T\mu^2}, \quad (7.35)$$

where

$$\mu = \frac{\sum_{t=0}^T N_{CO}(t)}{T}. \quad (7.36)$$

As d approaches d_C , FF increases drastically.

Fluctuations as a function of system size

An appropriate measure of the relative size of the fluctuations is the coefficient of variance, which is defined as the ratio of the variance to the mean square [172]. The stationary coefficient of the variance can be written as

$$CV = \frac{Var}{\mu^2}, \quad (7.37)$$

where

$$Var = \langle N_{CO}^2 \rangle - \langle N_{CO} \rangle^2, \quad (7.38)$$

and again

$$\mu = \langle N_{CO} \rangle. \quad (7.39)$$

In order to derivate analytical expressions for the variance, we calculate the stationary

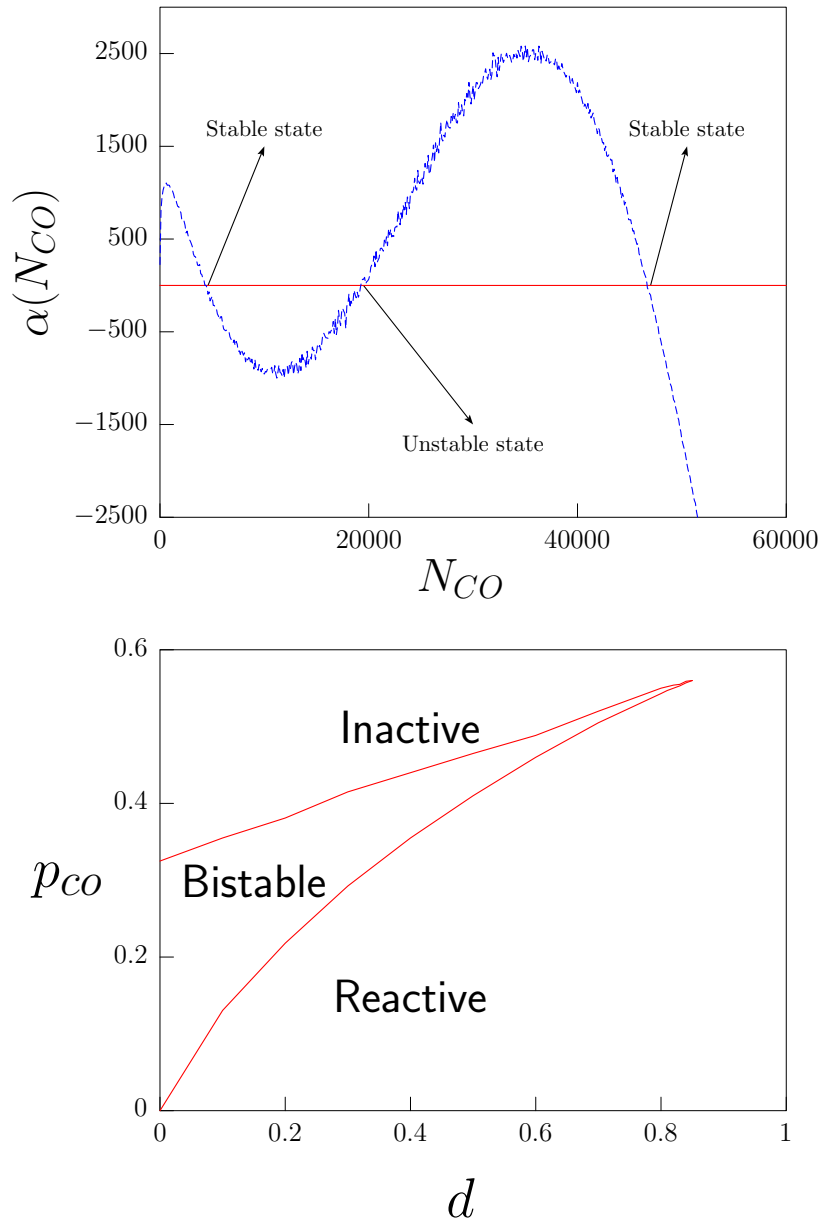


Figure 7.2: (a) $\alpha(N_{CO})$ as a function of N_{CO} for $A = 100000$, $p_{CO} = 0.4$, and $d = 0.4$. (b) Bifurcation diagram from the reduced model in the parameter space (d, p_{CO}) for $A = 1000$.

moments in the following way:

The general stationary master equation reads

$$0 = \tilde{W}_1(N_{CO} - 1)G^{st}(N_{CO} - 1) + \tilde{W}_2(N_{CO} + 1)G^{st}(N_{CO} - 1) - (\tilde{W}_1(N_{CO}) + \tilde{W}_2(N_{CO}))G^{st}(N_{CO}), \quad (7.40)$$

where the stationary moments we need are

$$\langle N_{CO} \rangle = \sum_{N_{CO}} N_{CO} G^{st}(N_{CO}; t), \quad (7.41)$$

and

$$\langle N_{CO}^2 \rangle = \sum_{N_{CO}} N_{CO}^2 G^{st}(N_{CO}; t). \quad (7.42)$$

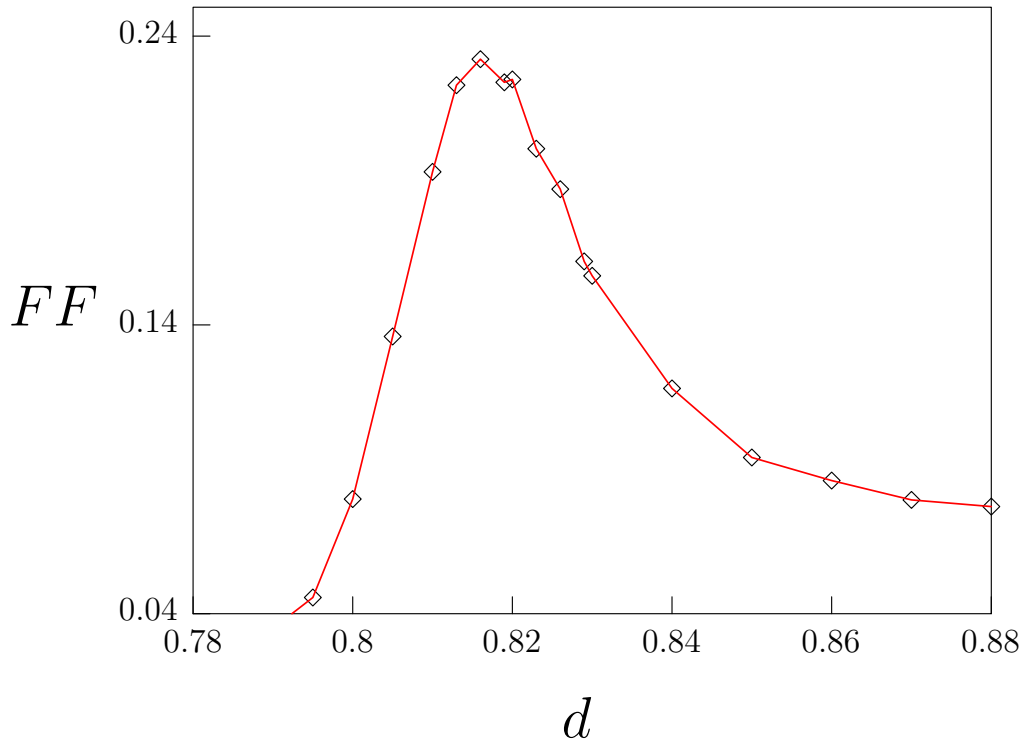


Figure 7.3: Amplitude of fluctuations versus d from the original system without adiabatic elimination of oxygen with $p_{CO} = 0.552$ and $A = 1000$.

After some algebra, it is easy to show that the "first moment" is derived from [4]

$$0 = \sum_{\rho=1}^2 v_{\rho} \langle \tilde{W}_{\rho}(N_{CO}) \rangle. \quad (7.43)$$

Thus, in our case

$$0 = p_{CO} \left[\frac{(A - 2N_O)^4}{(A - N_O)^3} - \langle N_{CO} \rangle \right] - d \langle N_{CO} \rangle - \frac{4k \langle N_{CO} \rangle N_O}{A}, \quad (7.44)$$

or

$$\langle N_{CO} \rangle = \frac{p_{CO}(A - 2N_O)^4 / (A - N_O)^3}{p_{CO} + d + 4N_O/A}. \quad (7.45)$$

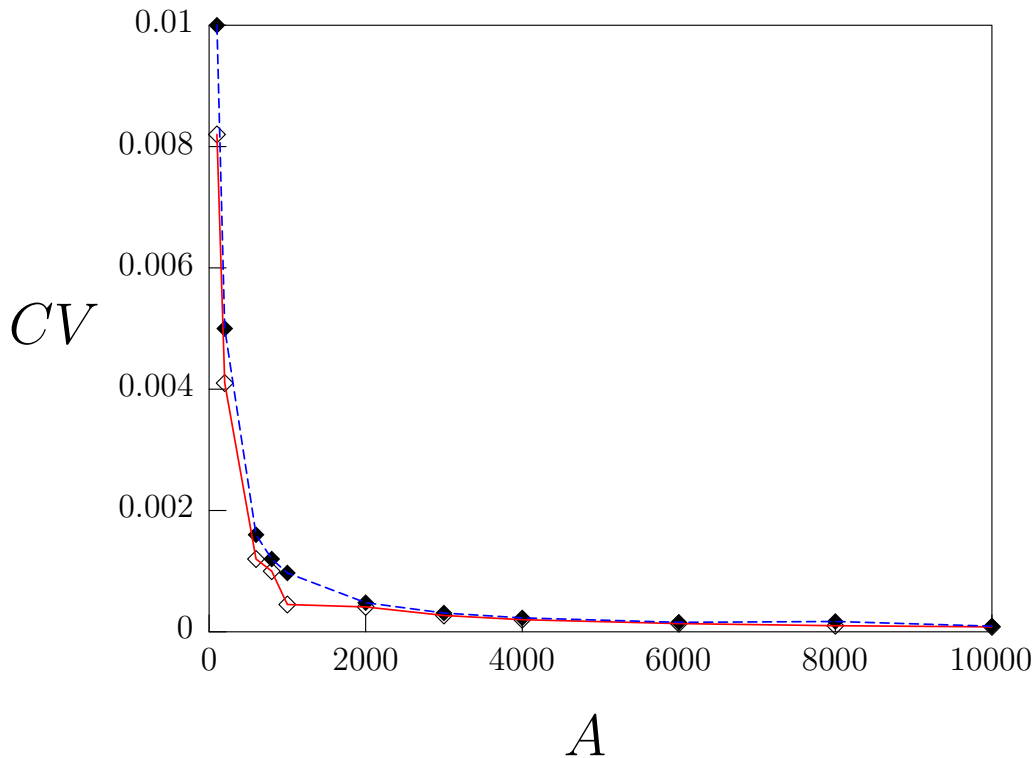


Figure 7.4: CV versus A with $d = 0.4$ and $p_{CO} = 0.5$. Dashed line correspond to simulations of the whole system, and solid line to Eq. 7.48.

On the other hand, to obtain the "second moment" we have to solve

$$0 = 2 \sum_{\rho=1}^2 v_{\rho} \langle N_{CO} \tilde{W}_{\rho}(N_{CO}) \rangle + \sum_{\rho=1}^2 v_{\rho}^2 \langle \tilde{W}_{\rho}(N_{CO}) \rangle. \quad (7.46)$$

Then, after some algebra

$$\langle N_{CO}^2 \rangle - \langle N_{CO} \rangle^2 = \frac{d + 4N_O/A}{p_{CO} + d + 4N_O/A} \langle N_{CO} \rangle. \quad (7.47)$$

Finally, for the reduced model the coefficient of the variance is

$$CV = \frac{1}{\langle N_{CO} \rangle} \frac{d + 4N_O/A}{p_{CO} + d + 4N_O/A} \propto \frac{1}{A}. \quad (7.48)$$

Figure 7.4 shows CV versus A . Dashed line corresponds to simulations of the original system, and solid line to Eq. 7.48.

7.3.4 Fluctuations about a stable state

We shall be concerned here with fluctuations about a stable state N_{CO}^{st} which is located in the highest point of a well resolved peak in the function $G^{st}(N_{CO})$. We start assigning to each stable state a nominal width $\chi(N_{CO}^{st})$. We shall define $\chi(N_{CO}^{st})$ to be the effective width of the Gaussian shaped curve that best fits $G^{st}(N_{CO}; t)$ in the immediate neighborhood of the peak point N_{CO}^{st} . To obtain an expression for $\chi(N_{CO}^{st})$, we begin by estimating the first derivative of $G^{st}(N_{CO})$ as

$$G^{st'}(N_{CO}) \approx \frac{G^{st}(N_{CO}) - G^{st}(N_{CO} - 1)}{1} = G^{st}(N_{CO} - 1) \frac{\tilde{W}_1(N_{CO} - 1)}{\tilde{W}_2(N_{CO})} - G^{st}(N_{CO} - 1). \quad (7.49)$$

A final approximation yields

$$G^{st'}(N_{CO}) \approx \frac{G^{st}(N_{CO})}{\tilde{W}_2(N_{CO})} \alpha(N_{CO}). \quad (7.50)$$

Using the properties of $\alpha(N_{CO})$, we find that the second derivative of $G^{st}(N_{CO})$ evaluated in N_{CO}^{st} is given by

$$\frac{dG^{st'}(N_{CO})}{dt} \approx -G^{st}(N_{CO}^{st}) \left| \frac{\alpha'(N_{CO}^{st})}{\tilde{W}_2(N_{CO}^{st})} \right|. \quad (7.51)$$

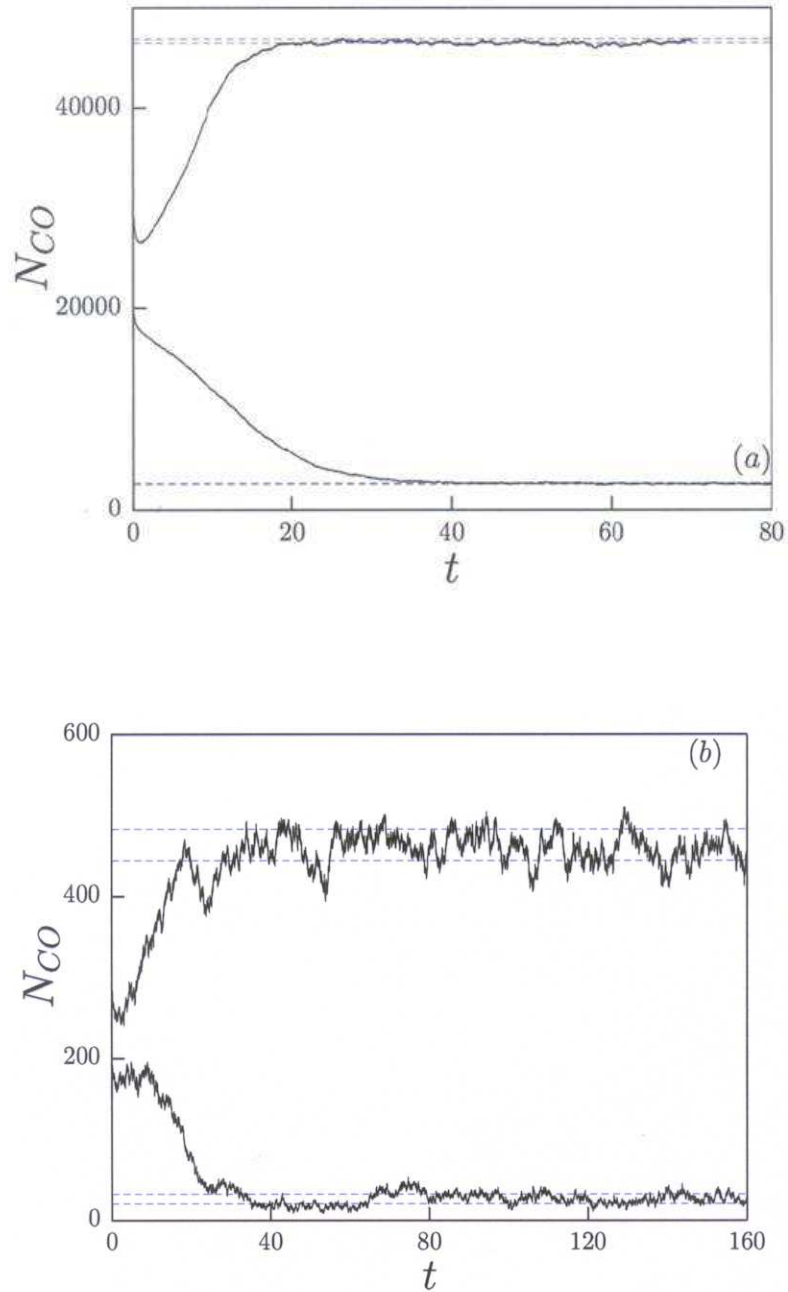


Figure 7.5: (Color online) Time series of $N_{CO}(t)$ with $p_{CO} = 0.4$, and $d = 0.4$. Dotted lines correspond to $N_{CO}^{st} \pm \chi(N_{CO}^{st})/2$. Simulations represented by the solid lines are obtained from the original system. (a) $A = 100000$. (b) $A = 1000$.

Finally, if we identify the previous calculations with the problem of estimating the width and area of a function peak, it is possible to show that [74]

$$\chi(N_{CO}^{st}) = \left| \frac{2\pi\tilde{W}_2(N_{CO}^{st})}{\alpha'(N_{CO}^{st})} \right|. \quad (7.52)$$

If the peak in the function $G^{st}(N_{CO})$ at N_{CO}^{st} is roughly symmetric and does not significantly overlap any adjacent peak, we shall say that

$$N_{CO}(t) \in [N_{CO}^{st} - \chi(N_{CO}^{st})/2, N_{CO}^{st} + \chi(N_{CO}^{st})/2]. \quad (7.53)$$

To illustrate this results, consider our reduced model inside the bistable range with $p_{CO} = 0.4$, and $d = 0.4$. For the case when $A = 100000$, the two stable states are $(N_{CO}^{st} = 2667, N_O^{st} = 25710)$ and $(N_{CO}^{st} = 46675, N_O^{st} = 683)$. Thus, one obtain from Eq. 7.52

$$N_{CO}^{st} \pm \chi(N_{CO}^{st})/2 \approx 2667 \pm 57.2, \quad (7.54)$$

and

$$N_{CO}^{st} \pm \chi(N_{CO}^{st})/2 \approx 46675 \pm 194.5. \quad (7.55)$$

On the other hand, for $A = 1000$ the two stable states are $(N_{CO}^{st} = 27, N_O^{st} = 263)$ and $(N_{CO}^{st} = 464, N_O^{st} = 7)$ and we obtain

$$N_{CO}^{st} \pm \chi(N_{CO}^{st})/2 \approx 27 \pm 5.8, \quad (7.56)$$

and

$$N_{CO}^{st} \pm \chi(N_{CO}^{st})/2 \approx 464 \pm 19.5. \quad (7.57)$$

Figure 7.5 summaries this results. Dotted lines correspond to $\chi(N_{CO}^{st})/2$. Simulations represented by the solid lines are obtained from the original system (without adiabatic elimination of oxygen coverage).

7.4 Summary and conclusions

A stochastic hybrid model for CO oxidation on metal surfaces with $CO-CO$ and $CO-O$ adspecies repulsions was introduced. After adiabatic elimination of the fast oxygen variable, an 1-d reduced version of this model is obtained. The fast N_O variable is simulated

using the Gillespie algorithm which produces numerical solutions of the master equation 7.18 for N_{CO} fixed. As in previous chapters we derived a master equation for N_{CO} which in our case is soluble. However, in some cases this type of master equations not soluble and other approximations are required. Motivated by this, we use a different method to study our reduced model. This method allows us to obtain the bistable phase diagram in the parameter space (d, p_{CO}) without having to solve solve Eq. 7.17. We derived expressions for the first two moments of N_{CO} in order to study the fluctuation behavior. These moments allow us to obtain analytical expression for the coefficient of the variance, and thus to study critical and system size fluctuations as well as the fluctuations around stable states. The results showed in this chapter correspond a starting point to more detailed studies of fluctuations in CO oxidation with adspecies repulsions.

Part IV

**CONCLUSIONS AND
PERSPECTIVES**

Chapter 8

Conclusions

8.1 Summary and outlook

The study of chemical processes on nanometer scale surfaces where the internal fluctuations are potentially large are not only of academical importance but provide also a challenge for the practical design of catalysts. This has been the motivation in recent years to study experimentally and theoretically these nanosystems. In this Thesis the role of internal fluctuations in the kinetic bistability of CO oxidation on unreconstructed metal surfaces of nanoscale dimensions was studied through a mean-field birth-death-type master equation framework and Gillespie-type kinetic Monte Carlo simulations. From this perspective, one only tracks the total numbers of different species and their increment and decrement using macroscopic rate laws to model the respective transition rates (see Chap. 3). The models used in this Thesis for CO oxidation on nanoscale surfaces incorporate both rapid diffusion of adsorbed CO, and adspecies repulsions. Three minimal interacting models are introduced, the first one is appropriate for homogeneous systems with a large diffusion length of CO, the second one is appropriate for limited diffusion conditions or inhomogeneous systems, and the last one can be used to analyse both, homogeneous and inhomogeneous systems.

It is well known that CO oxidation on structurally stable catalytical surfaces exhibits robust bistability (two stable kinetic stationary states coexist in the same parameter range). In particular, experimental studies of CO oxidation on a Pt field emitter tip and on Pd nanoparticle surfaces suggest that internal fluctuations can induce transitions between two stable states (see Chap. 2 and Refs. [13, 15]). At low enough pressure, CO molecules can diffuse very fast on a nanoscale surface and a well-stirred nanosystem is produced which exhibits only homogeneous coverage or internal fluctuations. Thus spatially homogeneous

transitions from one stable state to the other stable state and vice versa can be observed. In Chap. 4, we analyzed a hybrid model for CO oxidation on nanoscale surfaces which incorporates both rapid diffusion of adsorbed CO, and superlattice ordering of adsorbed immobile oxygen on a square lattice of adsorbed sites (eight-site adsorption rule). Transition probabilities for each reaction step are derived allowing us to construct a stochastic formalism through a mean-field birth-death-type master equation. This equation is reduced after adiabatic elimination of the oxygen variable. Finally, a reduced stochastic hybrid model was obtained which was used to study the role of fluctuations in CO oxidation under large diffusion length (Chap. 5 and 6). In Chap. 5, we analyzed the role of internal fluctuations in the kinetic bistability of CO oxidation on surfaces well mixed on a nanoscale. It was shown analytically that internal (coverage) fluctuations induce transitions between the two stable kinetic stationary states of the bistable region. These theoretical predictions derived from the reduced model have been found to be in reasonable agreement with stochastic simulation of the original system by the Gillespie-type kinetic Monte Carlo algorithm. In this way, our results are able to capture and to verify experimental observation for fluctuation-induced transitions in CO oxidation on a Pt field emitter tip and on Pd nanoparticle surfaces.

At high pressure, the diffusion length of CO molecules on surfaces is reduced and the effects of adspecies interactions become important. Stochastic patterns ('raindrop patterns'), experimentally observed in catalytic CO oxidation on Pt(110) at relatively high pressure, were recently interpreted as being initiated by stochastic density fluctuations (see Chap. 2 and Ref. [47]). In Chap. 6, stochastic effects are taken into account by dividing the surface into a square lattice of nanoscale cells, each containing A adsorption sites. A reaction-diffusion master equation for the probability of finding CO and oxygen coverage at a time t , that allows local fluctuations, is introduced. We are able to solve this complicated reaction-diffusion master equation after invoking the mean-field approach together with the adiabatic elimination of oxygen. We showed, using mean-field theory and adiabatic elimination techniques together with 2-d Gillespie-type kinetic Monte Carlo simulations, that a first-order phase transition exists in a stochastic model for catalytic CO oxidation under diffusion limited conditions. We were able to reproduce two-phase coexistence as well as nucleation and growth of active islands embedded in an inactive phase. Finally, in order to study the role of adspecies interactions in CO oxidation on nanoscale surfaces at high pressure, a stochastic hybrid model for CO oxidation on metal surfaces with $CO-O$ and $O-O$ adspecies repulsions was introduced in Chap. 7. In contrast to previous models, CO molecules can be randomly distributed on sites not occupied by oxygen if this sites

have not nearest-neighbor oxygen atoms. The eight-site adsorption rule for oxygen is also implemented together with the restriction imposed by the $CO - O$ adspecies repulsion. After adiabatic elimination of the fast oxygen variable, an 1-d reduced version of this model is obtained. We used a method that allows us to obtain the bistable phase diagram in the parameter space (d, p_{CO}) without having to solve any master equation. We derived also expressions for the first two moments of the number of CO molecules. These moments allowed us to study critical and system size fluctuations as well as the fluctuations around stable states.

This Thesis provides a first attempt to the development of a general theoretical framework in order to understand the role of internal fluctuations in the reaction kinetics of heterogenous catalysis, in particular for catalytic CO oxidation on metal surfaces. Nevertheless, we expect to observe fluctuation-induced effects, like those presented in this work, in many real catalytical reactions at high-, as well as in low-, pressure experiments, if these reactions exhibit multistability.

8.2 List of specific results

We will now summaries our main novel results divided by chapters. The results of this Thesis open many possible extensions, and some of the possible prospectives that could be studied in the future are discussed in the last section of this chapter.

Chapter 4: Reduced stochastic kinetic model (Ref. [51]).

- Using transition probabilities for each reaction step a hybrid master equation description of our model for CO oxidation which incorporates both rapid diffusion of adsorbed CO, and $O - O$ adsorbed repulsions was derived (Sec. 4.4). It was shown that this model in the deterministic limit exhibits bistability in the parameter space (d, p_{CO}) (Sec. 4.3). In the hybrid approximation CO adsorbed molecules are randomly distributed on sites not occupied by oxygen adsorbed atoms.
- After showing in Fig. 4.3(a) that the nullcline $d\theta_O/dt$ (solid line) is rapidly reached from any initial conditions, the oxygen variable is adiabatically eliminated from the master equation, and a reduced one-component model is obtained (Sec. 4.5).
- Based on the previous adiabatic elimination of the fast oxygen, the slow variable represented by the number of the CO adsorbed molecules is represented by a soluble one-step master equation. On the other hand, the fast oxygen variable is represented

by a more complicated master equation for $H_{st}(N_O : N_{CO} = const)$. In Fig. 4.3(b), it was shown that $H_{st}(N_O : N_{CO} = const)$ is a sharply peaked monomodal function around N_O . Using this results, the fast oxygen variable is modelled by the deterministic equation derived from the transition probabilities that only affect this fast variable (Sec. 4.5). The adiabatic elimination of fast oxygen signifies a great advance because it allows us to obtain analytical solutions in our model which can be compared with stochastic simulations and real experiments (Sec. 4.5).

Chapter 5: Fluctuation-induced transitions (Ref. [51]).

- It was shown that the reduced deterministic hybrid model still is able to produce bistability in the parameter space (d, p_{CO}) (Sec. 5.2.1).
- Using the Gillespie algorithm it was show that the stochastic version of the original model introduced in Chap. 4 is able to produce fluctuation-induced transitions which are similar to experiments with CO oxidation on a Pt field emitter tip and on Pd nanoparticle surfaces (Sec. 5.2.1).
- From previous results, it is clear that the deterministic description is not enough to describe kinetic processes at the nanoscale. Therefore, a stochastic description is fundamental. Using the reduced one-step master equation for the slow variable represented by the number of CO adsorbed molecules, probability distribution functions where obtained and verified by Gillespie stochastic simulations (Sec. 5.3.1).
- These analyses reveal an enhancement of fluctuations near the critical point for small surfaces (Sec. 5.3.3 and Sec. 5.3.3)
- Analytical equations for the transition time between stable state are derived and compered with stochastic simulations. Such analyses reveal that the rate of transitions between stable states decreases exponentially with surface area (Sec. 5.3.3).
- It is shown that the transition times approach the relaxation time for small surface areas. The relaxation time is theoretically derived.

Chapter 6: Fluctuation-induced first-order phase transitions (Ref. [52, 53]).

- In order to study stochastic effects under weak enough diffusion, a surface was divided into a square lattice of M cells denoted by i , which are smaller than the diffusion length. Each small cell was represented as a $L \times L = A$ square grid of

adsorption sites. A reaction-diffusion master equation of this system was introduced (Sec. 6.3).

- A mean-field approximation is applied to our reaction-diffusion master equation. This allows us to construct a reduced one-step mean-field coupling master equation which is analytically soluble after adiabatic elimination of the fast oxygen variable (Sec. 6.4 and Sec. 6.5). The fast oxygen variable is again simulated by a deterministic approach.
- An effective potential is introduced from the probability distribution function obtained above which was used to study the fluctuations (Sec. 6.6.1).
- An order parameter equation was derived from this analysis. The multiple solutions of this complicated equation reflected the possibility of bifurcations that break the ergodicity associated with the presence of a true first-order phase transition and two-phase coexistence between a low coverage active steady state and a high coverage inactive steady state. Bifurcation diagrams of the number of adsorbed CO molecules verified this finding. Finally, a phase diagram in the parameter space was constructed. This phase diagram is split in two regions. One region consists of two stable solutions and one unstable solution of the order parameter corresponding to three probability distribution functions. The second region is characterized by only one probability distribution function corresponding to one stable solution of the order parameter (Sec. 6.6.2).
- In order to verify the analytical predictions, simulations were carried out using two different extensions of the Gillespie algorithm: i) First, a version of the Gillespie algorithm with random local and nonlocal coupling was introduced. In this case, we have random connections between cell through CO adsorbed diffusion (Sec. 6.7.1). ii) In the second case, a different version of the Gillespie algorithm incorporating local coupling or normal diffusion, which describes correctly a 2-d surface, was constructed. Here, CO adsorbed molecules can jump only to nearest-neighbor cells (Sec. 6.7.2). The simulation results were in accordance with theoretical predictions.
- It was demonstrated that the phenomenon of nucleation and growth giving rise to transitions between the stable states of the phase diagram previously obtained from the theory. We observed that first one island with a composition corresponding to active state is formed and then this island starts to growth as a function of time.

This growth stops when the surface is completely covered by the active stable state (Sec. 6.7.3).

Chapter 7: A reduced stochastic hybrid model with adspecies repulsions (Ref. [54]).

- The so-called cluster approximation was used to construct a stochastic hybrid mean-field model for CO oxidation on nanoscale surfaces with $CO-O$ and $O-O$ adspecies repulsive interactions. In this case, CO molecules can be randomly distributed on sites not occupied by oxygen if this sites have not nearest-neighbor oxygen atoms (Sec. 7.2.1).
- An alternative method, where master equations have not to be solved, allows us to demonstrate that the reduced version of the original model presents bistability in the parameters space (Sec. 7.3).
- In order to study critical fluctuations and fluctuations depending on the system size, the first two moments of the number of CO molecules were analytically derived. They allow us to obtain an analytical expression for the coefficient of the variance which showed that the fluctuations increase near the critical point and that also increase decreasing surface area (Sec. 7.3.3).
- Finally, the fluctuations around the stable states are analytically estimated by using the effective width of the Gaussian shaped curve that best fits the probability distribution function of the number of CO adsorbed molecules in the immediate neighborhood of the peak point of stability (Sec. 7.3.4).

8.3 Open issues

A short list of possible extensions, open questions, and applications of the previous results is provided below:

- It could be interesting to compare the theoretical predictions and Gillespie-type kinetic Monte Carlo simulations of this thesis with lattice-gas atomistic Monte Carlo simulations. Typically, master equation descriptions of stochastic systems do not take into account spatial correlations induced by adspecies interactions [49].
- The simulation of the fast oxygen variable by a deterministic equation should be generalised to include the fluctuations that this variable produces.

- Due to limited diffusion length at high pressure we expect to observe strong fluctuation effects in a real catalytical reactions, if these reactions exhibit multistability. In order to adapt the model to such situations, we need to take into account the energetic interactions between the adparticles and non-isothermal conditions generated by the reaction heat.
- Our reaction-diffusion model can in principle be used to study fluctuations on inhomogeneous metal surfaces, where structural defects such steps or impurities are present. The structural defects can be considered as small regions on the surface with different kinetic parameters coupled by CO diffusion. An interesting extension could also be to use stochastic models, like the master equation used in this Thesis, in order to study an array of nanoparticles coupled globally through the gas phase [173, 174, 175, 176, 177, 178]. An extension of our model to study CO oxidation on a field-emitter tip is desirable.
- New experimental studies of the role of internal and external fluctuations in heterogeneous catalysis are desirable.
- The phase transition and the nucleation phenomena, described in this work, has to be study in more detail both by numerical and real experiments. At the same time new and more efficient spatial stochastic algorithmc must be development.
- The models used in this work are still simplistic. To precisely describe fluctuations in actual systems, some other ingredients must be considered [18, 19, 20, 21]. Some of these ingredients are:
 - 1) Energetic interactions between adparticles.
Island formation on the surface.
Kinetic parameters as a function of coverage.
Non-Fickian diffusion.
 - 2) Precursor kinetics for adsorption of CO molecules.
 - 3) Surface defects (locally different kinetic parameters).
 - 4) Substrate modification.
Adsorbate-induced structural phase transition.
Oxidation/reduction.
Catalytic activity.

5) Non-isothermal effects at high pressure.

Appendix A

Notation and Symbols

| | |
|------------------------------|---|
| N | Total population in a chemical reaction |
| $\tilde{\mathbf{Z}}$ | Population vector |
| \mathbf{v}_ρ | Stoichiometric vector |
| $P(\tilde{\mathbf{Z}}; t)$ | Probability of having a determinate number of molecules |
| $W_\rho(\tilde{\mathbf{Z}})$ | Reaction transition probability |
| P^{reac} | Reaction probability distribution function |
| P^{diff} | Diffusion probability distribution function |
| M_μ^i | Diffusion transition probability |
| L^2 | Cell area |
| n_j | Occupancy of site j |
| n | Configuration of the entire system |
| $P(n; t)$ | Probability for the system to be in a n configuration |
| ρ | Reaction steps |
| τ | Time for the next reaction in the Gillespie algorithm |
| N_Z | Number of sites not occupied by oxygen |
| N_A | Number of A |
| N_B | Number of B |
| θ_A | A coverage |
| θ_B | B coverage |
| k | CO_2 production rate |
| p_{CO} | CO adsorption rate |
| p_{O_2} | O adsorption rate |
| h_{CO} | CO diffusion rate |

| | |
|---------------------------|---|
| h_O | O diffusion rate |
| d | CO desorption rate |
| A | Surface Area |
| E | Empty sites |
| Z | Sites not occupied by oxygen adatoms |
| $\{J\}$ | Fraction of sites in state J |
| $\{KJ\}$ | Probability of a specific KJ pair |
| NN | Nearest-neighbor empty sites |
| N_{CO} | Number of CO molecules |
| N_O | Number of O atoms |
| θ_{CO} | CO coverage |
| θ_O | O coverage |
| N_{CO}^{local} | Local number of CO molecules in the hybrid approximation |
| $G(N_{CO})$ | Probability distribution for the number of N_{CO} molecules |
| $H(N_O : N_{CO})$ | Conditional probability distribution of oxygen |
| $\tilde{W}_{1,2}(N_{CO})$ | Conditional expectation of $W_{1,2}(N_{CO})$ |
| FET's | Field emitter tips |
| KMC | Kinetic Monte Carlo |
| $T^{ac}(N_{CO})$ | Transition time from N_{CO}^a to N_{CO}^c |
| $T^{ca}(N_{CO})$ | Transition time from N_{CO}^c to N_{CO}^a |
| $\phi(\theta_{CO})$ | Effective potential |
| τ_{rel} | Relaxation time |
| RDME | Reaction-diffusion master equation |
| PDF | Probability distribution functions |
| h | Microscopic hop rate |
| S_A^i | Normalized sticking probability for oxygen |
| M | Number of cells |
| N_{CO}^m | Average value of CO molecules inside each cell |
| $\beta(N_{CO}^m)$ | Order parameter |
| MFCME | Mean-field coupling master equation |
| P^{MF} | Mean-field probability distribution function |
| $F(N_O : N_{CO})$ | Conditional probability distribution of oxygen |
| $H_{1,2}(N_{CO})$ | Transition probabilities of the MFCME |
| Z^+ | Z site with nearest-neighbor oxygen atoms |
| Z^- | Z site with not nearest-neighbor oxygen atoms |

| | |
|---------------------|---|
| E^+ | Empty site with nearest-neighbor oxygen atoms |
| E^- | Empty site with not nearest-neighbor oxygen atoms |
| FF | Amplitude fluctuations |
| μ | Mean value |
| CV | Coefficient of the variance |
| Var | Variance |
| $\chi(N_{CO}^{st})$ | Nominal width |
| $\xi_{1,2}(t)$ | Gaussian white noise |

Appendix B

Cluster approximation for lattice models

The cluster approximation start with the probabilities $\{X_1X_2\cdots X_j\}$ that any j consecutive sites be in the states $X_1X_2\cdots X_j$. Any lattice model can be defined in terms of j -cluster processes, $X_1X_2\cdots X_j \rightarrow Y_1Y_2\cdots Y_j$, occurring at some specified rate. For example, a system where each site can be in only one of two states, A or B, with the process $AA \rightarrow BB$ taking place at rate k . Whenever the $AA \rightarrow BB$ process occurs the number of BB pairs is increased a least by one. If the site to the right (left) of the AA pair is in state B an additional BB pair is created. Thus

$$\frac{d\{BB\}}{dt} = k\{AA\} + k\{AAB\} + k\{BAA\}. \quad (\text{B.1})$$

Similarly, a rate equation for $\{BAA\}$ would involve four-site clusters; a BAA state is destroyed if the two rightmost sites in BAAA undergo a conversion to BB. This results an infinite hierarchy of rate equations for increasing cluster sizes. The cluster method consists in approximating large cluster probabilities in terms of the probabilities of no larger than n -site clusters (n is then called the size of the approximation).

Implicit in the cluster method is the assumption that the system is translationally symmetric; cluster probabilities are independent of the position of the cluster on the lattice. Consider a system where each site can either empty (state E) or occupied by an A particle (state A). Then, for example,

$$\{AA*\} = \{AAA\} + \{AAE\} = \{AAA\} + \{EAA\} = \{AA\}, \quad (\text{B.2})$$

where * indicates an unspecified state. The resultant relation $\{AAE\} = \{EAA\}$ follows solely from translation invariance. Finally, we can also consider the normalization condition:

$$\sum_{X_1 X_2 \cdots X_j} \{X_1 X_2 \cdots X_j\} = 1. \quad (\text{B.3})$$

B.1 The (n, m) approximation

Consider the following approximation

$$\{X_1 X_2 \cdots X_n X_{n+1} \cdots\} = \{X_1 X_2 \cdots X_n\} \{X_{n+1} \cdots\}. \quad (\text{B.4})$$

Because it assumes zero overlap between adjacent n -clusters, we term it the $(n, 0)$ approximation. In the next level of complexity, we allow for an overlap of one site between adjacent clusters and account for correlations resulting from this overlap. In the $(n, 1)$ approximation, we have then

$$\{X_1 X_2 \cdots X_n X_{n+1} \cdots\} = \{X_1 X_2 \cdots X_n\} \frac{\{X_n X_{n+1} \cdots\}}{\{X_n\}}. \quad (\text{B.5})$$

As an example, consider a six-cluster in the state ABCDEF. In the $(3, m)$ class its probability would be given by:

1) $(3, 0)$ approximation

$$\{ABCDEF\} = \{ABC\} \{DEF\}. \quad (\text{B.6})$$

2) $(3, 1)$ approximation

$$\{ABCDEF\} = \{ABC\} \frac{\{CDE\}}{\{C\}} \frac{\{EF*\}}{\{E\}}. \quad (\text{B.7})$$

3) $(3, 2)$ approximation

$$\{ABCDEF\} = \{ABC\} \frac{\{BCD\}}{\{BC\}} \frac{\{CDE\}}{\{CD\}} \frac{\{DEF\}}{\{DE\}}. \quad (\text{B.8})$$

Notice that only the expression for the $(3, 2)$ approximation satisfy translational

invariance. Care should be taken to properly account for all possibilities and to preserve thereby the fundamental property of translational invariance. The $(n, n-1)$ approximation is the most elegant, in that it takes care of translational symmetry automatically. In particular, the $(2, 1)$ approximation is the approximation used in this thesis. It is known as the "pair approximation" in the literature. We have considered in this analysis only an one-dimensional lattice, but an extension to two-dimensional lattices is easy.

Appendix C

Adiabatic reduction of fast variables

We consider the general chemical master equation of the reactive stochastic process with the number of reaction channels $\rho = 1, 2, \dots, r$. One can partition the systems in two subsets: the fast and the slow variables.

By splitting state vector $\tilde{\mathbf{Z}}$ into the slow variables vector \mathbf{X} and the fast variables vector \mathbf{Y}

$$\tilde{\mathbf{Z}} = \{\mathbf{X}, \mathbf{Y}\}, \quad (\text{C.1})$$

and

$$\mathbf{v}_\rho = \{\mathbf{v}_\rho^{\mathbf{x}}, \mathbf{v}_\rho^{\mathbf{y}}\}. \quad (\text{C.2})$$

We decompose the joint probability as

$$P(\mathbf{X}, \mathbf{Y}; t) = G(\mathbf{X}; t)H(\mathbf{Y} : \mathbf{X}; t), \quad (\text{C.3})$$

where $H(\mathbf{Y} : \mathbf{X}; t)$ is the conditional probability for \mathbf{X} kept constant. We also require

$$\sum_{\mathbf{X}} G(\mathbf{X}) = 1, \quad (\text{C.4})$$

$$\sum_{\mathbf{Y}} H(\mathbf{Y} : \mathbf{X}) = 1. \quad (\text{C.5})$$

Inserting Eqs. (C.3) into the master equation and summing up over \mathbf{Y} , we obtain

$$\frac{d}{dt}G(\mathbf{X}; t) = \sum_{\rho=1}^r [\tilde{W}_\rho(\mathbf{X} - \mathbf{v}_\rho^x/\mathbf{X})G(\mathbf{X} - \mathbf{v}_\rho^x; t) - \tilde{W}_\rho(\mathbf{X}/\mathbf{X} - \mathbf{v}_\rho^x)G(\mathbf{X}; t)], \quad (\text{C.6})$$

where

$$\tilde{W}_\rho(\mathbf{X}) = \sum_{\mathbf{Y}} W_\rho(\mathbf{X}, \mathbf{Y})H(\mathbf{Y} : \mathbf{X}), \quad (\text{C.7})$$

is the conditional expectation of $W_\rho(\mathbf{X}, \mathbf{Y})$.

Furthermore, we suppose that $H(\mathbf{Y} : \mathbf{X})$ approximately satisfies the one-dimensional chemical master equation obtained when \mathbf{X} is kept constant.

$$\frac{d}{dt}H(\mathbf{Y} : \mathbf{X}; t) = \sum_{\rho=1}^{r^n} [W_\rho(\mathbf{Y} - \mathbf{v}_\rho^y/\mathbf{Y})H(\mathbf{Y} - \mathbf{v}_\rho^y : \mathbf{X}; t) - W_\rho(\mathbf{Y}/\mathbf{Y} - \mathbf{v}_\rho^y)H(\mathbf{Y} : \mathbf{X}; t)], \quad (\text{C.8})$$

where r^n represents the number of reaction channels affecting the fast species.

To avoid time dependencies and dependence on the initial condition of the fast variable \mathbf{Y} in the conditional expectation $\tilde{W}_\rho(\mathbf{X})$ we assume time separation between \mathbf{Y} and \mathbf{X} . $H(\mathbf{Y} : \mathbf{X}; t)$ as the distribution of the fast variable will quickly relax to a conditional stationary distribution $H_{st}(\mathbf{Y} : \mathbf{X})$ with a vanishing left hand side in Eq. (C.8). $H_{st}(\mathbf{Y} : \mathbf{X})$ can be used to define the conditional moments in the transition population Eq. (C.7) and it is now possible to obtain $G(\mathbf{X}; t)$ from Eq. (C.6).

If $H_{st}(\mathbf{Y} : \mathbf{X})$ is a sharply peaked unimodal function one can replace the conditional moments by products of the first conditional moments, neglecting higher correlations. The latter can be obtained from finding the attracting stationary set of the corresponding deterministic equations, which are obtained from the chemical master equation when $A \rightarrow \infty$.

Appendix D

Mean-field approximation

Mean-field approximation (MFA) constitutes the first approach to the analysis of spatially extended systems. It is very useful to predict phase transitions, both in equilibrium [179] and away from equilibrium [5, 7]. It is more powerful than simple stability analysis. Nevertheless, it does not give accurate quantitative information, for example, it does not predict correctly either the position of transition points or the true values of the critical exponents. The MFA can be applied to stochastic partial differential equation (SPDE), to Fokker-Planck equation or to the master equation. Here for simplicity, we consider the use of this approximation as applied to a SPDE's, but a generalization to master equations is possible.

Consider a generic reaction-diffusion model with additive white noise¹,

$$\frac{d\theta}{dt} = f(\theta) + D\nabla^2\theta + \xi(r, t), \quad (\text{D.1})$$

where $\xi(r, t)$ is the white noise. Multiplicative noise can be considered as well [5, 7].

Eq. D.1 can be written in a lattice if the Laplacian operator is discretized as

$$\nabla^2\theta(x, t) = \sum_j \nabla_{ij}^2\theta_j(t) = \frac{1}{\Delta x^2} \sum_{j \in nn(i)} (\theta_j - \theta_i), \quad (\text{D.2})$$

where $nn(i)$ denotes the set of $2d$ nearest neighbors of cell i .

¹White noise is a random signal (or process) with a flat power spectral density. In other words, the signal's power spectral density has equal power in any band, at any centre frequency, having a given bandwidth. White noise is considered analogous to white light which contains all frequencies.

The MFA is implemented via the following assumption:

$$\sum_j \nabla_{ij}^2 \theta_j(t) = \frac{2d}{\Delta x^2} (\langle \theta \rangle - \theta_i). \quad (\text{D.3})$$

In that way, the MFA looks for uniform solutions of the field, $\theta = \langle \theta \rangle$, by neglecting its local fluctuations, $\sum_{j \in nn(i)} (\theta_j - \langle \theta \rangle) \approx 0$.

The MFA equation become exact or situations in which the field at each site interacts with all other sites in the thermodynamic limit. The next step is evaluation of the quantity $\langle \theta \rangle$, which is interpreted as the first statistical moment of the field, and accordingly it is defined as

$$\langle \theta \rangle = \beta \langle \langle \theta \rangle \rangle = \int d\theta \theta P(\theta, \langle \theta \rangle, t), \quad (\text{D.4})$$

where $P(\theta, \langle \theta \rangle, t)$ is the probability distribution, which obeys a Fokker-Planck equation [7].

Equation D.4 is a self-consistently equation, since the probability distribution depends itself on the unknown average $\langle \theta \rangle$. Hence, solving the MFA is reduced to finding the set of solutions of this self-consistency equation. $\langle \theta \rangle$ is the order parameter which can make predictions on the possible existence of a phase transition. A phase transition occurs, for instance, when the system leaves the state $\langle \theta \rangle = 0$, corresponding to a disordered phase, to reach a state $\langle \theta \rangle \neq 0$, representing an ordered phase.

Figures D.1(a) and D.1(b) show how to find these solutions graphically. Figure D.1(a) corresponds to a continuous phase transition, while Fig. D.1(b) depicts a discontinuous one, in which the empty circle is the unstable solution and the black circles are the stables states.

The MFA is very useful for predicting the existence of phase transitions, but the location of the transitions points is notoriously inaccurate. Several attempts have been made to improve the quantitative accuracy of the method [180, 181].

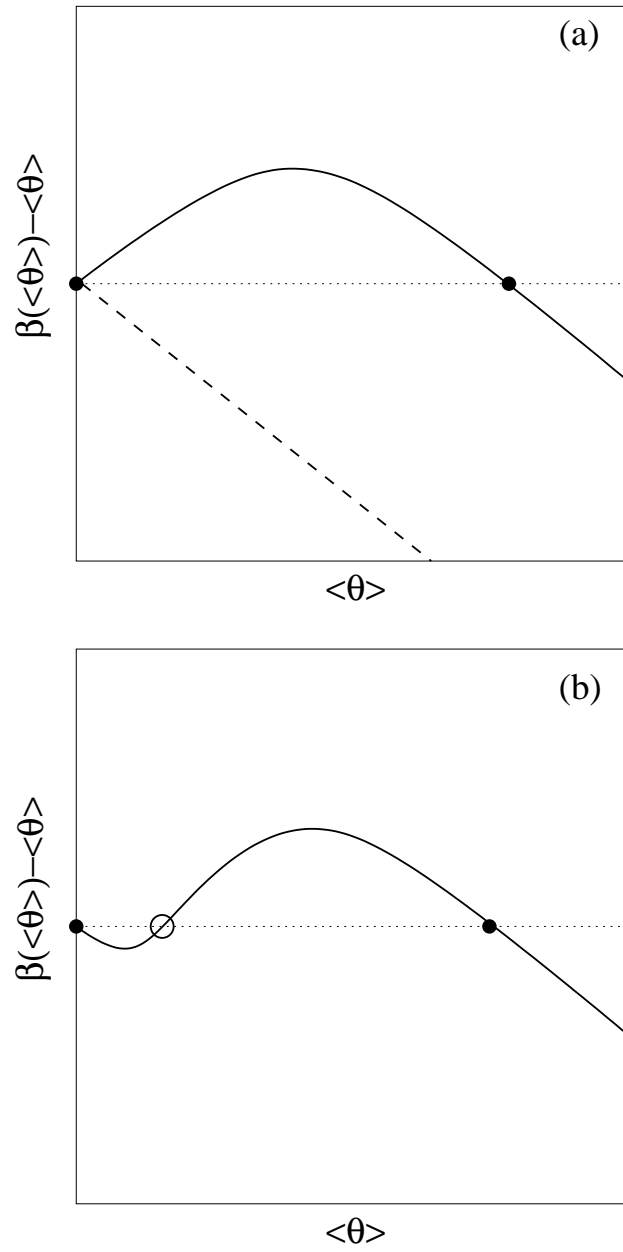


Figure D.1: Schematic figure describing the solution of the self-consistency equation D.4.

Appendix E

Spatial stochastic algorithm

The algorithm described below generates an exact realization of the Markov process described by the corresponding master equations. A surface is divided into a square lattice of $i = 1, \dots, N$ cells with periodic boundary conditions, which are at the same time regarded as well mixed and therefore are chosen to be smaller than the diffusion length. Each small cell is represented as a $L \times L = A$ square grid of adsorption sites. The idea is to determine in which subcell an event occurs first. A single event can change the state of only two subcells. If the event was a chemical reaction, the next event time has to be updated only for the subcell where it occurred. If the event was a jump out, next event times have to be updated for the subcell from which the jump occurred and for the subcell to which the molecule or atom jumped. Note that we consider in the following algorithms the adiabatic elimination of oxygen.

E.1 Random local and nonlocal interaction

Initialization

1. Distribute the initial numbers of molecules between the subcells.
2. Calculate the sum of the reaction rates for each subcell $m_i = \sum_{\rho=1}^r W_{\rho}$, where r is the number of reaction channels.
3. Calculate the sum of the random local and non local diffusion rates $s_i = \sum_{\rho=1}^2 W_{\rho}$, where 2 represents the jump out and the jump in channels.
4. For each subcell i :

- a) Sum the reaction and the random local and non local diffusion rates $m_i + s_i$ (total rate).
- b) Generate a random number $rand(1)$ uniformly distributed between 0 and 1.
- c) Calculate the first event time for each subcell as

$$\tau = \frac{1}{m_i + s_i} \ln \left[\frac{1}{rand(1)} \right]. \quad (\text{E.1})$$

5. Choose the subcell where the next event occurs first.

Iterations

6. Assume that i_α is the subcell in which the next event occurs. Generate a random number $rand(2)$ between 0 and 1, choose a channel according to

$$\sum_{\mu=1}^{\mu=\rho-1} W_\mu < rand(2)(m_i + s_i) \leq \sum_{\mu=1}^{\mu=\rho} W_\mu, \quad (\text{E.2})$$

note that $\rho = 1, \dots, r + 2$.

7. Reaction event:

- a) Update the state of the subcell i_α according to the state changes by reaction
- b) Recalculate $m_{i_\alpha} + s_{i_\alpha}$ for the subcell i_α , generate a new random number $rand(3)$ and calculate the time of the next event as

$$\tau_{i_\alpha} = \frac{1}{m_{i_\alpha} + s_{i_\alpha}} \ln \left[\frac{1}{rand(3)} \right] + t. \quad (\text{E.3})$$

- c) Recalculate the total rate for the other cells as well as the times of the next reaction.

8. Diffusion event:

- a) The direction of the diffusion event is chosen by "randomly selecting any subcell".
- b) Update the state of both subcells i_α and the other cell i_β .
- c) Recalculate the sum $m_{i_\alpha} + s_{i_\alpha}$ and $m_{i_\beta} + s_{i_\beta}$, sample the time to the next event in the subcells as in 7b.

9. Return to 6 for the next iteration.

E.2 Local (diffusive) interaction

Initialization

1. Distribute the initial numbers of molecules between the subcells.
2. Calculate the sum of the reaction rates for each subcell $m_i = \sum_{\rho=1}^r W_\rho$, where r is the number of reaction channels.
3. Calculate the sum of the random local and non local diffusion rates $s_i = \sum_{\rho=1}^2 W_\rho$, where 2 represents the jump out and the jump in channels.
4. For each subcell i :
 - a) Sum the reaction and the random local and non local diffusion rates $m_i + s_i$.
 - b) Generate a random number $rand(1)$ uniformly distributed between 0 and 1.
 - c) calculate the first event time for each subcell as

$$\tau = \frac{1}{m_i + s_i} \ln \left[\frac{1}{rand(1)} \right]. \quad (\text{E.4})$$

5. Choose the subcell where the next event occurs first.

Iterations

6. Assume that i_α is the subcell in which the next event occurs. Generate a random number $rand(2)$ between 0 and 1, choose a channel according to

$$\sum_{\mu=1}^{\mu=\rho-1} W_\mu < rand(2)(m_i + s_i) \leq \sum_{\mu=1}^{\mu=\rho} W_\mu, \quad (\text{E.5})$$

note that $\rho = 1, \dots, r + 2$.

7. Reaction event:
 - a) Update the state of the subcell i_α according to the state changes by reaction
 - b) Recalculate $m_{i_\alpha} + s_{i_\alpha}$ for the subcell i_α , generate a new random number $rand(3)$ and calculate the time of the next event as

$$\tau_{i_\alpha} = \frac{1}{m_{i_\alpha} + s_{i_\alpha}} \ln \left[\frac{1}{rand(3)} \right] + t. \quad (\text{E.6})$$

c) Recalculate the total rate for the nearest-neighbor cells as well as the times of the next reaction.

8. Diffusion event:

a) The direction of the diffusion event is chosen by "*randomly selecting a nearest-neighbor subcell*".

b) Update the state of both subcells i_α and the "*neighbor*" cell i_β .

c) Recalculate the sum $m_{i_\alpha} + s_{i_\alpha}$ and $m_{i_\beta} + s_{i_\beta}$, sample the time to the next event in the subcells as in 7b.

d) Recalculate the total rate for the nearest-neighbor cells of i_α and i_β as well as the times of the next reaction.

9. Return to 7 for the next iteration.

Appendix F

Rate equations from the (2,1) approximation

F.1 Rate equation for θ_{CO}

Consider the following equation

$$\frac{d\{CO\}}{dt} = p_{CO}\{E^-\} - d\{CO\} - 4k \left\{ \begin{array}{c} O \\ CO \end{array} \right\}. \quad (\text{F.1})$$

Using the (2,1) or pair approximation, it is possible to write

$$\{E^-\} = \left\{ \begin{array}{ccc} & Z & \\ Z & Z & Z \\ & Z & \end{array} \right\} - \{CO\} = \frac{\{ZZ\}^4}{\{Z\}^3} - \{CO\}, \quad (\text{F.2})$$

and

$$\left\{ \begin{array}{c} O \\ CO \end{array} \right\} \approx \{CO\}\{O\}. \quad (\text{F.3})$$

Then using

$$\{ZZ\} = 1 - \{OO\} - 2\{O\}, \quad (\text{F.4})$$

with

$$\{Z\} = 1 - \{O\}, \quad (\text{F.5})$$

where $\{OO\} = 0$, it is easy to show that

$$\frac{\{ZZ\}^4}{\{Z\}^3} = \frac{(1 - 2\{O\})^4}{(1 - \{O\})^3}. \quad (\text{F.6})$$

Finally considering that $\{O\} = \theta_O$ and $\{CO\} = \theta_{CO}$, we obtain

$$\frac{d\theta_{CO}}{dt} = p_{CO} \left[\frac{(1 - 2\theta_O)^4}{(1 - \theta_O)^3} - \theta_{CO} \right] - d\theta_{CO} - 4k\theta_{CO}\theta_O, \quad (\text{F.7})$$

F.2 Rate equation for θ_O

Consider the following equation

$$\frac{d\{O\}}{dt} = 2p_{O_2} \left\{ \begin{array}{cccc} & & E & \\ & E & E^- & E \\ E & E^- & E & \\ & & E & \end{array} \right\} - 4k \left\{ \begin{array}{c} O \\ CO \end{array} \right\}. \quad (\text{F.8})$$

Using the hybrid approximation, it is possible to write

$$\left\{ \begin{array}{cccc} & & E & \\ & E & E^- & E \\ E & E^- & E & \\ & & E & \end{array} \right\} = \left\{ \begin{array}{cccc} & & E & \\ & E & Z^- & E \\ E & Z^- & E & \\ & & E & \end{array} \right\} \left[1 - \frac{\{CO\}}{\{Z^-\}} \right]^2. \quad (\text{F.9})$$

Then, after apply the pair or (2,1) approximation

$$\left\{ \begin{array}{cccc} & & E & \\ & E & Z^- & E \\ E & Z^- & E & \\ & & E & \end{array} \right\} = \frac{\{EZ^-\}^8}{\{E\}^2\{Z^-\}^6}, \quad (\text{F.10})$$

where

$$\{EZ^-\} = \{E^-Z^-\} + \{E^+Z^-\} = \{Z^-Z^-\} \left[1 - \frac{\{CO\}}{\{Z^-\}} \right] + \{Z^+Z^-\}, \quad (\text{F.11})$$

and

$$\{Z^+Z^-\} + \{Z^-Z^-\} = \{Z^-\}, \quad (\text{F.12})$$

or

$$\{Z^+Z^-\} = \{Z^-\} - \{Z^-Z^-\}, \quad (\text{F.13})$$

Finally, it is easy to shown that

$$\{EZ^-\} = \{Z^-\} - \{Z^-Z^-\} \frac{\{CO\}}{\{Z^-\}}, \quad (\text{F.14})$$

where

$$\{Z^-Z^-\} = \left\{ \begin{array}{cccc} & Z & Z & \\ Z & Z & Z & Z \\ & Z & Z & \end{array} \right\} = \frac{\{ZZ\}^7}{\{Z\}^6}. \quad (\text{F.15})$$

Using previous equations and after some algebra

$$\{EZ^-\} = \frac{(1 - 2\{O\})^3}{(1 - \{O\})^3} (1 - 2\{O\} - \{CO\}), \quad (\text{F.16})$$

$$\frac{\{EZ^-\}^8}{\{E\}^2\{Z^-\}^6} = \frac{(1 - 2\{O\} - \{CO\})^8}{(1 - \{O\})^6(1 - \{O\} - \{CO\})^2}, \quad (\text{F.17})$$

and

$$\left[1 - \frac{\{CO\}}{\{Z^-\}}\right]^2 = \left[1 - \frac{(1 - \{O\})^3\{CO\}}{(1 - 2\{O\})^4}\right]^2. \quad (\text{F.18})$$

Finally considering that $\{O\} = \theta_O$ and $\{CO\} = \theta_{CO}$, we obtain

$$\frac{d\theta_O}{dt} = 2p_{O_2} \left[\frac{(1 - 2\theta_O - \theta_{CO})^8}{(1 - \theta_O)^6(1 - \theta_O - \theta_{CO})^2} \right] \left[1 - \frac{(1 - \theta_O)^3\theta_{CO}}{(1 - 2\theta_O)^4} \right]^2 - 4k\theta_{CO}\theta_O. \quad (\text{F.19})$$

Bibliography

- [1] Richard P. Feynman, *The Character of Physical Law*, (Random House, Inc. New York 1994).
- [2] D. Ruelle, *Physics Today* **57**, 48 (2004).
- [3] N. G. van Kampen, *Stochastic Processes in Physics and Chemistry*, (North-Holland, Amsterdam, 1987).
- [4] C. W. Gardiner, *Handbook of Stochastic Methods for Physics, Chemistry and the natural science*, (Springer-Verlag, Berlin, 1985).
- [5] F. Sagués, J. M. Sancho and J. Garcia-Ojalvo, *Rev. Mod. Phy.* **79**, 829 (2007).
- [6] W. Horsthemke and R. Lefever, *Noise-Induced Transitions*, (Springer, Berlin, 1984).
- [7] J. Garcia-Ojalvo and J. M. Sancho, *Noise in Spatially Extended Systems*, (Springer-Verlag, New York, 1999).
- [8] M. Löcher, *Noise Sustained Patterns*, (World Scientific, Singapore, 2003).
- [9] B. Lindner, J. Garcia-Ojalvo, A. Neiman, and L. Schimansky-Geier, *Phys. Rep.* **392**, 321 (2004).
- [10] L. Yang, Z. Hou, and H. Xin, *J. Chem. Phys.* **109**, 2002 (1998).
- [11] L. Yang, Z. Hou, B. Zhou, and H. Xin, *J. Chem. Phys.* **109**, 6456 (1998).
- [12] I. Derényi, C. Lee, and A. L. Barabási, *Phys. Rev. Lett.* **80**, 1473 (1998).
- [13] Y. Suchorski, J. Beben, E. W. James, J. W. Evans, and R. Imbuhl, *Phys. Rev. Lett.* **82**, 1907 (1999).
- [14] Y. Suchorski, J. Beben, R. Imbuhl, E. W. James, Da-Jiang Liu, and J. W. Evans, *Phys. Rev. B.* **63**, 165417 (2001).
- [15] V. Johánek, M. Laurin, A. W. Grant, B. Kasemo, C. R. Henry, and J. Libuda, *Science* **304**, 1639 (2004).

- [16] S. Wehner, P. Hoffmann, D. Schmeißer, H. R. Brand and J. Küppers, *Phys. Rev. Lett.* **95**, 038301 (2005).
- [17] P. Hoffmann, S. Wehner, D. Schmeisser, H. R. Brand, and J. Küppers, *Phys. Rev. E.* **73**, 056123 (2006).
- [18] I. Chorkendorff and J. W. Niemantsverdriet, *Concepts of Modern Catalysis and Kinetics*, (VCH, Weinheim, 2003).
- [19] J. Hagen, *Industrial Catalysis: a practical approach*, (VCH, Weinheim, 2006).
- [20] J. Libuda, S. Schuermann, M. Laurin, T. Schalow and H.-J. Freund, *Monatshefte für Chemie* **136**, 59 (2005).
- [21] R. I. Masel, *Principles of Adsorption and Reaction on Solid Surfaces*, (Wiley-Interscience, New York, 1996).
- [22] G. Ertl and H.-J. Freund, *Physics Today* **52**, 32 (1999).
- [23] G. Ertl, *Science* **254**, 1756 (1991).
- [24] R. Imbihl and G. Ertl, *Chem. Rev. (Washington, D.C)* **95**, 397 (1995).
- [25] G. Ertl, *Adv. Catal.* **37**, 231 (1990).
- [26] F. Schüth, B. E. Henry and L. D. Schmidt, *Adv. Catal.* **39**, 51 (1993).
- [27] H. H. Rotermund, *Surf. Sci. Rep.* **29**, 265 (1997).
- [28] R. Imbihl, *Prog. Surf. Sci.* **44**, 185 (1993).
- [29] M. Eiswirth and G. Ertl, in *Chemical Waves and Patterns*, edited by R. Kapral and K. Showalter (Kluwer, Dordrecht, 1994).
- [30] V. P. Zhdanov and B. Kasemo, *Surf. Sci. Rep.* **20**, 111 (1994).
- [31] G. Blyholder, *J. Phys. Chem.* **68**, 2772 (1964).
- [32] T. Engel and G. Ertl, *Adv. Catal.* **28**, 1 (1979).
- [33] P. Hugo, *Ber. Bunsen-Ges. Phys. Chem.* **74**, 121 (1970).
- [34] H. Beusch, D. Fieguth, and D. Wicke, *E. Chem. Eng. Tech.* **44**, 445 (1972).
- [35] L. F. Rázon and R. A. Schmitz, *Catal.. Rev. Sci. Eng* **28**, 89 (1986).
- [36] G. Ertl, P. R. Norton, and J. Rüstig, *Phys. Rev. Lett.* **49**, 177 (1982).
- [37] M. Ehsasi, M. Matloch, M. Frank, O. Block, J. H. Christman, K. Rys, and F. S. Hirschwald, *J. Chem. Phys.* **91**, 4949 (1989).
- [38] K. Krischer, M. Eiswirth, and G. Ertl, *J. Chem. Phys.* **96**, 9161 (1992).
- [39] N. Hartmann, K. Krischer, and R. Imbihl, *J. Chem. Phys.* **101**, 6717 (1994).

- [40] S. Jakubith, H. H. Rotermund, W. Engel, A. von Oertzen, and G. Ertl, *Phys. Rev. Lett.* **65**, 3013 (1990).
- [41] S. Nettesheim, A. von Oertzen, H. H. Rotermund, and G. Ertl, *J. Chem. Phys.* **98**, 9977 (1993).
- [42] H. H. Rotermund, S. Jakubith, A. von Oertzen, and G. Ertl, *Phys. Rev. Lett.* **66**, 3083 (1991).
- [43] K. C. Rose, D. Battogtokh, A. Mikhailov, R. Imbihl, W. Engel, and A. M. Bradshaw, *Phys. Rev. Lett.* **76**, 3582 (1996).
- [44] R. Imbihl and G. Vesper, *J. Vac. Sci. Technol. A* **12**, 2170 (1994).
- [45] R. Imbihl, *New J. Phys.* **5**, 62.1 (2003).
- [46] Y. Suchorski and W. Drachsel, *Top. Catal.* **46**, 201 (2007).
- [47] J. Starke, C. Reichert, M. Eiswirth, H. H. Rotermund, and G. Ertl, *Europhysical Letters.* **73**, 820 (2006).
- [48] D. J. Liu and J. W. Evans, *J. Chem. Phys.* **117**, 7319 (2002).
- [49] D. J. Liu and J. W. Evans, *Phys. Rev. B* **75**, 073401 (2007).
- [50] V. P. Zhdanov and B. Kasemo, *Surf. Sci. Rep.* **39**, 25 (2000).
- [51] M. Pineda, R. Imbihl, L. Schimansky-Geier, and Ch. Zülicke, *J. Chem. Phys.* **124**, 044701 (2006).
- [52] M. Pineda, L. Schimansky-Geier, and R. Imbihl, *Phys. Rev. E* **75**, 061107 (2007).
- [53] M. Pineda, L. Schimansky-Geier, and R. Imbihl, *To be published*.
- [54] M. Pineda, R. Imbihl, and J. W. Evans, *To be published*.
- [55] R. W. Wood, *Phys. Rev.* **5**, 1 (1899).
- [56] R. H. Fowler and L. W. Nordheim, *Proc. Roy. Soc.* **A119**, 173 (1928).
- [57] E. W. Müller, *Z. Phys.* **37**, 838 (1936).
- [58] D. P. Woodruff and T. A. Delchar, *Modern Techniques of Surface Science*, (Cambridge University Press, 1994).
- [59] M. F. H van Tol, A. Gielbert, and B. E. Nieuwenhuys, *Catal. Lett.* **16**, 297 (1992).
- [60] V. Gorodetskii, J. H. Block, W. Drachsel, and M. Ehsasi, *Appl. Surf. Sci.* **67**, 198 (1993).

- [61] J. R. Oppenheimer, *Phys. Rev.* **31**, 67 (1928).
- [62] E. W. Müller, *Z. Phys.* **131**, 136 (1951).
- [63] E. W. Müller, *Chemistry and Physics of Solid Surfaces*, (Vanselow and Tong, Cleveland: CRC, 1977).
- [64] M. Rezep, J. Pitters, and R. Wolkow, *J. Chem. Phys.* **124**, 204716 (2006).
- [65] A. Zangwill, *Physics at Surfaces*, (Cambridge University Press, 1988).
- [66] W. Gerlach and O. Stern, *Z. Phys.* **8**, 110 (1921).
- [67] A Benninghoven, *Surf. Sci.* **35**, 427 (1973).
- [68] S. Günther, B. Kaulich, L. Gregoratti, and M. Kiskinova, *Prog. Surf. Sci.* **70**, 187 (2002).
- [69] H. H. Rotermund, W. Engel, M. E. Kordesh, S. Jakubith, A. Von Oertzen, and G. Ertl, *Ultramicroscopy* **36**, 164 (1991).
- [70] H. H. Rotermund, *Surf. Sci.* **386**, 10 (1997).
- [71] M. Berdau, G. G. Yelenin, A. Karpowicz, M. Ehsasi, K. Christmann, and J. H. Block, *J. Chem. Phys.* **110**, 11551 (1999).
- [72] R. Imbihl, *New. J. Phys.* **5**, 62-1 (2003).
- [73] Y. Suchorski, J. Beben, and R. Imbihl, *Prog. Surf. Sci.* **59**, 343 (1998).
- [74] D. T. Gillespie, *Markov Processes: An Introduction for Physical Scientists*, (Academic, San Diego, 1992).
- [75] L. K. Doraiswamy and B. D. Kulkarni, *The Analysis of Chemically Reacting Systems: A Stochastic Approach*, (Gordon and Breach Science, Switzerland, 1987).
- [76] E. Joos, H. D. Zeh, C. Kiefer, D. Giulini, J. Kupsch, and I.-O. Stamatescu, *Decoherence and the Appearance of a Classical World in Quantum Theory*, (Springer-Verlag, Berlin, 2003).
- [77] H. Hinrichsen, *Physica A* **369**, 1 (2006).
- [78] M. Delbrück, *J. Chem. Phys.* **8**, 120 (1940).
- [79] G. Nicolis and I. Prigogine, *Self-organization in Nonequilibrium Systems*, (Wiley-Interscience, New York, 1977).
- [80] H. Risken, *The Fokker-Planck equation: Methods of Solutions and Applications*, (Springer-Verlag, Berlin, 1989).

- [81] N. Metropolis, A. W. Rosenbluth, A. H. Teller, and E. Teller, *J. Chem. Phys.* **21**, 1087 (1953).
- [82] T. Liggett, *Interacting Particles Systems*, (Springer-Verlag, Berlin, 1985).
- [83] D. T. Gillespie, *J. Chem. Phys.* **22**, 403 (1976).
- [84] M. A. Gibson and J. Bruck, *J. Phys. Chem. A* **104**, 1876 (2000).
- [85] D. J. Wilkinson, *Stochastic Model of System Biology*, (Chapman and Hall/CRC Press London, 2006).
- [86] R. Gomer, *Rep. Prog. Phys* **53**, 917 (1990).
- [87] M. Silverberg and A. Ben-Shaul, *J. Chem. Phys.* **87**, 3178 (1989).
- [88] H. C. Kang, T. A. Jachimowiski and W. H. Weinberg, *J. Chem. Phys.* **93**, 1418 (1990).
- [89] A. Fitchthorn and W. H. Weinberg, *Langmuir* **7**, 2539 (1991).
- [90] J. Marro and R. Dickman, *Nonequilibrium Phase Transitions in Lattice Models*, (Cambridge University Press, 1999).
- [91] M. Tammaro, M. Sabella and J. W. Evans, *J. Chem. Phys.* **103**, 10277 (1995).
- [92] N. G. van Kampen, *Phys. Rep.* **124**, 69 (1985).
- [93] T. Turányi, A. S. Tomlin and M. J. Pilling, *J. Phys Chem.* **97**, 163 (1993).
- [94] W. Klonowski, *Biophys. Chem.* **18**, 73 (1983).
- [95] H. Malchow and L. Schimansky-Geier, *Noise and Diffusion in Bistable Non-equilibrium Systems*, (Teubner, Berlin, 1985).
- [96] M. Bär, Ch. Zülicke, M. Eiswirth, and G. Ertl, *J. Chem. Phys.* **96**, 8595 (1992).
- [97] S. Ladas, R. Imbihl, and G. Ertl, *Surf. Sci.* **219**, 88 (1989).
- [98] S. Völkening and J. Wintterlin, *J. Chem. Phys.* **114**, 6382 (2001).
- [99] J. Wintterlin, S. Völkening, T. V. W. Janssens, T. Zambelli, and G. Ertl, *Science* **278**, 1931 (1997).
- [100] D.-J Liu and J. W. Evans, *Phys. Rev. B.* **70**, 193408 (2004).
- [101] D.-J Liu and J. W. Evans, *Multiscale Modelling Simul.* **4**, 424 (2005).
- [102] E. W. James, C. Song, and J. W. Evans, *J. Chem. Phys.* **111**, 6579 (1999).
- [103] J. W. Evans and M. S. Miesch, *Surf. Sci.* **245**, 401 (1991).
- [104] R. D. Vigil and F. T. Willmore, *Phys. Rev. E.* **54**, 1225 (1996).
- [105] J. J. Luque, *Phys. Rev. A.* **42**, 3319 (1990).

- [106] J. C otes, A. Narv aez, H. Puschmann, and E. Valencia, *Chem. Phys.* **288**, 77 (2003).
- [107] M. C. Lemos, J. J. Luque and F. Jim enez-Morales, *Phys. Rev. E.* **51**, 5360 (1995).
- [108] J. J. Luque, F. Jim enez-Morales, and M. C. Lemos, *J. Chem. Phys.* **96**, 8535 (1992).
- [109] G. L. Hoenicke and W. Figueiredo, *Phys. Rev. E.* **62**, 6216 (2000).
- [110] C. R. Brundle, R. J. Behm, and J. A. Barler, *J. Vac. Sci. Technol. A* **2**, 1038 (1984).
- [111] S.-L. Chang and P. A. Thiel, *Phys. Rev. Lett.* **59**, 296 (1987).
- [112] J. W. Evans, *J. Chem. Phys.* **87**, 3038 (1987).
- [113] G. A. Somorjai, *Introduction to Surface Chemistry*, (Wiley, New York, 1994).
- [114] R. M. Ziff, E. Gulari and Y. Barshad, *Phys. Rev. Lett.* **56**, 2553 (1986).
- [115] N. Pavlenko, R. Imbihl, J. W. Evans, and D. -J. Liu, *Phys. Rev. E.* **68**, 016212 (2003).
- [116] D. -J. Liu, N. Pavlenko, and J. W. Evans, *J. Stat. Phys.* **114**, 101 (2004).
- [117] J. A. M. Janssen, *J. Stat. Phys.* **57**, 171 (1989).
- [118] M. O. Vlad and A. Pop, *Physics A.* **155**, 276 (1989).
- [119] E. L. Haseltine and J. B. Rawlings, *J. Chem. Phys.* **123**, 164115 (2005).
- [120] J. Elf and M. Ehrenberg, *Genome Research.* **13**, 2475 (2003).
- [121] M. Frankowicz, M. Moreau, P. P. Szczesny, J. Toth, and L. Vicente, *J. Phys. Chem.* **97**, 1891 (1993).
- [122] C. V. Rao and P. Arkin, *J. Chem. Phys.* **118**, 4999 (2003).
- [123] M. R. Roussel and R. Zhu, *J. Chem. Phys.* **121**, 8716 (2004).
- [124] A. Samant and D. G. Vlachos, *J. Chem. Phys.* **123**, 144114 (2005).
- [125] K.-H. Chiam, C. M. Tan, V. Bhargava and G. Rajagopal, *Phys. Rev. E.* **74**, 051910 (2006).
- [126] Y. Cao, D. T. Gillespie, and L. R. Petzold, *J. Chem. Phys.* **122**, 04116 (2005).
- [127] Y. Cao, D. T. Gillespie, and L. R. Petzold, *J. Chem. Phys.* **123**, 144917 (2005).
- [128] Y. Cao, D. T. Gillespie, and L. R. Petzold, *J. Comput. Phys.* **206**, 395 (2005).

- [129] R. Kawai, X. Sailer, L. Schimansky-Geier, and C. Van den Broeck, *Phys. Rev. E* **69**, 051104 (2004).
- [130] M. Eiswirth and H. H. Rotermund, *Physica D* **84**, 40 (1995).
- [131] V. P. Zhdanov and B. Kasemo, *Surf. Sci.* **496**, 251 (2002).
- [132] V. P. Zhdanova, *Phys. Rev. B* **63**, 153410 (2001).
- [133] N. V. Peskov, M. M. Slinko, and N. I. Jaeger, *J. Chem. Phys.* **116**, 2098 (2002).
- [134] C. Reichert, J. Starke, and M. Eiswirth, *J. Chem. Phys.* **115**, 4829 (2001).
- [135] E. S. Kurkina and N. L. Semydyayeva, *Surf. Sci. Lett.* **558**, 122 (2004).
- [136] F. Shloegl, *Z. Phys.* **253**, 147 (1972).
- [137] A. S. Mikhailov, *Foundations of synergetics I*, (Springer-Verlag, Berlin, 1990).
- [138] X. Guo, D. -J. Liu, and J. W. Evans, *Phys. Rev. E* **75**, 061129 (2007).
- [139] D. T. Gillespie, *Physica A* **95**, 69 (1979)
- [140] D. T. Gillespie, *Physica A* **101**, 535 (1980)
- [141] D. T. Gillespie, *J. Chem. Phys.* **74**, 5295 (1981)
- [142] V. Seshadri, B. J. West, and K. Lindenberg, *J. Chem. Phys.* **72**, 1145 (1980)
- [143] W. Ebeling and L. Schimansky-Geier, *Physica A* **98**, 587 (1979).
- [144] M. M. de Oliveira and R. Dickman, *Physica A* **343**, 525 (2004).
- [145] R. Müller, K. Lippert, A. Kühnel and U. Behn, *Phys. Rev. E* **56**, 2658 (1997).
- [146] N. Pavlenko, J. W. Evans, D. -J. Liu, and R. Imbihl, *Phys. Rev. E* **65**, 016121 (2002).
- [147] Y. Suchorski, W. Drachsel, V. V. Gorodetski, V. K. Medvedev, and H. Weiss, *Surf. Sci.* **600**, 1579 (2006).
- [148] H. Rosé, H. Hempel, and L. Schimansky-Geier, *Physica A* **2006**, 421 (1994).
- [149] M. Malek-Mansour and G. Nicolis, *J. Stat. Phys.* **13**, 197 (1975).
- [150] M. Hildebrand and A. S. Mikhailov, *J. Phys. Chem.* **100**, 19089 (1996).
- [151] F. Baras and M. M. Mansour, *Phys. Rev. E* **54**, 6139 (1996).
- [152] M. V. Velikanov and R. Kapral, *J. Chem. Phys.* **109**, 281 (1998).
- [153] J. Gorecki, A. L. Kawczyński, and B. Nowakowski, *J. Phys. Chem. A* **103**, 3200 (1999).
- [154] C. Van den Broeck, J. M. R. Parrondo, J. Armero, and A. Hernández-Machado, *Phys. Rev. E* **49**, 2639 (1994).

- [155] M. Morillo, J. Gómez-Ordóñez, and J. M. Casado, *Phys. Rev. E.* **52**, 316 (1995).
- [156] J. S. Smart, *Effective field theories of magnetism*, (W.B. Saunders, Philadelphia, 1966).
- [157] M. DelleDonne and P. Ortoleva, *J. Stat. Phys.* **18**, 319 (1978).
- [158] M. Shiino, *Phys. Rev. A.* **36**, 2393 (1987).
- [159] R. Erban, I. G. Kevrekidis, D. Adalsteinsson, and T. C. Elston, *J. Chem. Phys.* **124**, 084106 (2006).
- [160] D. Bernstein, *Phys. Rev. E.* **71**, 041103 (2005).
- [161] A. Chatterjee and D. G. Vlachos, *J. Chem. Phys.* **124**, 064110 (2006).
- [162] H. Hinrichsen, *J. Stat. Mech.: Theor. Exp.* P07066 (2007).
- [163] J. Cisternas, P. Holmes, I. G. Kevrekidis and J. X. Li, *J. Chem. Phys.* **118**, 3312 (2003).
- [164] J. Libuda and H. -J. Freund, *Surf. Sci. Rep.* **57**, 157 (2005).
- [165] V. P. Zhdanov, *Langmuir* **17**, 1793 (2001)
- [166] M. Nagasaka, H. Kondof, I. Nakai, and T. Ohta, *J. Chem. Phys.* **126**, 044704 (2007).
- [167] M. Silverberg and A. Ben-Shaul, *J. Stat. Phys.* **52**, 1179 (1988).
- [168] V. P. Zhdanov and B. Kasemo, *Eur. Phys. J. B* **27**, 541 (2002).
- [169] C. A. Voigt and R. M. Ziff, *J. Chem.* **107**, 7397 (1997).
- [170] D. J. Liu and J. W. Evans, *J. Phys.: Condens. Matter* **19**, 065129 (2007).
- [171] H. Uecker, R. Imbihl, M. Rafti, I. M. Irurzun, J. L. Vicente, and E. E. Mola, *Chem. Phys. Lett* **382**, 232 (2003).
- [172] T. B. Kepler, and T. C. Elston, *Biophys. J.* **81**, 3116 (2001).
- [173] M. M. Slinko, A. A. Ukharskii, and N. I. Jaeger, *Phys. Chem. Chem. Phys* **3**, 1015 (2001).
- [174] E. S. Kurkina and E. D. Tolstunova, *Appl. Surf. Sci.* **182**, 77 (2001).
- [175] N. V. Peskov, M. M. Slinko, and N. I. Jaeger, *J. Chem. Phys.* **118**, 8882 (2003).
- [176] N. V. Peskov, *Physica D* **137**, 316 (2000).
- [177] M. M. Slinko, E. S. Kurkina, M. A. Liauw, and N. I. Jaeger, *J. Chem. Phys.* **111**, 8105 (1999).

- [178] E. S. Kurkina, N. V. Peskov, M. M. Slinko *Physica D* **118**, 103 (1998).
- [179] L. P. Kadanoff, *Statistical Physics : Statics, Dynamics and Renormalization*, (World Scientific, 2000).
- [180] Van den Broeck, C. J. M. Parrondo, and R. Toral, *Phys. Rev. Lett.* **73**, 3395 (1995).
- [181] Van den Broeck, C. J. M. Parrondo, R. Toral, and R. Kawai, *Phys. Rev. E.* **55**, 4084 (1997).

Publications of this Thesis

- **M. Pineda**, R. Imbihl, L. Schimansky-Geier, and CH. Zülicke:
Theoretical analysis of internal fluctuations and bistability in CO oxidation on nanoscale surfaces
J. Chem. Phys. Vol. 124, 044701 (2006)
- **M. Pineda**, L. Schimansky-Geier, and R. Imbihl:
Fluctuation-induced phase transition in a spatially extended model for catalytic CO oxidation
Phys. Rev. E. **75**, 061107 (2007)
- **M. Pineda**, L. Schimansky-Geier, and R. Imbihl:
First-order phase transition in a phenomenological model for CO oxidation driven by internal fluctuations
In preparation

CURRICULUM VITAE

SURNAMES: Pineda Rodriguez

FIRST NAMES: Miguel Arnaldo

DATE OF BIRTH: 05 October 1979

CITIZENSHIP: Venezuelan

PLACE OF BIRTH: Valera, Venezuela

SEX: Male

ACADEMIC INFORMATION

10/2004 - 01/2008: **Dr.rer.nat.(PhD)**

Leibniz University Hannover, Germany

(Supervisor: Prof. Dr. Ronald Imbihl)

(Co-Supervisor: Prof. Dr. Lutz Schimansky-Geier)

Thesis: *"Fluctuations in heterogeneous catalysis: CO oxidation as a case study"*

1996 - 2001: **Licentiate in Physics** (*Magna Cum Laude*)

Universidad de los Andes, Venezuela

(Supervisor: Prof. Dr. Mario Cosenza)

Thesis: *"Spatiotemporal patterns in chaotic systems with local and global interactions"*

OTHER ACADEMIC APPOINTMENTS

2001 - 2002: **Graduate Student**

Universidad de los Andes (ULA)

Mérida, Venezuela

2003 - 2004: **Graduate Student**

Max-Planck-Institute for Physics of Complex Systems (MPIPKS)

Dresden, Germany

03/2006 - 04/2006: **Visiting Scientist**

Ames Laboratory-USDOE

Iowa State University

Ames, USA

PUBLICATIONS

Authors: M. G. Cosenza, **M. Pineda**, and A. Parravano

Title: *Emergence of patterns in drive and in autonomous spatiotemporal systems*

Journal: *Physical Review E* **67**, 066217 (2003).

Authors: **M. Pineda** and M. G. Cosenza

Title: *Synchronization in driven versus autonomous coupled chaotic maps*

Journal: *Physical Review E* **71**, 057201 (2005).

Authors: **M. Pineda**, R. Imbihl, L. Schimansky-Geier and Ch. Zülicke

Title: *Theoretical analysis of internal fluctuations and bistability in CO oxidation on nanoscale surfaces*

Journal: *The Journal of Chemical Physics* **124**, 044701 (2006).

Authors: O. Alvarez-Llamoza, K. Tucci, M. G. Cosenza and **M. Pineda**

Title: *Random global coupling induces synchronization and nontrivial collective behavior in networks of chaotic maps*

Journal: *The European Physical Journal ST* **143**, 245 (2007).

Authors: **M. Pineda**, L. Schimansky-Geier and R. Imbihl

Title: *Fluctuation-induced phase transition in a spatially extended model for CO oxidation*

Journal: *Physical Review E* **75**, 061107 (2007).

Acknowledgements

First of all my sincere gratitude to Prof. Dr. R. Imbihl and Prof. Dr. L. Schimansky-Geier for the stimulating supervision of this Thesis. In particular, I would like acknowledgement to Prof. Dr. R. Imbihl for illuminating discussions related to the fascinating experimental aspects of heterogeneous catalysis and to Prof. Dr. L. Schimansky-Geier for the motivating introduction to the theory of stochastic process.

I would like to thanks my senior collaborator Dr. Ch. Zülicke for his appreciated contributions to this Thesis, particularly in aspects related to fluctuation-induced transitions in CO oxidation on nanoscale surfaces.

I am specially thankful to Prof. Dr. J. W. Evans, for allowing me to spend a joyful period at the Ames Laboratory-USDOE, Iowa State University and for stimulating discussions concerning to nonequilibrium processes in heterogeneous catalysis. I would also like to thanks Dr. Da-Jiang Liu at the Ames Laboratory-USDOE for his valuable discussions related to the numerical implementation of realistic atomistic kinetic Monte Carlo simulation to heterogeneous catalysis.

Many thanks also to all colleagues and staff of the Institute of Physical Chemistry and Electrochemistry at the Gottfried-Wilhelm-Leibniz-Universität Hannover, specially those of the Prof. Imbihl's research group, for the motivating experimental environment.

I am especially acknowledgement Dr. Edward Arévalo for his help and advice in difficult moments for me. He played a primordial role in the fruitful culmination of my doctoral studies in Germany.

I would like to thanks FUNDAYACUCHO for the financial support through a fellowship as a part of a cooperation between DAAD (Germany) and FUNDAYACUCHO (Venezuela). Finally, I would like acknowledgement to Prof. Dr. R. Imbihl for financial support during the final period of this work.

